NATIONAL AERONAUTICS AND SPACE ADMINISTRATION.

Technical Report No. 32-700

Ranger VII

Part II. Experimenters' Analyses and Interpretations

R. L. Heacock
G. P. Kuiper
E. M. Shoemaker
H. C. Urey
E. A. Whitaker

N65-22162
(ACCESSION NUMBER)
156
(PAGES)
CR-62347
(NASA CR OR TMX OR AD NUMBER)
1
(THRU)
(CODE)
30
(CATEGORY)
FACILITY FORM 602

GPO PRICE $ _____
OTS PRICE(S) $ _____
Hard copy (HC) 5.00
Microfiche (MF) 1.00

jpl
JET PROPULSION LABORATORY
CALIFORNIA INSTITUTE OF TECHNOLOGY
PASADENA, CALIFORNIA

February 10, 1965

NATIONAL AERONAUTICS AND SPACE ADMINISTRATION

Technical Report No. 32-700

Ranger VII

Part II. Experimenters' Analyses and Interpretations

R. L. Heacock
G. P. Kuiper
E. M. Shoemaker
H. C. Urey
E. A. Whitaker

H. M. Schurmeier
Ranger Project Manager

JET PROPULSION LABORATORY
CALIFORNIA INSTITUTE OF TECHNOLOGY
PASADENA, CALIFORNIA

February 10, 1965

Copyright © 1965
Jet Propulsion Laboratory
California Institute of Technology

Prepared Under Contract No. NAS 7-100
National Aeronautics & Space Administration

CONTENTS

I. Introduction *by Raymond L. Heacock* 1
A. Experimenter Team 1
B. Television Description 3
C. Impact-Area Selection 5
D. Publication of Data 5

II. Preview of Scientific Results *by the Experimenter Team* 7

III. Interpretation of *Ranger VII* Records *by Gerard P. Kuiper* 9
A. The Gross Structure of Lunar Maria 12
B. Colors and the Meso-Structure of the Maria 29
C. On the Structure of Mare Cognitum 39
D. The Structure of Crater Rays 44
E. Classes of Craters and Depressions 49
F. The Structure of the Mare Floor 55
G. The Frequency of Lunar Craters 59
H. Small-Scale Lineaments on the *Ranger VII* Photographs 62
I. The Mare Ridges 69
J. The Scientific Significance of the *Ranger VII* Mission 71
References 73

IV. Preliminary Analysis of the Fine Structure of the Lunar Surface *by Eugene M. Shoemaker* 75
A. Major Facts Established by *Ranger VII* Photographs 75
B. Cratering as the Dominant Surface Process 115
C. Preliminary Model of Fine Structure 130
References 133

V. Observations on the *Ranger VII* Pictures *by Harold C. Urey* . . . 135
A. Erosion 135
B. Secondary Craters 136
C. Rocks in Craters 138
D. Perfect and Imperfect Craters 138
E. Wrinkles on the Lunar Surface 143
F. Dimples, Valleys, and Cracks 143
G. Summary 145
References 148

VI. Further Observations on the *Ranger VII* Records *by Ewen A. Whitaker* 149

I. INTRODUCTION

Raymond L. Heacock
Jet Propulsion Laboratory
Pasadena, California

On July 31, 1964, the *Ranger VII* spacecraft transmitted to the Earth over 4300 photographs of the Moon. The photographs were of excellent quality and provide a unique set of new data about the Moon for scientific and engineering study. This Report presents results of the first phase of the analysis of these photographs by a team of scientists appointed as investigators by the National Aeronautics and Space Administration. The emphasis thus far has been placed on a qualitative interpretation of the pictures in an effort to hypothesize a surface model. Work is now underway to accomplish the long-term quantitative analysis of the entire set of photographs. The major items planned are photometric and photogrammetric mapping. A number of other items such as geologic mapping and a statistical analysis of heights are also planned.

A preliminary presentation of scientific results from the *Ranger VII* flight was made at a special session of the International Astronomical Union Meeting in Hamburg, Germany, on August 31, 1964. The name Mare Cognitum was officially adopted by the Union for the previously unnamed mare in which *Ranger VII* impacted. The preferred broad translation of Mare Cognitum is "the sea that has become known."

A. Experimenter Team

The National Aeronautics and Space Administration initiated the *Ranger* Block III program, which included *Ranger VII*, in mid-1961. The primary objective of this program was to obtain close-up photographs of the Moon. Such photographs were to provide information about small topographic features of the Moon's surface needed for Projects *Surveyor* and *Apollo*. The television camera payload was conceived as a follow-on to the earlier *Ranger* Block II photographic experiment. NASA appointed an experimenter group made up of a technical team and a scientific team to aid in the planning of this photographic mission. These teams worked with the Jet Propulsion Laboratory to ensure that the photographs obtained from successful *Ranger* flights would provide significant new information about the Moon, and they were responsible for reporting the scientific results. The

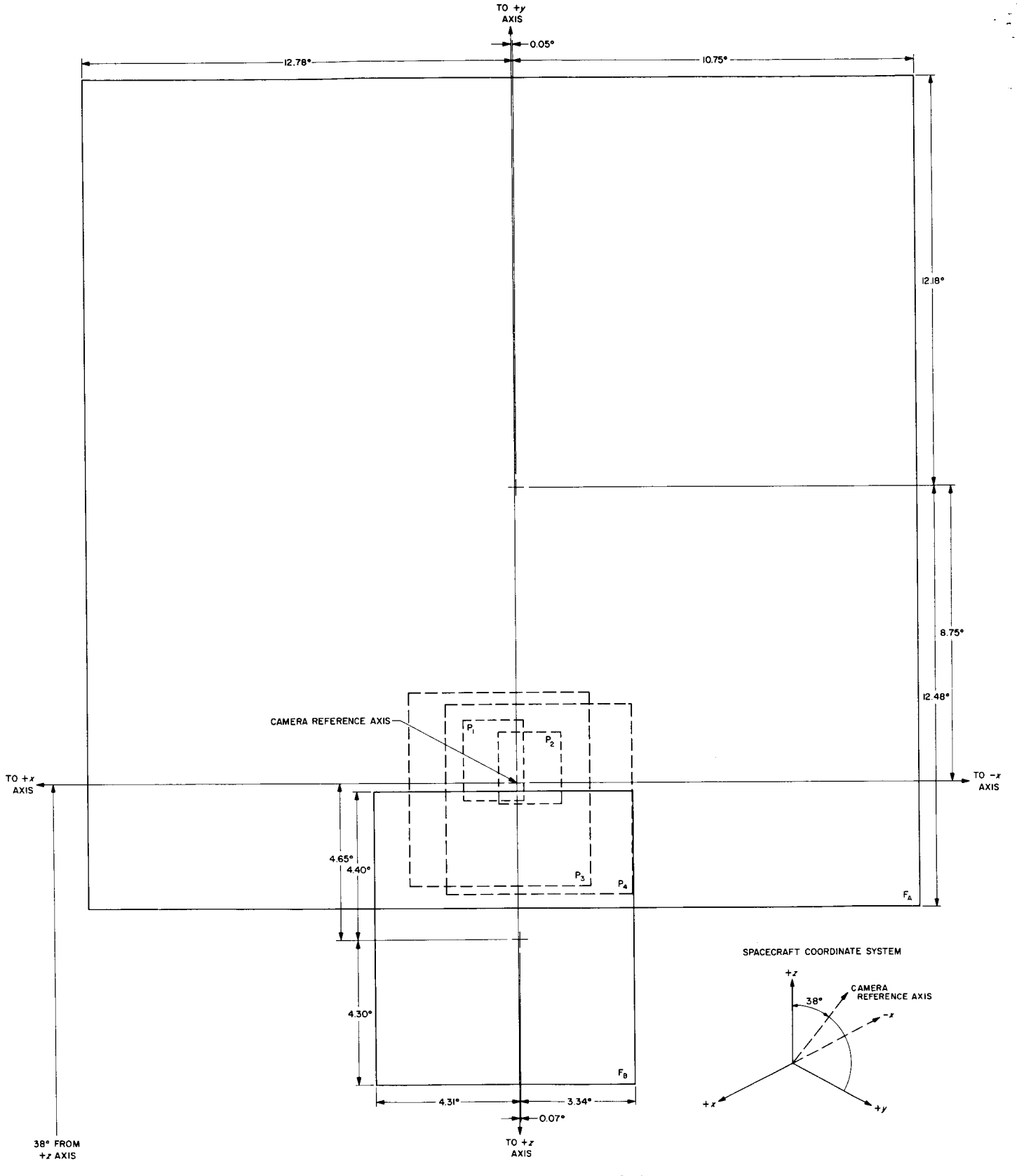

Fig. 1. A- and B-camera fields of view

original experimenter group for the *Ranger* Block II photographic experiment was:

Scientific Team:
Dr. G. P. Kuiper, University of Arizona
Dr. E. M. Shoemaker, U.S. Geological Survey
Dr. H. C. Urey, University of California, San Diego

Technical Team:
Mr. E. F. Dobies, Jet Propulsion Laboratory
Mr. R. L. Heacock, Jet Propulsion Laboratory
Dr. A. R. Hibbs, Jet Propulsion Laboratory

This group also carried the responsibility for the experiment in the early phases of *Ranger* Block III. The present appointments were formalized in July of 1963. Dr. A. R. Hibbs and Mr. E. F. Dobies had accepted other positions and were no longer associated with the *Ranger* Project. Dr. G. P. Kuiper was appointed as Principal Investigator, and Mr. E. A. Whitaker, University of Arizona, was added to further strengthen the scientific team.

B. Television Description

The *Ranger VII* spacecraft carried six television cameras that transmitted over two separate channels designated F and P (for full-scan and partial-scan). The F channel contained cameras A and B, while the four P-channel cameras were designated P_1 through P_4. One-inch diameter vidicons were used for image sensing in all six cameras. The F cameras utilized an active image area 11 mm square which was scanned with 1152 lines in 2.5 sec. The P-camera image area was 2.8 mm square and was scanned with 300 lines in 0.2 sec. The faster cycling of the P-channel cameras allowed 12 pictures to be taken between the exposure of the last F picture and the impact of the *Ranger VII* spacecraft.

One F and two P cameras carried 1.0-in. f/1 lenses, and the other F and P cameras carried 3.0-in. f/2 lenses. A 5.0-msec exposure was used for the F cameras and a 2.0-msec exposure for the P cameras. The fields of view and relative pointing directions for all six cameras are shown in Figs. 1, 2, and 3. Coverage of the lunar surface with the two F cameras is shown in Fig. 4.

The *Ranger VII* photographs were recorded at two receiver sites in the Mojave Desert of California. Recording equipment consisted of both kinescope film recorders and magnetic tape recorders. The quality of both forms of recordings was excellent. However, the magnetic-tape records have yielded the best pictures, after digital computer processing.

The *Ranger VII* television system was calibrated before launch for light-transfer characteristics, sine-wave response (modulation transfer function), system noise,

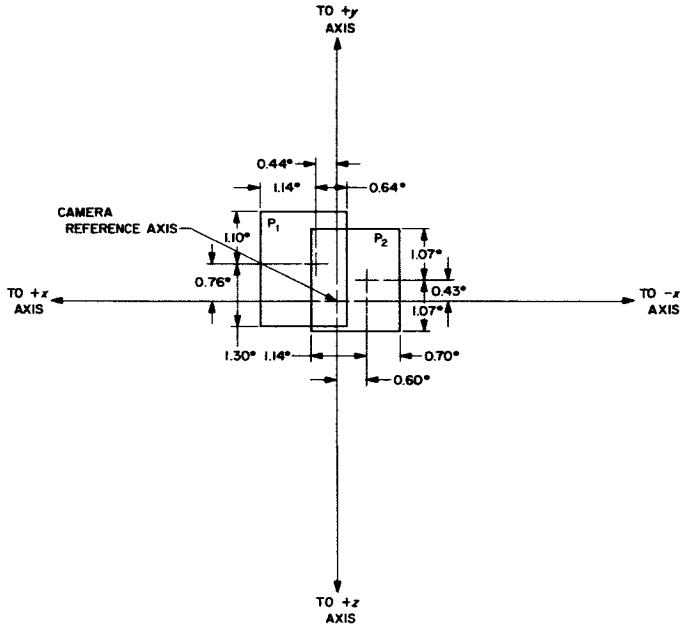

Fig. 2. P_1- and P_2-camera fields of view

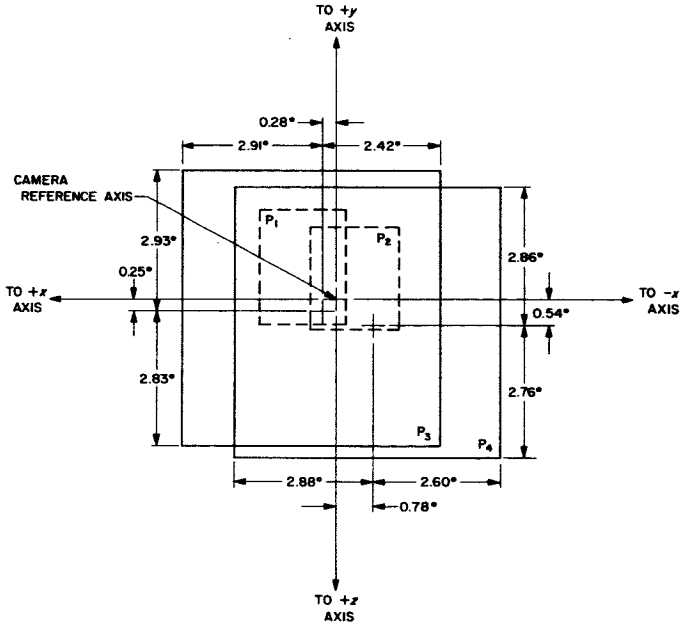

Fig. 3. P_3- and P_4-camera fields of view

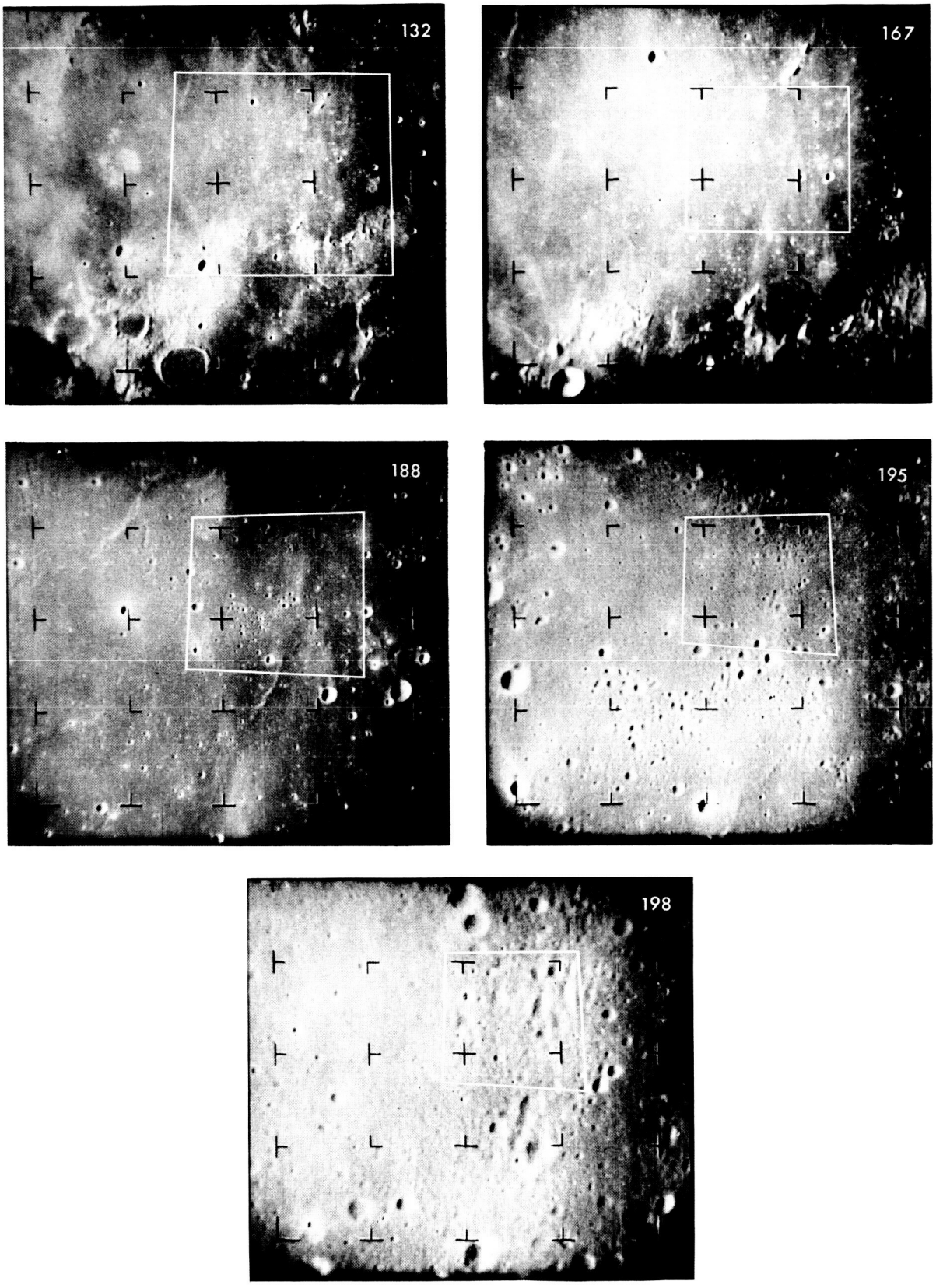

Fig. 4. Camera nesting and coverage

and geometrical distortion. A series of slides displayed through collimators were used for calibration standards. The camera system signal was recorded on magnetic tape and then played back into the ground receiver system to obtain a kinescope film record. The film was read with a microphotometer and compared with the standard slides to obtain the four principal aspects of camera performance listed above.

C. Impact-Area Selection

Ranger VII was launched on July 28, 1964. At the time of impact, on July 31, the terminator was located at approximately 2°E longitude. Preferred impact sites were chosen prior to launch on the basis of the camera calibrations, system constraints, and considerations of the lunar terrain. The mare area between Mare Nubium and Oceanus Procellarum was selected as the primary site because it had a relatively typical mare surface, it was a large enough target to hit with good probability, and it was fairly close to the lunar equator and a region of interest for landing Apollo spacecraft. The selected aiming point was 21°W and 11°S selenographic coordinates. The actual impact point measured from the photographic data was 20.6°W and 10.6°S.

D. Publication of Data

The quality of the *Ranger VII* photographs prompted their immediate release as a series of photographic atlases. *Ranger VII Photographs of the Moon, Part I: Camera "A" Series,* was released on August 27, 1964, and *Ranger VII Photographs of the Moon, Part II: Camera "B" Series,* on December 15, 1964. A third atlas of selected P-camera photographs was published on February 10, 1965. The atlases have been produced in two forms: a limited scientific edition consisting of high-quality photographic prints and a halftone edition printed by the Government Printing Office.

The photographs in the atlases were dodged to adjust for the variations in sensitivity of the vidicons and to reduce the surface brightness change with longitude in the early pictures. The dodging helps bring the data content of the film within the dynamic range of the photographic prints. Mr. E. A. Whitaker produced the negatives used for the photographic atlas, and he and Dr. G. P. Kuiper supervised the printing. In addition to vidicon sensitivity variations, residual images, erase cycle interference, and shutter microphonic noise are present in the pictures. These forms of photometric anomaly and noise are easily interpreted and can be removed by computer processing of the magnetic tape data. (See *Ranger Mission Report: Part I,* Technical Report No. 32-700, Jet Propulsion Laboratory, December 15, 1964.)

The United States Air Force, Aeronautical Chart and Information Center (USAF ACIC), have used the *Ranger VII* photographs to refine their shaded relief maps of this area of the Moon. Their LAC 76 map at a scale of 1:1,000,000 was the largest-scale map previously available for the impact area. The USAF ACIC has now published a new series of maps, based upon the *Ranger* photographs, at scales of 1:1,000,000, 1:500,000, 1:100,000, 1:10,000 and 1:1,000 (*ACIC Ranger VII Lunar Charts RLC 1–5*). These maps give in condensed, but qualitative, form much of the new topographic data acquired by *Ranger VII.*

II. PREVIEW OF SCIENTIFIC RESULTS

Experimenter Team

Prior to the *Ranger VII* flight, knowledge of the detailed topographic and physical characteristics of the Moon's surface was based almost entirely on observations made with optical and radio telescopes (including radar). With optical telescopes, topographic features as small as 200 m had been visually resolved by observation under exceptionally favorable astronomical conditions, and a few photographs had been obtained in which lunar surface features of about 400 m could be distinguished. Vertical relief of the order of 10 m was detectable near the terminator for broad features which could easily be resolved through the telescope.

The topographic features observed through telescopes consist primarily of craters but include the relatively smooth plain-like maria, ridges, valleys, and rugged mountains. Slopes observed on these features range from 0 to about 50 deg. Average slopes on the maria, measured over lengths of 1 km, are a few tenths of a degree and range between 5 and 10 deg in the most rugged mountains of the Moon. Some of the mountainous regions of the Moon are comparable in relief and frequency distribution of slopes (but not in mode of origin) to mountain systems in the United States, such as the Sierra Nevada and the Rocky Mountains.

In addition to the direct observations of topography, many physical measurements of various parts of the Moon's surface have been made with instruments mounted on optical telescopes. Chief among these are the photometric properties and color, the polarizing properties, and the infrared radiation, from which certain characteristics of the near-surface material may be calculated. The photometric and polarimetric data show that the texture of all measured parts of the lunar surface is extremely rough at the microscopic or near-microscopic scale and that the surface is covered for the most part with minute particles considerably less than 1 mm in average grain size. The infrared measurements show that the upper few millimeters of surface material have an abnormally low thermal inertia, implying that the material is exceptionally porous.

Measurements of radiofrequency emission and of reflected microwave radiation from the lunar surface have provided information on the thermal properties of the material at slightly greater depths beneath the Moon's surface and can also be used to infer average slopes on the lunar surface for slope lengths in the range of about 10 cm to a few meters. The emission measurements show that the material down to depths of the order of 1 m also

has a very low thermal inertia over much of the Moon and is thus relatively porous in most places. The average slopes over the sub-Earth side of the Moon estimated from measurements of reflected microwaves increase with decreasing slope lengths in a manner analogous to terrestrial terrain.

The area selected for detailed topographic investigation with the *Ranger VII* spacecraft was a relatively smooth mare. The region was known to have several ray systems and ridges and a relatively high crater density. The *Ranger VII* photographs have yielded much new information on the small features of the target mare surface and on the detailed characteristics of some of the rays.

The progressive increase in resolution with decreasing area of coverage in successive photographs taken as the spacecraft approached the Moon provides a smooth transition from features known from Earth-based observations to new features never before seen. One of the most immediately apparent new facts is that craters are the dominant topographic features of the mare surface at all scales down to the smallest features observed in the last photographs (less than 1 m across). The crater distribution is not uniform in the area photographed in that craters are more abundant in the rays than in the areas between the rays. The number of craters increases so rapidly with decreasing crater size that, in general, they occupy an increasing proportion of the field of view in successive photographs. The craters in areas outside of the rays occupy about 20% of the field of view in the last photographs, and more than 50% of the field of view is occupied by craters in some of the photographs of a part of the surface that is mainly within a ray. In the small area covered by the last full-scan photograph, the craters are so closely spaced that the smallest craters (10 to 50 m in diameter) are abundantly distributed over the larger ones.

The highest-resolution photographs are of a ray-covered area identified with the large crater Tycho. The distribution of small craters within this ray and within other rays of the Tycho system is revealed in new detail by the photographs. A large number of craters, less than a kilometer in diameter, are found to be clustered within these rays. The largest craters of the clusters occur near the ends of each ray nearest Tycho. Some of the small craters clustered in the Tycho rays photographed by *Ranger VII* are shallow and elongated, like known secondaries; others are relatively deep and circular.

Most of the craters smaller than 250 or 300 m in diameter, both within and outside the rays, have smoothly rounded rims. In this respect, they differ strikingly from most of the larger craters on the lunar maria observed through a telescope. This is one of the most significant new facts established by the *Ranger VII* photographs. In addition, the craters less than 300 m across have a large variation in depth-to-diameter ratio, and the majority of them are proportionately shallower and have gentler interior slopes than the larger craters on the maria. These differences give a "smoothed" appearance to the highest-resolution photographs.

However, a few sharp-rimmed steep-walled craters of nearly conical shape may be observed in most of the photographs. They range in size from the craters known from telescopic observations down to craters a few meters in diameter. Some of these craters are surrounded by bright halos and small systems of rays and others are not. The smallest crater with a bright halo found in the *Ranger VII* photographs is about 30 m across. These steep-walled craters are remarkable for their uniformity of shape over a very large range of size, from a few meters up to several kilometers in diameter.

Another major fact revealed by the *Ranger VII* photographs is the scarcity of small positive-relief features—small surface bumps or isolated protuberances. Except for crater rims and certain ridges on the mare surface, which had been known from Earth-based telescopic observation, protuberances are so rare in the high-resolution photographs as to require very careful search to be discovered.

Slopes may be estimated from the *Ranger VII* photographs by photometric methods. A survey of slopes in the last partial-scan photograph revealed that slopes over about 10% of the area photographed were less than 1 deg (measured over 1-m slope lengths), slopes over 50% of the area were less than about 5 deg, and slopes over 90% of the area were less than about 15 deg. The roughness of a surface of this type does not appear to present an unreasonable risk to landing *Surveyor* or *Apollo* spacecraft. Direct tests of the bearing strength of the lunar surface will be needed, however, before the safe landing of men on the Moon can be assured.

In the Parts that follow, a more detailed review of the facts established by *Ranger VII* is given by individual members of the investigator team, and selected aspects of the interpretation of the data are presented in their reports.

III. INTERPRETATION OF RANGER VII RECORDS*

Gerard P. Kuiper
Lunar and Planetary Laboratory
University of Arizona, Tucson, Arizona

The pictorial records obtained by *Ranger VII* have provided the first close-up views of our satellite. They have led to important advances in our factual knowledge of the lunar surface.

This report is an attempt to interpret the *Ranger VII* photographs and to assess their impact on lunar science. The principal assets of the *Ranger* photographs are (1) the truly remarkable quality of the TV records, transmitted over a distance of 60 Earth radii; (2) their high resolution, exceeding the best Earth-based photography by factors up to 2000; and (3) their adequate redundancy, giving confidence in the reality of the image content. Their limitations, though obvious, must also be borne in mind: (1) the records covered a limited area, and image resolutions of better than 0.1 arc sec, as seen from the Earth are confined to about 10,000 km^2 or $\frac{1}{1000}$ of an orthogonally projected hemisphere; (2) the Sun was 23 deg above the horizon at the impact point (selected for reasons that have been described elsewhere), whereas Earth-based photography can extend to 1 deg or less, giving a relative gain in vertical resolution of some 20 times. For extended terrain features, therefore, the vertical resolution of Earth-based photography competes favorably with the *Ranger* records; and it is available over the entire visible disk.

It follows that the interpretation of the *Ranger VII* records is best made in the context of all available data. This at the same time allows an assessment of the question as to whether the results on Mare Cognitum are representative of lunar maria in general, and what is indicated for future missions.

The program of this report follows the above considerations. It starts with a classification of the *lunar maria*, based on their gross structure as found from Earth-based photography (resolution about 1 km). Mare Cognitum is seen to be an impact mare, its basin having been formed well before that of Mare Imbrium. Most of the surrounding mountain walls were destroyed before the basin was flooded. Then follows a study of the vertical structure of

*This paper was written with the collaboration of Messrs. R. G. Strom, E. A. Whitaker, and W. K. Hartmann of the Lunar and Planetary Laboratory, as indicated in the text.

maria in general at the intermediate scale (vertical resolution about 10 m), based on Earth-based photography at very low Sun angles and on color photography with a wide baseline (3800–8000Å). Two of the maria (Imbrium and Serenitatis) appear to consist of a *succession of flows*, each flow being roughly 30–200 m thick and having a characteristic color. Successive flows may differ in color, with the most recent (top-level) tending to be the bluest. While no direct similar evidence exists for the other maria, partly because the data are less precise, it seems reasonable to assume that all maria have essentially similar structure.

Next are presented the results concerning the presence or absence of a *cosmic dust layer*. From high-resolution color photography it is concluded that no such layer covers the Moon, although the uppermost meter or more has undoubtedly been contaminated with cosmic debris. From the sharpness of the color boundaries it is further found that, since the formation of the maria, a general horizontal migration of dust by electrostatic forces, if it has occurred at all, was limited to subtelescopic dimensions. That some material has been widely scattered over the surface during major impacts is shown by the many scars and crater rays having distant sources. The existence of the color provinces in the maria indicates, however, that far from the large craters, with their swarms of secondaries extending to several crater diameters (and outside visible crater rays, secondaries, and scars), the scattering process has been inappreciable—not enough to erase the sharp color contrasts. This observation is of decisive importance in all that follows.

The *Ranger* records have yielded abundant data on lunar *craters* and *crater rays*, and these data are reviewed in this report. They have raised the question of the relationship between the swarms of secondary craters known to surround all major post-mare primary craters and the newly discovered clusters of secondary craters accompanied by short ray elements. The *Ranger* photographs demonstrated the existence of these clusters, but re-examination of Earth-based photography indicated that this basic structure of lunar rays is general. One is led to assume that the swarms of individual secondaries (having no rays) are due to lunar surface materials ejected during major impacts, but that the clusters of secondaries and their associated ray elements have a different cause, presumably fragments blown away from the impacting body itself. This explanation requires the impacting body to be of a different composition than the Moon. It may be postulated that it was a comet, as suggested by H. C. Urey and E. A. Whitaker. This assumption would also explain the nature of the crater rays, as is shown by E. A. Whitaker in Part VI. The hypothesis is examined quantitatively and found satisfactory.

The *Ranger* records have also provided a clue to the morphology of the *ridges* in the maria. These ridges appear to belong to two classes: (1) those showing local or mare-wide patterns and (2) those that are part of the "grid system," a global pattern of structural lines that seems connected with the dynamics of the lunar globe as a whole. In either case, the hypothesis can be made that ridges follow a pattern of fractures in the lunar crust along which up-welling magmas caused dikes to erupt sporadically through the lunar surface. This hypothesis can be tested on the *Ranger* photographs, notably some of the last B and P frames (especially B196), through the fortunate circumstance that one ridge was dissected by a crater that has laid bare the ridge substructure. It is found that the ridges are basically strips of the lunar mare surface pushed up by dike-forming intrusive magmas which locally spread out horizontally between crustal layers and widened the overlying ridges. The *Ranger* photographs may be regarded as having clarified the morphology of the ridges; but the interesting dynamical problems of fissure formation and the related clues to the tidal history of the Moon remain unsolved.

The third major problem with respect to which the *Ranger* photographs supply decisive information is the physical and mechanical structure of the *upper layers* of the mare floor. Of particular interest is the average thickness of the layer of lunar debris scattered between observable craters within 1–2 km from its source (within the sharpness of the observed color boundaries). Regardless of whether or not this debris has subsequently been consolidated into metamorphic rock as a result of vacuum welding or other processes, the layer will not possess the tectonic properties and the fine structure of the original flows at the time of mare deposition. Two approaches lead to an estimated thickness of this disturbed layer. One is based on the study of lineaments, the other on the morphology of craters and crustal depressions. A study of the *lineaments*, made by R. Strom using standard geological methods, is included in this report. It is found that Mare Cognitum possesses three main lineament directions, down to the smallest scale observable on the *Ranger* records. Two of these are identical to the directions found in adjacent test areas and belong to the global lunar grid system. The third direction is composite in nature, and its interpretation is complex. On the basis of these lineament studies, it is concluded that the average thickness of the disturbed layer between observable craters is less than 2 m.

The interpretation of the craters and depressions observed on the *Ranger* photographs is incomplete. A basic question in the analysis is the initial state of the mare floor. Recent experiments by Dobar *et al.* (Ref. 1) and at this Laboratory have confirmed occasional speculations that the upper layers of a lunar lava flow may be composed of a *low-density rock froth*, whose thickness might attain several meters or possibly tens of meters. This conclusion would not be important if the maria were not lava but dust. With the maria apparently consisting of a succession of flows, the physical processes of a lava deposit in a vacuum on a body with a low surface gravity are relevant. With the bulk density of the upper layers of the mare floors estimated at 0.1–0.3, the impact mechanics of secondary craters will be quite different from impacts in rock, alluvium, or sand. The properties of both primary and secondary craters are likely to reflect this unfamiliar medium. The bearing strength found for such material (roughly 3–8 kg/cm^2) further accounts for the virtual absence on the Moon of loose blocks and fragments tossed out of primary craters. Rocks of 1-m size and larger could have remained on the surface only if they originated in the immediate vicinity ($D < 100$–200 m); otherwise, they would have penetrated the rock-froth surface. Finally, the observed infrequency of very small ray craters might thus be accounted for, rays having been formed only when the deeper and more compact layers were struck.

In addition to objects that are clearly craters, the *Ranger* records have shown a new class of objects—*shallow depressions* and *dimple craters*. These have no rims, and the outer portions are identical in that their shape approximates an inverted Gaussian curve, rotated around its vertical axis. The depressions continue on the Gaussian profile and thus have a roundish, nearly level bottom; whereas the dimple craters are pointed at their centers or end in a short horizontal line. These depressions closely resemble the karst-type depressions, usually perfectly circular, well known on the Earth. The latter are partial cave-ins (sinkholes) in limestone country, caused by subsurface removal of limestone by solution. On the Moon, withdrawal of magma, cave-ins of deeper frothy layers by the new flow, shrinkage in volume upon solidification and subsequent cooling, and possibly venting of subsurface gases are held responsible. The apparent absence of a conical section on the slopes of the dimple craters indicates that the thickness of loose material on the maria capable of forming talus slopes is inappreciable.

Two additional sources of information about the lunar crust exist: (1) the rate of particle influx on the Moon and (2) the structure of the upper meter or two as derived from radio emission and radar reflections, supplemented by the emission of the upper few millimeters observed at shorter wavelengths. There is still some numerical uncertainty about the rate of particle influx on the Moon. A recent summary by McCracken and Dubin (Ref. 2) fixes the rate as 1 g/cm^2/4.5 $\times$ 10^9 years for particles of mass less than 10^4 g, a value supported by more recent work by W. G. Elford and G. S. Hawkins. Particles larger than 10^4 g would cause primary craters well visible on the *Ranger* photographs ($D > 5$ m), and very large impacting masses would also produce numerous secondaries. If these secondaries are excluded as much as possible, by considering areas outside crater rays and outside the concentrations of secondaries around primaries, the quoted primary impact rate of roughly 1 g/cm^2 during the history of the lunar maria appears appropriate; Dr. Dubin regards the numerical value uncertain by a factor of nearly 10. The 1964–65 *Mariner* mission to Mars is accumulating data that will make the value more precise.

One might assume that the initial post-mare impact rate was much larger than it is at present, both because the Moon was probably closer to the Earth and because the post-mare period came at the close of a period of very active lunar bombardment. However, the cosmic component for the entire post-mare period has been too small to have obliterated the sharply defined color differences on the lunar maria; further, most of the impacting mass below 10^4 g, at least now, consists of submillimeter particles (Ref. 2) which cannot penetrate the lunar crust to great depth. It therefore appears that the McCracken–Dubin primary impact rate, when applied to the entire post-mare period, is not grossly underestimated. The color differences also indicate that the secondary spray from distant impact craters is not important either except where visible as craters or scars.

The photometric results show that the top layer of the Moon (a few millimeters or centimeters thick) is a very open structure, only some 10% of the volume being occupied (Ref. 3). This is consistent with the thermal measurements at 10 μ made during eclipses, which require the presence of a loosely open or dust-like layer at least a few millimeters thick. Ray craters such as Tycho appear only thinly covered (< 1 mm) with such a layer (Ref. 4). For deeper layers, the radar reflections at $\lambda = 68$ cm indicate a bulk density of 0.4–0.5 of solid rock (Ref. 5); or less, according to other authors.

The high-resolution *Ranger* records are limited to a region in and near a weak Tycho crater ray. On the last P frames, this region is partly resolved into a remarkable continuing pattern not unlike a tree bark (e.g., Ponderosa

pine). This *tree-bark* pattern probably represents the surface structure of a lava flow, modified by karst-type collapse, which may have added surface cracks. The raised elements are typically of the order of 20–30 m long, 10 m wide, and 1–2 m high. Among them is the boat-like structure illustrated in Section F (Figs. 37 and 38), and several structures like it, less well covered by the *Ranger* records. The tree-bark structure appears soft and rounded off, with a scale of 0.5–1 m. The rounding off is presumably due to erosion.

A linear mountain range (Bonpland γ) occurs near 21°E, 10°S, situated in one of the most prominent ridges of Mare Cognitum. It and similar mountain ridges on the south shore of the mare (one at 21°E, 13°30'S) show by the calderas on their crests that they are of *igneous* origin. This observation has important implications for the origin of many such linear mountains in the Carpathians and elsewhere, also situated along structural lines (in the case of the Carpathians, radial to Mare Imbrium).

The highest resolution obtained by *Ranger VII* occurs on two photographs of the last P frame (979), namely, 0.25 and 0.4 m. The hope that high-resolution photography would yield basic new evidence on lunar crustal structure and, thus, on lunar history and development, has been fulfilled. The *Ranger* results have further stimulated an intensive re-examination of the Earth-based photographs, which, in turn, has decisively assisted in the evaluation of the *Ranger* data. Since high-resolution photography will, for some time to come, necessarily be limited to selected regions of the lunar surface, Earth-based photography pushed to the highest attainable resolution (about 0.1 arc sec) has become a prime requisite.

Continued laboratory experiments and studies of terrestrial craters will also be needed. There are two classes of such craters, those that occur naturally near volcanoes and those produced by artificial surface or subsurface explosions in desert terrain. The first class is represented by the extraordinary crater field produced in 1960 on the slopes of Laimana Crater, Hawaii. We discovered this field in the course of the preparation of this report, and some photographs taken there are reproduced in a later section. In addition to hundreds of "secondary" impact craters, we found some craters and crater chains, somewhat resembling features on the Moon, that were due to drainage. The dimple craters, however, are different in shape from drainage craters. Artificial secondaries have recently been described by W. A. Roberts* and others.

*Roberts, W. A., "Secondary Craters," *Icarus*, Vol. 3 (1964), p. 348, and references given there.

Attention is called to the excellent maps of the area covered by *Ranger VII* published by the Air Force Aeronautical Chart and Information Center, at scales of 1:1,000,000; 1:500,000; 1:100,000; 1:10,000; 1:1,000; and 1:350. These maps portray, in condensed form, the essential information contained on the more than 4300 *Ranger VII* photographs, on coordinates, nomenclature, and qualitative relief, as well as the dimensions and orientation of the numerous features included. The maps were produced in record time and will be an indispensable aid in the further reduction and evaluation of the data.

AF-ACIC has also called attention to the treasure of information contained in the stereo coverage of the Ptolemaeus to Mare Nubium area, obtained by combining Earth-based photography with the B series of *Ranger VII* photographs.

The studies of Mare Cognitum refer to one of the older impact maria on the Moon. It has a rather yellow surface, almost certainly antedating bluer maria such as Mare Tranquillitatis. Studies of one of the bluer maria will be needed before general conclusions can be drawn. The impact area on Mare Cognitum was selected to avoid prominent lunar landscape features such as faults, rilles, graben, mountain chains, large craters, or intense crater rays. The *Ranger* pictures therefore are less spectacular than they would have been had such major structural features been chosen instead. The choice was made in part in support of future landing operations, unmanned and manned, which require the type of terrain actually encountered. Continued scientific exploration of the Moon will benefit if close-up photography of such major structural elements can be included.

A. The Gross Structure of Lunar Maria

Since the impact of *Ranger VII* occurred in one of the lunar maria, the *Ranger* data of highest resolution pertain to a mare surface. Since, additionally, the impact occurred in a minor crater ray, with other minor rays in the vicinity, the data also provide information on the fine structure of lunar crater rays. In order that the specific conclusions derived from the *Ranger* records may be related to the problems of lunar maria and crater rays in general, these problems are reviewed first.

The lunar maria are of two main types: (1) those that are nearly circular and are surrounded by near-circular mountain arcs or fault scarps; these maria also show some circular symmetry in the peripheral rille systems and in the ridge systems of the mare floors, and (2) those that are

irregular. Examples of class 1 are Mare Crisium (Figs. 1, 2), Mare Nectaris (Fig. 3), and Mare Orientale (Fig. 4). Mare Crisium is surrounded by one prominent mountain wall (D=450 km) and fragments of two weaker walls (D=670 and 1060 km); Mare Nectaris is surrounded by three rings (D=400, 600, and 840 km); and Mare Orientale is surrounded by at least five rings (D=320, 480, 620, 930, and 1300 km). Examples of class 2 (irregular maria) are Mare Nubium (part of which is shown in Fig. 5) and Mare Tranquillitatis (Figs. 6–8). Here the ridge systems show patterns of a regional nature, with several such systems covering the entire mare. The outlines of these maria are irregular, probably the result of flooding onto terrain with irregular contours and complex tectonic origin; and no peripheral mountain walls or scarps are observed.

Among the various hypotheses that have been advanced to account for the existence and general appearance of the maria, the following are of interest:

1. The maria are lava fields, though not necessarily identical in composition or fine structure to terrestrial lava beds. It is usually assumed that the nearly circular maria were caused by impact and subsequent flooding; the irregular maria, without surrounding walls and associated rille systems, by flooding only. The source of the lava requires a separate explanation, which is discussed below.

2. The same classification of maria is made, but the explanation for the dark mare material is not lava but dust, or lava and dust. It is assumed that this dust resulted from the impacts that formed the mare basins.

3. The mare basins were filled with dust that accumulated in those low-lying areas during the long lunar history, the source of the dust being erosional and the transportation to the basins by electrical forces.

4. The maria are the oldest regions on the Moon, with the dark surfaces caused by solar radiation effects.

Hypothesis 4 may be ruled out if it is assumed, as is done on excellent grounds (Section G), that the great majority of the lunar craters are caused by impacts. It then follows, from the crater densities in the maria and on the terrae, that the maria do not constitute the oldest parts of the lunar surface but the most recent. Hypothesis 3 would require that the floors of the oldest lunar craters be covered with the largest amount of dark material and those of the most recent craters with the smallest amount. This is contrary to fact. The craters with dark floors, such as those in Fig. 2, appear to be of intermediate age, with both the oldest and the most recent craters having light-colored floors. Also, the mare basins would be expected to be essentially featureless. In reality, structural details related to the general basin geometry may be found all over the maria when observed under favorable conditions of illumination and resolution (cf. Figs. 5–12), and these structural units show the nature of the lunar maria to be basically plutonic.

A compelling argument against a general migration of dust across the surface of the Moon is based on the sharp boundaries observed for the different color provinces, shown in Figs. 13–15. These boundaries often coincide with structural units such as flows (discussed in Section B) and are so sharp that any migration must be within subtelescopic dimensions.

The plates selected for reproduction here emphasize structural features especially relevant to the interpretation of the *Ranger VII* photographs, with the object of determining the nature of a typical mare surface. They were taken in part from the *Consolidated Lunar Atlas* now in preparation, which includes the results of new Earth-based lunar photography carried out under federal sponsorship. For a more general description and systematic photographic coverage of the lunar maria, reference is made to a paper by Hartmann and Kuiper, entitled *Concentric Structures Surrounding the Lunar Basins* (Ref. 6). This paper contains 77 photographic reproductions, many of them rectified, with a summary for each of the maria on the ridge and rille systems, indicating the presence or absence of concentric surrounding mountain walls or faults. A sequel to this study is contained in two papers by Hartmann on *Radial Structures Surrounding Lunar Basins* (Ref. 7), which, incidentally provide much additional photographic coverage. Earlier systematic lunar photography is reproduced in the *Photographic Lunar Atlas* and the *Rectified Lunar Atlas.*

Figure 5 shows the southeastern corner of Mare Nubium, including the region of the Straight Wall, about 20 deg from Mare Cognitum. It is noted that the mare floor exhibits a complex system of ridges, unlike Mare Crisium (Fig. 1), Mare Nectaris (Fig. 3), and other near-circular maria such as Mare Serenitatis (Figs. 9 and 10) and Mare Humorum (Fig. 12).

Other regions, showing local rather than mare-wide structural patterns, are portrayed in Figs. 6–8. Figures 6 and 7 show, under opposite illumination, the western part of Mare Tranquillitatis in the region of the crater Arago, containing the impact point of *Ranger VI.* It is

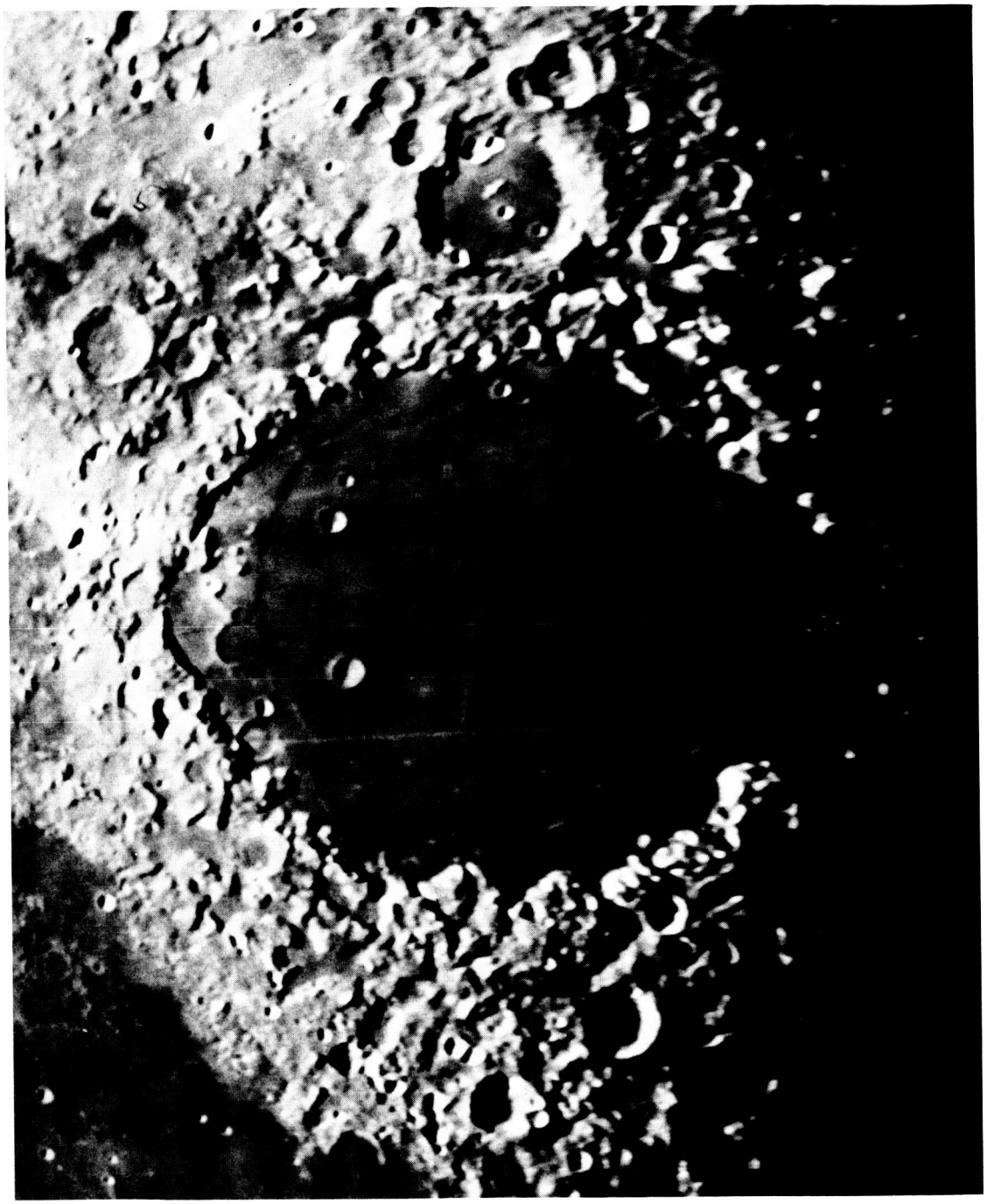

Fig. 1. Mare Crisium, rectified, showing surrounding walls (Plate Y369).



Fig. 2. Mare Crisium and neighboring small flooded craters, rectified (Plate Y738).

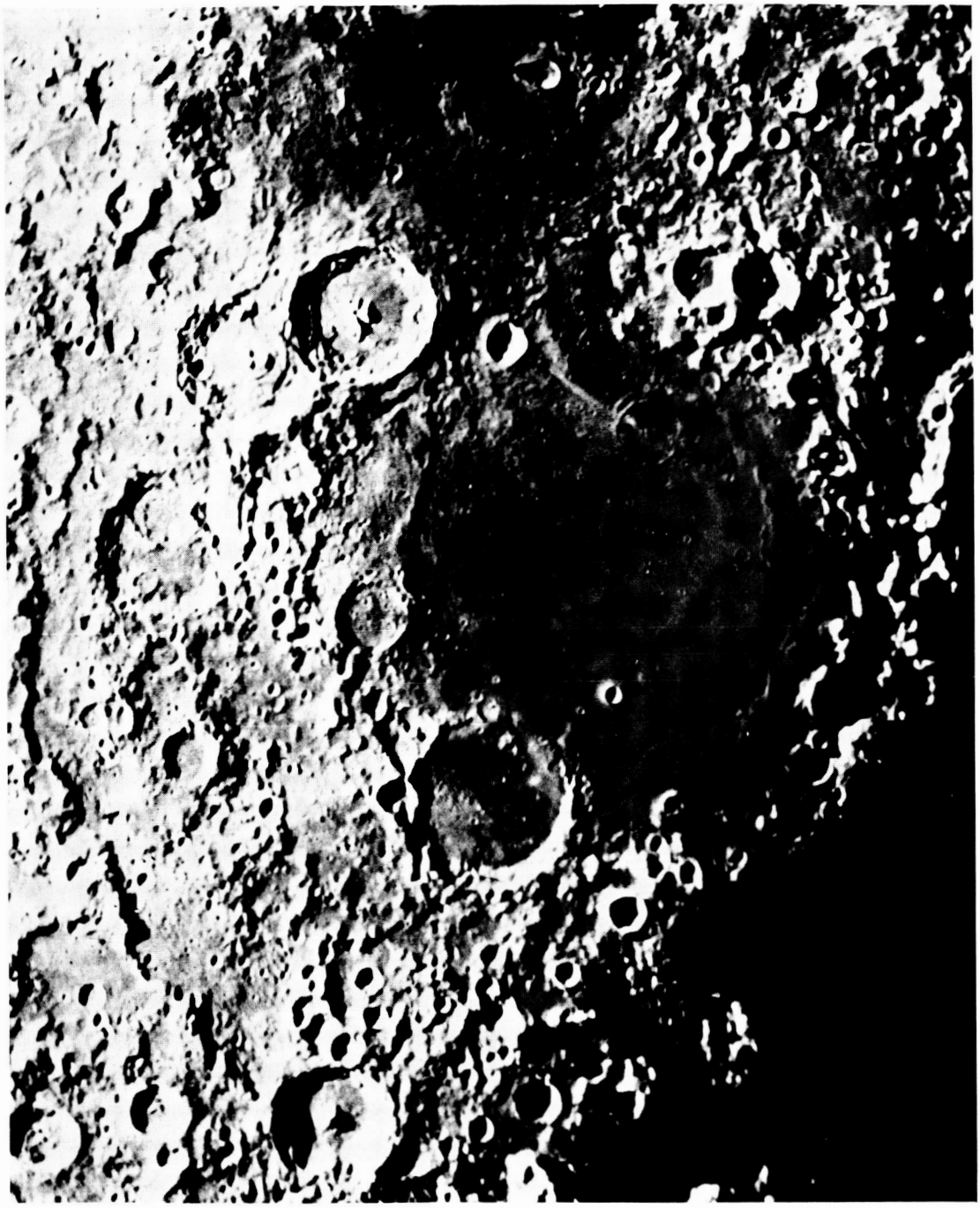

Fig. 3. Mare Nectaris, rectified, showing three surrounding walls (Plate Y1334).

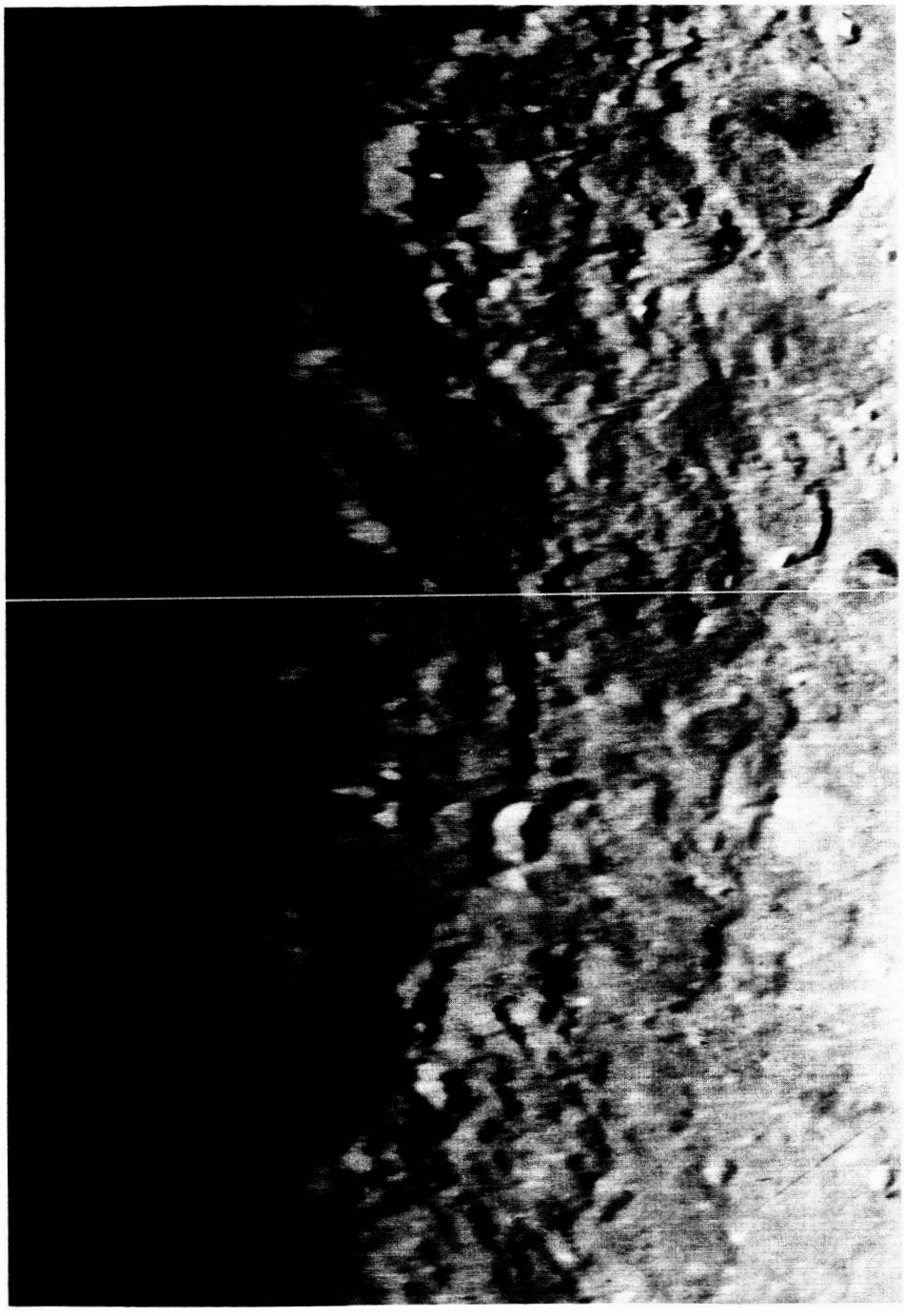

Fig. 4. Arcuate fault scarps surrounding Mare Orientale, rectified (Plate M372).

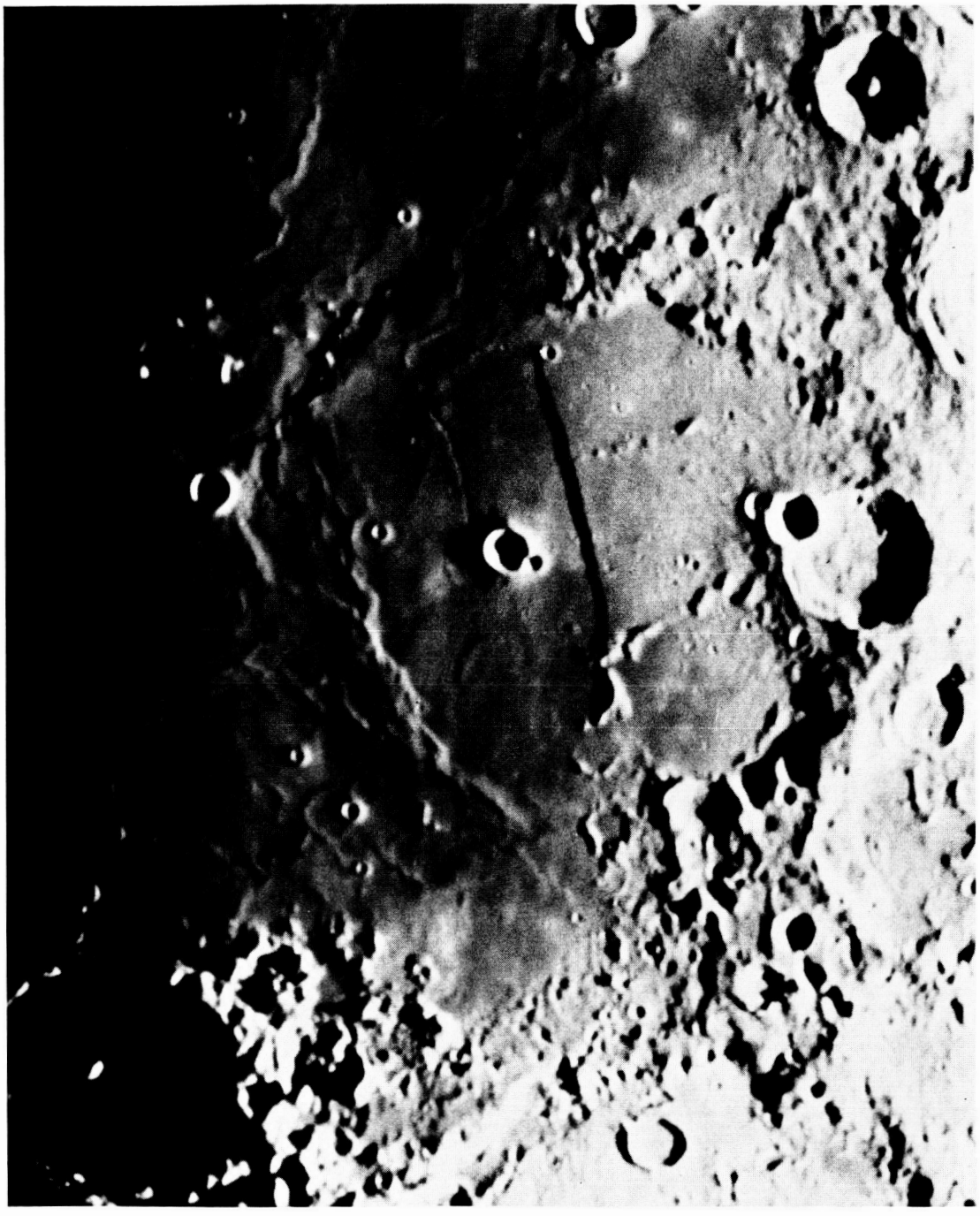

Fig. 5. Southeast corner of Mare Nubium, including Straight Wall (Plate Y1271).

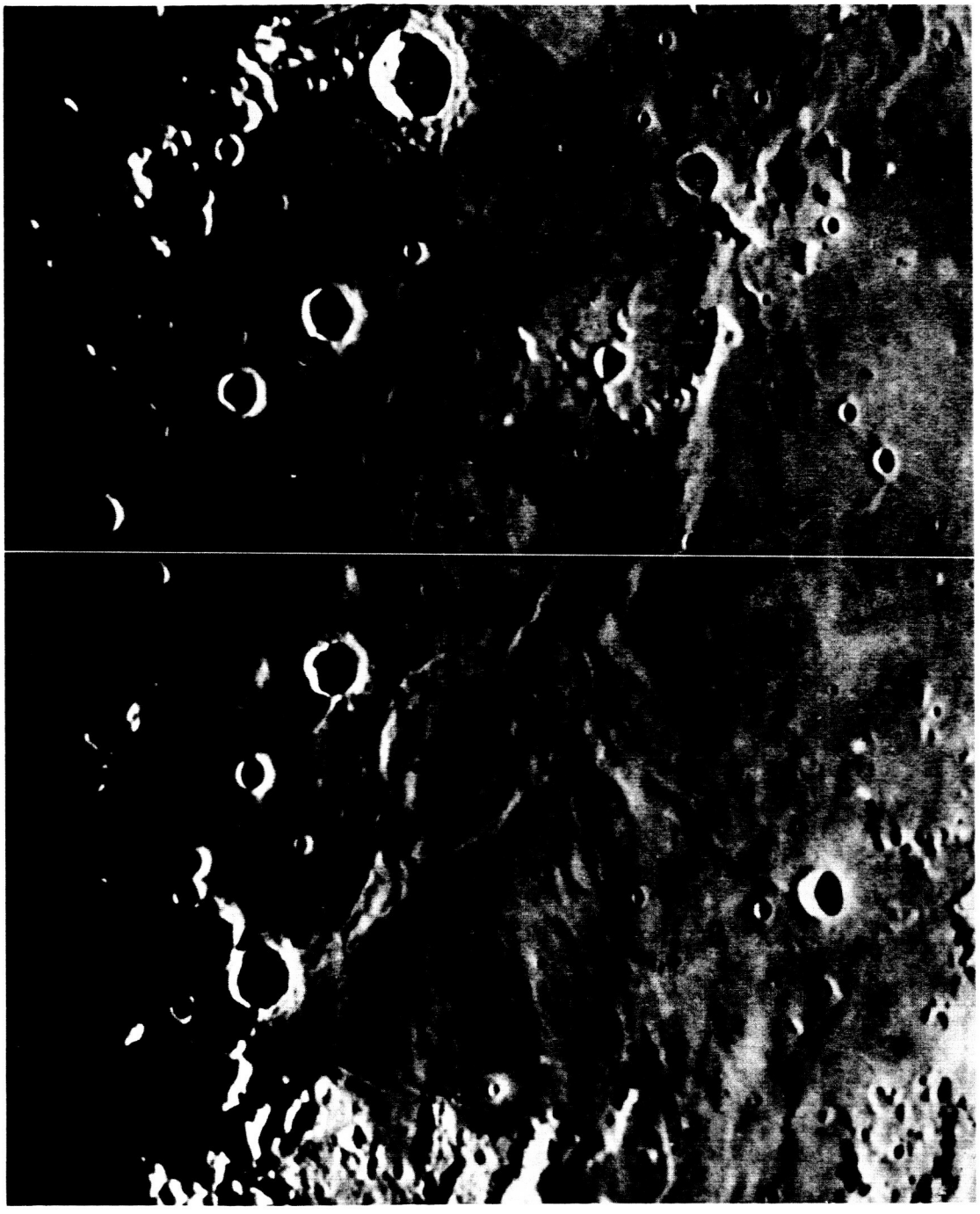

Fig. 6. Part of Mare Tranquillitatis near Arago, at sunrise (*Ranger VI* impact area; Plate Y936).

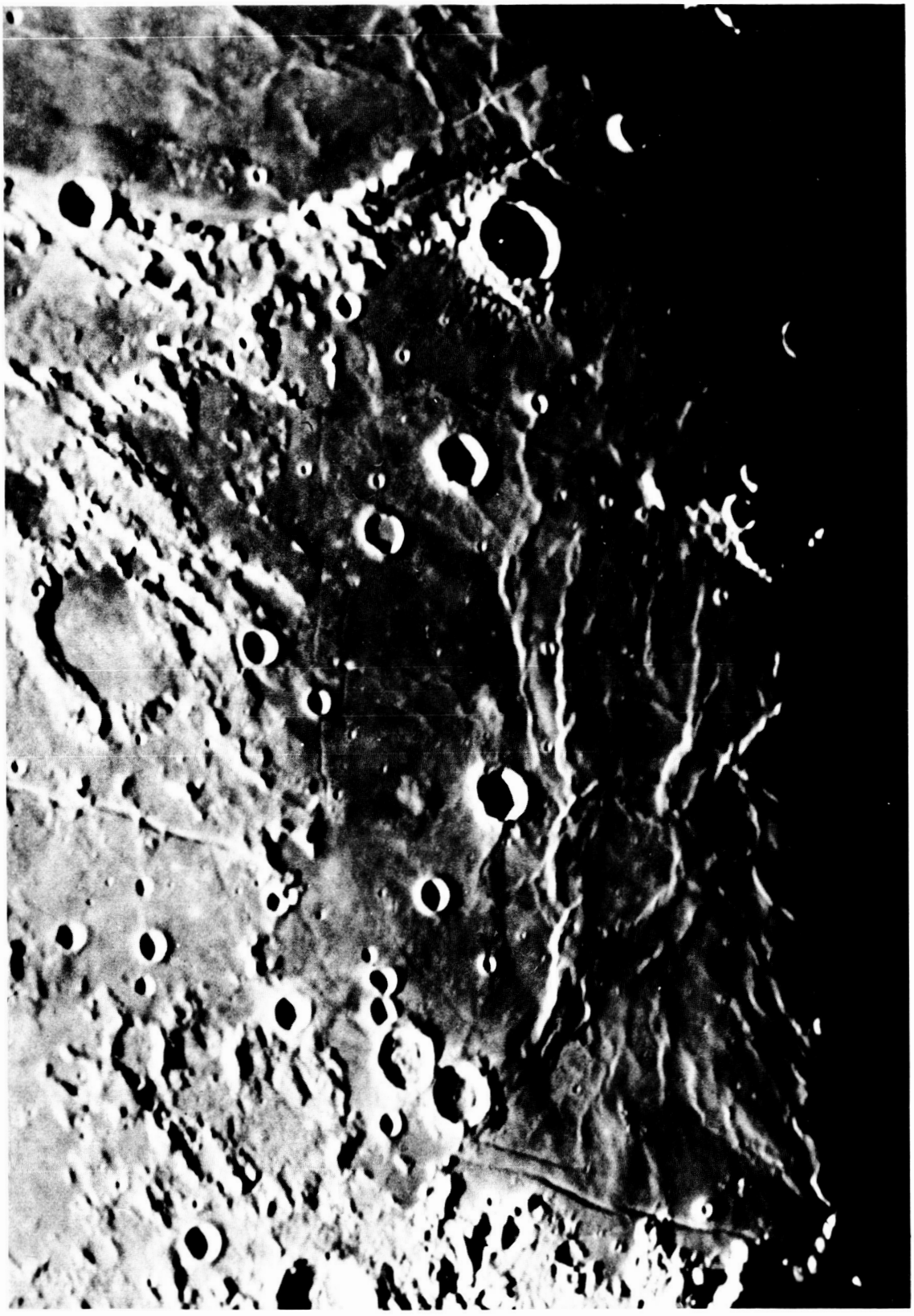

Fig. 7. Part of Mare Tranquillitatis near Arago at sunset (Plate M816).

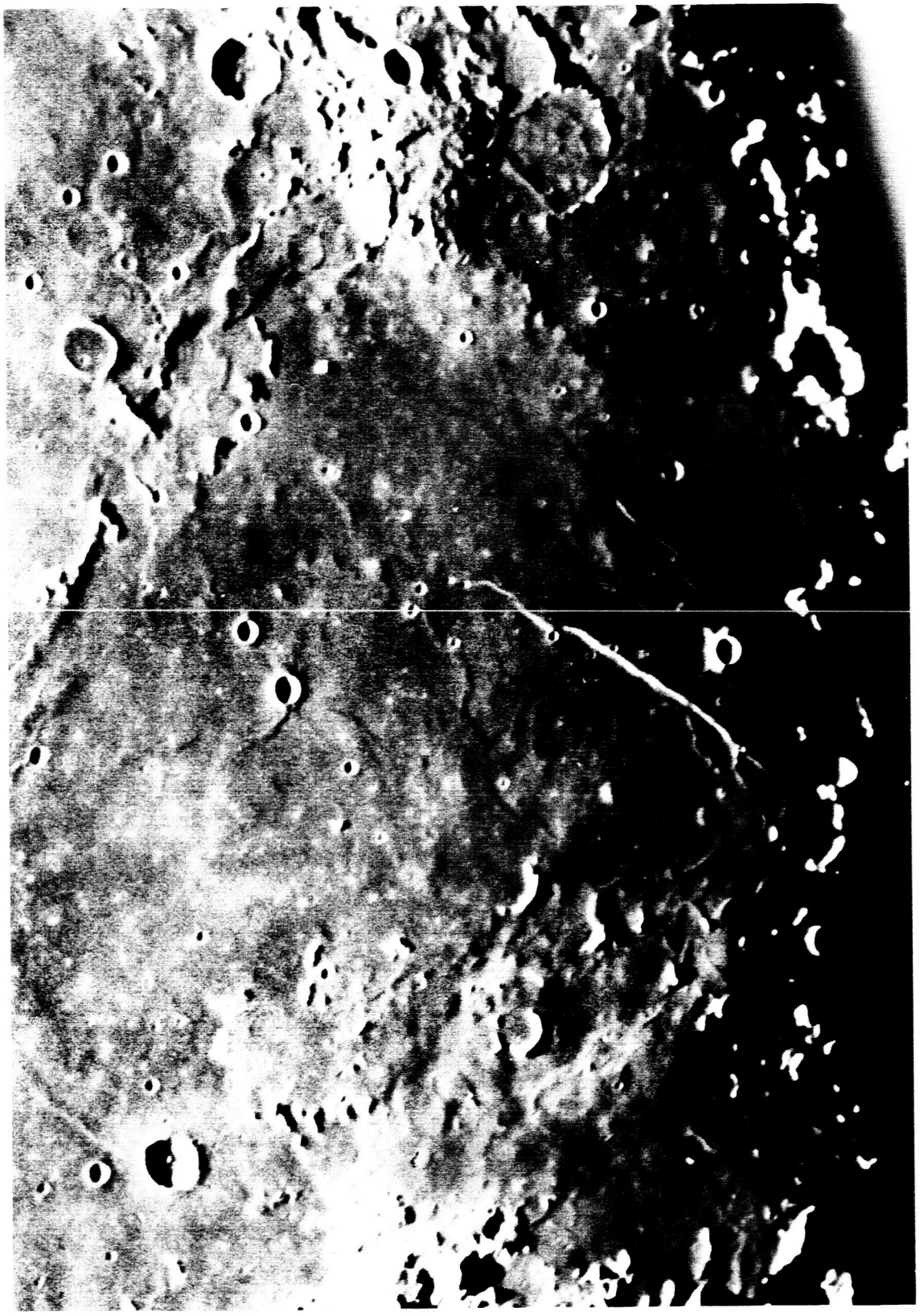

Fig. 8. Part of Mare Tranquillitatis, showing Cauchy Fault and numerous volcano-like structures (Plate Y1338).

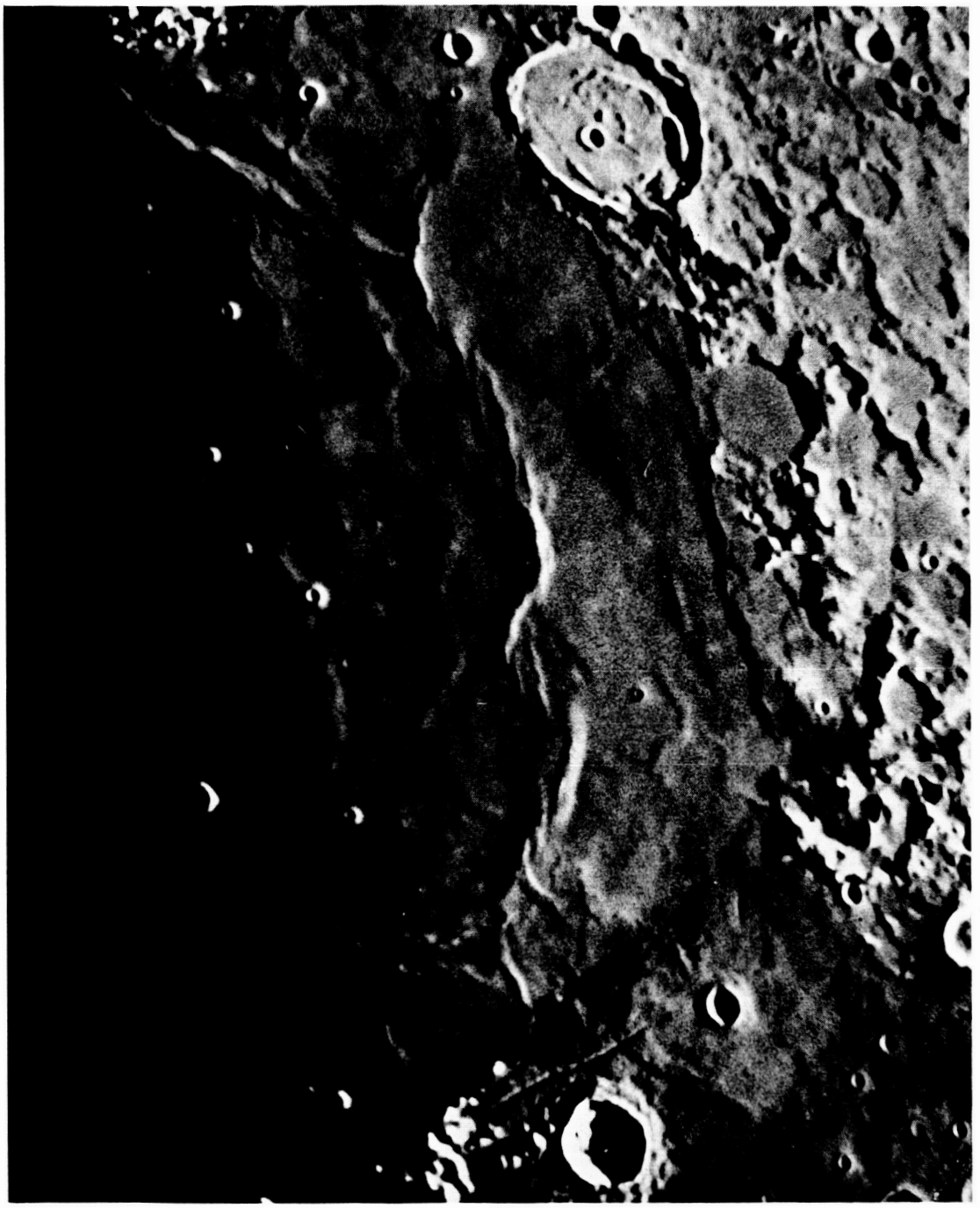

Fig. 9. Mare Serenitatis from Posidonius to Plinius. (Note *en échelon* structure in ridge system and Tranquillitatis flow entering Serenitatis north of Plinius, shown to be bluish on Fig. 14; Plate Y936.)

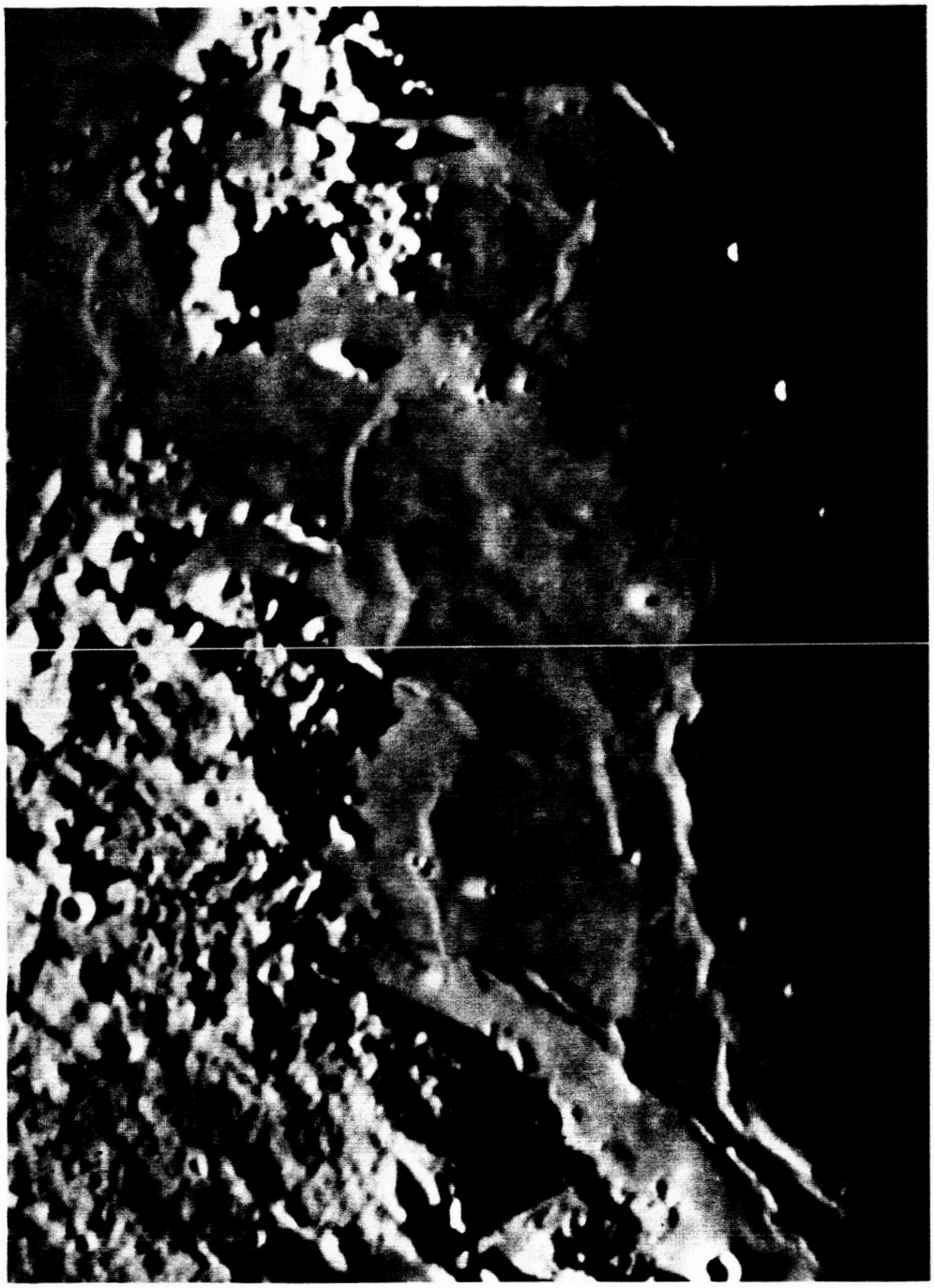

Fig. 10. Braided ridges, troughs, and flows in Mare Serenitatis (Plate M826).

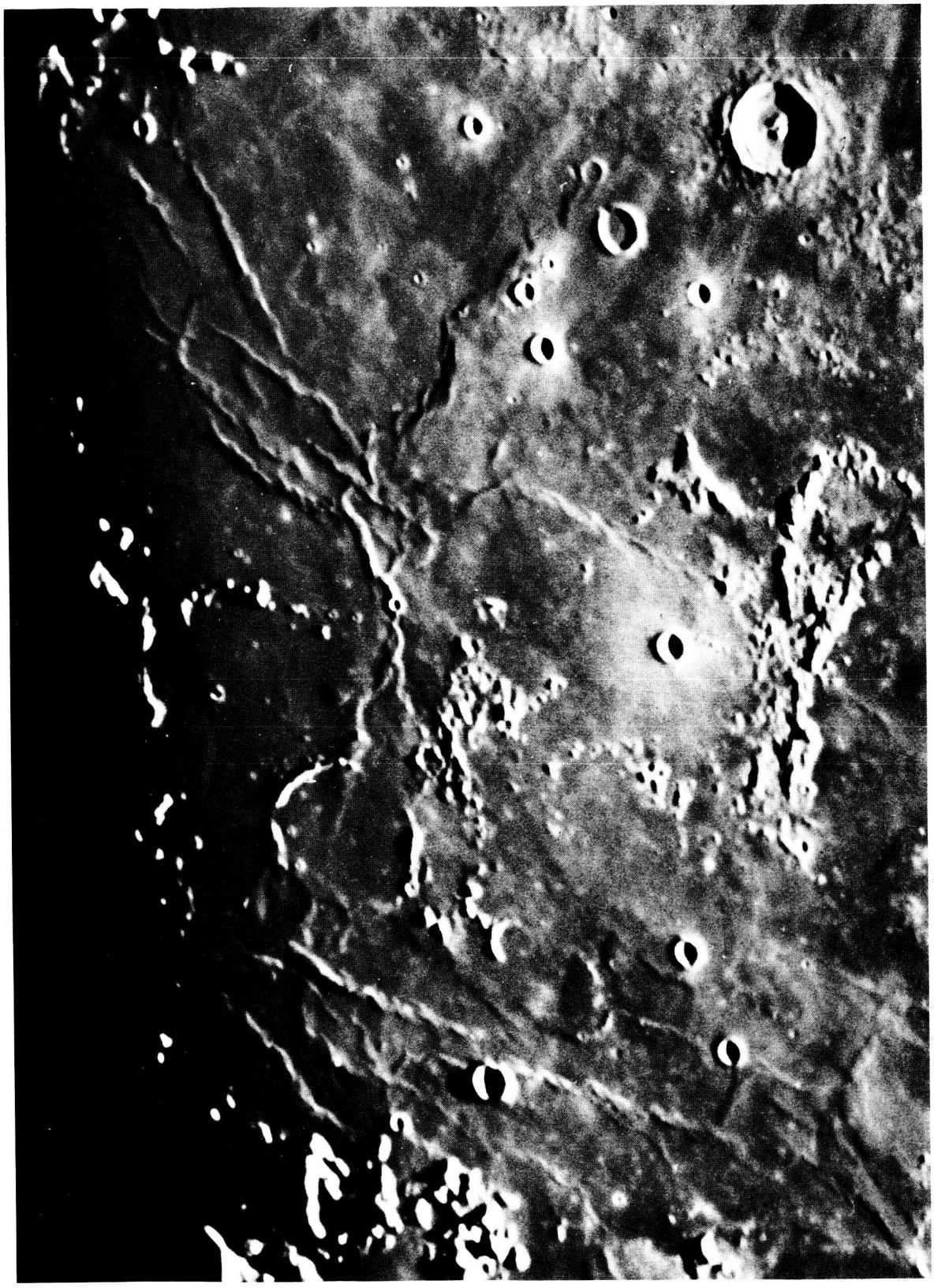

Fig. 11. Part of Oceanus Procellarum, west of Montes Riphaeus, ridges showing braided structure (Plate M613).

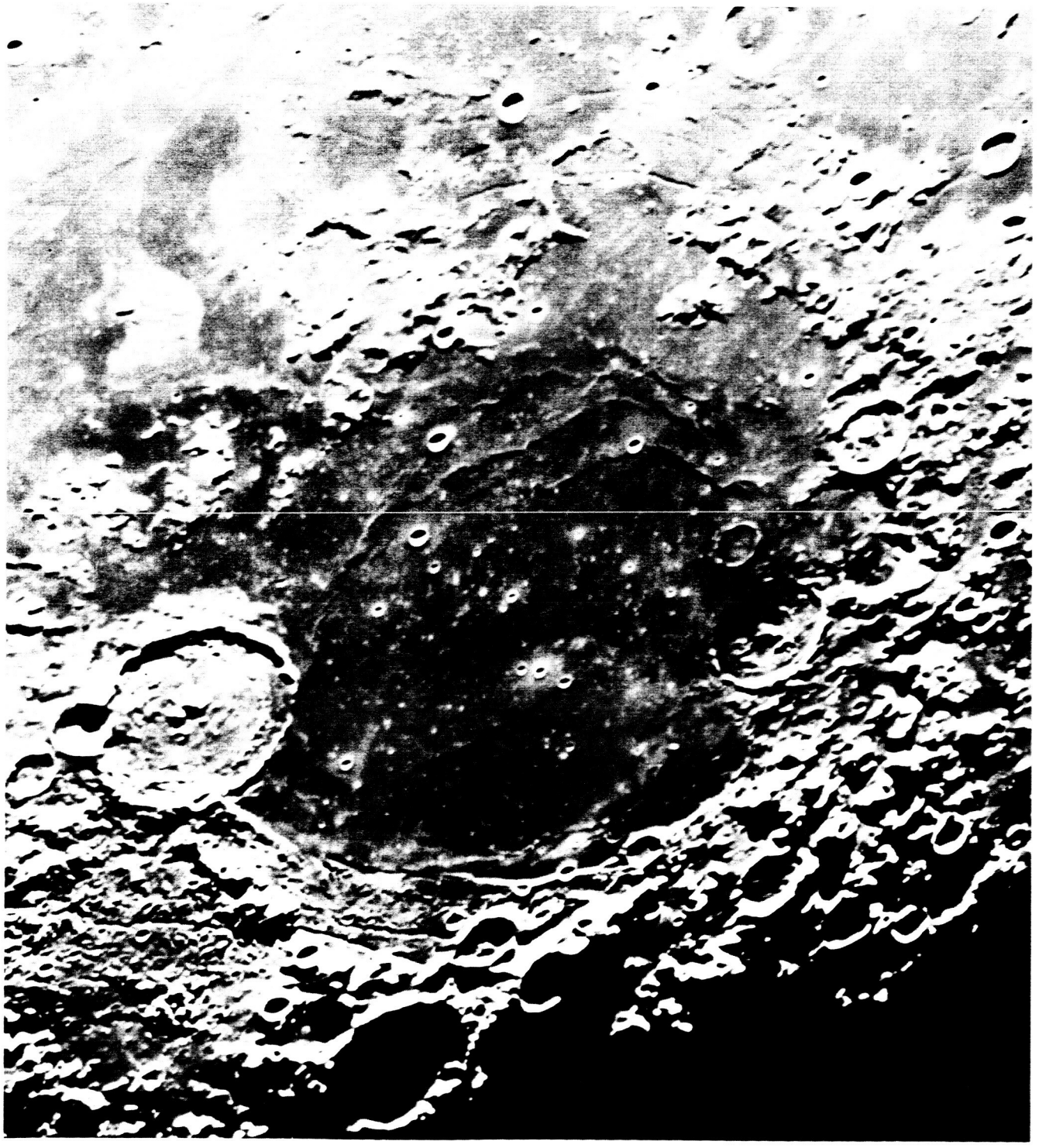

Fig. 12. Mare Humorum, concentric rilles and ridges, and tilted craters on shoreline (Plate M630).

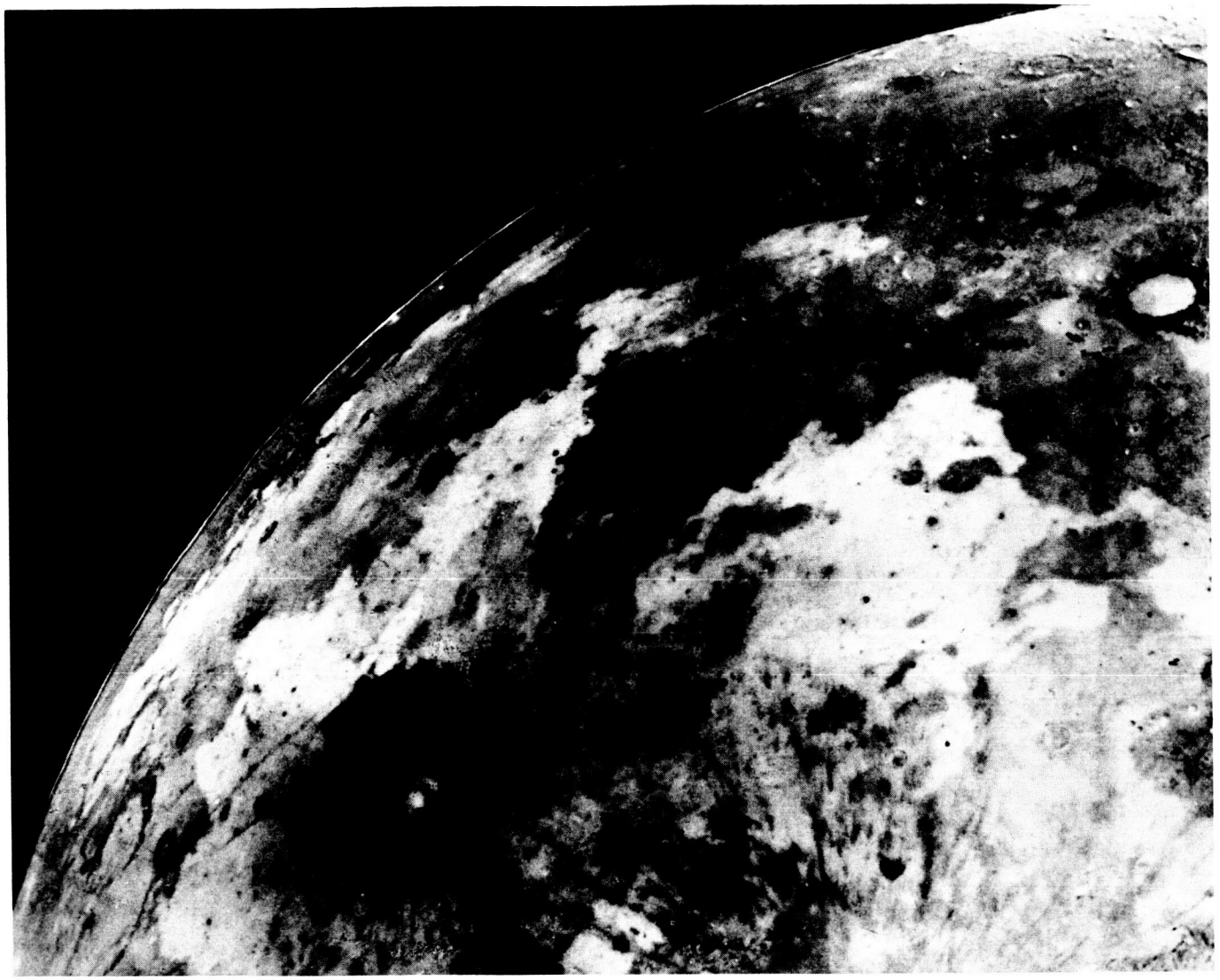

Fig. 13. Colors of the Mare Imbrium region. (The darker the tone, the redder the lunar surface. Printed from a sandwich consisting of an original negative ultraviolet plate and a positive copy of an original negative infrared plate, both taken at the 82-in. telescope of the McDonald Observatory of the University of Texas on May 29, 1964. The color differences were verified by photo-electric calibration by T. Gehrels of the LPL staff; E. Whitaker.)

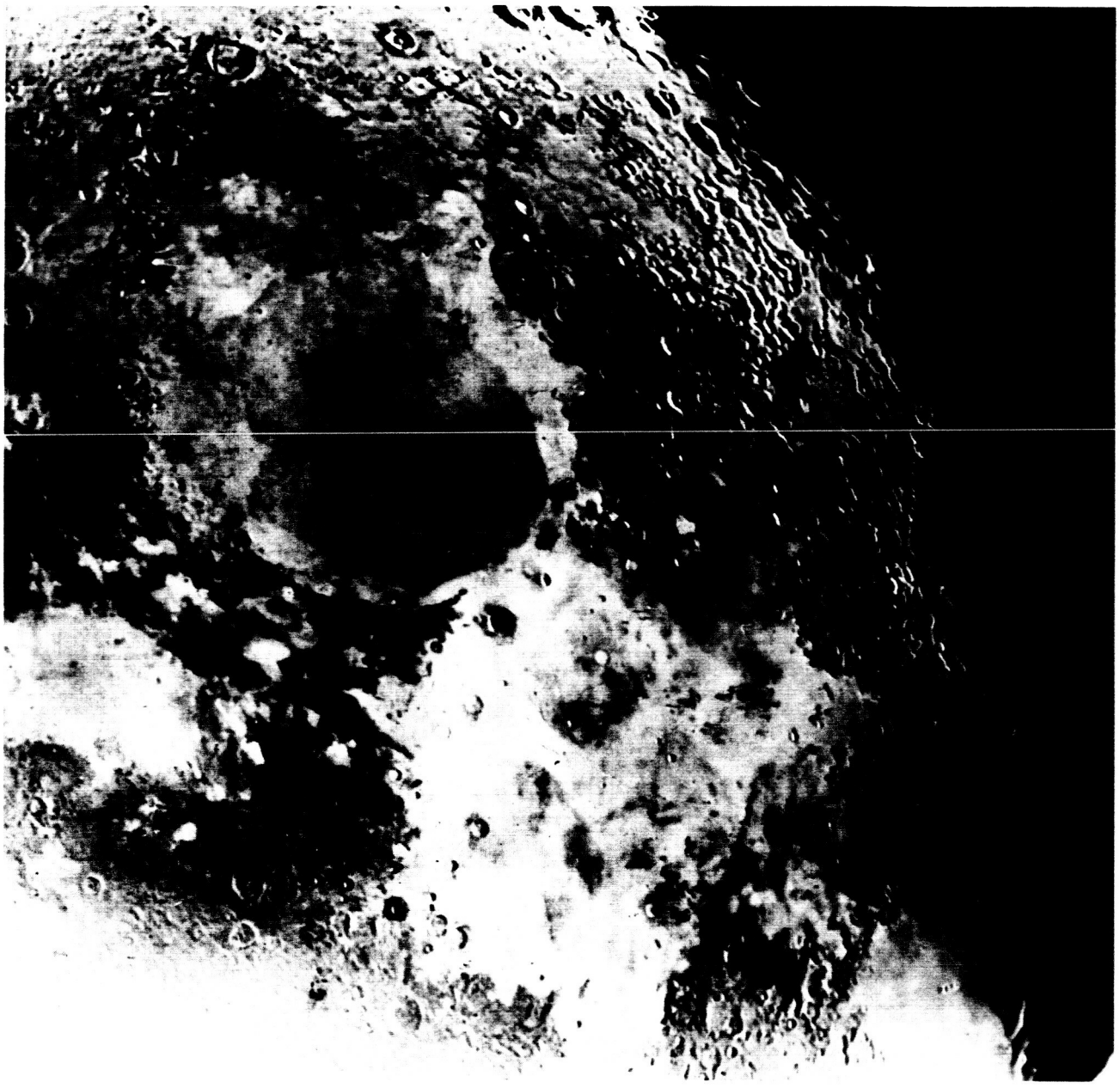

Fig. 14. Colors of Mare Serenitatis and Mare Tranquillitatis. (Shades as in Fig. 13; E. Whitaker.)

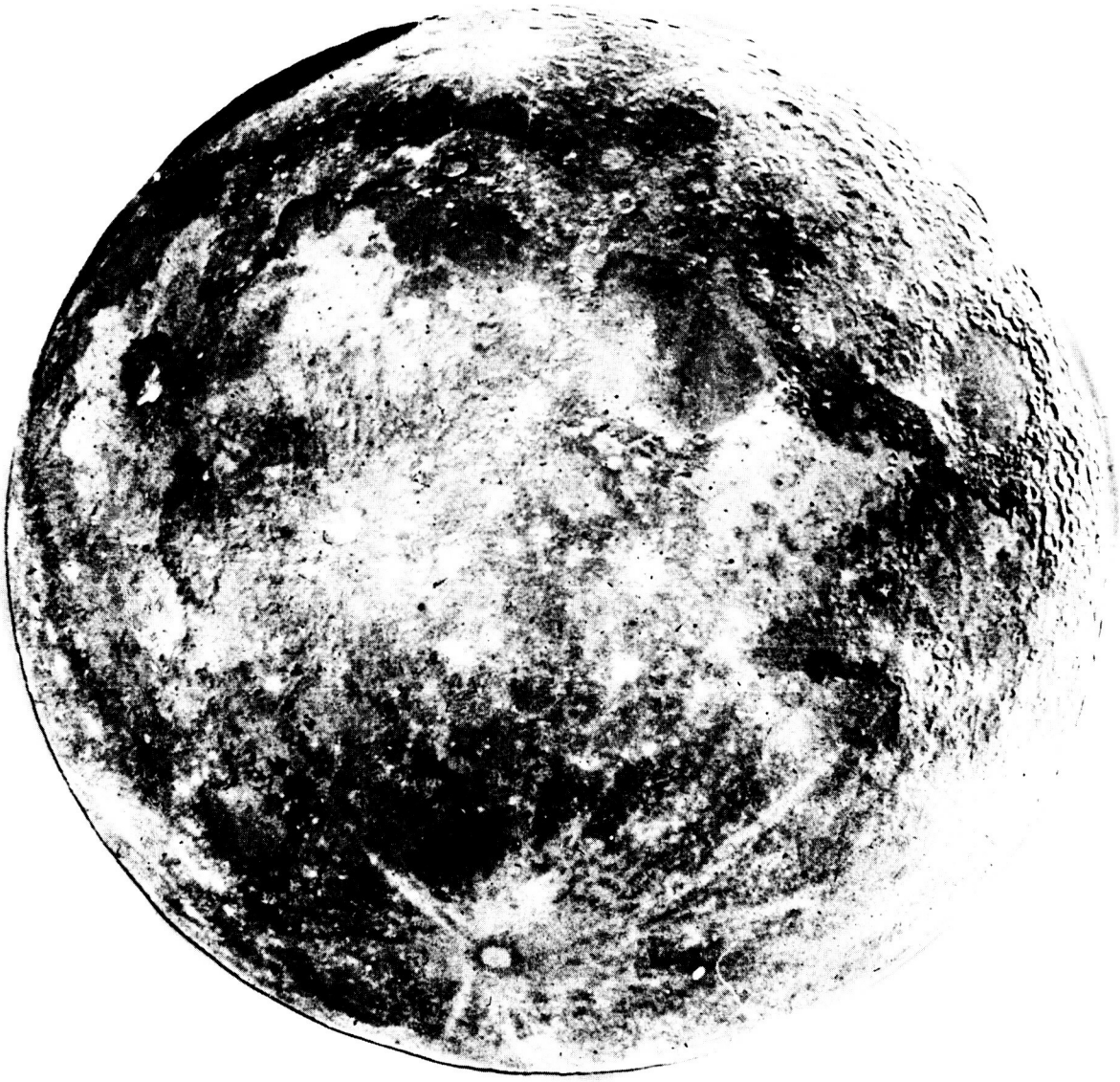

Fig. 15. Colors for the entire visible lunar disk. (Shades as in Fig. 13; E. Whitaker.)

at once evident that the prominent ridge system reflects a complex deep-seated structure that is probably related to one or more major impacts and old craters, all preceding the filling of the mare basin. The complex structure is again in contrast with the rather simple concentric ridge patterns found in Mare Crisium, Mare Nectaris, and Mare Humorum; nevertheless, the pattern is not random and appears in principle interpretable in terms of one or two main events. Very close to the terminator, elevation differences of 3–10 m can easily be detected on ridges sufficiently long to be shown on the photographs. The straight diagonal ridges seen on Fig. 6 crossing the radial pattern emanating from Lamont agree in direction with lineaments found in the nearby terrae, indicating a basic crustal pattern continuing into the mare region. This fact and the detailed appearance of the ridge system, as well as the prominent mounds near Arago, are unmistakable signs of plutonic activity extending right up to the visible surface. The color differences within the mare (Fig. 15), to be discussed below, reinforce this conclusion.

Figure 8 shows the eastern half of Mare Tranquillitatis. No simple symmetry properties are apparent, but the Cauchy Fault, the numerous volcano-like structures (domes showing calderas), the prominent rille, and other structural features again point to tectonic and plutonic activity extending to the lunar surface.

Figures 9 and 10 show the eastern and western sectors of Mare Serenitatis. Because of its near-circular outline, its roughly symmetrical ridge pattern, and its surrounding mountain walls in the southern and eastern sectors, this mare is considered to have been formed by impact early in the lunar history (prior to the formation of Mare Imbrium). Attention is called to the *en échelon* structure of the Serpentine Ridge presented in Fig. 9, the dark threshold just north of Plinius, which is shown in Fig. 15 to have a bluer color than the remainder of the mare basin, and the very remarkable crossing and intertwining of ridges in the vicinity of Plinius. Figure 10 shows a complex system of ridges, plateaus, and the well known threshold of the "lava" flow directed toward Archimedes, just past the gate between the Apennines and the Caucasus Mountains. This entire complex of features again is unmistakably tectonic and plutonic in nature.

Figure 11 shows a region of Oceanus Procellarum just west of the Riphaean Mountains, at approximately the same latitude as Mare Cognitum but less than one mare diameter to the west. Certain structural directions clearly predominate. These are known to be part of the grid pattern that also pervades Mare Cognitum, as is shown in Section F. The "braided" structure of the ridges is noteworthy. The positions of the larger craters bear no relationship to the tectonic pattern, consistent with the hypothesis of their impact origin. That this conclusion does not extend to all of the small craters is evident from an analysis of the *Ranger VII* photographs. While the larger craters appear invariably to be of impact origin, some small craters are found by their linear arrangement or position on mountain tops to be related to plutonic effects.

Figure 12 illustrates the occurrence of several major craters near the shoreline of Mare Humorum, whose rims are not level but are inclined toward the mare. Similar structures are observed on the shorelines of Mare Crisium, Mare Nectaris, and elsewhere. Apparently these craters were caused by impact after the basin had formed (since they interrupt and locally destroy the mountain wall surrounding the mare) but prior to the flooding of the basin, as follows from the details of the mare level where the craters were invaded. The concentric ridge system of Mare Humorum is shown also, though not as well as on photographs taken at a low Sun angle.

B. Colors and the Meso-Structure of the Maria

An important source of information is the color of the lunar surface. Figures 13–15 show the color contrasts for the principal maria facing the Earth. It is seen that the color boundaries between bluish and reddish areas are usually very sharp; and by comparison with direct photographs, it is found that these boundaries often coincide with visible flows, as shown in Figs. 9, 10, 16, and 17. In Fig. 18, eight flows have been mapped in a limited region of Mare Imbrium; the boundaries of five or six of these are recognizable also on Fig. 13 as edges of color provinces. These color contrasts indicate, first, that the lunar maria are not covered with even 1 mm of cosmic dust, which would have obliterated the color differences, and that the color contrasts seen on the lunar surface are, in many instances, related to observable structural units, such as the flows shown in Figs. 9, 10, 16, and 17. The uppermost flows, obviously the most recent ones, are often the bluest; the older deeper-lying flows, which are partly covered, are often (but not always) the reddest. The color differences may be due to differences in the state of oxidation, possibly related to variations in the water content of the magmas. On Mauna Loa, Hawaii, one often observes a reddish coloration of vents, which is attributed to escaping steam. Color differences might be due also to differences in age (cosmic weathering effects). The adjacent terrae, and particularly the islands

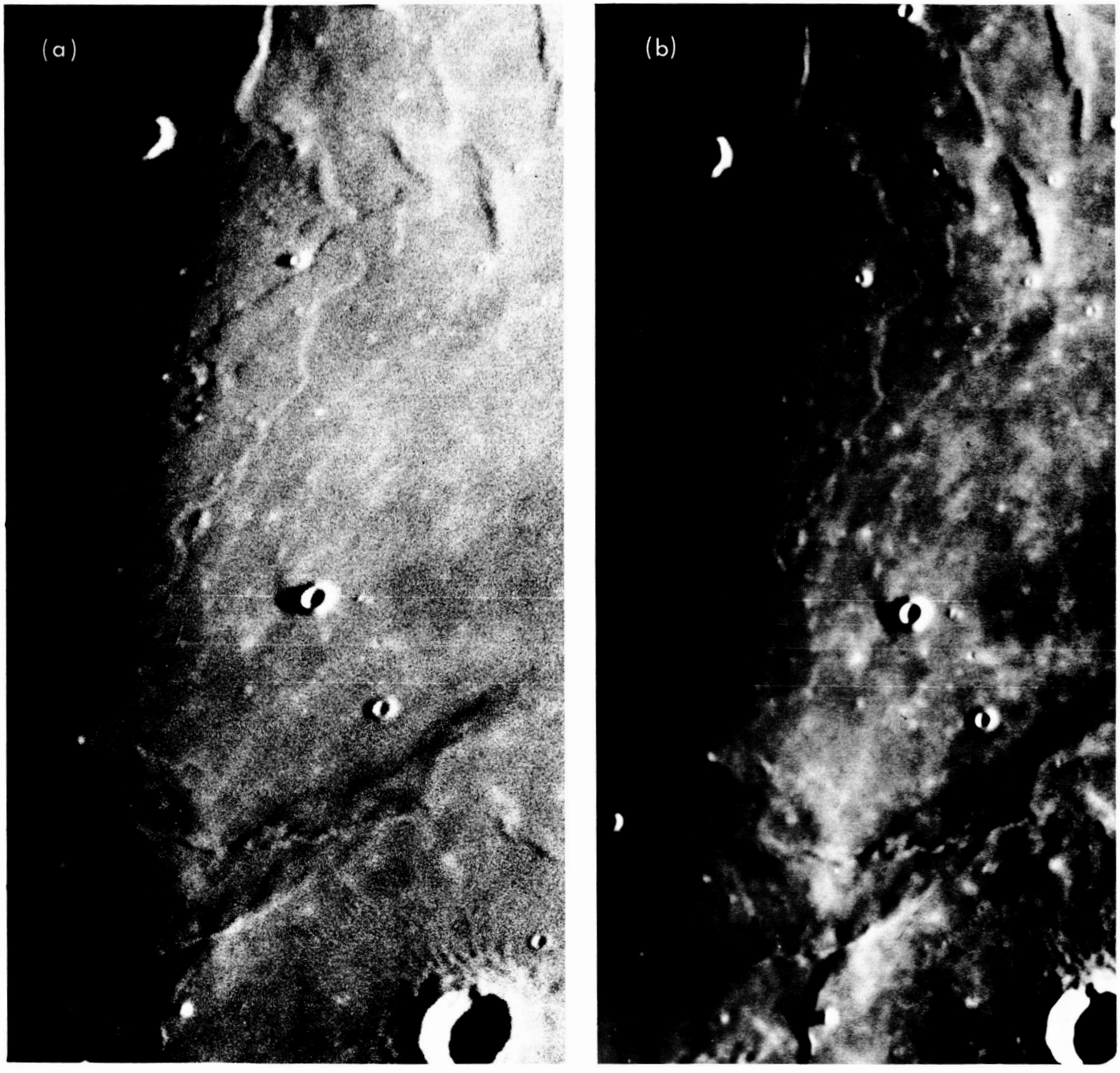

Fig. 16. Flows on Mare Imbrium. (Boundary of lower flow coincides with boundary of a color province shown in Fig. 13 [cf. Fig. 18]; a, Plate M284, b, Plate M690.)



Fig. 17. Flows on Mare Imbrium. (Boundary of flow 1–2 in. from margin coincides with color boundary of Fig. 13 [cf. Fig. 18]; Plate W252.)

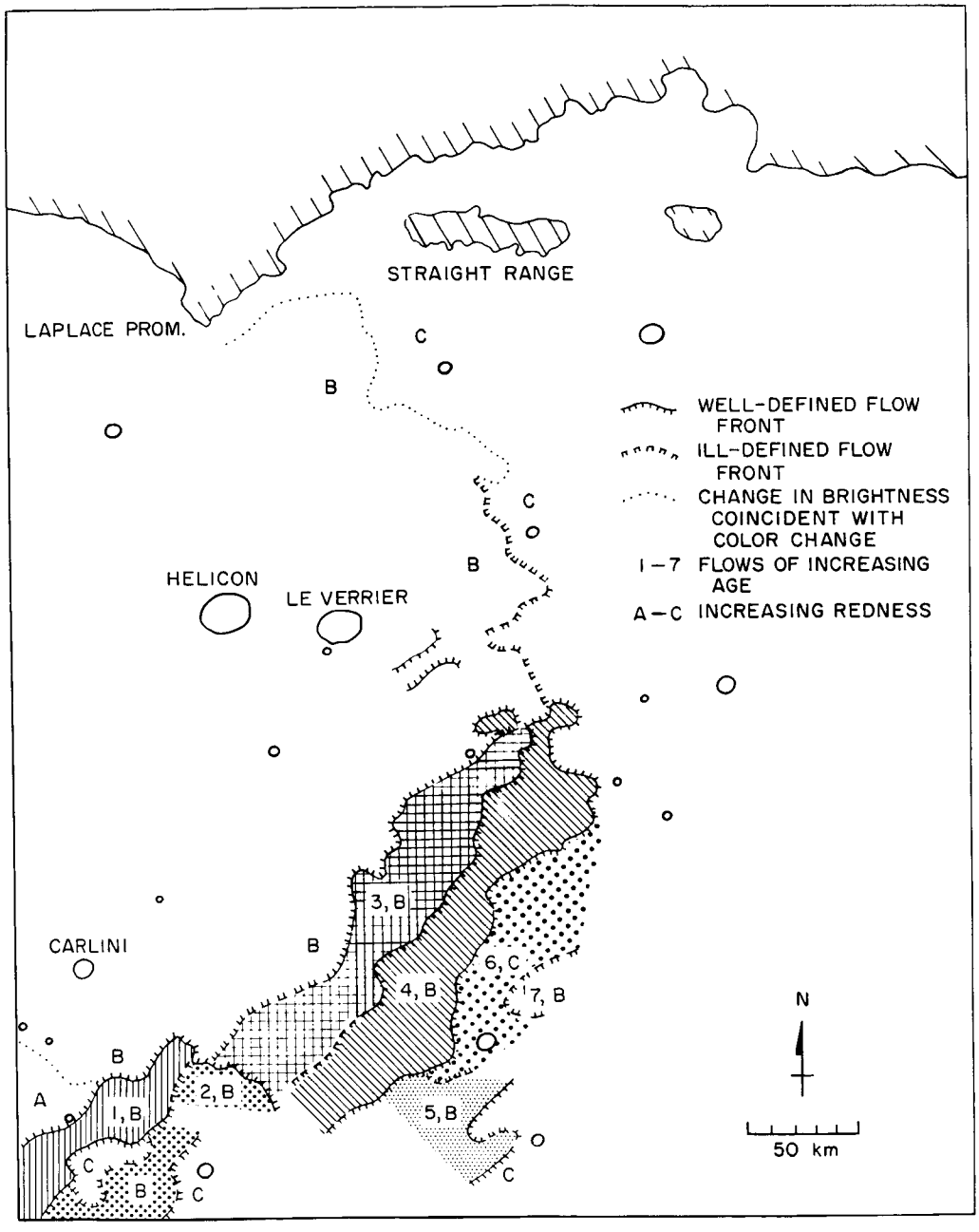

Fig. 18. Map of flows photographed in Mare Imbrium (R. Strom; cf. Figs. 16 and 17).

in the maria, are often redder than the maria themselves. This holds also for much of the crater-ray material deposited on the maria. Regardless of the causes of the observed colors, the existence of successive well marked flows as part of a general tectonic pattern unmistakably supports hypothesis 1 of Section A.

There is another important observation that bears on the choice between hypotheses 1 and 2. It is that the flooding of the circular maria did not occur immediately upon the formation of the basins but after a considerable interval, apparently different for the different basins, in some cases perhaps as long as a few million years. This follows from the study of the inclined and partly flooded craters near the borders of Mare Nectaris, Mare Humorum, Mare Crisium, and others. These craters are tipped, clearly having been formed on an inclined surface, apparently the floor of the basin before it was flooded. Since the number of such structures differs for different maria, it appears that the intervals between formation and flooding may not be constant. In any case, the intervals must have been many thousands or possibly a few million years. Hypothesis 2 does not explain this phenomenon, whereas it is compatible with hypothesis 1 provided the formation of the lavas was not the result of the impact itself but of a general heating process of the Moon, causing subsurface magmas to be available during a certain period of lunar history. The assumption of the Moon having passed through such a period of considerable internal heat and partial melting is consistent with the observation that the parent bodies of the meteorites, which by all indications were even smaller than the Moon, have gone through a similar process of melting, differentiation, and freezing. It is difficult, if not impossible, to explain various other lunar phenomena without the assumption of a period of maximum melting. Among these are the isostatic adjustment that has taken place in approximately twenty large pre-maria craters, such as Clavius and Hevelius, which show convex rather than concave floors, and the flooding and filling of many craters with elevated flat, dark floors, such as Wargentin (Fig. 19). The hypothesis that the flooding was indeed by available magmas, caused by previous lunar heating and not by the impacts themselves, is further supported by the fact that several very large pre-mare craters were never flooded, whereas even small craters dating from the period of maria formation are flooded (Fig. 2) and that distinctly post-mare craters, such as Tycho and Copernicus, show no sign of flooding.

There is a related observation bearing on the choice between hypotheses 1 and 2. Because of the severe damage to the walls of Mare Cognitum it would probably

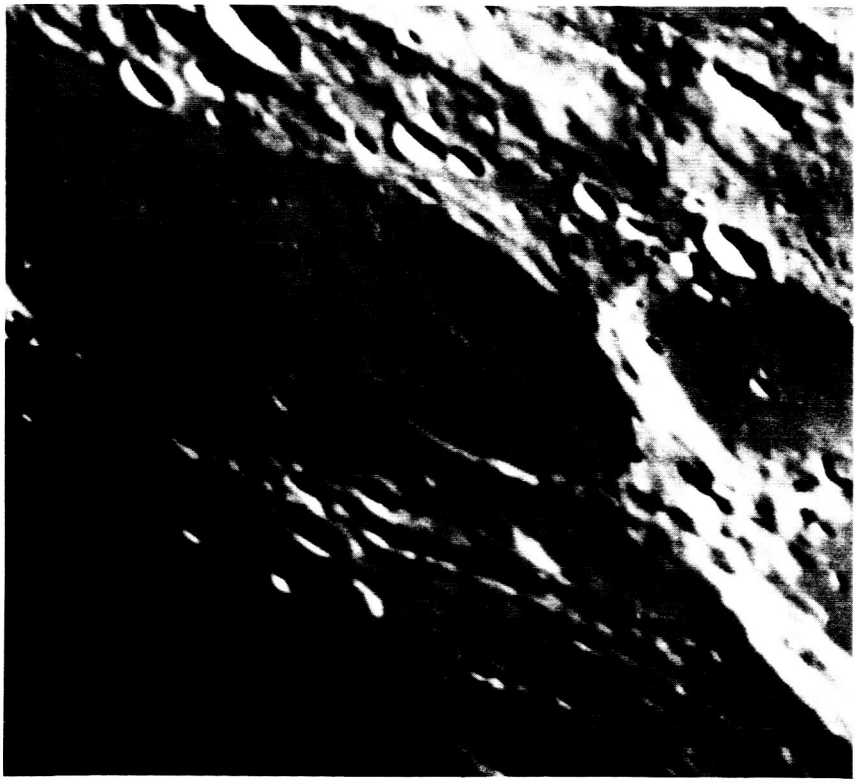

Fig. 19. Elevated floor of Crater Wargentin (Lick Observatory).

be generally conceded that it is older than Mare Imbrium. If so, the striking color contrast between the islands in Mare Cognitum (such as Darney χ) and the mare itself proves that no dense dust cloud from the Mare Imbrium impact has struck there.

The conclusion that hypothesis 1 is consistent with the observed features does not mean that the structure and density of the lunar lava, as exposed in the maria, are the same as those of terrestrial lavas. The deposition in a vacuum, the much lower surface gravity of the Moon, and the subsequent erosion by particles and solar radiation will have caused departures which must be ascertained.

The lunar surface lavas will, upon deposition, probably be *extremely porous and vesicular,* like pumice or reticulite found, e.g., in Hawaiian lava flows, but probably more extreme. The pressures occurring in terrestrial lavas at a depth of 10 cm would be encountered on the Moon at a depth of some 120 m if the lunar surface rock has a bulk density of 0.5.

That the uppermost layers may have an even lower density is indicated by the experiments of Dobar *et al.* (Ref. 1), who found a value of about 0.12 for the bulk density of solid silica extruded as a liquid into a vacuum. These authors introduced the name "simolivac" for such material (silica molten in vacuum). Almost certainly, the surface of the original lunar laval flows will have had a rock-froth structure somewhat like simolivac. It will not be identical because the lunar rock will probably have no more than about 70% SiO_2 content, and dissolved gases will cause further complexities. In addition, a rapid boiling off of many substances will occur when the magmas reach the surface, since the sublimation points of SiO_2, MgO, BaO, ZnO, Al_2O_3, and other oxides, as well as the metals Ca, Cr, Cu, Fe, Mg, Ni, Si, Zn, etc., are much below the melting points even at such "high" lunar pressures as 10^{-5} mm Hg. We are indebted to Dr. Alvar Wilska of this University for calling these facts to our attention. Because of the low thermal velocities, the substances that boil off will precipitate on colder rock surfaces in the neighborhood and cause powdery deposits not unlike "fairy castles."

Recent experiments with extruded basalt by Dr. S. Hoenig at this Laboratory yielded 0.3 for the bulk density of this material. The author has found that basaltic material thrown up in liquid form by the Laimana volcano on Hawaii in 1960 and solidified in free fall (very low effective gravity) has a bulk density of 0.10–0.18. It is therefore very probable that at the time of deposition, the lunar maria were covered with a layer of material of bulk density 0.1–0.3.

Some estimate on the thickness of a rock-froth layer on each of the lava flows may be made on the basis of the Mare Imbrium (Figs. 16–18) and Mare Serenitatis (Figs. 9, 10) observations. The flows on Imbrium are about 50–100 m thick, and the most extensive are some 200 km long (Fig. 16). These Imbrium flows appear to have issued not from the mare shoreline but from fissures well inside the mare, within a rather confined area. The slopes of the flows have not been measured (this could probably be done photometrically) and may not be the original ones at the time of deposition. They seem to be of the order of 1 deg. In Mare Serenitatis, near the south shore (Fig. 9), a distinctly steeper slope of perhaps 3 deg occurs, though other flows are found nearby with very small slopes.

The composition of these flows cannot, of course, be inferred with any certainty by inspection from the Earth. O'Keefe and Cameron (Ref. 8) have drawn an analogy with terrestrial ash flows because of their great fluidity and suitable composition, if it be adopted that tektites are of lunar origin and their composition (about 70% SiO_2) is indicative of that of the lunar crust, and that lunar ash flows would lead to a material of similar composition as on Earth (ignimbrite). On the other hand, as R. Strom has pointed out, unlike the lunar flows (Fig. 16), terrestrial ash flows spread in all directions from the source and have no appreciable terminal walls, whereas the observed lunar flows rather resemble the Hawaiian flows illustrated in Figs. 20–22.

While most terrestrial lava flows have fronts inclined over 20 deg, Dr. H. Powers of the Hawaii Volcano Observatory informs us that some Hawaiian flows have fronts inclined less than 7 deg. Estimates based on Figs. 16 and 17 indicate average slopes of about 3–7 deg for the fronts there shown; the well known flow between the Apennines and the Caucasus, toward Archimedes, has a front slope of about 17 deg (R. G. Strom, E. A. Whitaker). These low figures are not necessarily representative, because the limited resolution used reduces the values. It is further noted that ash flows tend to sweep over low hills and other obstacles in their paths, whereas the slower lava flows avoid and bypass them. In Figs. 16–17, a number of hills are seen to have been bypassed, in curved arcs, by the principal flow. On the Earth, ash flows are associated with explosive volcanism, and basaltic lava flows are quiescent. The topography of the lunar maria appears to fit the second description

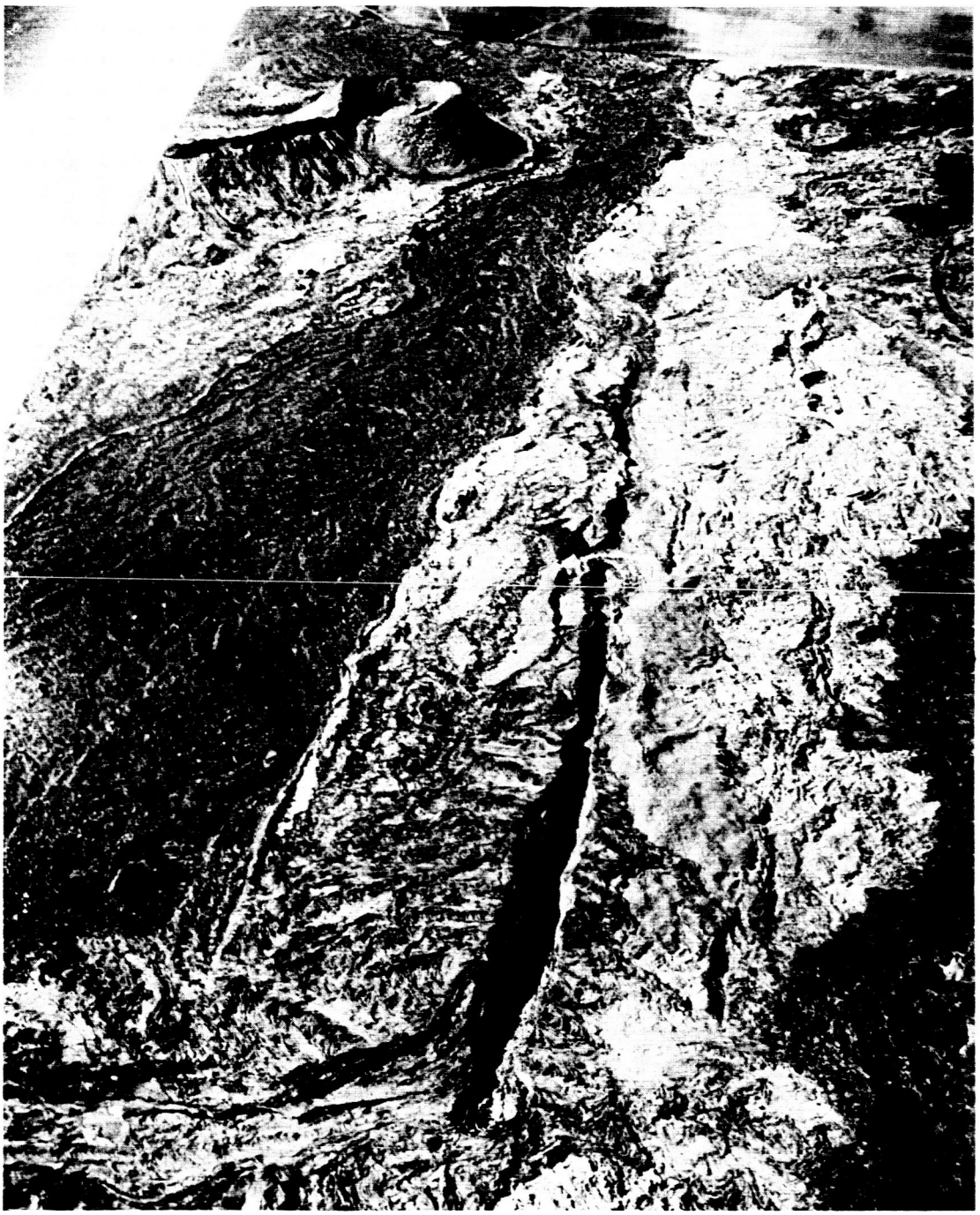

Fig. 20. Aerial view of lava fields and rifts on Mauna Loa, Hawaii.
(Approximate elevation, 12,000 ft; LPL photograph.)



Fig. 21. Crater, crater chain, rift, and edge of lava flow, Mauna Loa, Hawaii. (Window reflection superposed on upper right corner; LPL photograph.)

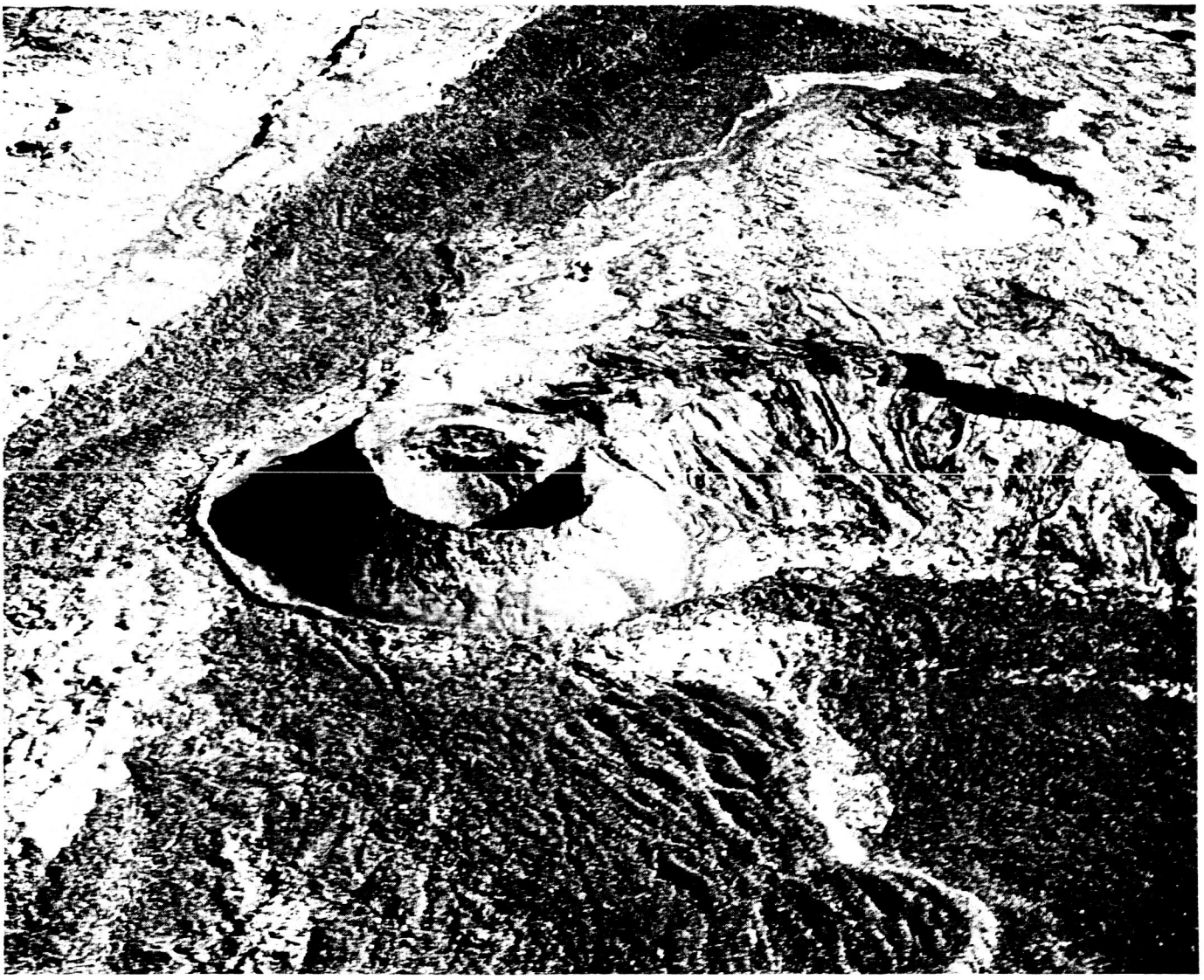

Fig. 22. View of lava vent and lava channel as well as surrounding lava streams showing "moraine" effect (LPL photograph).

better. It is true that some authors have assumed the craters on the maria to be of volcanic origin; however, there is nothing to indicate that the observed lava flows and the craters are related.

The retention of the carrier gas in an ash flow in the lunar vacuum would be difficult to understand unless it is assumed that the flow is promptly sealed off at the surface with a layer of sufficient strength to confine the gas. Also, ash flows are normally associated with lava flows. There thus appear to be reasons to assume that the observed flows are lavas, not ash, although allowance must be made for the different lunar conditions before one can be certain. If they are ash flows, the composition is likely to be rhyolitic; if they are lavas, they are likely to be basaltic.*

The *mare ridges* cut through the color provinces without visible interference. They are not the edges of lava flows. Instead, they appear to have a dynamical cause, some being related to the symmetrical pattern of the near-circular maria and others to the lunar grid system, of which some ridges are parts. This may be verified by inspection of Figs. 5–12, 16, and 17, and Fig. 25 in Section C. Also, the ridges are quite invisible at high Sun, showing that the lunar surface is essentially continuous across them. There are no close analogs of the lunar ridges on the Earth. Their non-interference with the color provinces and their invisibility at high Sun indicate that they were formed by uplift. In some cases, the uplift appears to have been so large that the surface has split open; and often it may be observed that out of such fissures, a new dike-like rock mass has been extruded, usually whiter in color than the original mare floor (and thus visible at high Sun). These whitish "lunar dikes" have been known to exist (Ref. 9), and some are clearly seen on several of the *Ranger* photographs.

The phenomenon of lunar dikes indicates that the ridges are surface manifestations of subcrustal structural planes along which upwelling of magmas has taken place. These structural planes presumably resulted from tension followed by compression. This model accounts for the presence of ridges as part of the grid system and also as roughly concentric and radial structural units of the impact maria, because, as the lava basins cooled to increasingly great depths, the deeper spherical layers of the Moon shrank, narrowed the support base for the overlying maria, and caused radial compression. Figure 11 shows a region adjacent to Mare Humorum where the grid-system pattern was deflected by the local stress pattern of the mare.

The formation of ridges by a laccolithic-type uplift of the lunar crust above dynamically determined fracture planes is facilitated by the layered structure of the lunar maria noted above (individual layers typically 50–100 m thick), particularly if alternate layers are very vesicular and weak structurally. The low surface gravity would also facilitate the vertical displacements. Thus, it is not surprising that the equivalent of lunar ridges has not been found on the Earth.

The ridges are therefore assumed to date from an early post-mare period and to have resulted from effects accompanying the cooling of the mare basins. Later in lunar history, magmas will not have been available except possibly in isolated "volcanic" regions. The apparent absence of ridges from the terrae is consistent with their presumed nature as consolidated dust to great depth and the absence of near-surface magmas.

On the basis of the findings discussed in Sections A and B, the following conclusions about the lunar maria have been drawn that may be used as a basis for the discussion of the *Ranger VII* data. The maria are low-level areas flooded by lunar lavas. Some of these depressions were caused by large impacts that resulted also in extensive surrounding tectonic structures, both peripheral and radial. The lavas were not caused by the impacts themselves but resulted from extrusion of available magmas. Some mare surfaces show clear evidence of several successive lava flows. Each flow is found to have a homogeneous color throughout, but different flows may have different colors. The most recent (upper) flows tend to be the bluest, but the age sequence is not everywhere the same as the color sequence. Composition differences, rather than mere age differences, are therefore held responsible. These composition differences may reflect the state of oxidation, possibly related to the water content of the magmas. There is again a remarkable analogy with recent terrestrial basaltic lava flows; on Mauna Loa, Hawaii, each flow has a characteristic uniform color, but the colors of adjacent flows may differ markedly.

The lunar flows are bounded by terminal walls, and some large flows (up to 200 km in length) are comparatively narrow. By terrestrial analogy, this would indicate

*R. Strom points out that gradations exist such as described by R. L. Smith in the *Bulletin of the Geological Society of America*, Vol. 71 (1960), p. 809, that might closely resemble the lunar flows.

that the flows are basaltic lavas rather than ash. According to the small slopes of the flows and their great lengths, the lavas must have been very fluid. Yet their terminal walls show the presence of a substantial solid crust during the flow. On this basis, and in view of the presumed rock-froth nature of the upper layers, it is assumed that the lunar flows consist of two layers each, an upper viscous and later highly vesicular layer, some 10–20 m thick, and a layer of more compacted rock that resulted from the low-viscosity lava.

Subsequent meteorite or cometary impacts as well as cosmic abrasion will have occurred in this multilayered structure. Very small craters will have formed in the rock froth only, and larger craters will extend into the denser rock; but the succession of flows on the maria may have caused irregular local alterations between very vesicular and denser rock material. Regional unevenness in crater shape is therefore to be expected.

Dobar *et al.* (Ref. 1) found the bearing strength of simolivac to be 1–4 tons/ft^2 or 1–4 kg/cm^2 for static loads. For the low-*g* Hawaiian basalt, the author found essentially the same value (2–3 kg/cm^2), which increases to about 6–8 kg/cm^2 after surficial crushing of a few millimeters. It is probable that the bearing strength of the lunar maria will be of the same order of magnitude, with impacts that have pulverized and compressed the rock froth having caused some local fluctuations in value. The expected occurrence of cavities and lava tunnels makes it unsafe to use this number indiscriminately.

The *Ranger* photographs, with their high resolution, potentially add much information on the texture of the upper 10–20 m of the mare surface. The upper layer is not likely to react like solid rock or even like sand or alluvium because of its very high compressibility, over 90% of the volume being open. This is particularly true for material stemming from the unconsolidated upper layers of a terra region impacting on a rock-froth mare.

C. On the Structure of Mare Cognitum

Figures 23–25 are Earth-based photographs of the Mare Cognitum region showing the aiming and impact points as well as two low obliques. The mare is less regular than Mare Crisium, presumably because of the greater age of the basin, and is only two thirds of its size (diameter roughly 280 km versus 450 km for the inner wall of Crisium). In size, the mare resembles the inner basin of Mare Orientale (inner ring 320 km), the inner ring of Mare Humboldtianum (300 km), or the giant craters Bailly and Pingré near the South Pole (ring diameters 320 and 300 km) (Ref. 6). As is true for Mare Crisium, the east wall is destroyed, although the destruction is much more severe in Mare Cognitum. The ridge system shown in Fig. 25 and the area of the Riphaean Mountains are the most regular remaining parts of the mare. Most of the ridges are visible with more resolution on the *Ranger* photographs despite the higher Sun angle (23 deg).

A group of islands occurs in the mare at 12°S, 26°W, the largest of which is called Darney χ. These islands are remarkable for their deep yellow color (in stark contrast with the dark gray, slightly yellow, mare floor; cf. Fig. 15) and for the large number of crater pits piercing their surface (several dozen can be seen telescopically). The islands appear to be remnants of the pre-mare lunar crust.

Figure 26 shows the full-Moon appearance of Mare Cognitum. The mare is seen to be traversed by a number of narrow crater rays, most of which are traceable to Tycho or Copernicus, although a single thin ray issuing from Lalande passes almost squarely through the impact area. The craters responsible for these rays are denoted by symbols in Fig. 26.

All rays in Fig. 26, particularly those in the eastern half of the mare, are readily identified on the *Ranger* photographs. The Copernicus ray in the far eastern part of the mare (11°S, 18°W) is found to contain a band of craters up to about 500 m in diameter, seen in B frames 165, where the band of craters occurs in the upper central section of the frame, through 180, after which the area moves out of the field. Apart from a few minor features, grooves are found to be nearly absent on these photographs. The resolution on B180 is 100–150 m. The photographs strongly indicate that *the brightness of the ray is not due primarily to secondary craters but instead to uniformly spread fine ray material.* The area is well mapped on the AF-ACIC chart RLC 2, scale 1:500,000. The distance from Copernicus is 20 deg or 600 km.

The second Copernicus ray, crossing the mare just east of the prominent mountain ridge near the mare center at 10°S, 21.3°W, is shown clearly on the A frames as a brighter fan-shaped area, but right up to the last frame (A183, resolution 250 m), showing an appreciable area of the ray, few if any secondary craters appear. Again, the uniformity of the ray indicates that its brightness is not primarily due to unresolved secondary craters. The distance from Copernicus is 20 deg or 600 km.

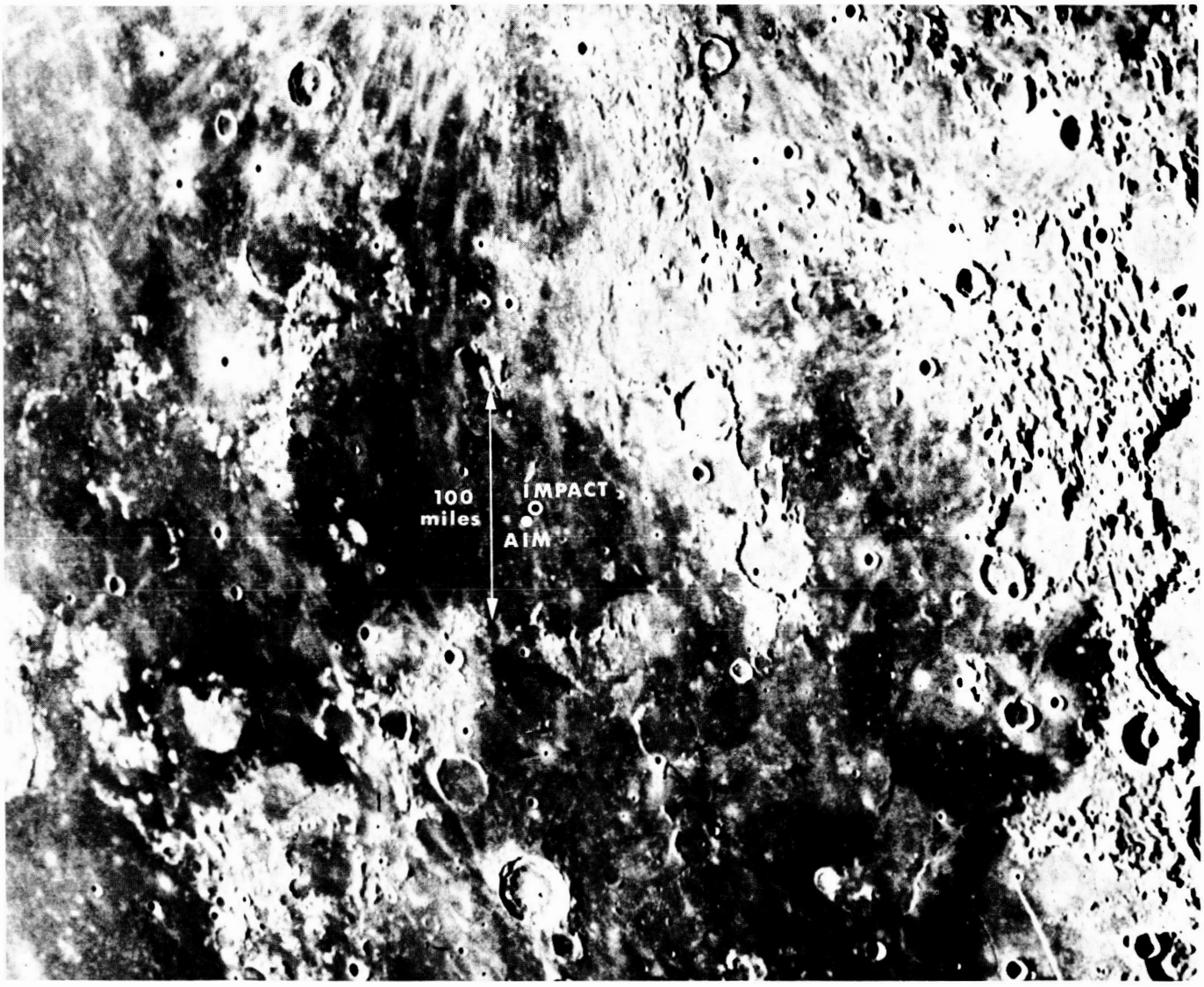

Fig. 23. Earth-based photographs of Mare Cognitum showing aiming and impact points of *Ranger VII*. (Illumination similar to that in *Ranger* photographs.)

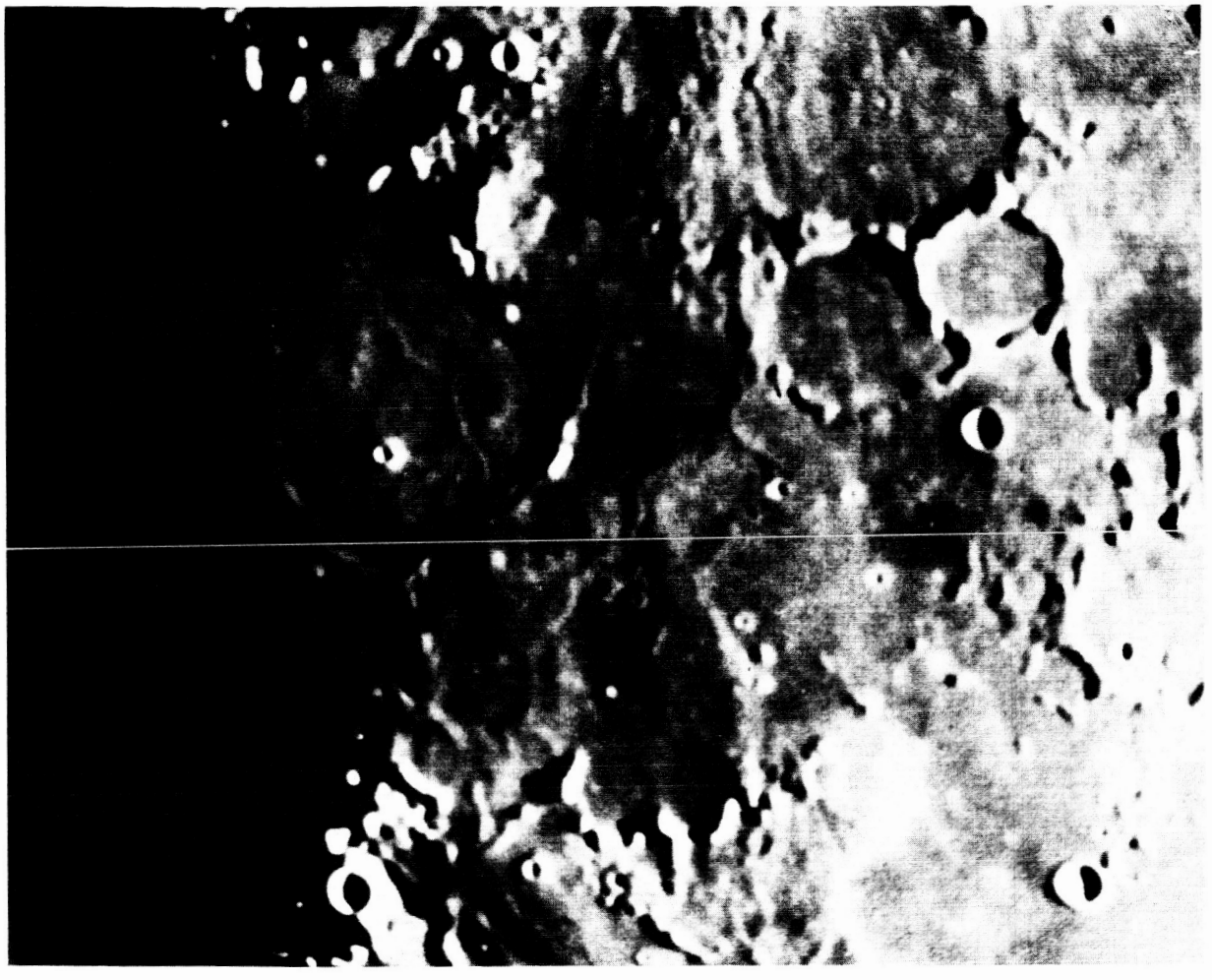

Fig. 24. Eastern half of Mare Cognitum under low Sun, showing ridge system (Plate Y883).

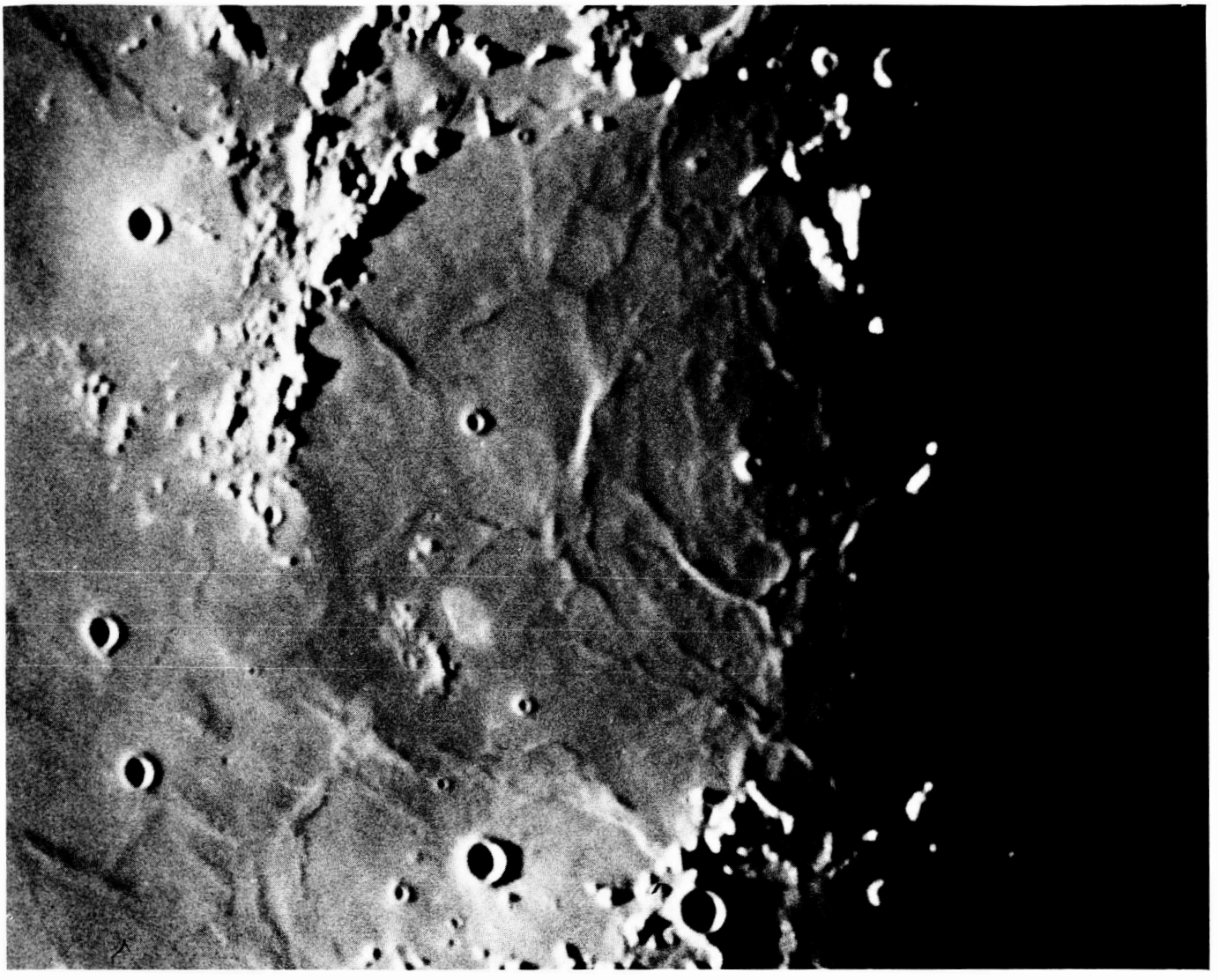

Fig. 25. Western half of Mare Cognitum under low Sun, including Riphaean Mountains (Plate M195).

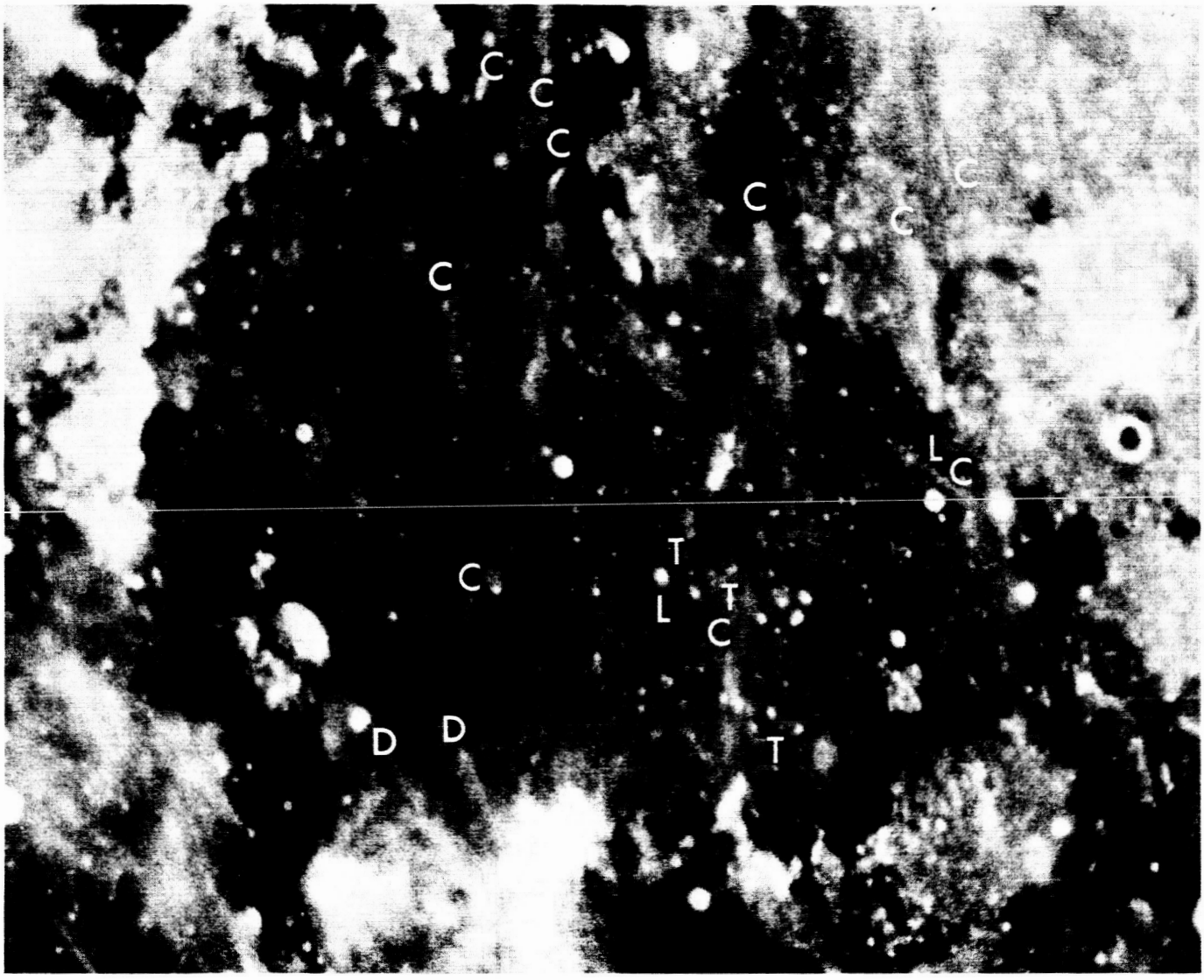

Fig. 26. Full-Moon view of Mare Cognitum, showing numerous crater rays and some dark areas essentially free from ray material. (Four sets of rays are identified as follows: C, Copernicus; D, Darney; L, Lalande; T, Tycho. The Lalande ray stretches between the two L's crossing the impact area. The Darney rays issue from Darney, within the Figure. The Copernicus rays extend downward from the symbols, the Tycho rays upward.)

Several small Tycho rays and some Copernican rays occur close to the impact area of *Ranger VII* and are thus shown with higher resolution. The *Ranger* records have provided the first information on the detailed structure of such rays.

D. The Structure of Crater Rays

Figure 27 shows a reprojected photograph of the Tycho ray system, with Tycho itself placed centrally on the lunar disk. The strongest Tycho rays are seen to miss Mare Cognitum, but numerous smaller rays spread toward the mare. Comparison of Figs. 26 and 27 will clarify the Tycho ray pattern in this region.

On A180, the prominent mountain at 10°S and 21°W, referred to before, is seen near the upper margin, with its crest pierced by a small crater. About 3.5 cm southwest of this crater, a cluster of five whitish craters occurs (at 10°30′S, 21°04′W; see ACIC map RCL-3, scale 1:100,000) from which a whitish band approximately 2 cm long extends upward. This feature is readily identified in Fig. 26, where it is marked with a **T**, and may be observed with increasing resolution (from approximately 300 to 75 m) in the successive A frames, 180–195. It is also shown on the upper central margin of Fig. 28, reproduced from A187. On these A frames, it is seen that the ray starts at a cluster of four or five prominent craters and numerous smaller ones in a confined area, from which a whitish band extends like a comet tail from the comet head. This whitish band crosses a complex ridge, shown in Fig. 28, and contains some shallow craters and grooves oriented North and South, in the direction of the ray itself, which is away from Tycho.

A similar observation may be made with respect to the Tycho ray that passes through the impact point of *Ranger VII*. The "head" of this ray is seen as early as frame A170, with two craters shown located at 10°52′S, 20°37′W, each about 1 km in diameter. On A180, many smaller craters are seen, and a fan-shaped ray issues from the cluster northward for about 1 cm. In Fig. 28 (A187), some structure is visible in the ray and evolves in the later A frames (cf. Fig. 29, frame A194). The analysis is complicated by the proximity and partial overlap of four Copernican clusters also identified on Figs. 28 and 29. In fact, there may be a continuous arc of minor Copernican secondaries extending through the entire central and upper central section of Fig. 29, crossing the Tycho cluster.

A spectacular event has occurred in the crater (1.4 km in diameter) just below and left of the central reticle on Fig. 28. The splashing Tycho material has cut through its rim and caused a bright ray about 0.5 km wide to extend northward from the crater for about 4.5 km. This is best seen on frames A194 (Fig. 29) and A195.

The concept of secondary impact craters occurring at the head of short crater rays is not new. It was observed many years ago, both visually and photographically, on the three or four short but prominent Tycho rays on the floor of Pitatus (Ref. 10). This floor is notable for its absence of confusing surface detail. At the head of each of the rays, a shallow crater can be seen.

In considering (e.g., in Fig. 29) the shapes of the secondary craters in the crater rays, it must be borne in mind that a given impact area can be struck by ejecta arriving at different angles and with different velocities. For example, the distance from Tycho is 32 deg or 980 km, so that the impact velocity for Tycho secondaries must have exceeded 1.1 km/sec (Ref. 11). Velocities of up to 2.0 km/sec could have occurred, provided that the impacts were nearly vertical. For velocities less than 1.67 km/sec, both low-angle and high-angle impacts could have reached the target (Ref. 11), but clusters are unlikely to contain both types in comparable numbers. Near-vertical impacts probably lead to roundish clusters, low-angle impacts to elongated clusters. Since the observed clusters are roundish, it is assumed that they are due to high-angle impacts. This is consistent with the fact that most craters are also round. Two exceptions occur in the first cluster, being groove-like craters, visible in Fig. 29 but best seen on A197. Figure 29 also shows some shallow grooves in the tail part of the ray. A larger groove of similar orientation, marked **b**, is seen in Fig. 28. The direction points to Bullialdus, which is 10 deg or 300 km away from the *Ranger* impact point. Figure 30 shows the relationship on an Earth-based photograph. With the resolution of Fig. 30, however, the Bullialdus scars or grooves are seen to only about half the distance from the *Ranger* impact point, marked **I**.

While there is little doubt that a causal relationship exists between clusters of secondary craters and their ray elements pointing away from the central ray crater (Tycho or Copernicus), the nature of the lesser features within the rays is not obvious. We shall return to this subject after a more general review of lunar craters and depressions seen on the *Ranger* photographs.

The presence of clusters of secondary craters at the head of ray elements appears to represent a rather general phenomenon, as was noted upon re-examination of high-resolution Earth-based photographs. It became

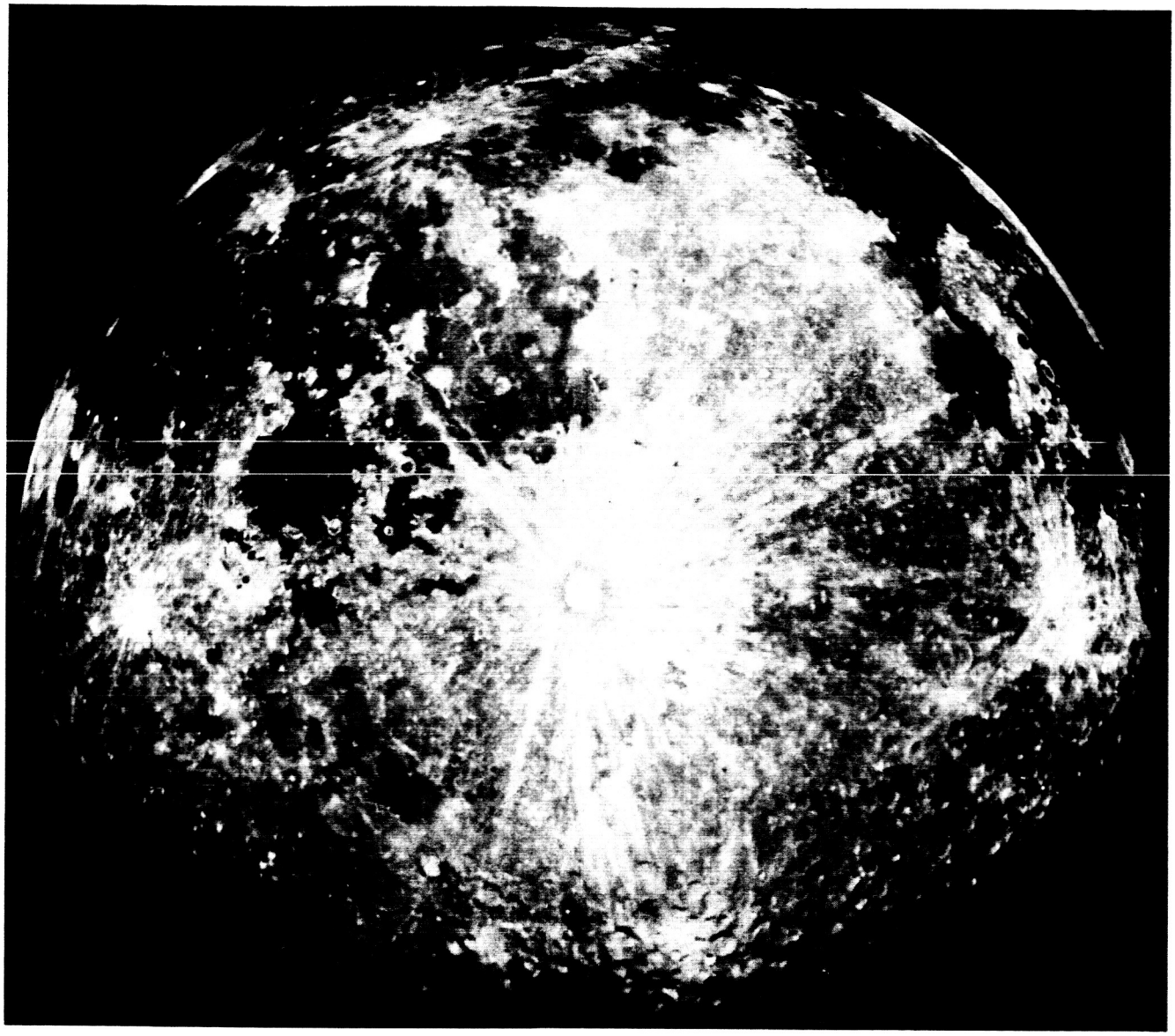

Fig. 27. Tycho ray system seen from above, reprojected.

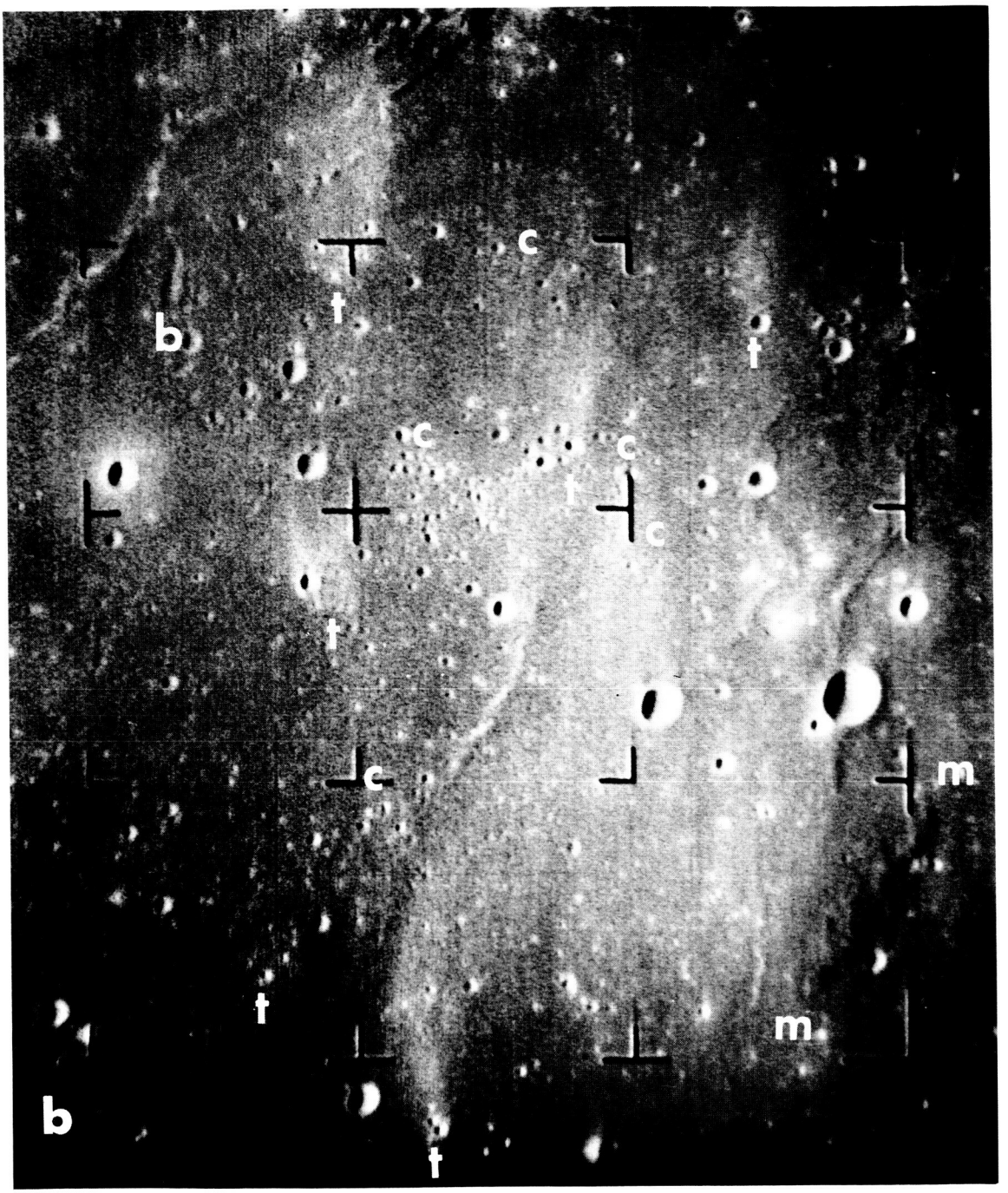

Fig. 28. Part of *Ranger* photograph A187 showing Tycho (t) and Copernicus (c) clusters of secondaries and associated rays, identified. North is up; the Tycho rays point North, the Copernicus rays South; b = Bullialdus scar; m–m is a nearly black mountain range which appears distinctly post-mare and is possibly comparatively recent (Ref. 16).



Fig. 29. Reproduction of A194 showing with higher resolution several features marked on Fig. 28.



Fig. 30. Earth-based photograph of Bullialdus and *Ranger* impact region (I) showing grooves caused by crater in its immediate vicinity. (Distance from crater to impact point is 10 deg or 300 km. Plate Y160.)

apparent that the ray craters have *two classes of secondaries,* those with normal dark walls and scattered at random around the crater, very frequent within about 4 crater diameters from the main crater walls and rapidly thinning out beyond; and those with bright walls, usually having ray elements associated with them, not distributed at random near the crater but falling along great circles passing through it. These bright secondaries, together with their oriented ray elements, form the observed ray pattern.

E. A. Whitaker shows in Part VI that the relationship between the secondaries and the ray elements can be understood by assuming that a blast from the central crater (Tycho or Copernicus) was responsible for the deposition of the ray material originating from the secondary impact. This interesting suggestion would require the central crater to have been formed by an explosion whose ejected gases did not condense upon cooling during the flight time (15–30 min). A comet might serve this requirement. The mass of a Halley-type comet has been estimated to be 10^{17}–10^{19} g (Ref. 12). If its velocity of impact was 52 km/sec (corresponding to the comet radially approaching the Sun with parabolic velocity), the kinetic energy was 10^{30}–10^{32} ergs. Baldwin (Ref. 13) estimates that the energy required to produce Tycho (and Copernicus, having nearly equal dimensions) was 10^{30} ergs. The kinetic energy of Halley-type comets is thus adequate to produce these craters, even if the cometary nucleus is a composite body.

A rough calculation suffices to show that the expanding gas cloud would have cooled rapidly as a result of radiation losses to space. With a total energy of 10^{30} ergs, the thermal energy of the cloud is estimated to be of the order of 10^{29} ergs. If it expands as a hemisphere, initially optically thick to its own radiation, with a velocity $v \sim 10^5$ cm/sec, then its radius will be 10^7 cm after 100 sec and its total luminosity $L = 2\pi R^2 \sigma T^4 = 3.6 \times 10^{15}\, T^4$ ergs/sec. This quantity must be less than 10^{29} ergs/100 sec, the initial radiation presumably having been the most intense. Hence, T (100 sec) $< 730°$K. Adiabatic effects will reduce the temperature further. One finds similarly that T (1000 sec) $< 130°$K, a value probably too low because it neglects solar irradition, reduced optical opacity, and possible sublimation.

In order for the Tycho gases not to sublimate before reaching Mare Cognitum ($\Delta t \simeq 1000$ sec) and thereby lose their aerodynamic effect on the particle spray ejected by the clusters of secondary craters, the gases must have been highly volatile, consistent with their proposed cometary origin and contrary to a meteoritic origin. The comet hypothesis thus appears to be self-consistent. It appears very plausible that some material from the comet nucleus, being additionally separated from the main mass by the Moon's tidal effects, should be propelled to greater distances from the central crater than the lunar surface materials, which apparently produced the non-ray secondaries near the rim.

It remains to be shown that the frequency of comets passing the Earth is adequate to account for the occurrence of cometary impacts on the Moon. I am indebted to Dr. G. Van Biesbroeck for deriving the number of cometary encounters with the Earth since the year 1800 to within 0.1 AU, as based on the *Table of Cometary Orbits* published by J. C. Porter. Among the 648 parabolic comets that have been well observed since 1800, three have passed within 0.1 AU of the Earth, namely, Tebbut 1881 III, Morehouse 1908 III, and Jurlof 1938 III. It is certain that, in addition, uncounted smaller comets have passed the Earth; and it is significant also that all three of the comets listed fall within the past century, when the observers were more active. Among the 125 known periodic comets, five have *orbits* which come within 0.1 AU of the Earth; again, this list is incomplete for faint comets. All but one of the five (Tempel–Tuttle, $P = 33.2$ years) have periods of 5–7 years. It can be shown from probability considerations that statistically much less than one of the five came within 0.1 AU of the Earth since 1800. With three bright parabolic comets during the past 100 years having come within 0.1 AU, we derive that impacts on the Moon by such objects will occur at the rate of 1 per 2.5×10^9 years. On the basis of Oort's theory on the evolution of comet orbits, it may be assumed that the rate was greater in the early history of the solar system. With the strong reasons presented in favor of the major ray craters on the Moon having been caused by comet impacts, the argument may be reversed and the comet size distribution for the interior part of the solar system derived from the observed ray-crater distribution on the Moon. This subject will be dealt with elsewhere.

E. Classes of Craters and Depressions

In Section D, we referred to two classes of secondary craters associated with major ray craters such as Tycho and Copernicus. The rayless secondaries are crowded around the main crater, with elongated grooves or scars found sporadically at greater distances; these craters and scars do not have bright walls and are essentially invisible at full Moon. The second class are the bright secondaries,

often occurring in small clusters and associated with ray elements. These are located in the crater rays, which may extend to great distances from the main central crater.

In addition to these two rather easily identifiable classes, a third category is found, scattered rather uniformly over the Moon, consisting of primary craters. These primaries, where they occur in the maria, are usually very regular in shape, showing a rather deep floor and elevated crater walls often surrounded by a small white halo, a few crater diameters in size.

The *Ranger VII* pictures have shown the existence of a fourth class of craters or depressions without surrounding walls but having a form approximating an inverted Gaussian curve rotated around its vertical axis of symmetry. The majority of these *depressions* are quite shallow, and their bottoms, though roundish, are nearly flat at the center. Examples of such depressions are found on the last A and B frames, particularly A199 (Fig. 31). There appears to be a variant of these depressions shaped somewhat like dimples and aptly called *dimple craters* by H. C. Urey. Figure 31 shows some examples of such formations. These depressions and dimple craters occur in a variety of dimensions and depth-to-diameter ratios. In Fig. 31, the depressions vary from less than 150 to 300 m in diameter, the dimple craters from less than 60 to 150 m. It is probable that at a lower Sun angle than 23 deg, even shallower depressions would be seen and that most of the mare surface would be found covered by them. These shallow depressions show no sign of explosive violence, the slopes being extremely smooth. The deeper depressions have breaks in the walls or even rock ledges, as seen in Fig. 31.

One might at first suppose that these structures could be explained by a surface heavily cratered by post-mare impacts and subsequently buried by dust. But this is most unlikely on several grounds: (1) no single thickness can explain both the large and small dimple craters of similar proportion, and the shallow and deep depressions; (2) fine fractures (scale $\sim$ 1–2 m) are observed that are structurally related to the depressions in a manner suggesting a brittle rock surface; (3) lineaments are observed over the entire mare surface to the smallest resolved dimension, apparently part of a global lineament pattern (see Section H); (4) an observable primary cosmic dust layer and a lunar secondary dust layer of distant origin are essentially absent (see above), while the post-mare impact rate of particles below 10^4 g is only about 1 g/cm^2/4.10^9 years (Ref. 2); and (5) the fractures in the walls of these depressions are unlike those seen in impact craters.

Instead, one appears to observe here a *karst-type formation,* which it closely resembles in appearance and scale (Ref. 14). An aerial photograph of typical karst terrain in Southern Indiana (obtained for this report by Dr. M. S. Burkhead of Indiana University) is shown in Fig. 32. (A high wind unfortunately caused ripples in the fresh snow; an effort will be made to repeat the observation under better conditions.)

There are three causes that could have led to karst-type depressions on the lunar maria: (1) the relocation or even local drainage of magmas below the surface rock-froth layer into lower subsurface vesicular lava beds; (2) the volume decreases in the subsurface materials resulting from solidification and cooling; and (3) the escape of gases. These three mechanisms are the equivalent of solution of subsurface limestone in the karst formations. Cave-ins of the ceilings of cavities will lead to dimple craters. On the basis of the above identification, the sinkholes and dimple craters are early post-mare in age. The absence of an appreciable straight conical section on the slopes of the dimple craters, so typical of Hawaiian drainage craters (Fig. 33), indicates that the profile is not due to drainage but cave-in. The shallow depressions shown on the *Ranger* records are reminiscent of the much larger round and very shallow depressions observed on the floors of Ptolemaeus, Albategnius, and Hipparchus. The score of Ptolemaeus depressions are typically about 10 km in diameter, the others 2–5 km. They are seen only at very low Sun angles. The fact that the Ptolemaeus depressions are so large may be connected with the high elevation of the Ptolemaeus floor, well above Mare Nubium or the floor of Alphonsus. The shallow craters within the Tycho rays shown on A199 (Fig. 31) appear also to be of the collapse type, not due to flying fragments. This conclusion is supported by the orientation of the tree-bark structure reviewed in Section F and the lineaments shown over the entire region, well portrayed on the ACIC maps. The relationship between the crater rays and the collapse features has not been fully elucidated; it may be in part photometric, the ray deposit enhancing the visibility of pre-existing structures.

One of the craters in Fig. 31 is found to have several rock masses on its floor and step-wise rock ledges on one of its inner walls. Because of their dark color and dimensions, the rock masses are assumed to be unrelated to the impacting material and to be extrusive igneous masses instead.

At least half a dozen craters on the B frames have rock-like masses on their floors, sometimes more than one per

crater. Presumably, these are either remnants of the impacting masses, such as shown on the Hawaiian craters of Fig. 34, or the result of slumping of the crater walls.

A test of the impact hypothesis is readily made. B200 shows one crater with a central rock mass about 15 × 20 m in size. The crater is 90 m in diameter. According

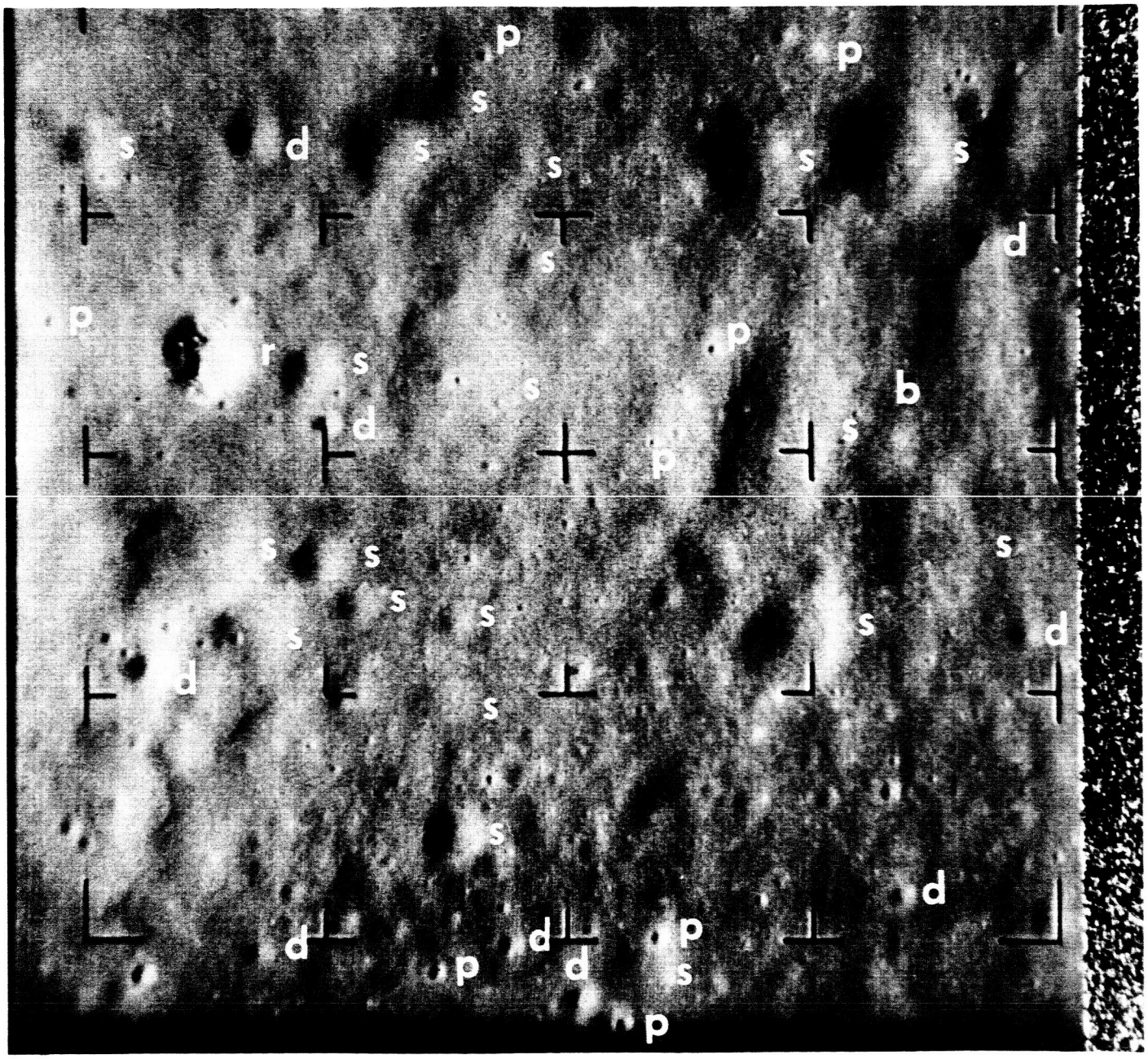

Fig. 31. Reproduction of A199 showing examples of small primary impact craters (p); depressions (sink holes) (s), dimple craters (d), and a crater with internal rock masses (r). (b designates the location of the "boat" [Figs. 36-38]. The distance between the central reticle and the mark to the left is 0.65 km on the Moon. Smallest craters visible are about 10 m diameter. Approximate scale 1:15,000; 1 mm = 15.5 m.)

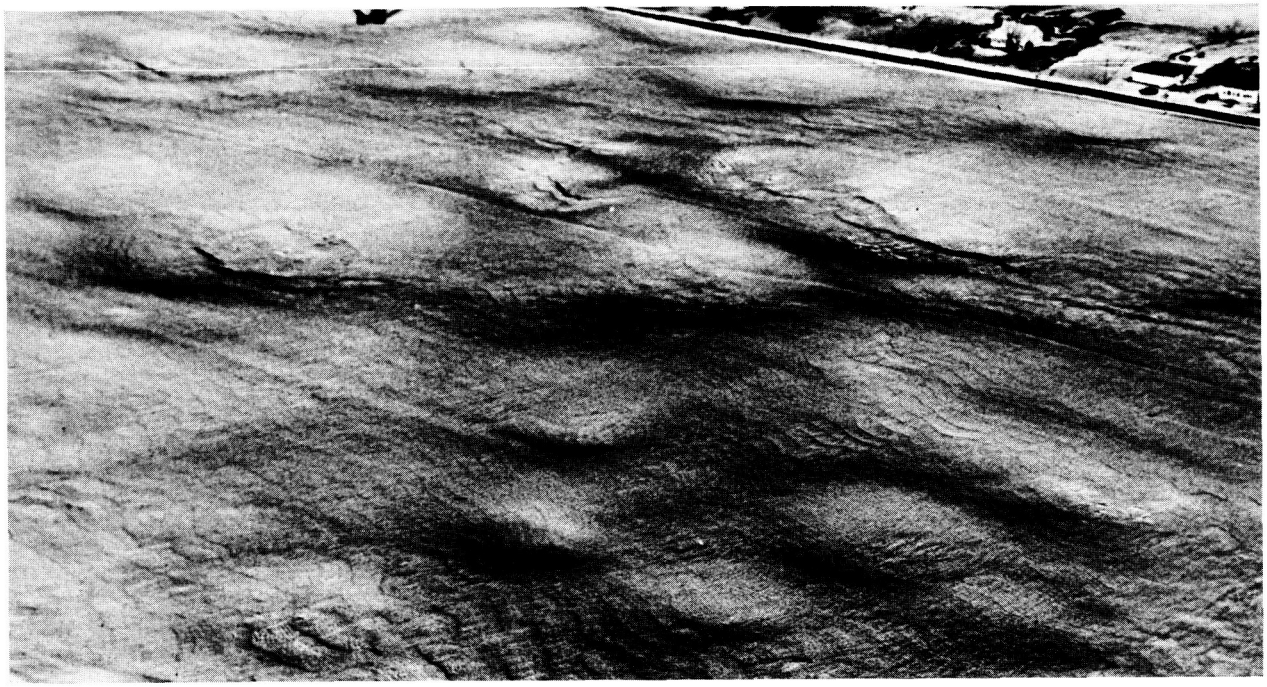

Fig. 32. Snow-covered karst topography in Southern Indiana. (Ripples due to wind pattern on snow; courtesy Dr. M. S. Burkhead, University of Indiana.)

to a table by Baldwin (Ref. 13), the energy required to make the crater was $10^{19.7}$ ergs. If the rock mass struck with $v = 1.0$ km/sec and all the kinetic energy was used in making the crater, the rock mass was $10^{10.0}$ g or 22 m in diameter if spherical and of mean density 1.9. With half the impacting velocity, the mass required would be 4 times, the diameter 34 m. The secondary nature of the crater and the impacting mass are therefore confirmed.

Frame B199 yields additional tests. A crater of 220 m diameter contains a rock about 30 × 50 m in size; a crater 320 m diameter contains three masses, measuring approximately 30 × 40, 15 × 20, and 30 × 30 m. These two craters required approximately $10^{21.0}$ and $10^{21.5}$ ergs to produce, that is, spherical rock masses with $v = 1.0$ km/sec and diameters 58 and 87 m, respectively. Again, these figures are consistent with the hypothesis of secondary origins of the craters and rocks.

It remains to be shown that these rock masses can indeed be propelled to the velocities assumed without break-up. If the velocity of 1.0 km/sec was acquired during a uniform acceleration over an interval equal to the radius of the primary crater ($R = 45$ km for Copernicus), one finds $g = 1100$ cgs. If, for simplicity, the rock mass is now assumed cubical, with one surface normal to the pressure gradient, the pressures required to accelerate a $(30\text{ m})^3$ and $(100\text{ m})^3$ rock mass to $v = 1.0$ km/sec are, respectively, 5.3 and 21 × 10^6 dynes/cm^2 (5 and 21 atm). The peak pressures will be higher than these averages, but the figures suffice to show that rock masses of the sizes considered can indeed be hurled over the lunar surface to several hundred kilometers. They also suggest, however, that this is not true for much larger masses without rupture. In fact, impacts at the largest distances from their primaries appear invariably as complex scars or depressions, indicating that they were formed not by single bodies but clusters of fragments. This correlation of crater shape with distance from the primary was called to my attention by R. Le Poole of this Laboratory.

Many larger craters observed on the B frames have a banded, almost flame-like pattern on their inside walls. The pattern resembles that shown, e.g., on the outer wall of Puu Poliahu (13,630 ft, 4160 m), one of the summit mountains of Mauna Kea, Hawaii (Fig. 35). This pattern is due to a combination of weathering and slumping which has exposed fresh deposits.

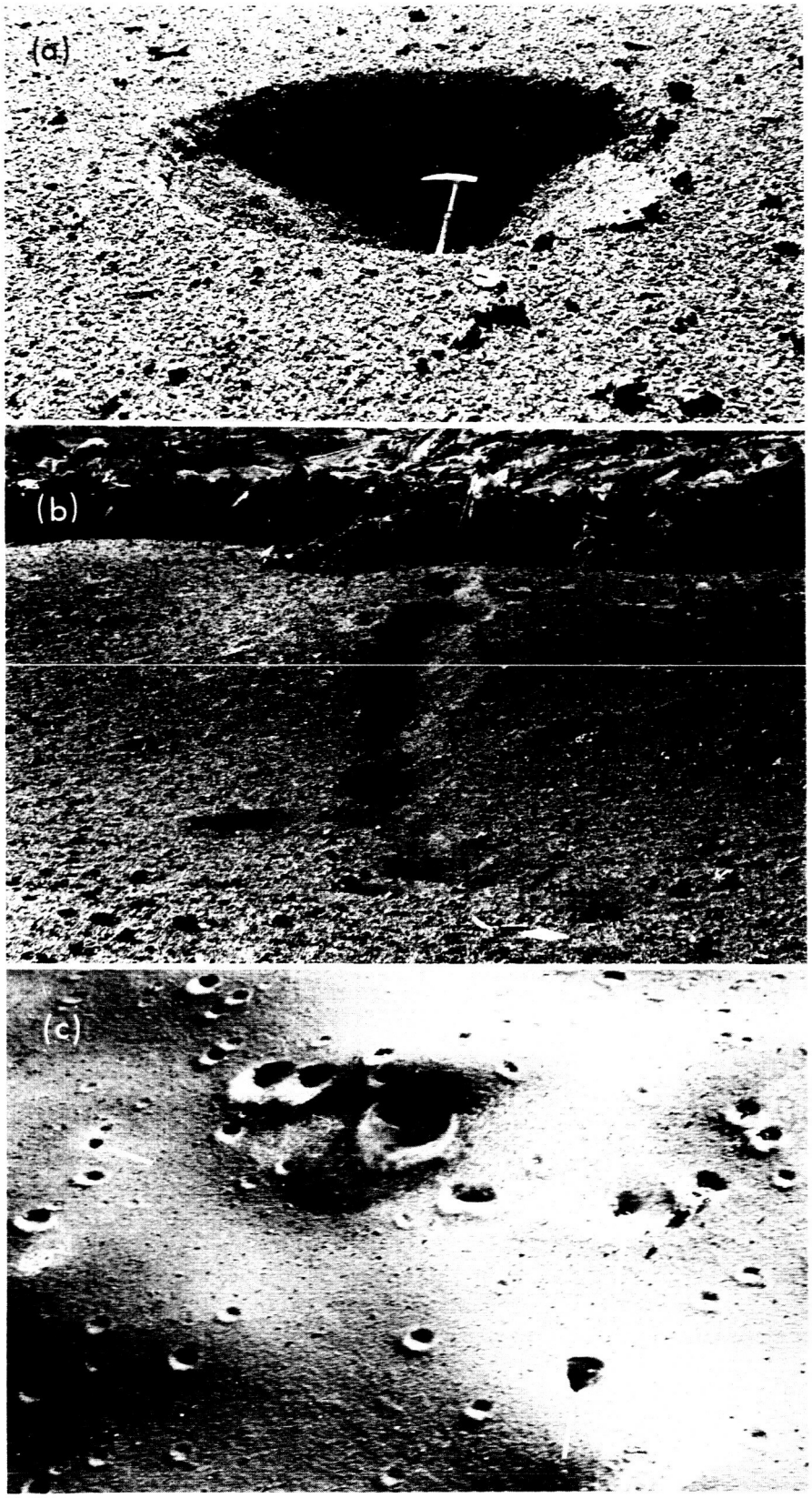

Fig. 33. Examples of craters and a crater chain on a slope of Laimana Crater, Hawaii, due to drainage of surface materials: (a) a 6-ft crater, (b) a crater "chain" due to drainage into a crack, (c) a field on a moderate slope covered with scoria showing conical drainage craters (marked with white lines) and "secondary" impact craters. (Note that impact craters in this material show crater walls accentuated on the down side; LPL photograph.)

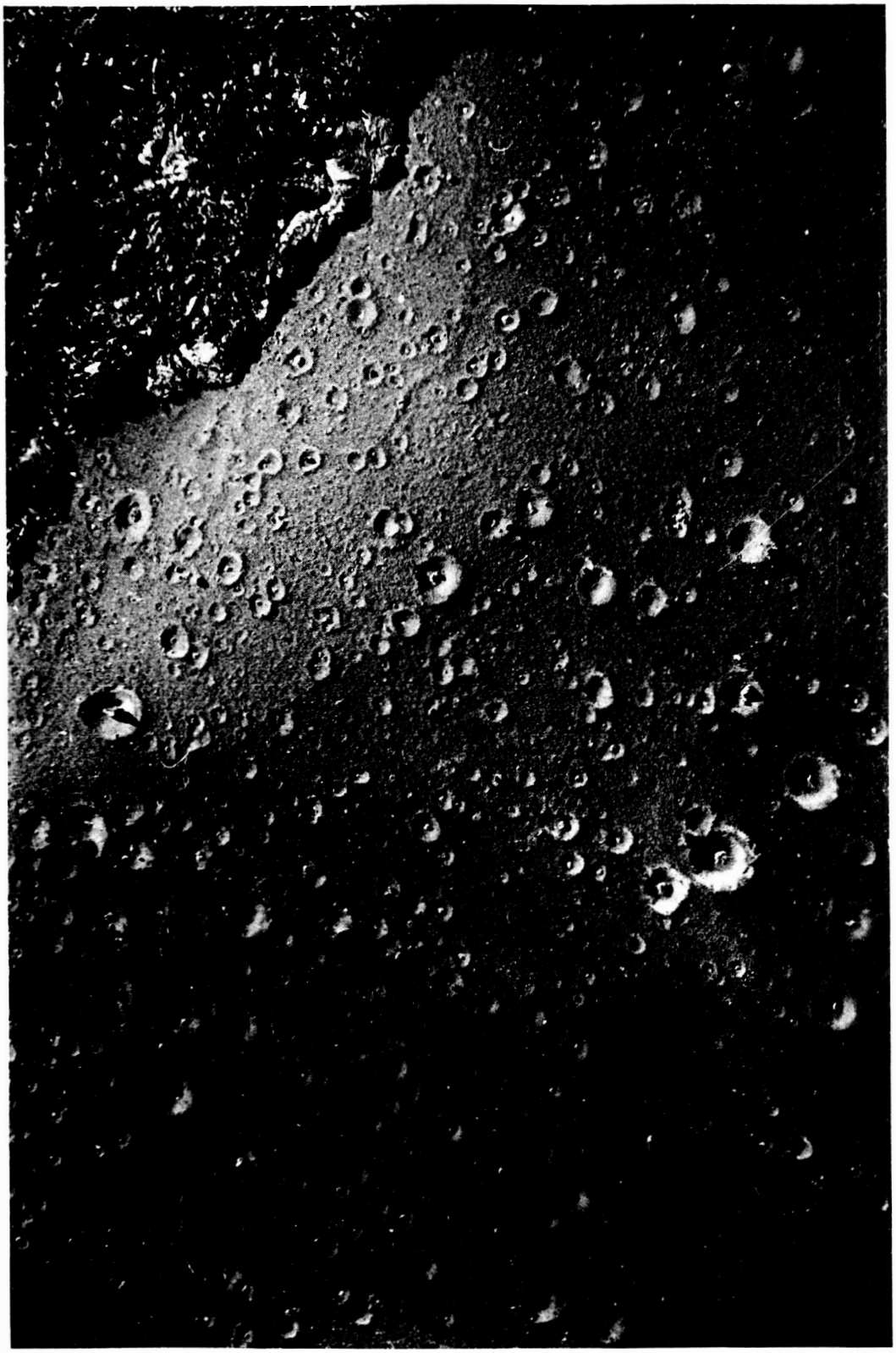

Fig. 34. Aerial photograph of impact craters produced February 1960 on a gentle slope covered with scoria of Laimana Crater, Hawaii. (Lava stream in upper right. Craters up to 3 m diameter formed by solid basalt blocks ejected nearly vertically from volcano. Sun angle corresponds to *Ranger VII* photographs; courtesy L. Nichols.)

A fuller discussion of the different types of craters encountered on the *Ranger VII* records will be published elsewhere.

F. The Structure of the Mare Floor

The mare floor was observed with the highest resolution on the last several P frames. Two photomosaics of these were made by placing appropriately enlarged P frames on enlargements of A199 (no rectification was applied to A199 for the 25-deg deviation from normal viewing). The results are shown in Fig. 36. It is seen that the darker areas running between the various shallow craters as continuing bands are resolved into much structural detail, similar in appearance to tree bark (e.g., Ponderosa pine) or glacial moraines. The continuing flow pattern on the P frames somewhat resembles patterns observed in terrestrial lava flows, as seen in Figs. 20–22. These are aerial views of recent (uneroded) lava flows on Mauna Loa, Hawaii, at approximately 12,000 ft elevation, near the northeast fissure emanating from the main caldera. Particularly, the pattern shown in the foreground of Fig. 22 is similar to the pattern seen in Fig. 36. The Hawaii pattern is that of a basaltic flow of aa, a clinkery mass pushed in place by an underlying lava flow. Its resemblance to a glacial moraine stems from the similarity of the mechanism of motion and deposition, a two-layered process.

Reference has been made to extensive flows in Mare Imbrium (up to 200 km long) which indicate highly fluid lavas as the carriers. The terminal walls of some of these flows (Figs. 16, 17) are very similar to those shown in Fig. 22 (right edge) and indicate a damming action by the solid crustal cover. Since pumiceous lavas are viscous and do not produce the nearly level flows shown in Figs. 16 and 17, one surmises that only the upper 10 m or so of the mare surface are structured as pumice, reticulite, or rock froth, the deeper layers being much less vesicular.

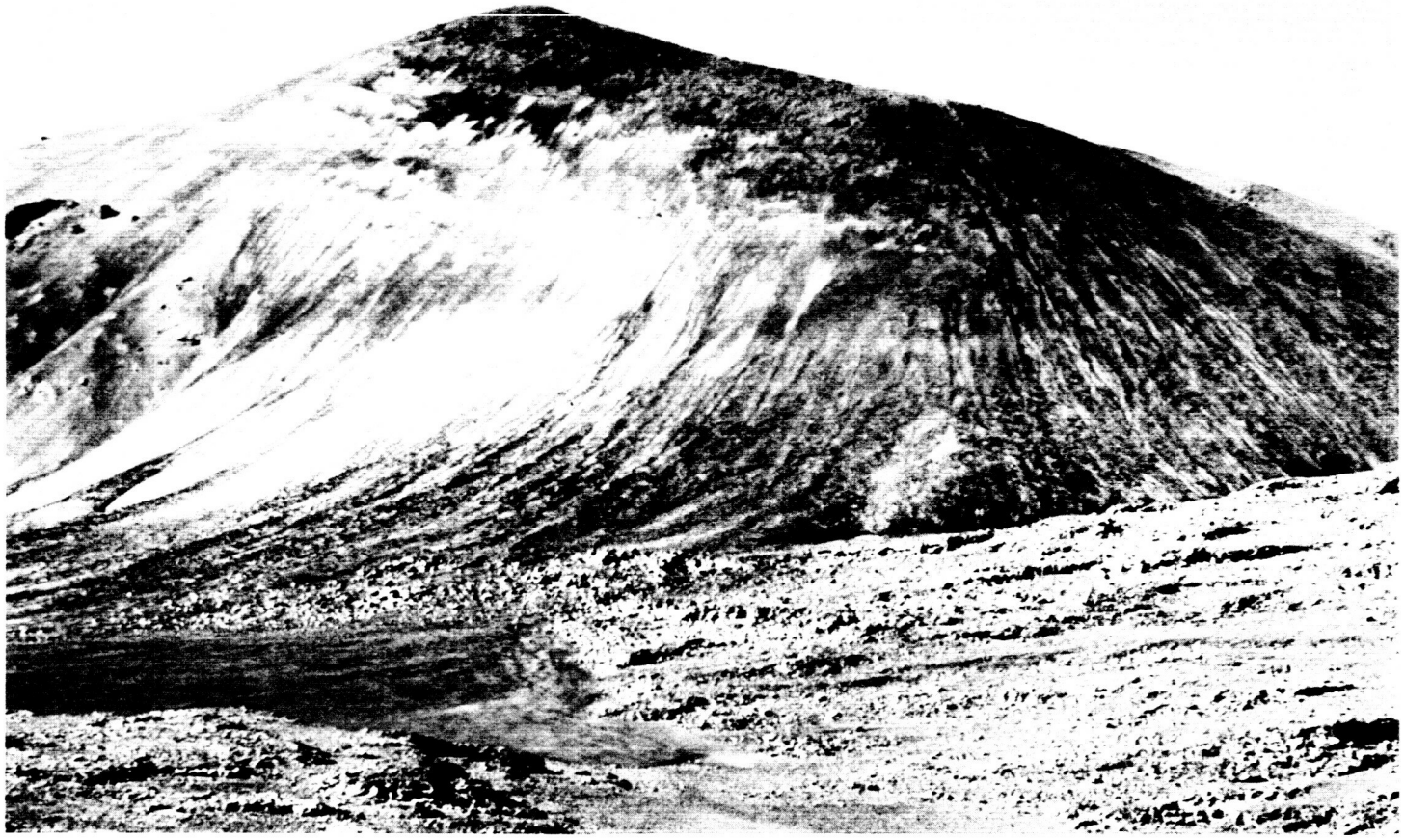

Fig. 35. Patterns of slumping on weathered surface of Puu Poliahu, Hawaii, resembling patterns on interior walls of lunar craters.

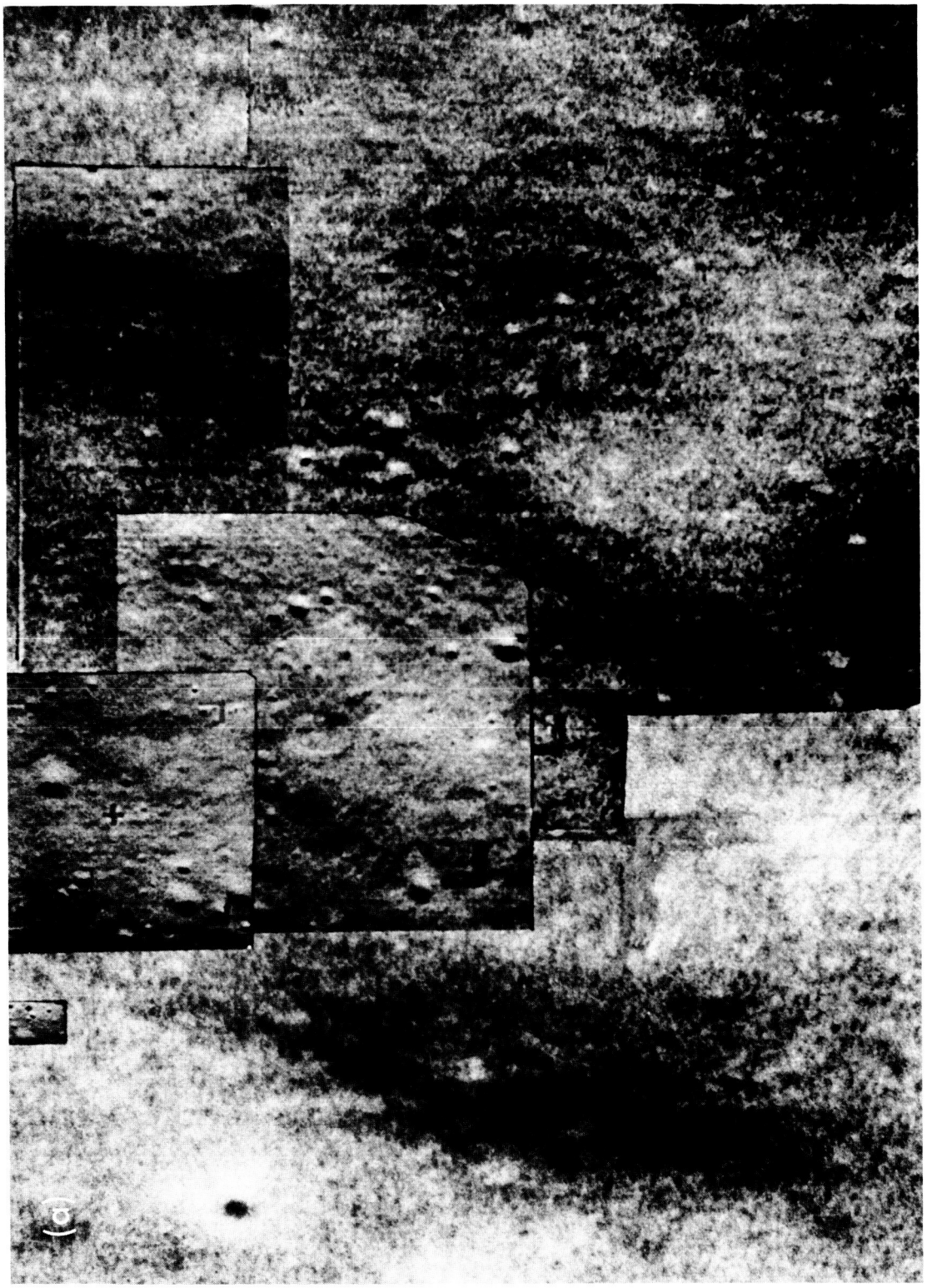

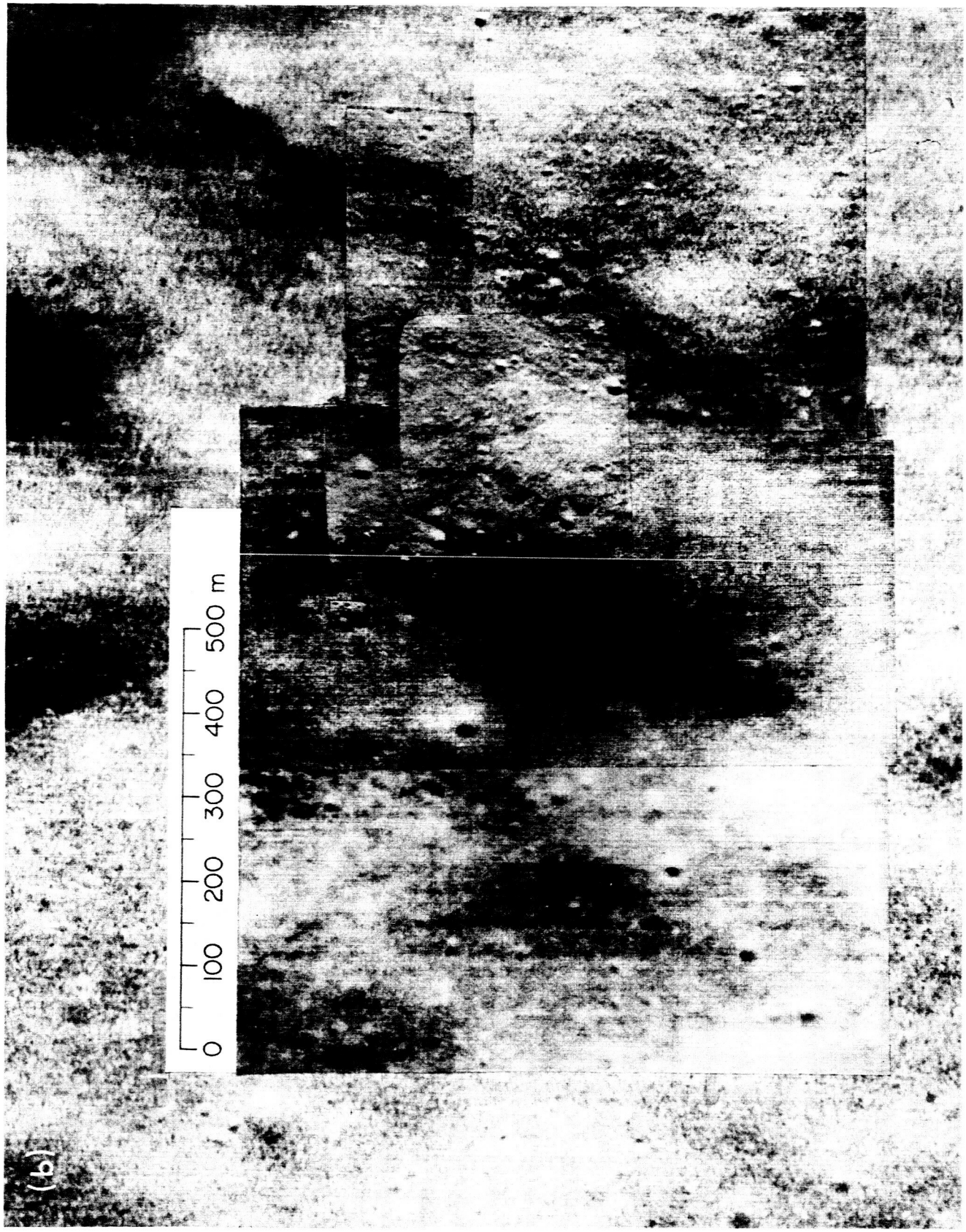

Fig. 36. (a) Photomosaic on A199 with several P frames superposed; (b) independent composition of (a) with computer clean-up from A199 by Dr. R. Nathan (JPL).

The darker areas on Fig. 36, resolved into the tree-bark structure, could, in principle, either be slopes inclined away from the Sun and thus be both darker and show more detail; or they could be nearly level terrain and actually be darker (true mare surface, without the overlay of Tycho ray material), as well as possessing more true relief. The first factor appears to dominate. Some tree-bark-type relief is weakly shown even on frame P979(2), which is in a brighter area. The pattern is seen over a somewhat wider area on the mosaic composed by E. A. Whitaker, presented in Part VI.

One striking impression gained is that the fine ridges and troughs shown on the last P frames have a rounded appearance, with a rounding-off scale of roughly 1 m, as if a buffeting action on the lunar surface had reduced all sharp relief. If further study sustains this conclusion, the effects of micrometeorite bombardment and spray of secondary material may be held responsible.

Essential in further studies will be a maximum effort of picture clean-up and enhancement. Preliminary results by analog methods on the "boat" structure on P977(2) are found in Fig. 37. A scale model at 1:500 of the region best covered has been composed with great care by the sculptor R. Turner at this Laboratory, with the author's collaboration, using A199 and the last P frames. Marginal detail was entered only when confirmed on at least one other frame. The smooth areas in the model are not necessarily devoid of structural detail on the Moon but are areas where the Sun angle was too high to bring out the low relief. A photographic reproduction of this model, exposed to the Sun at 23 deg elevation, is shown in Fig. 38; its scale is about 1:2,000.

The gain of about 5 in average resolution over the last A frame (Fig. 31) has clearly been of decisive importance for revealing the mare surface. The field of Fig. 38 partly overlaps with ACIC map, RLC 5 (scale 1:1,000), but our model was constructed directly from the *Ranger* records and somewhat exceeds the ACIC representation in detail extracted. Many of the lineaments shown in Fig. 38 appear to belong to the lineament families reviewed in Section H.

The last eleven B frames, 190–200, show that the shallow dips noted in Fig. 31 are typical of the mare surface, also outside the Tycho ray. They appear to cover an appreciable fraction of the lunar surface and, on the B frames, are mostly between 150–300 m in diameter, in agreement with the prominent dips seen in Fig. 31.

This distribution indicates that the dips antedate the (recent) Tycho event and that instead, as suspected earlier, their visibility on the lower-resolution photographs was enhanced by the ray, much as snow may enhance the aerial visibility of terrestrial topography.

In addition to several extremely shallow dips and a few deeper ones, again mostly in the diameter range of 150–300 m, frame B200 shows a prominent dimple crater near the center of the frame nearly 100 m wide and some 10 m deep. A very similar object is seen in the extreme upper margin. The fields of B197, 198, and 199 are covered by the shallow dips for at least half the surface area. Frames B193–197 indicate that *the dips avoid mare ridges,* not inconsistent with the structure of these ridges as sills, as discussed in Section I, and with the explanation of the dips as due to collapse.

The depressions appear to have some preferential depth, near 10 m, although both much shallower and somewhat deeper dips also occur. This depth may conceivably be related to the depth of the rock-froth layer.

There is some evidence for a second preferred depth, at about 100 m; at least, some craters are found that single out this depth by showing a layer of a different color. Bonpland G has a dark band at about 100 m on B185–186; Bonpland HB shows a light band on B196; Bonpland JJ seems to have a flat layer on A197, and a crater just northwest of Bonpland JF shows a band on A198 at this depth.

Several members of the Experimenter Team have commented on the low frequency of ray craters with diameters less than about 30 m (although exceptions are found; cf. Fig. 31). This also could be attributed to the thickness of the rock-froth layer. A 30-m primary crater will have a depth of 6–8 m. A small crater found in the rock froth would probably not show crater rays; but a larger crater, penetrating into the denser rock below, could have such rays. The thickness of 6–8 m might possibly be a measure of the average depth of the layer of rock froth.

The absence of rocks strewn all over the lunar surface is a striking aspect of the *Ranger* photographs. As reviewed above, this absence is likely to be attributable to the rock-froth structure of the upper layers of the mare.

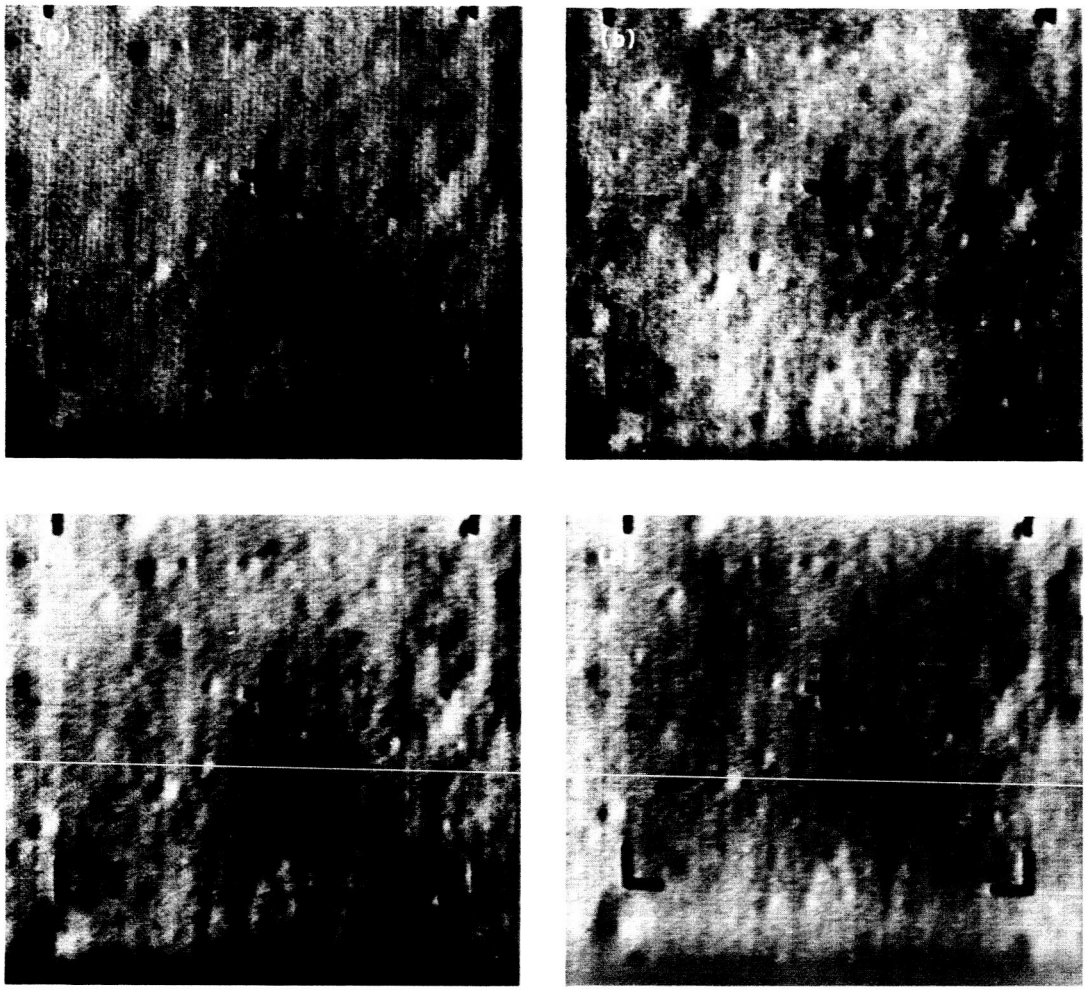

Fig. 37. Frame P977 (2): (a) original film record; (b) vertical lines removed by hand (E. A. Whitaker); (c) by compensation with noise mask (E. A. Whitaker); (d) from two superposed negatives displaced half a spacing (T. Coffeen).

G. The Frequency of Lunar Craters

The frequency distribution of crater diameters can be used both to estimate the age of lunar formations and to investigate the nature of the craters themselves. The following account is based on W. K. Hartmann's work.

The age of a lunar province can, in principle, be determined from the number of its craters and a knowledge of the mean rate of crater formation since the formation of the maria. A preliminary estimate of the latter has been made on the basis of studies of the current influx of meteorites and of fossil meteorite craters on the Earth. It is found that the lunar rate for craters of diameters larger than 1 km is approximately $5 \times 10^{-4}/\text{km}^2/10^9$ years.

Earth-based photographs have been used to determine the number of craters per square kilometer in the mare regions of the Moon. Resolution limitations prohibit complete counts below 5 km diameter. The *Ranger VII* photographs have been used to extend the counts to craters much smaller than 1 km. These counts, which apply to Mare Nubium and Mare Cognitum, fall precisely on the curve for all the maria in the northern hemisphere, as determined from the Earth-based photographs. The number of craters larger than 1 km was found to be about $18 \times 10^{-4}/\text{km}^2/10^9$ years and, based on the mean cratering rate given above, implies an age of about 3.6×10^9 years. This agrees well with estimates of the age of the Moon based on isotopic age determinations of meteorites, i.e., 4.5 to 4.7×10^9 years.



Fig. 38. Photograph of a scale model of the part of the lunar surface covered by high-resolution P frames. (Produced by the sculptor Ralph Turner with the collaboration and supervision of the author, using shadow lengths and stereo viewing to estimate vertical relief. The model is the result of a painstaking intercomparison of all *Ranger* data available. Approximate scale, 1:2000; 2 m to 1 mm.)

Hartmann's studies are based on the new catalogs of crater diameters published by Arthur, Agnieray, Horvath, Wood, and Chapman (Ref. 15). With the numbers of post-mare craters plotted on a log-log diagram in equal increments of log diameter, Hartmann has found that for them, the relationship is linear over the entire range of 5 to 100 km. Older groups of craters show a linear relationship only at larger diameters, and it appears that among the oldest groups, some erosion or destruction mechanism has erased the smaller craters.

The *Ranger VII* photographs allow these studies to be extended by nearly four orders of magnitude. The areas selected for the crater counts were, for each range of crater diameter (i.e., image resolution), those that were as free as possible of clusters of secondary craters. The last frames were in a region in which crater rays were nearby or partly overlapping, so that secondary craters were not completely absent. Since *Ranger VII* impacted in a mare, we are concerned with the post-mare distribution, which is illustrated in Fig. 39. The linear relationship found from Earth-based photographs extends down to at least 5 km. The fitting of the *Ranger* data to the Earth-based data is excellent, which means that the crater density in Mare Nubium and Mare Cognitum equals the average for the maria in the northern hemisphere. At diameters of 32–1000 m, however, there are more craters than expected on the basis of a linear extrapolation from larger diameters. The craters from 250–1000 m give rise to a new slope in the distribution curve, whereas at diameters less than 32 m, the numbers again approach the extrapolation.

The interpretation of this curve is not complete. The excess of craters from 32 to 1000 m probably represents the inclusion of secondary craters in spite of efforts to avoid them and of the depressions and dimple craters noted in Section G. It is possible that the diameter distribution observed of primary craters is linear over the entire diameter interval from 2 m to 1000 km and that the depressions and dimple craters cause the excess from 32 to 1000 m, peaking at 250 m.

Since (1) there is no clear evidence for a shortage of primary craters less than 1 km in diameter, (2) the shapes of the secondary craters and the depressions cannot simply be used as a criterion for age because they are formed in all shapes and depth-to-diameter ratios down to $\frac{1}{20}$ or less, and (3) the Tycho impact is probably a comparatively recent event in lunar history in any case, it is concluded that the varied shapes observed are not a reliable basis for an estimate of the rate of lunar erosion.

A direct estimate of the erosion rate may be made from the influx of particles onto the Moon. The term erosion with reference to the Earth includes all processes by which matter or rock is loosened and moved. On the Moon, erosion is caused by incoming particles ranging in mass from asteroidal to atomic.

The influx rates are such that for particles of mass greater than 1 g, impacts are infrequent and widely dispersed; they result in distinct craters, so that we can refer to the effect of large masses as "cratering." Cratering does not erode the surface in-between except insofar as secondary throwout strikes such areas, and this must be estimated for a given spot, such as the *Ranger VII* impact point.

In the mass range from 1 g to atomic masses, a given square centimeter of mare will have been hit repeatedly; this effect is referred to as "sandblasting." Most of the sandblasting mass influx is concentrated in particles of the order of 10^{-4} to 1 g in mass. A total mass of about 1 g/cm^2 has fallen on the maria in the form of sandblasting particles. Secondary particles of lunar material thrown out onto the lunar surface in the sandblasting process form a layer of perhaps 20 g/cm^2. It should be noted that when impacting particles of less than 1-g mass strike an open, porous surface such as hypothesized for the Moon, ejection of secondary particles is severely impeded. Therefore, although the impacting particle may dislodge up to 100 or 1000 times its own mass, the secondary throwout will be much less. Each sandblasting particle may knock nearly its own mass off the Moon, and the net effect of sandblasting erosion may be a slight mass loss by the Moon.

Atomic-sized particles and radiation cause "sputtering" of material. It has been estimated that a layer on the order of 10 cm deep has been lost in this way.

The net effect of sandblasting and sputtering will be a softening of relief on a scale of 10 to 100 cm. The secondary throwout by cratering in the region of the *Ranger VII* impact blankets the surface by a layer probably less than 1 m in depth. This follows from the fact that not even the brightest rays are as much as 10 m deep, as their relief cannot be detected from the Earth, and the *Ranger VII* impact site is only very weakly rayed.

It is concluded that the total effect of the direct influx of cosmic material and secondary throwout material in the region of the *Ranger VII* impact has been a softening of vertical relief and a mixing of surface layers on the order of 10 to 100 cm in depth.

The impact origin of lunar craters as a class is given strong support by both the frequency distribution and the form of the primary craters as revealed by the *Ranger VII* photographs. Since the frequency distribution of meteoritic and asteroidal masses is known, one may use the theory of cratering to predict the diameter distribution of primary lunar craters. This has been done, and it is found that (1) the straight line in the log-frequency–log-diameter plot in Fig. 39 is predicted, (2) the slope of the predicted line is very close to that observed, and (3) the number of lunar craters is compatible with the observed flux of meteoritic material. If the lunar craters were volcanic, the correctness of these conclusions would be fortuitous, and one would have to explain why no meteoritic craters were present.

In addition, the *Ranger VII* photographs give detailed views of craters of about 1 km diameter, which we may compare with terrestrial examples. The lunar craters are shown to be bowl-shaped, as are the nuclear explosion craters on the Earth. They do not have vertical walls, as do volcanic collapse craters such as Halemaumau in Hawaii. Furthermore, there is no evidence of cinder-cone structures, which are common in regions of collapse craters on the Earth. Yet, in the continental regions, which are not covered by the mare material, one can commonly see small craters (up to a few kilometers in diameter) arranged in chains, graben, and other structures that attest to volcanic activity. In addition, the maria themselves give every evidence of being lava flows, eroded by the same rain of material discussed above. Therefore, the Moon's surface, considered *in toto*, has been shaped both by internal volcanic agencies, responsible for the flooding of maria, small volcanic structures, and probably the collapse craters mentioned; and by external meteoritic and cometary impacts, responsible for primary and secondary craters and the mild surface erosion.

H. Small-Scale Lineaments on the Ranger VII Photographs*

The *Ranger VII* photographs reveal faint linear structures consisting of crater chains, elongate craters, shallow linear depressions, and several ridges. These features have been mapped on three rectified ACIC photomosaics of the *Ranger VII* photographs and are visible on the last P_1 and P_3 frames. Several of the lineaments are illustrated by white lines in Fig. 40. The three photomosaics cover areas of 2,856, 13.5, and 0.139 km^2 (R1, R2, and R3 in Fig. 40), while the last P_1 and P_3 photographs encompass areas of approximately 1,200 and 1,600 m^2, respectively. Azimuth–frequency diagrams of the lineaments have been constructed and compared with similar diagrams of lineaments in the terra regions adjacent to the *Ranger VII* impact site. The latter lineaments were mapped from Earth-based photography in a previous study, and their length and true selenographic azimuths were computed on the IBM 7072 computer of the University of Arizona Numerical Analysis Laboratory. The terra regions consist of two areas (T1 and T2 in Fig. 41) to the south and northeast of the *Ranger VII* impact site. Each area encompasses 64,380 km^2. Figure 42 shows the area mapped for lineaments from *Ranger VII* photography and several neighboring major lineaments which are intermediate in size between those resolved on Earth-based photographs and those on the *Ranger VII* photographs.

Figures 43 and 44 are lineament azimuth–frequency diagrams of the terra areas adjacent to the *Ranger VII* impact site. They show that the lineaments are oriented in three principal directions (NE–SW, NW–SE, and N–S) and form parts of three global systems of lineaments (Ref. 15). The strong north–south peak in Fig. 44 is part of the Imbrium radial system, while the peak in Fig. 43 may be part of the global north–south system or the Imbrium radial system.

Small-scale lineaments in the *Ranger* photographs were separated into negative features (linear depressions, crater chains, and elongate craters) and positive structures (linear segments of ridges). Azimuth–frequency diagrams of the negative structures are presented in Figs. 45–49. Figure 50 is a similar diagram of linear portions of mare ridges in Mare Cognitum. These features occur within the area encompassed by the ACIC *Ranger VII* chart RLC 2, and were mapped from low-phase-angle Earth-based photography and the *Ranger* photographs. Figure 51 is an azimuth–frequency diagram of the small-scale segmented ridge structure in area R1. The directions of Tycho, Copernicus, and Bullialdus are shown on the diagrams of the negative structures in the *Ranger* areas. In addition, the azimuths of four major linear features, shown in Fig. 42, are illustrated in Figs. 43–47. These features are in the immediate vicinity of the mapped *Ranger* areas and consist of (1) a 10-km linear mountain

*This Section was prepared by R. G. Strom.

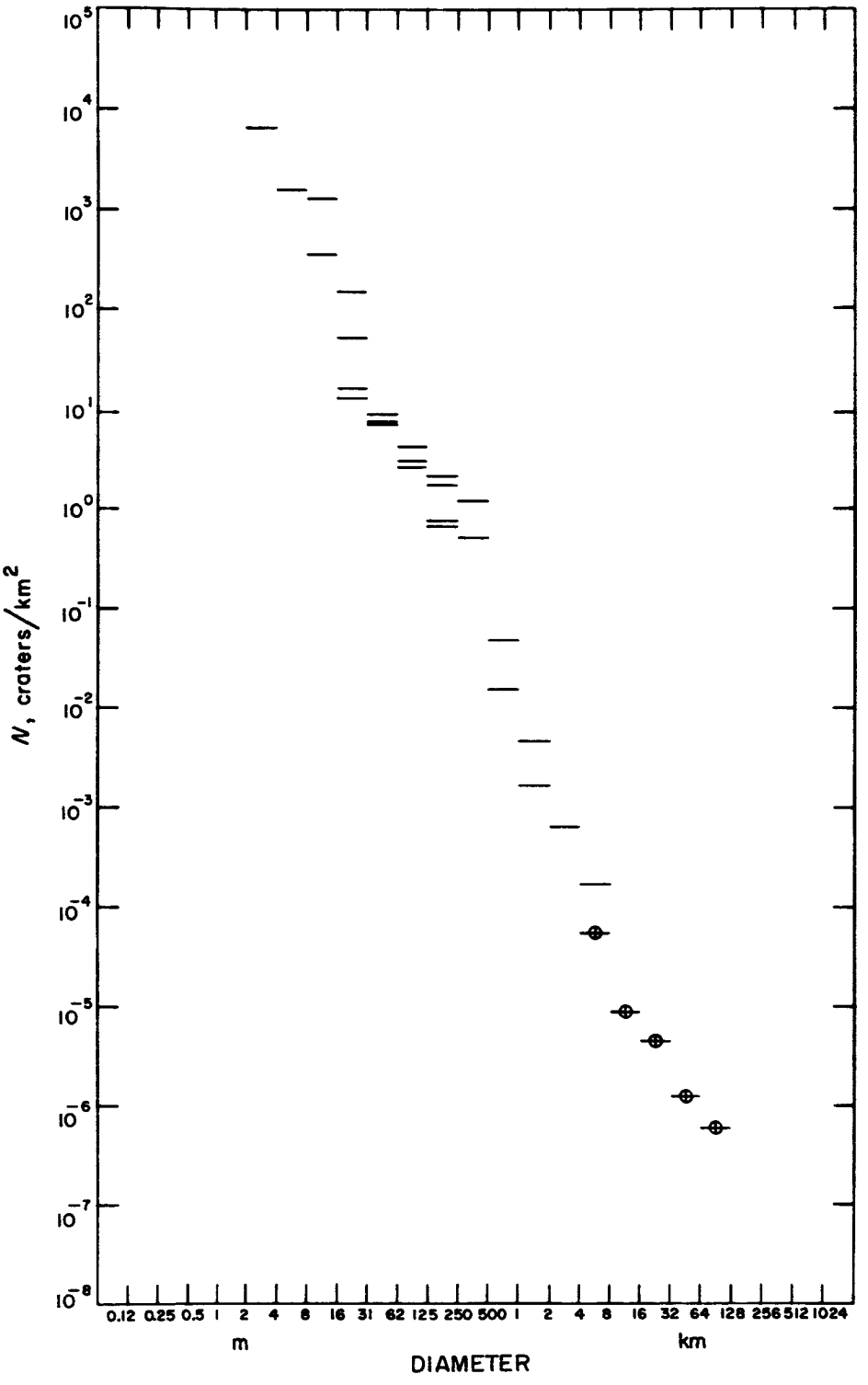

Fig. 39. Post-mare diameter distribution of lunar craters from Earth-based and *Ranger* photographs (Hartmann).



Fig. 40. ACIC rectified photomosaic of *Ranger VII* photographs, showing location and relative size of mapped areas. (White lines indicate several linear structures.)

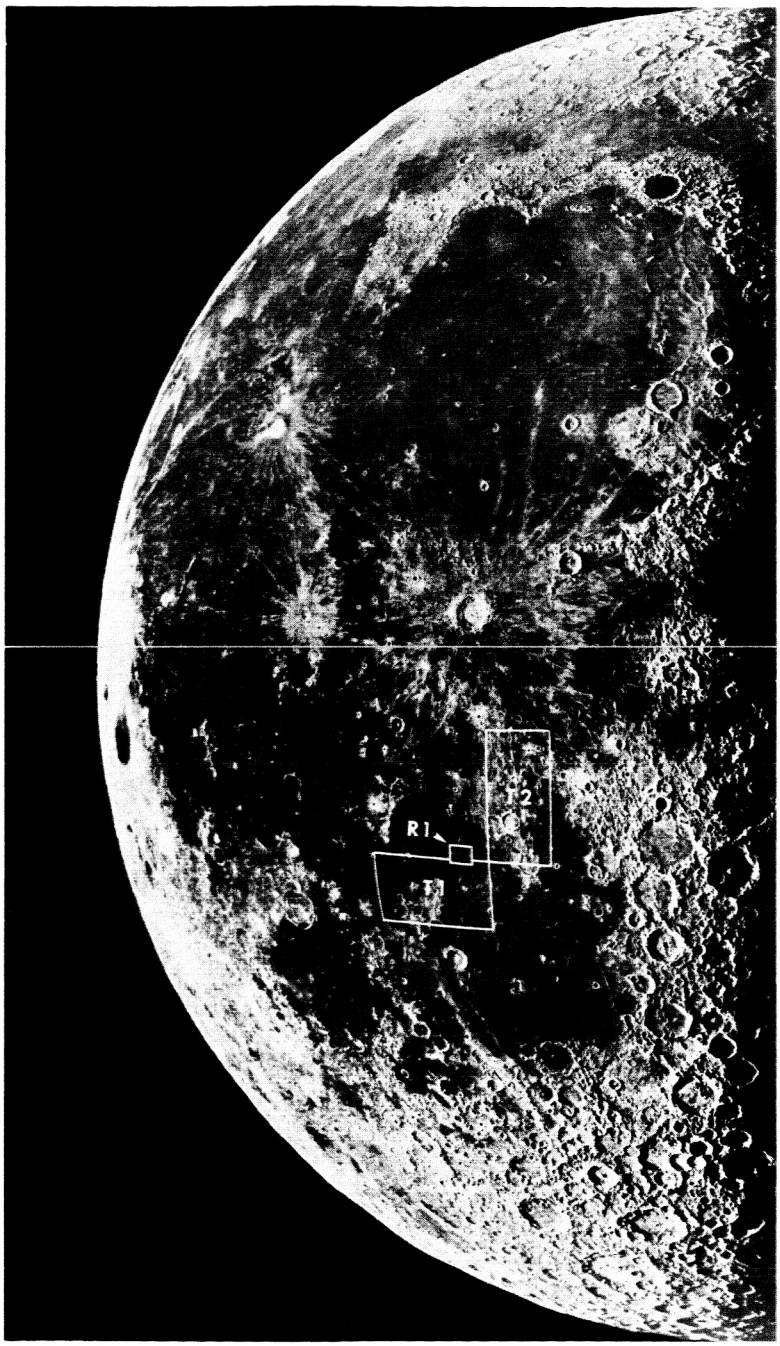

Fig. 41. Location of areas mapped for lineaments from Earth-based (T1 and T2) and *Ranger VII* (R1) photographs.

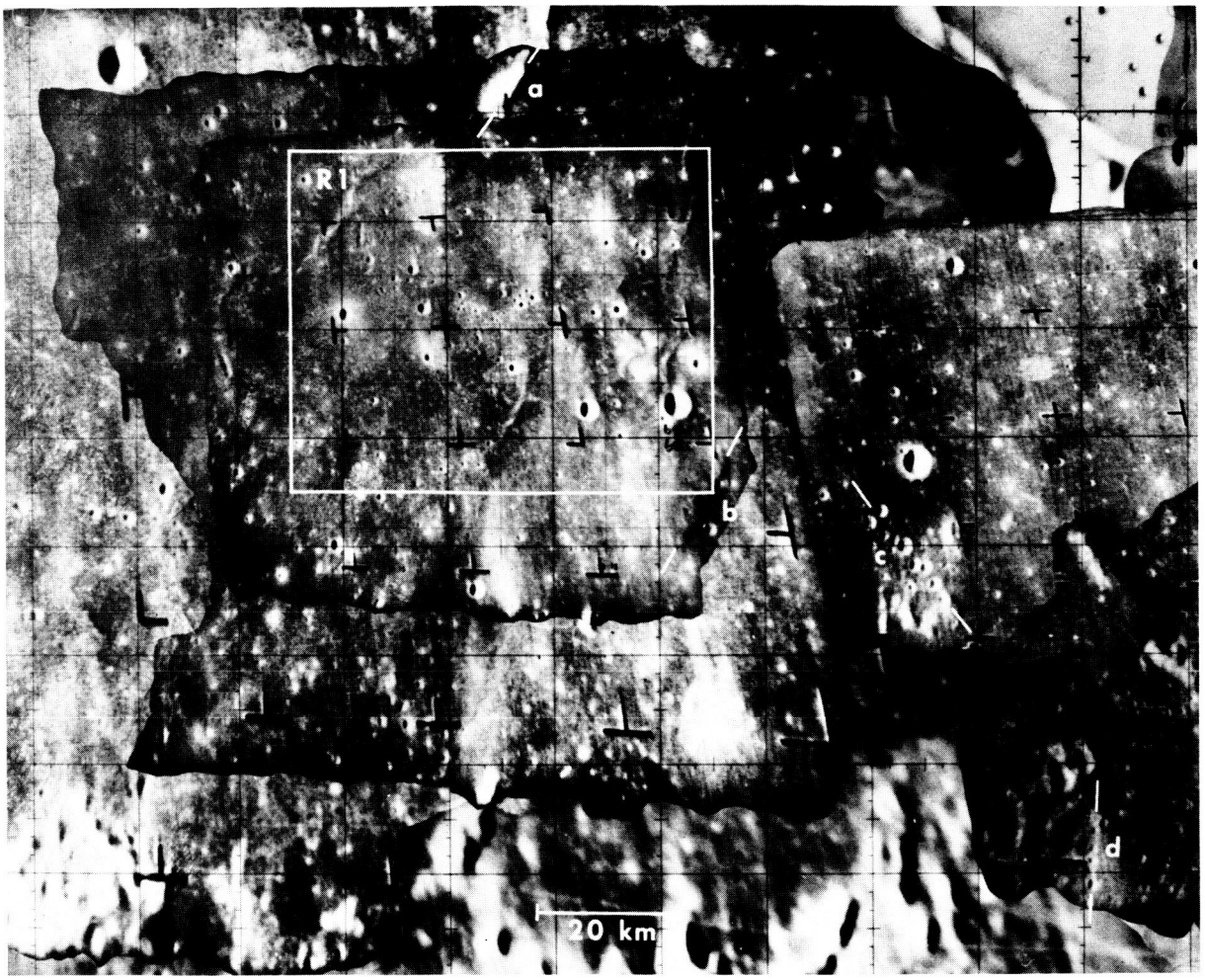

Fig. 42. ACIC rectified photomosaic of *Ranger VII* photographs showing major linear structures which coincide with directions of lineaments in areas R1, R2, R3, T1 and T2. (Linear structures are between white lines at a, b, c, and d.)

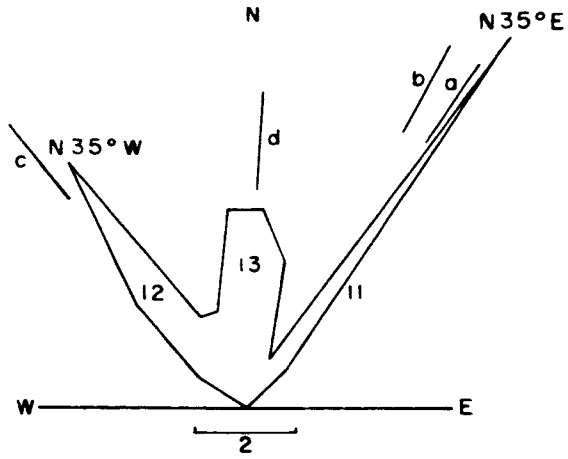

Fig. 43. Azimuth–frequency diagram of lineaments in area T1. (Number of lineaments represented by each peak and directions of lineaments a, b, c, and d, shown in Fig. 42, are indicated. Lineament length = 8–39 km; average length = 18.7 km.)

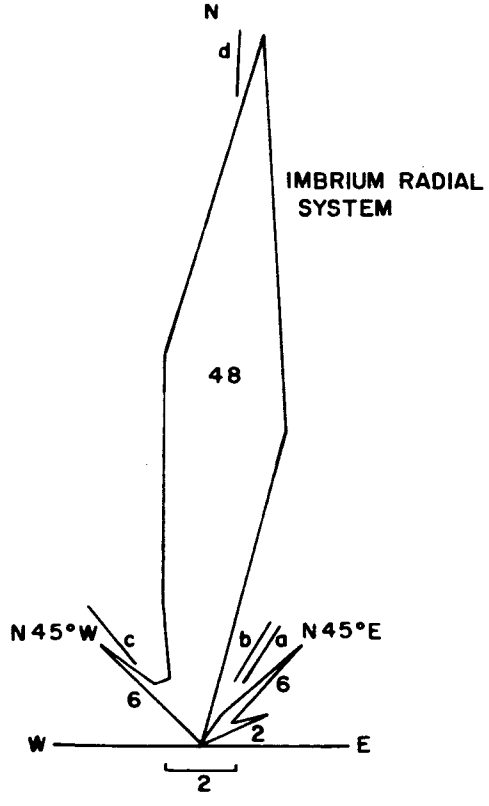

Fig. 44. Azimuth–frequency diagram of lineaments in area T2. (Indications are the same as in Fig. 43. Lineament length = 5–63 km; average length = 19.8 km.)

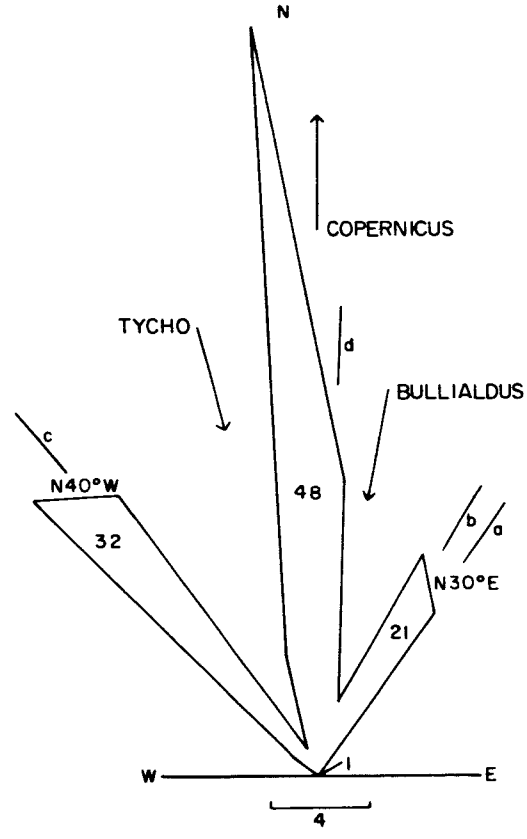

Fig. 45. Azimuth–frequency diagram of lineaments in area R1. (Number of lineaments represented by each peak, directions to Tycho, Copernicus, and Bullialdus and azimuths of lineaments a, b, c, and d, shown in Fig. 43, are indicated. Lineament length = 0.4–6 km; average length = 1.1 km; lineament density = 0.04 lineament/km².)

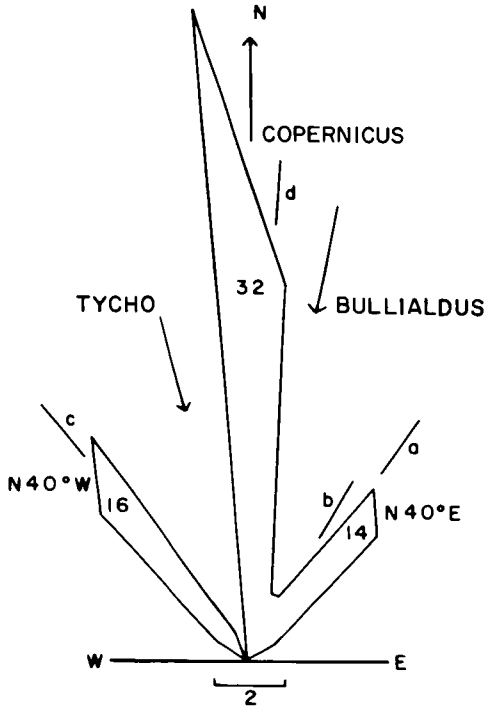

Fig. 46. Azimuth–frequency diagram of lineaments in area R2. (Indications are the same as in Fig. 45. Lineament length = 50–380 m; average length = 114 m; lineament density = 4.7 lineaments/km^2.)

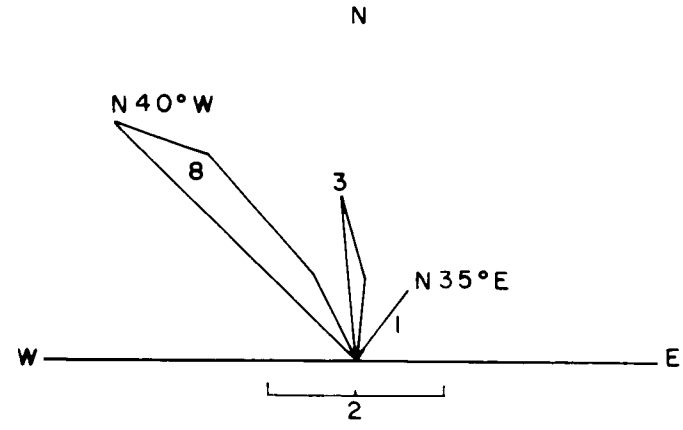

Fig. 48. Azimuth–frequency diagram of lineaments on last P_3 photograph. (Number of lineaments represented by each peak is indicated. Lineament length = 2.8–9.3 m; average length = 5.4 m; lineament density = 7094 lineaments/km^2.)

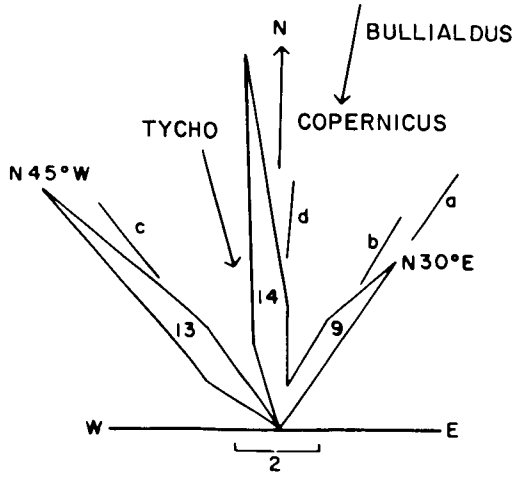

Fig. 47. Azimuth–frequency diagram of lineaments in area R3. (Indications are same as in Fig. 45. Lineament length = 12–53 m; average length = 21.4 m; lineament density = 252 lineaments/km^2.)

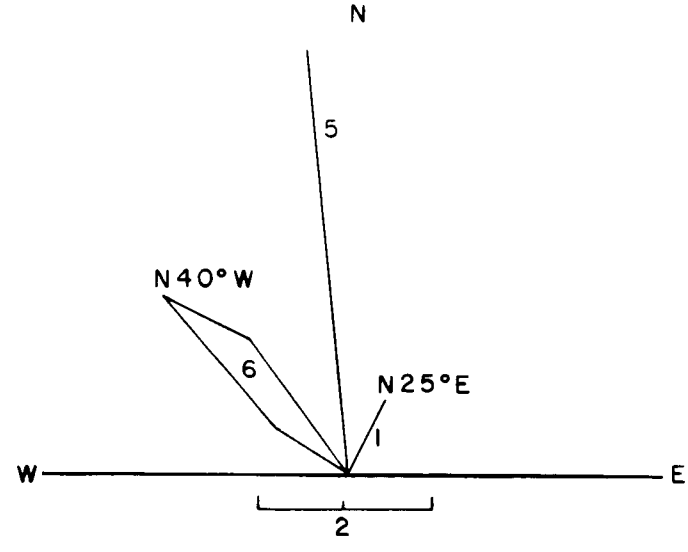

Fig. 49. Azimuth–frequency diagram of lineaments on last P_1 photograph. (Number of lineaments represented by each peak is indicated. Lineament length = 3–17.5 m; average length = 4.5 m; lineament density = 9876 lineaments/km^2.)

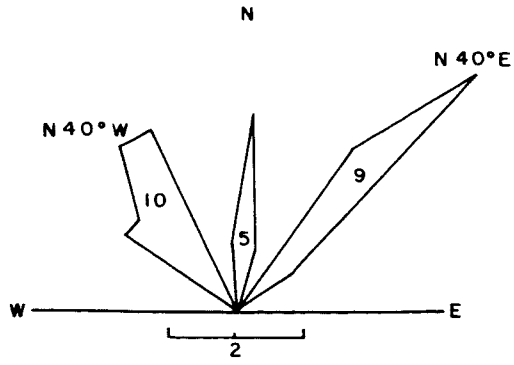

Fig. 50. Azimuth–frequency diagram of linear mare ridges occurring in western Mare Cognitum.

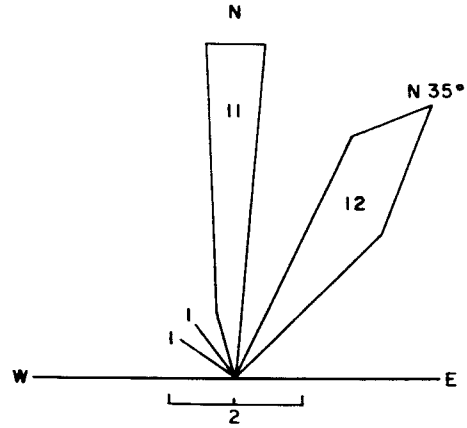

Fig. 51. Azimuth–frequency diagram of fine segmented ridge structure in *Ranger* area R1.

with a crater on its crest, (2) a 15-km dark ridge which is probably a lava extrusion along a fracture, (3) a 17-km linear cluster of craters, and (4) a 10-km-long crater chain.

A comparison of the azimuth–frequency diagrams demonstrates that the directions of small-scale negative and positive lineaments on the *Ranger VII* photographs coincide with the azimuths of large-scale lineaments in the adjacent terra areas (T1 and T2). The four linear structures shown in Fig. 42 also coincide with these azimuths. It has been suggested that the small-scale negative structures are secondary features which have resulted from clots of ejecta from Copernicus, Tycho, or Bullialdus. These ejecta could have rotated in flight and landed in three preferred orientations. To test this hypothesis, the azimuths of linear Copernican secondaries were measured in four areas radial to Copernicus. These areas are located in Mare Imbrium at distances of 6–16 deg north of the center of Copernicus. The *Ranger VII* impact site is 21 deg south of the center of Copernicus. Azimuth–frequency diagrams of the secondary features are illustrated in Fig. 52. The two lines near the top of each diagram are the radial boundaries of the areas. The diagrams show that the linear secondaries form fan-shaped patterns which coincide closely with the directions radial to Copernicus. There has apparently been some rotation of ejecta because not all lineations are exactly radial to Copernicus. Two notable exceptions occur in Fig. 52 (b) and (d). However, both these linear features coincide with the directions of lineament systems in the adjacent terrae and neither lies on ray material. Therefore, they may be structurally controlled and related to the major lineament systems. In any case, the Copernican diagrams do not resemble the typical three-peaked diagrams of the *Ranger* areas.

The fact that the directions of lineaments on the *Ranger VII* photographs coincide with the directions of the global fracture systems in the adjacent terrae indicates that at least the *Ranger* lineaments which trend in a NE–SW and NW–SE direction are structurally controlled and form part of the global lineament systems. Also, the similarity in direction of the linear segments of mare ridges—which are definitely tectonic in origin (see Section I)—and the small-scale negative lineaments supports the above contention. The north–south *Ranger* lineaments may be (1) fractures associated with the global north–south lineament system, (2) fractures related to the Imbrium radial system, or (3) secondary ejecta from Copernicus, Tycho, and Bullialdus. However, it is probable that some of the north–south lineaments are structurally controlled, because many of the segmented mare ridges and large-scale terra lineaments follow this direction.

The size of the small-scale lineaments has a bearing on the nature of the lunar surface. On the last P_1 and P_3 photographs, they average about 5 m in length and are as narrow as 1 m. The delicate nature of these lineaments —particularly those trending in a northeast direction— suggests that if a layer of fine debris is present, it is probably relatively thin (≤ 2 m); otherwise, these delicate features would be completely buried. If a debris layer were deposited prior to the formation of the fractures, then the layer would have to be relatively cohesive and strong in order to fracture.

I. The Mare Ridges

The *Ranger VII* photographs include many excellent records of ridges on Mare Cognitum. These ridges have been well portrayed in the ACIC *Ranger* series. Special

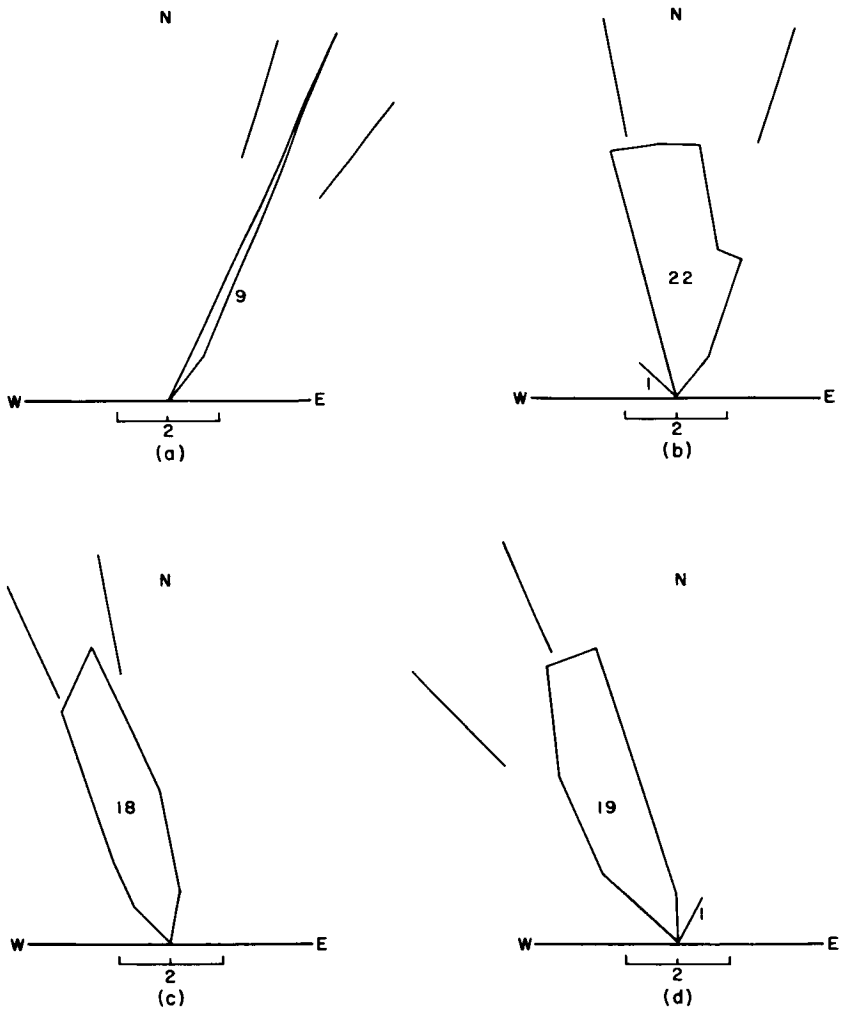

Fig. 52. Azimuth–frequency diagrams of linear features formed by Copernicus secondary ejecta.

reference is made to RLC 3 for the three ridges shown there, their structure and width, and the directions of the *en échelon* elements. It is noted that the ridges have these directions in common; they belong to the grid system discussed in Section H.

The narrowest dike-like ridge element shown on the *Ranger* photographs is found on B197. The element is about 50 m wide, 500 m long, and reaches about 10 m above the lunar surface. Except for the narrow dikes (and not in all of these), the ridges show no break through the lunar surface but are merely uplifted. The width of a ridge may be 250–500 m or exceed 1 km. That a dike has formed at depth, and that the general explanation developed in Section B applies, is seen from the test case on Bonpland HB, where a ridge crosses a crater. This crossing may be observed on B196 and on several P frames which were combined stereoscopically with B196. The dike crosses the crater floor centrally from southwest to northeast, casting a minor shadow below the northeastern half of the crossing. A bright band extends horizontally at a higher level (about 0.9 km down to the floor) along the west and north walls. This band appears to represent the cross section of the laccolithic intrusion by the dike responsible for the uplift of the western branch of the ridge, which continues narrow southwest of the crater. The broader branch of the ridge located just south of the center appears uplifted by a laccolith fed by three dikes that stem from a single main dike at depth and branch upward and outward along three planes. Together with the branch noted above, these would, in vertical cross section, resemble four branches in a river delta, spreading upward. This observation also explains how a ridge develops satellite branches roughly parallel with the main branch. Thus, the pattern of the dikes determines the number of branches; the width of each branch, if appreciable, may be due to a laccolith or sill. The concept of laccoliths is consistent with the result of the mare having bedding planes from successive lava flows, causing an alternation of weak and stronger

layers. If the structure planes possess *en échelon* fine structure, the ridges will likewise show this structure. This explains the "braided" appearance on lower-resolution telescopic photographs. A crossing of structure planes may lead to crossing ridges such as the remarkable system located northwest of Plinius (Fig. 9), the system in Mare Tranquillitatis near Lamont (Figs. 6, 7), and that shown in Oceanus Procellarum (Fig. 11).

It is also apparent from the *Ranger* photographs that some of the higher mountain ridges shown in Mare Cognitum are volcanic extrusions. The double-peaked range near the impact point, shown central on Fig. 26, is located on the crest of a ridge and is seen on A180–186 to have several craters on its crest and two remarkably symmetrical low volcanoes on its southern toe. A number of similar mountains on the south shore also appear to be formed on structural lines and crowned with volcanoes on their crests. By implication, the many linear mountains of the Carpathians, oriented in the Imbrium direction, may similarly be regarded as being of extrusive origin.

It is very remarkable that these extrusives, be they segments of ridges broken out to the surface, linear mountains such as those near Bonpland γ, or volcanoes such as occur near the toe of the Bonpland γ complex, are all *whitish*, much brighter than the mare floor. There seems to be again a parallel with Hawaii: the Mauna Loa lavas, which have been compared with the lunar maria (Sections B and F), do not show whitish coloration; but cinder cones, such as Laimana Crater, were initially covered with brilliant white material that was dissolved by rain. On the Moon, such deposits would remain within the bounds of surface erosion, which appears to have been limited.

J. The Scientific Significance of the Ranger VII Mission

The comments in this Section are restricted to the impact of *Ranger VII* on lunar science. The tremendous technological achievements of the mission need no emphasis.

The scientific impact has several aspects:

1. *Gain in resolution.* The best resolution ever achieved in ground-based lunar photography is 0.″15 or 270 m in a series of records covering a small part of the Moon, obtained by G. Herbig with the Lick 120-in. telescope in 1963. All previous "top-quality" lunar photography has resolutions of 500–1000 m; 1–2 km is considered "good quality." Frame P979 has two records, one having a resolution of 25, the other of 40 cm. The gain in resolution achieved by *Ranger VII* is therefore 1000–2000 ×. This achievement may be compared with the invention of a powerful microscope in medical science.
2. *Quality of the records.* The quality of the records is uniformly good to excellent. This is attested by the photographic reproductions of the A and B frames, now available. The B records in particular cannot fail to elicit the admiration of anyone familiar with astronomical photography. Steps are being taken to reduce the minor electronic interference that affects some of the P frames. Some additional information may be extracted from all records, particularly on small and shallow craters, by machine reduction methods.
3. *Ranger VII target selection.* In retrospect, no serious criticism can be made of the target selection. The mare region showed a variety of terrain, from the coastal area of Mare Nubium to a nearly bare mare floor to patches veiled by crater-ray material. Although nearly any site selected for a first *Ranger* mission would have yielded a wealth of new data, the choice of a mare has made it possible to solve, to a first order, several key problems and leads to a logical sequence of further steps in lunar exploration.
4. *Chief scientific results of the mission.* Outstanding among the results obtained are, first, the resolution of crater rays into clusters of secondary craters and their associated ray elements; the discovery that these ray secondaries are invariably bright at full Moon, contrary to the well known swarms of secondaries surrounding all post-mare impact craters, which are invisible at full Moon; the explanation, justified quantitatively, of ray craters as being due to impacts by comets. Next is the discovery of shallow depressions and dimple craters, covering much of the mare floor, and their interpretation as a karst phenomenon. Third, the interpretation of the ridges as due to dikes extruded into fissures caused by both global and mare-wide tensional forces; with these dikes branching and also spreading locally as sills or laccoliths, thus causing *en échelon* or braided ridge structures and also giving the ridges locally considerable width. These broad expanses do not appear to contain depressions or dimple craters, consistent with the explanation of these features as due to collapse. Fourth, the discovery of the "fine structure" of the mare floor where it is exposed. This structure somewhat resembles lava flows, but there appears to be a "rounding off" effect on the surface blocks, presumably caused by

particle impact; and there is much evidence for after-effects due to subsidence of the depressions and dimple craters. The numbers of primary craters appear to continue on a -2.5 power law in a log-frequency–log-diameter plot, with these craters covering less than 1% of the mare surface down to the meter range. Non-ray secondary craters are observed, some with central rock masses still visible. It is shown that for these, the crater and rock sizes are compatible with being caused by ejecta from primary impacts less than 1000 km away, and that there will be a progression of secondary crater shapes with distance from the primary, with the most distant secondaries likely to be complex grooves caused by a cluster of fragments. Another important observation concerns the presence and the azimuthal distribution of lineaments. These findings lead to the conclusion that the structural pattern found on Earth-based photography in the lunar crust in regions adjacent to the mare persists in the mare itself, down to scales in the meter range. This shows that the fracture pattern in the lunar crust is very basic in nature and omnipresent, extending right up to the lunar surface. The diagonal patterns are not due to Tycho or Copernicus or even Mare Imbrium. They resemble the pattern to be expected from a general north–south compression, as first pointed out by R. Strom, who studied some 10,000 lineaments within 60 deg from the center of the face of the Moon (Ref. 16).

Important conclusions can be derived on the nature of mountain chains, both within Mare Cognitum and on the shore lines. These mountains show small craters on their crests, clearly by their distribution not of meteoritic origin, indicating the plutonic nature of these ranges. By implication, such mountain ranges as the Carpathians are not ejecta from Mare Imbrium either, but similarly due to magmatic upwellings along structural planes radiating from the Imbrium impact region. A dark, presumably late post-mare structure, is shown in Fig. 28 (**m** – **m**), to which J. O'Keefe (Ref. 17) has called attention. It is composed of some 20 nearly parallel blocks, steeply inclined to the main direction of the mountain, an example of a composite pattern of the two diagonal lineament directions in Mare Cognitum.

5. *The ACIC maps.* It is fortunate that the Aeronautical Chart and Information Center, with its experienced staff and excellent production facilities, has undertaken to construct a series of maps on the basis of the *Ranger VII* records. These maps are made in the best tradition of lunar mapping and are a most convenient summary of the new surface data obtained. They are especially useful for nomenclature, coordinates, dimensions, orientations, and the location of lineaments which are so important in the interpretation of the lunar surface.
6. *Required further research.* One of the principal questions left open is the detailed explanation of the variety of crater forms and depressions recorded on the *Ranger* photographs. This problem will require theoretical as well as laboratory and field research.

   Another problem is the determination of contours by stereoscopy of the portions of the lunar disk suitably covered. A determined effort must be made to obtain improved Earth-based photography matching the *Ranger VII* records in solar phase angle. The construction of lunar section models would be incidental to this program.
7. *Economy of Ranger vs. Earth-based lunar photography.* In principle, very high image resolution can be obtained either by telescopes on the Earth with very large optics or by spacecraft near the Moon provided with modest equipment. As may be seen from the graphs included in the *Whitford Report on Astronomy* recently issued by the National Academy of Sciences, the cost of a 300–400-in. telescope would be in the vicinity of $100 million. Assuming that a site can be found for this supertelescope having sufficient atmospheric stability for its occasional use to the full limit of its potential, the resolving power obtainable would be 20–25 m. *Ranger VII* achieved a maximum resolving power 100 times larger. It is therefore obvious that detailed exploration of the lunar surface must be made by the general methods employed on *Ranger VII.* It is also apparent that the economy of the *Ranger* operation compares favorably with a maximum ground-based effort.
8. *Name of the mare.* It was fortunate that the impact area of *Ranger VII* was an unnamed small mare, situated between Mare Nubium and Oceanus Procellarum. With the mission successful and a wealth of entirely novel information on the mare obtained, it appeared appropriate to take advantage of this combination of circumstances in proposing a name for the mare that would henceforth commemorate and symbolize this scientific achievement. The name Mare Cognitum was proposed to and adopted by the International Astronomical Union on August 31, 1964, during its Twelfth General Assembly at Hamburg, Germany.

REFERENCES

1. Dobar, W. L., Tiffany, O. L., Gnaedinger, J. P., "Simulated Extrusive Magma Solidification in Vacuum," *Icarus,* Vol. 3 (1964), p. 323.
2. McCracken, C. W., and Dubin, M., *Dust Bombardment on the Lunar Surface,* NASA TN D-2100, 1963; also in *Lunar Surface Layer, Materials and Characteristics,* ed. by J. W. Salisbury and P. E. Glaser, New York: Academic Press (1964), pp. 179–214; Dubin, M., Personal communication on recent data evaluation.
3. van Diggelen, J., *Recherches Astronomiques de l'Observatoire Utrecht,* Vol. XIV, No. 2 (1958); reprinted as NASA TT F-188, 1965; Hapke, B., *Journal of Geophysical Research,* Vol. 68 (1963), p. 4571.
4. Shorthill, R. W., *Measurements of Lunar Temperature Variations During an Eclipse and Throughout a Lunation,* Report D1. 82-0196, Boeing Scientific Research Laboratories, 1962.
5. Evans, J. V., and Hagfors, T., "On the Interpretation of Radar Reflections from the Moon," *Icarus,* Vol. 3 (1964), p. 151.
6. Hartmann, W. K., and Kuiper, G. P., "Concentric Structures Surrounding Lunar Basins," *Communications of the Lunar and Planetary Laboratory,* University of Arizona, Vol. 1, p. 51.
7. Hartmann, W. K., "Radial Structures Surrounding Lunar Basins, I: The Imbrium System;" *Ibid.,* Vol. 2 (1963), p. 1; "II: Orientale and Other Systems; Conclusions," *Ibid.,* Vol. 2 (1964), p. 174.
8. O'Keefe, J. A., and Cameron, W. S., "Evidence from the Moon's Surface Features for the Production of Lunar Granites," *Icarus,* Vol. 1 (1962), p. 271.
9. Kuiper, G. P., 1958, *Vistas in Astronomy,* Vol. 2, ed. by M. Alperin and H. F. Gregory, London and New York: Pergamon Press, pp. 299–302.
10. Kuiper, G. P., *et al., Photographic Lunar Atlas,* Sheet D5, Chicago: University of Chicago Press (1960).
11. Wright, F. E., Wright, F. H., and Wright, H., "The Lunar Surface: Introduction," *The Solar System,* Vol. 4, Chicago: University of Chicago Press (1963), p. 37 ff.
12. Whipple, F. L., "Structure of the Cometary Nucleus," *The Solar System,* Vol. 4, Chicago: University of Chicago Press (1963), pp. 644–646.
13. Baldwin, R. B., *The Measure of the Moon,* Chicago: University of Chicago Press (1963), Table 13, p. 157 and Table 18, p. 177.
14. Thornbury, W. D., *Principles of Geomorphology,* New York and London: Wiley (1954), p. 321 ff.
15. Arthur, D. W. G., Agnieray, A. P., Horvath, R. A., Wood, C. A., and Chapman, C. E., "The System of Lunar Craters, Quadrant I," *Communications of the Lunar and Planetary Laboratory,* University of Arizona, Vol. 3 (1963), p. 1.
16. Strom, R. G., "Analysis of Lunar Lineaments I: Tectonic Maps of the Moon," *Communications of the Lunar and Planetary Laboratory,* University of Arizona, Vol. 2, No. 39 (1964).
17. O'Keefe, J. A., "Interpretation of Ranger Photographs," *Science,* Vol. 146 (1964), pp. 514–515.

IV. PRELIMINARY ANALYSIS OF THE FINE STRUCTURE OF THE LUNAR SURFACE IN MARE COGNITUM

Eugene M. Shoemaker
United States Geological Survey
Flagstaff, Arizona

The principal new facts obtained from the *Ranger VII* photographs pertain to features of the Moon's surface less than 300 m across and to the small details on larger features in the region of Mare Cognitum. These facts, when combined with prior knowledge about the Moon obtained with Earth-based telescopes, permit the formulation of a comprehensive model of the fine structure of the surface of Mare Cognitum and the development of hypotheses about processes which have led to the formation of the observed small topographic features. The formulation of a model of the fine structure and the development of hypotheses about the surface processes are important for two reasons: (1) such a model and set of hypotheses may be used to predict the nature of the surface to be expected elsewhere on the Moon and (2) formulation of a model consistent with the available facts is an essential first step in drawing inferences about the physical characteristics of the Moon's surface which are not directly observable in the photographs. Coherence and bearing strength, properties important in the problem of landing spacecraft on the Moon, are among the unknown physical characteristics of the lunar surface which we might attempt to infer. The predictions and inferences made from the model and working hypothesis that will be presented here are subject to test by further lunar exploration. I will start by reviewing the basic new facts that may be established from the *Ranger VII* photographs and by introducing previously known facts about the Moon that are necessary to formulate a model of the fine structure of a mare surface.

A. Major Facts Established by Ranger VII Photographs

Two basic kinds of facts about a planetary surface can be obtained from photographs or television imagery: (1) the topographic configuration and (2) photometric characteristics. Information drawn from a photograph about other physical characteristics, the processes acting on the surface, the structure, and the history of the surface are necessarily inferences based on the first two basic kinds of information. In the *Ranger VII* pictures, the new information obtained concerns chiefly small topographic features. These may be classified, for purposes of discussion, into negative- and positive-relief features. A certain amount of information important to constructing a model

of the fine structure may also be derived from detailed observations of the photometric heterogeneity of the surface.

1. Negative-Relief Features

The small topographic features revealed by the *Ranger VII* photographs of Mare Cognitum are almost all craters. Craters thus are not only the dominant large topographic features on the Moon but also the dominant small topographic form revealed by *Ranger VII*. The new craters observed show a wide range of shapes. Some of them may be recognized as belonging to certain classes of craters observed through the telescope, but a large number of the craters less than 300 m across cannot be classified by shape alone in the categories previously recognized by telescopic observations. In my opinion, there are, with one minor exception, no unequivocally identifiable negative-relief features less than 300 m in length in the *Ranger VII* photographs that cannot be classified either as a form of crater, a group of craters, or a topographic detail within a crater.

a. Shapes of craters. Two basic types of craters well known from telescopic observations can be readily identified in the *Ranger* photographs: (1) primary craters and (2) secondary craters.* These types are defined on the basis of morphology and distribution. Small telescopically observable primary craters are typically very uniform in shape. They are nearly circular in plan and have a distinct smooth raised rim, generally of nearly uniform height. The inner walls are also smooth, uniform, and steep. The walls are slightly concave upward; typical slopes of the wall near the rim crest are greater than 35 deg and, near the foot, about 25 deg. The average slope of the crater walls is typically between 30 and 35 deg. In primary craters larger than about 7 km in diameter, the steep wall terminates, at the foot, against a relatively smooth, level, circular floor. The diameter of the floor diminishes with size and is very small or absent in primary craters less than 7 km across; the walls thus extend to the center, or almost to the center, of these small craters. As has been remarked by Kuiper (Ref. 1), these remarkably uniform craters look as though they had been turned out on a lathe. They are scattered across the maria and other parts of the Moon without apparent control by other surface features. Some of them are surrounded by a bright halo, or a system of rays; others are not.

*Other classes of craters known from telescopic observations, such as chain craters and craters at the summits of domes, are apparently not represented in the high-resolution *Ranger VII* photographs and will not be discussed here.

With increased diameter, the primary craters are less regular in form. At 25 km diameter, some irregular hummocks are found in the rim, terraces occur on the crater walls, and irregularities begin to appear on the primary crater floor. At 50 or 60 km diameter, the rims are typically rugged and hummocky, the rim crest is uneven and commonly roughly hexagonal in plan, the walls are terraced, and the floor is marked by scattered hills and one or more prominent irregular peaks near the center of the crater. A swarm of small craters, which are barely resolvable through the telescope, surrounds a primary crater of this size. The greatest areal density of small craters in the swarm occurs at a distance of about one crater diameter from the rim crest of the primary. At greater distances, the secondary craters are clustered within rays or within arcuate and loop-shaped bands extending outward, in some cases hundreds of miles, from the primary crater. These small craters, whose forms can be distinguished only in the swarms that occur around very large primaries, are called secondary craters. Several thousand of them can be observed in the swarms that surround large primary craters such as Tycho (Fig. 1), Copernicus (Fig. 2), Aristoteles (Fig. 3), and Langrenus (Fig. 4).

The secondary craters that can be photographed with Earth-based telescopes (generally 1 km across or larger) are in most cases readily distinguishable in form from very small primary craters. The secondary craters are typically elongate, are generally shallower than primaries of corresponding size, and in most cases have low irregular rims, or in some cases no rims at all. Many elongate secondaries, when observed visually through the telescope under favorable conditions, are found to be composite, consisting of several small craters strung end to end or merged together. The secondary craters are found around primary craters with rays and also around those without rays. Around the ray craters, the secondaries occur within the rays and within the bright halo surrounding the ray crater. Secondary craters associated with primary ray craters, which are referred to the Copernican System of Shoemaker and Hackman (Ref. 2), generally exhibit raised rims and are commonly observed to be composite (Fig. 5). In the swarms of secondaries around rayless primaries, the secondary craters are generally devoid of rims and are commonly long shallow trenches of simple form (Fig. 6). Secondary craters on the maria associated with rayless primaries are referred to the Eratosthenian System of Shoemaker and Hackman (Ref. 2). Both Copernican and Eratosthenian secondaries are represented in the *Ranger VII* photographs.



Fig. 1. Telescopic photograph of Tycho showing part of its associated swarm of secondary craters. (The secondary craters appear as very small, closely spaced craters, many of which have diameters just above the limit of resolution and are scattered over much larger older craters surrounding Tycho. The diameter of Tycho is 88 km. Photograph from Lick Observatory.)



Fig. 2. Telescopic photograph of Copernicus showing part of its associated swarm of secondary craters. (The secondary craters are distributed over both mare surfaces and over the more rugged terrain surrounding Copernicus. Several hundred secondaries appear as very small craters which are just barely resolved. Distinct bands or loops of secondary craters are easily observed in the lower right-hand corner. The diameter of Copernicus is 91 km. Photograph from Mt. Wilson Observatory.)



Fig. 3. Telescopic photograph of Aristoteles showing part of its associated swarm of secondary craters. (A well defined loop of secondary craters extends to the upper right from Aristoteles on to the surface of Mare Frigoris. The diameter of Aristoteles is 91 km. Photograph from Lick Observatory.)



Fig. 4. Telescopic photograph of Langrenus showing part of its associated swarm of secondary craters. (The secondary craters extend outward from the hummocky rim of Langrenus as subradial bands of elongate craters on Mare Fecunditatis. Langrenus, 131 km in diameter, is the largest ray crater on the sub-Earth side of the Moon. Photograph from Lick Observatory.)



Fig. 5. Diagrammatic sketch of a composite secondary crater of Copernican age. (Copernican secondary craters that can be resolved with Earth-based telescopes generally have distinct raised rims and may show internal cusps. Based on telescopic observations of M. H. Carr.)

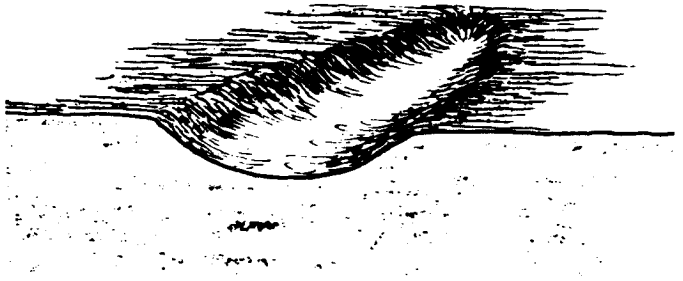

Fig. 6. Diagrammatic sketch of a secondary crater of Eratosthenian age. (Eratosthenian secondary craters generally have no observable raised rims or internal cusps. Based on telescopic observations of M. H. Carr.)

Primary craters. Primary craters are well represented in the *Ranger VII* photographs. They range in size from craters previously known from telescopic observation—such as Bullialdus, 62 km in diameter, and Darney, 16 km in diameter—down to 2 m in diameter, the size of the smallest identifiable primary craters shown in the last photographs obtained from the P cameras. For craters smaller than 7 km in diameter, the shape is essentially the same down to the smallest crater observed. On all photographs obtained from *Ranger VII,* from the smallest to the largest scale, the primary craters occupy a very small fraction of the mare surface, typically less than 1%. At all scales, they appear to be randomly scattered over the field. Over the range of size from 30 m diameter to the largest primaries photographed, some primary craters are surrounded by bright halos or rays, and some are not (Figs. 7–10). Discrete bright halos are associated exclusively with primary craters, but no demonstrable variations in albedo have been found to be localized around craters smaller than 30 m in diameter.

Secondary craters. Secondary craters are abundantly represented in the *Ranger VII* photographs. In Mare Cognitum, a majority of them may be identified with three major secondary crater swarms. Two of these swarms coincide with major ray systems—one with the ray system of Copernicus and one with that of Tycho. Only relatively large secondary craters of Copernicus are resolved in the *Ranger VII* photographs, as Copernicus rays are not present in the highest-resolution pictures. These large secondary craters of Copernicus are best portrayed near the northern margins of A-camera photographs 155 to 158. Most of the secondary craters in the highest-resolution photographs are in a ray belonging to the Tycho system. The third major swarm of secondary craters is associated with the Eratosthenian primary crater Bullialdus, and the differences in form between the larger Copernican and Eratosthenian secondaries are well illustrated in the A-camera photographs.

The swarm of secondary craters within the Tycho ray shown in the last four A-camera photographs (Figs. 11–14) exhibit details of form and spacing too small to be seen through the telescope. The majority of readily identifiable secondary craters in this ray range from 200 to about 400 m across and from about 200 m to 1 km in length. Most of the more elongate craters are found to be composite, composed of two, and in some cases three, craters merged together. Craters of this type are closely spaced, forming a rough crescent-shaped pattern opening to the northwest (astronautical coordinates). The convex boundary of the crescent is the approximate margin of the ray, and the largest secondary craters tend to occur along the southern part of the crescent, which is the part nearest Tycho. Along the northern arm of the crescent, the secondary craters are smaller and shallower in proportion to their width, and the rims are distinctly more rounded.

In the southern or proximal part of the crescent-shaped secondary crater cluster are a number of circular, relatively deep craters ranging in diameter from about 400 to 900 m. Except for the lack of well developed rims, some of these circular craters could be mistaken for primaries, were they not clearly members of the swarm. In another small Tycho ray northwest of the crescent-shaped cluster, all of the largest craters, which form a loose cluster on the end of the ray nearest Tycho, are

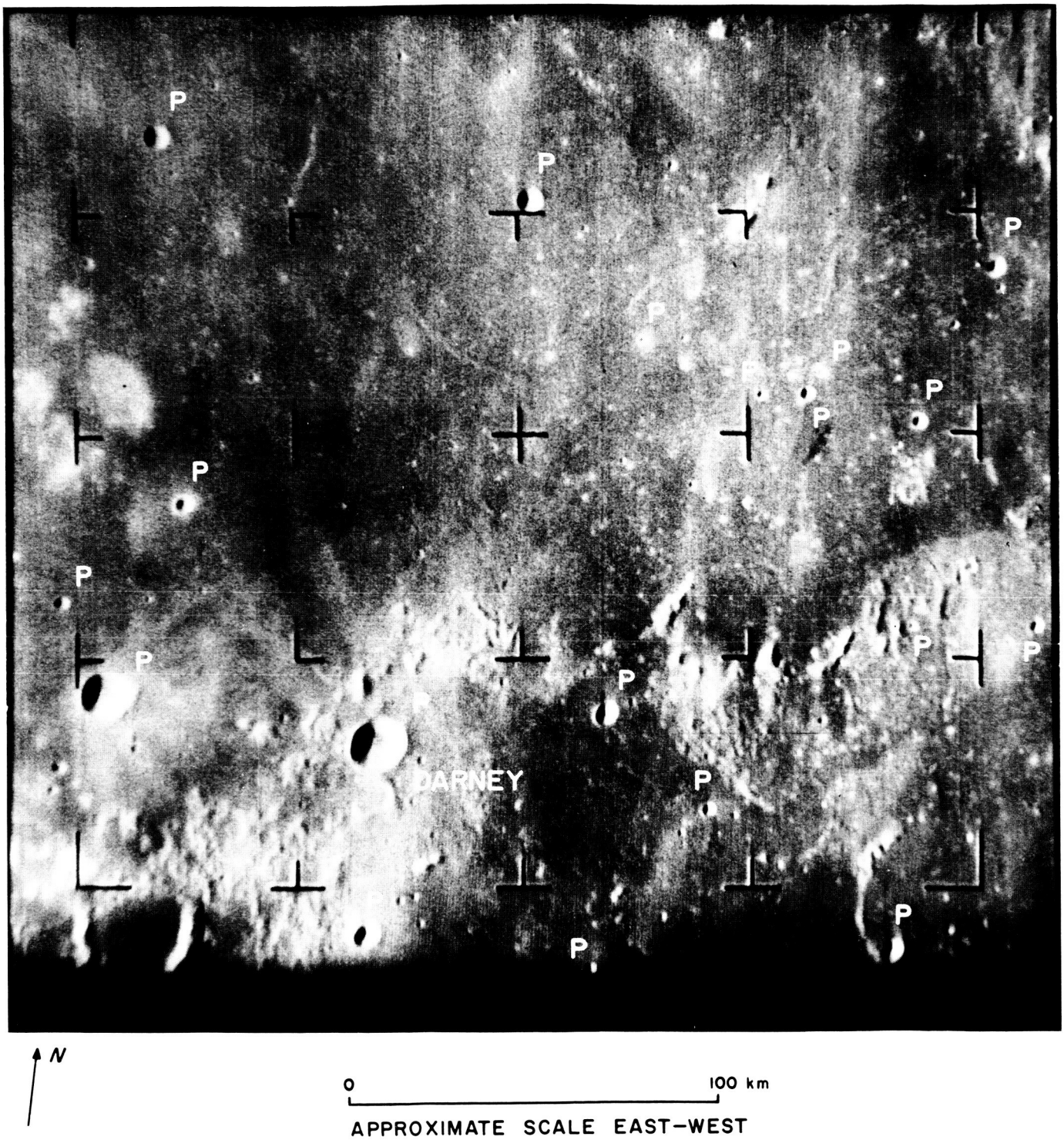

Fig. 7. A-camera photograph 151 showing distribution of telescopically resolvable primary craters (designated P).

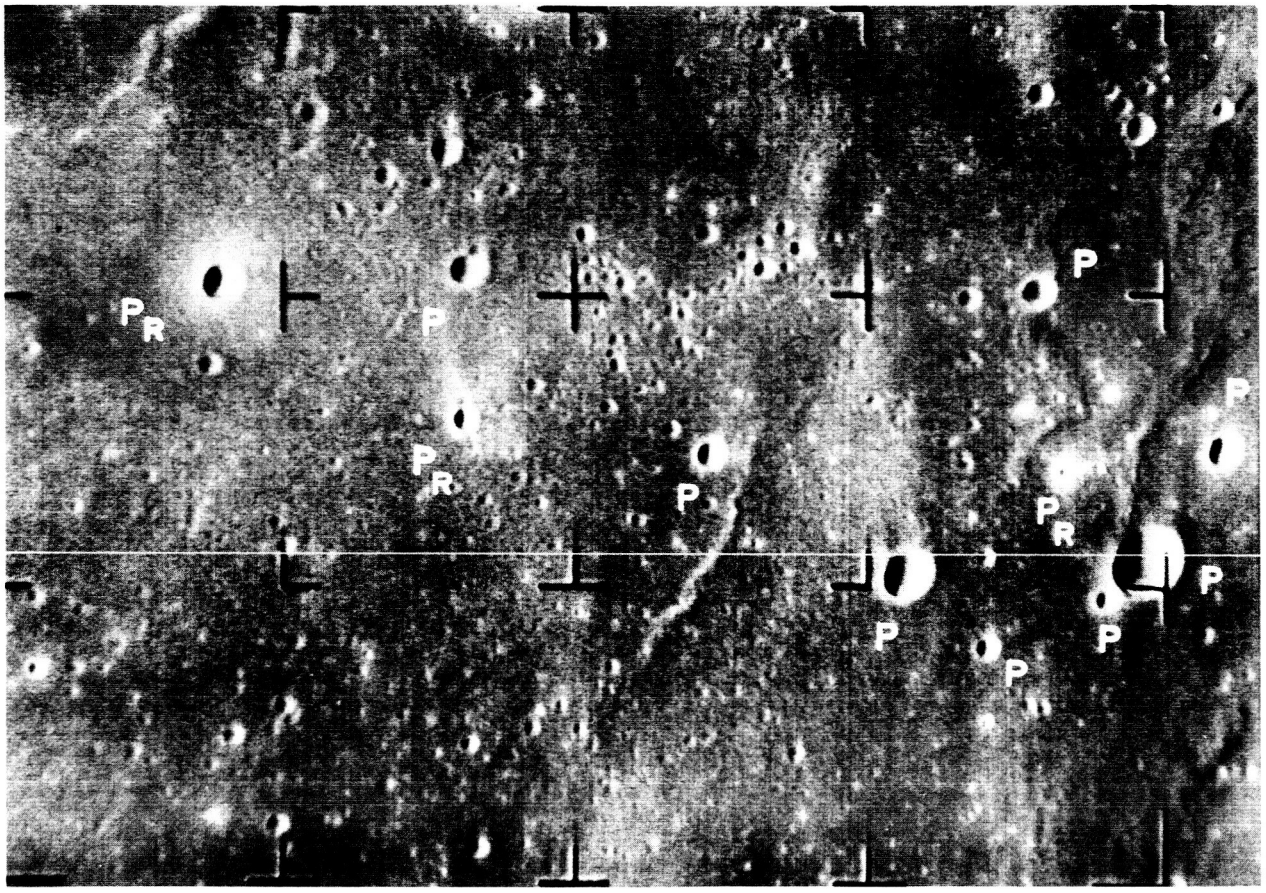

Fig. 8. Part of A-camera photograph 189 showing group of primary craters of intermediate size. (Primary craters without rays are designated P, and primary craters with rays are designated P_R.)

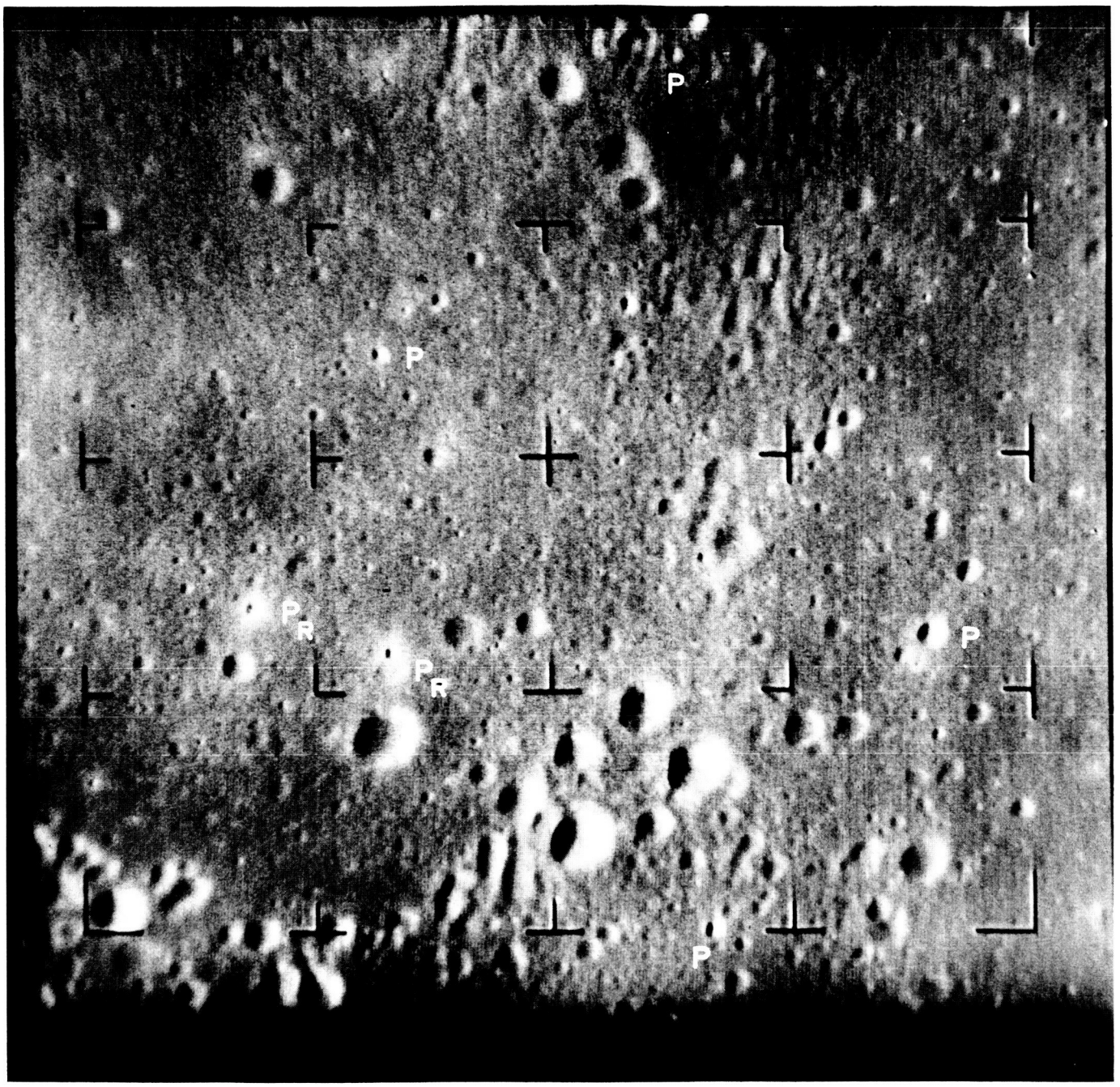



Fig. 9. A-camera photograph 197 showing identifiable primary craters. (Primary craters without rays are designated P, and primary craters with rays are designated P_R. Most of the primary craters identified are too small to be resolved with Earth-based telescopes.)

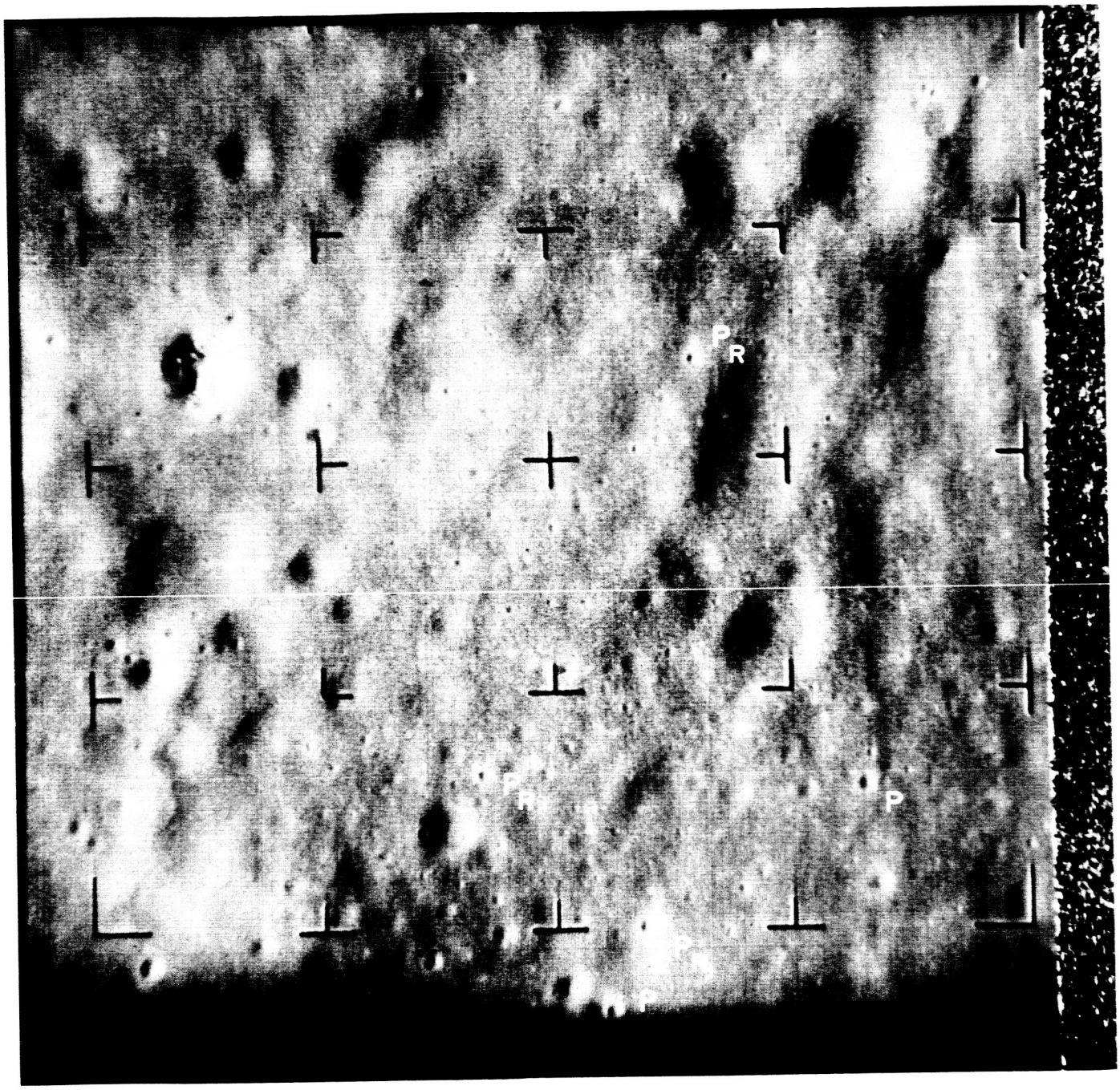

Fig. 10. A-camera photograph 199 showing identifiable primary craters. (Primary craters without rays are designated P, and primary craters with rays are designated P_R. The smallest ray craters identified are about 30 m in diameter and are the smallest ray craters so far identified on the Moon.)

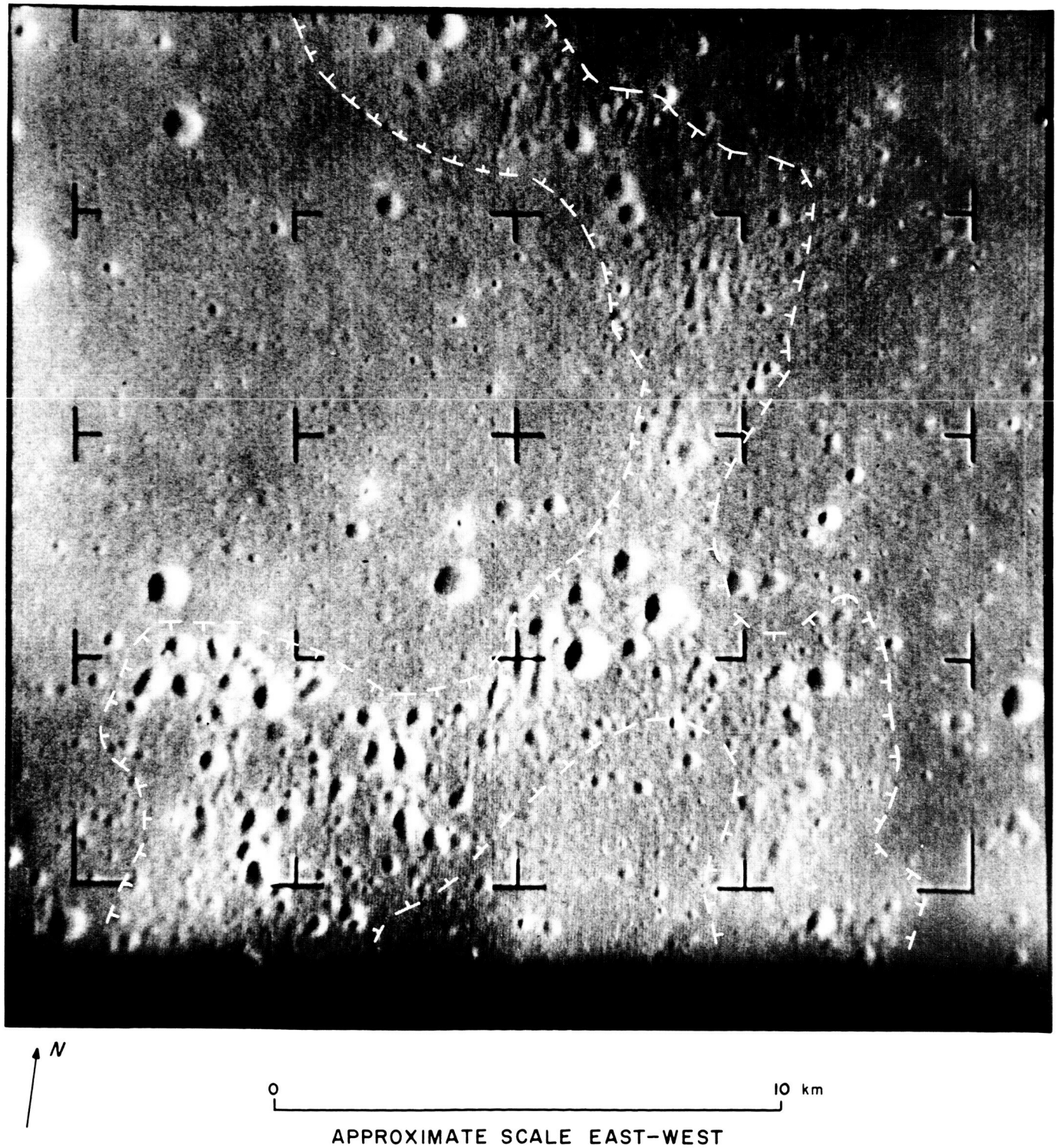

Fig. 11. A-camera photograph 196 showing approximate boundaries of Tycho ray and distribution of secondary craters within the ray. (Dashed lines with tick marks are ray boundaries; tick marks are on ray. Note the abundance of elongate, composite craters in the ray. Nearly all of the elongate craters and most of the circular craters in the ray are interpreted as secondary craters of Tycho.)

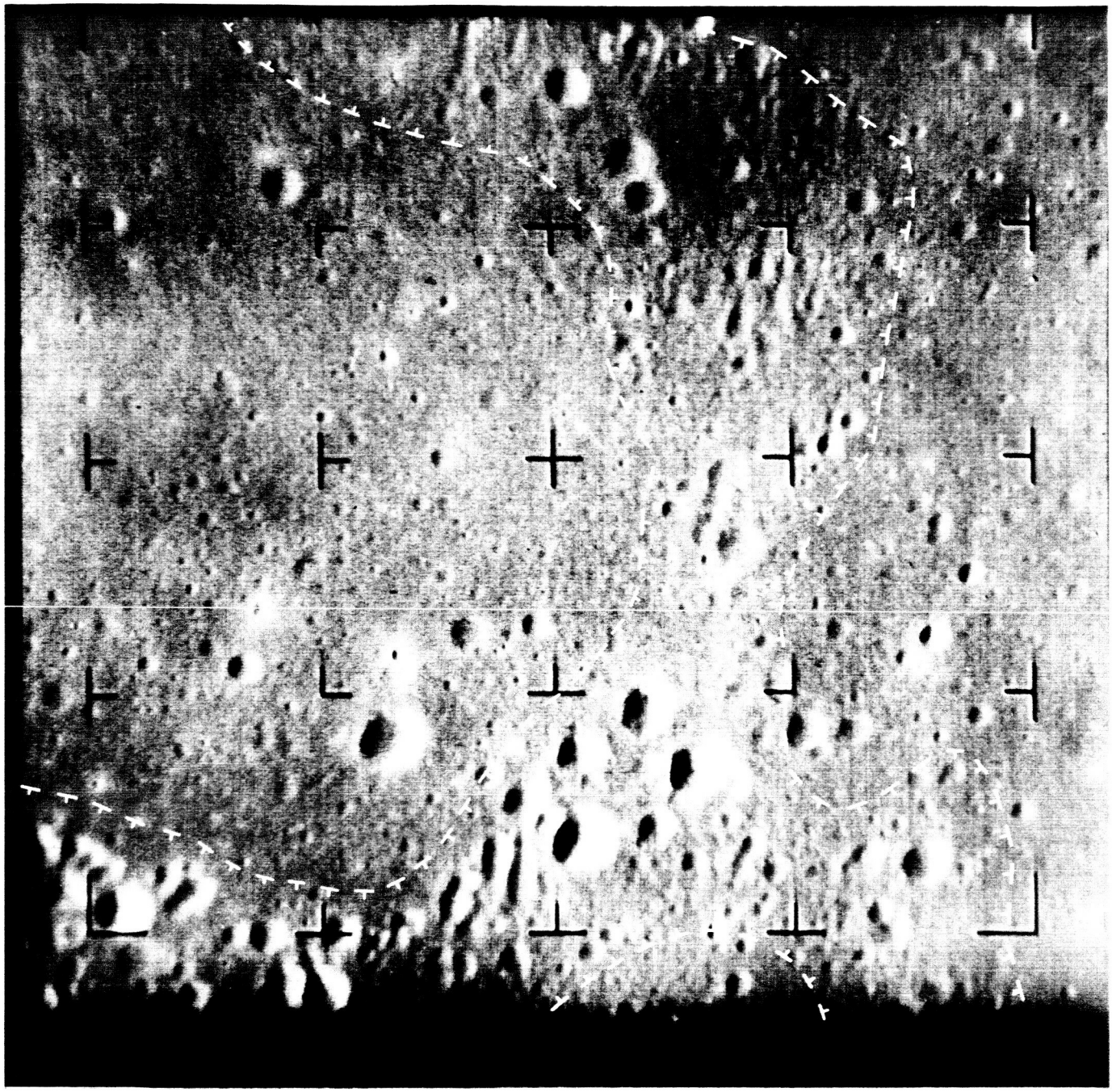

Fig. 12. A-camera photograph 197 showing approximate boundaries of Tycho ray and distribution of secondary craters within the ray. (Dashed lines with tick marks are ray boundaries; tick marks are on ray. Note the abundance of elongate, composite craters in the ray. Nearly all of the elongate craters and most of the circular craters in the ray are interpreted as secondary craters of Tycho.)

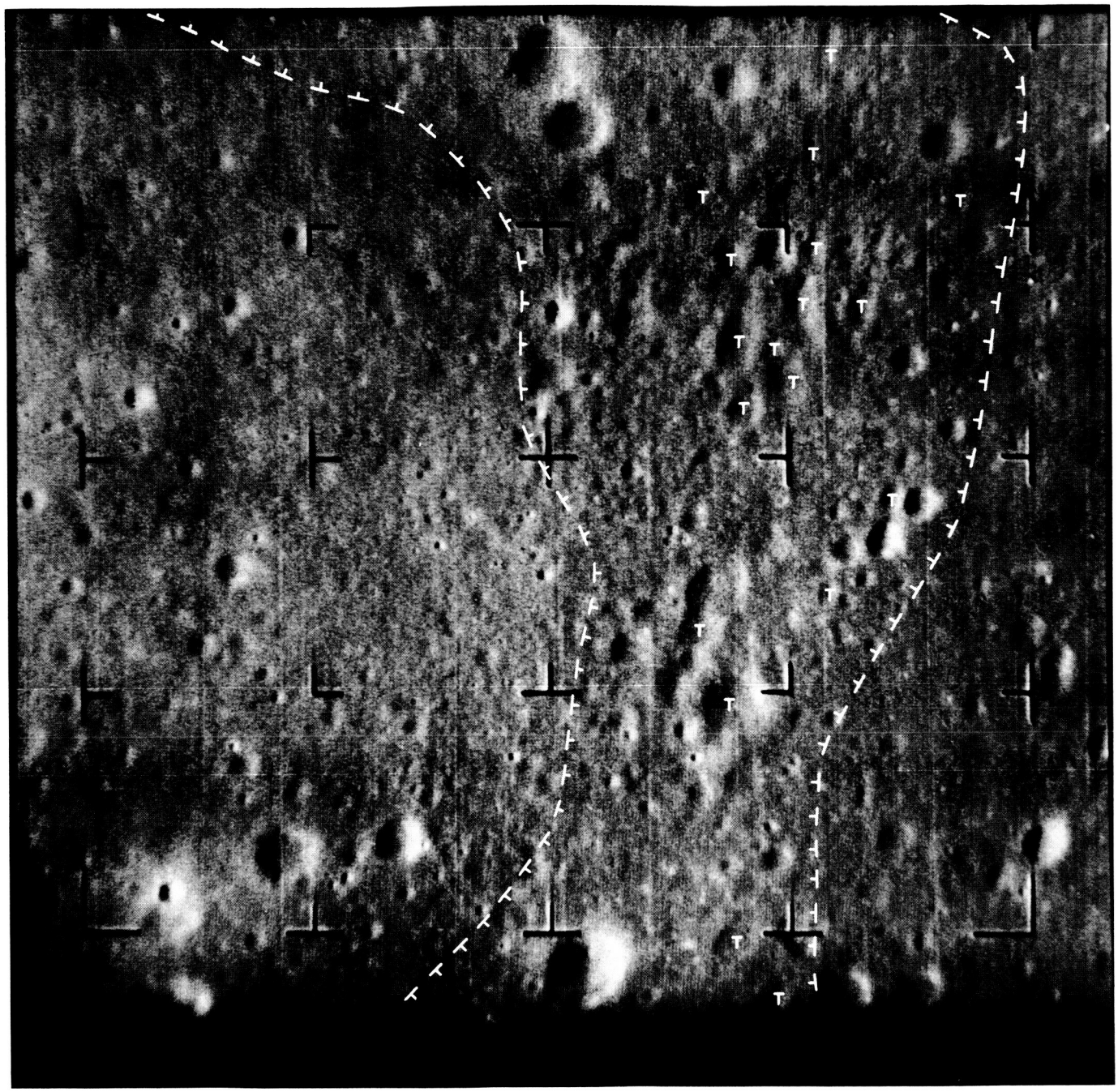

Fig. 13. A-camera photograph 198 showing approximate boundaries of Tycho ray and elongate secondary craters of Tycho. (Dashed lines with tick marks are ray boundaries, tick marks are on ray. Elongate Tycho secondary craters are designated T. Only the largest elongate secondary craters that may be identified with reasonable confidence as belonging to the Tycho secondary crater swarm are marked.)

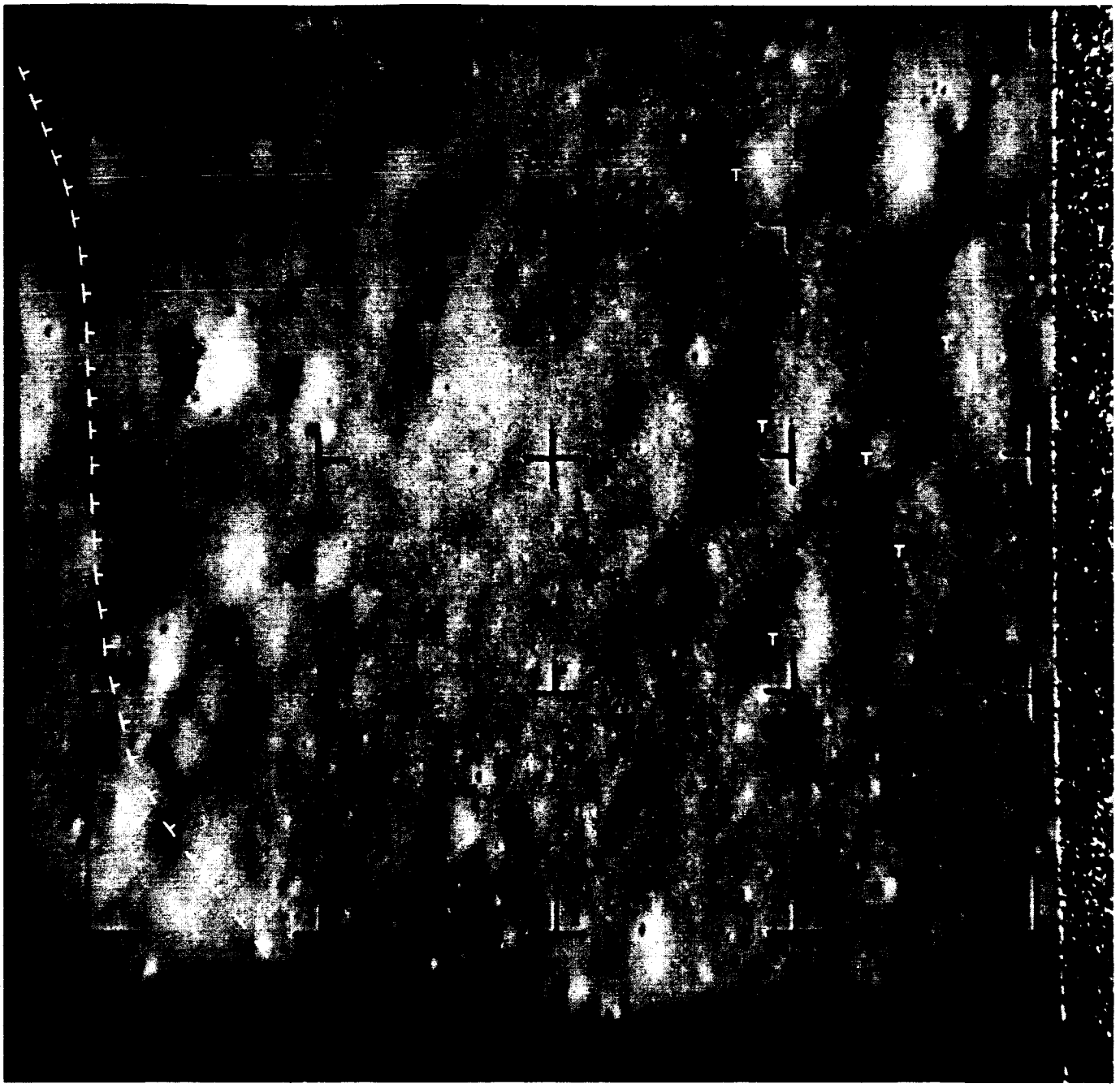

Fig. 14. A-camera photograph 199 showing approximate boundaries of Tycho ray and elongate secondary craters of Tycho (cf. Fig. 13).

circular in form. From the fact that they form a cluster and occur within the ray, it is inferred that these also must be secondary craters. It appears that the more open the cluster, the greater is the tendency for the secondaries to be circular.

A somewhat higher proportion of circular to elongate secondaries occurs in the rays of Tycho shown in the highest-resolution A-camera photographs than in the typical swarms of secondaries observed through the telescope. It appears that, in a given secondary swarm, the smaller and more widely spaced the craters become, the greater is the tendency for individual circular rather than elongate composite craters to be formed.

Large Eratosthenian secondary craters, most of which are probably related to Bullialdus, are widely scattered over the southern part of Mare Cognitum. A row or band of secondary craters may be traced north from Bullialdus crossing the southern margin of the mare (Figs. 15 and 16). Near the north end of this row is a very prominent elongate crater over 3 km in length and about 1 km in maximum width (Figs. 17 and 18). It is devoid of any discernible rim. The edges of the crater are rounded, and it is much shallower than primaries of 1 km diameter. The elongate crater has a vague internal structure and appears to be composed of about four barely recognizable smaller craters strung end to end. Three closely similar composite secondary craters of about the same size may be seen in this general region of the mare. The one which lies closest to the *Ranger* impact point is shown with highest resolution in photographs A191–193 (Figs. 19–21). Between the rays, in this same general region, are a large number of smaller, less well defined secondary craters, most of which are also probably a part of the Bullialdus swarm. They can be distinguished best in photographs A182–186 (Figs. 22–25). In the northwest corner of photographs A187 and 188 (Figs. 26 and 27) is a series of extremely shallow and very elongate faintly marked features which may belong to an unidentified Eratosthenian secondary swarm, possibly older than that of Bullialdus.

Elongate small secondaries can be recognized in the *Ranger VII* photographs over the range of length from 3 km down to 1 m. At least two sets of very small secondaries appear in the last part of the sequence of photographs obtained by the P cameras, one set with long axes tending north-northwest and the other set north-northeast (Figs. 28 and 29). These small secondary craters are probably related to two or more nearby primary craters in Mare Cognitum, possibly two primaries about 1 km across or smaller with conspicuous bright halos that lie south of the *Ranger* impact point (Fig. 8).

Craters less than 300 m in diameter. Nearly all craters in Mare Cognitum shown on the *Ranger VII* photographs that are greater than 1 km across can be classified as primary or as secondary craters. The majority of them are primary. In the diameter range from 300 m to 1 km, most of the craters can also be classified as primary or as secondary, but craters of this size are predominantly secondary. Beginning at a diameter of about 500 m and extending to smaller sizes, a number of craters are observed in the *Ranger* photographs that are not clearly assignable either to the primary or to the secondary class. These craters are circular in plan but have low rounded rims and are shallower than typical primary craters (Figs. 30 and 31). In the areas between the rays, these shallow circular craters do not clearly belong to any recognizable secondary crater swarm. They may be degraded primary craters or isolated round degraded secondary craters. At diameters less than 300 m, the crater population is dominated by this third indefinite type.

All gradations in form may be observed among circular craters less than 300 m across. They range from steep-walled primaries to craters with no discernible raised rim and with such gentle interior slopes that the craters are barely detectable in the photographs. For each size class from 2 to 300 m diameter, a complete sequence of crater forms with varying depth and slope of wall may be found between the primary and the shallowest, barely detectable craters. The edges of the shallow craters are invariably rounded and, in fact, are generally so smooth in the shallowest ones as to defy precise location.

Many very shallow round-edged elongate or irregular craters less than 300 m in diameter are also represented in the high-resolution photographs (Fig. 31). They occur both in and between the major rays.

Irregular features of craters. Certain unusual features of the small craters photographed by *Ranger VII* have attracted comment and speculation out of all proportion to the frequency of their occurrence. Foremost among these is the cluster of somewhat angular protuberances in the bottom of the deepest crater (the so-called rock) shown in A199 (Fig. 32). There are perhaps as many as half a dozen other small craters, seen in the highest-resolution A and B photographs, that also have irregularities near the crater center (for example, in Fig. 33), but none are shown with the same clarity of detail as the

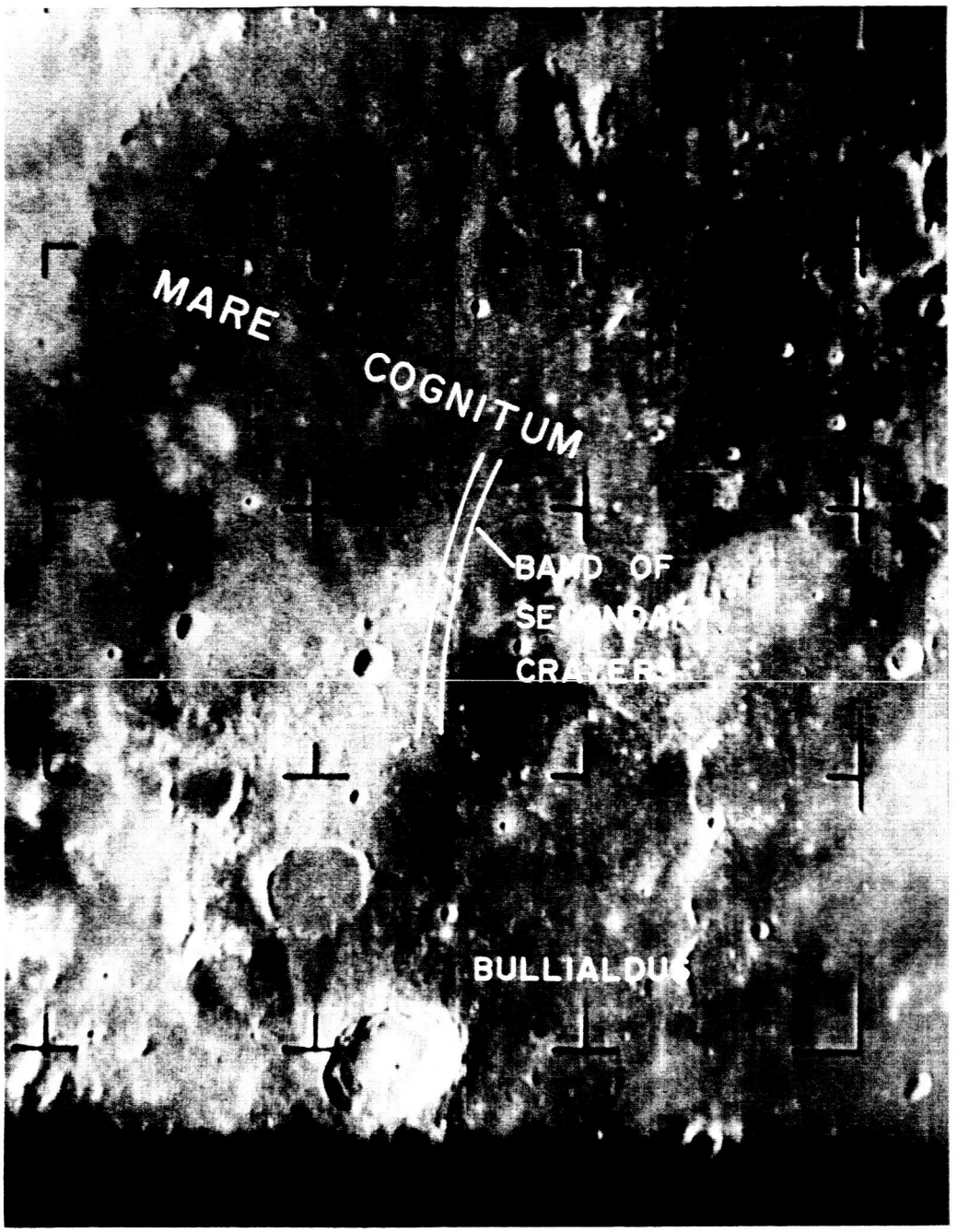

Fig. 15. Part of A-camera photograph 108 showing Bullialdus, position of band of Bullialdus secondary craters, and Mare Cognitum. (Secondary craters of Bullialdus are not resolved in this photograph.)

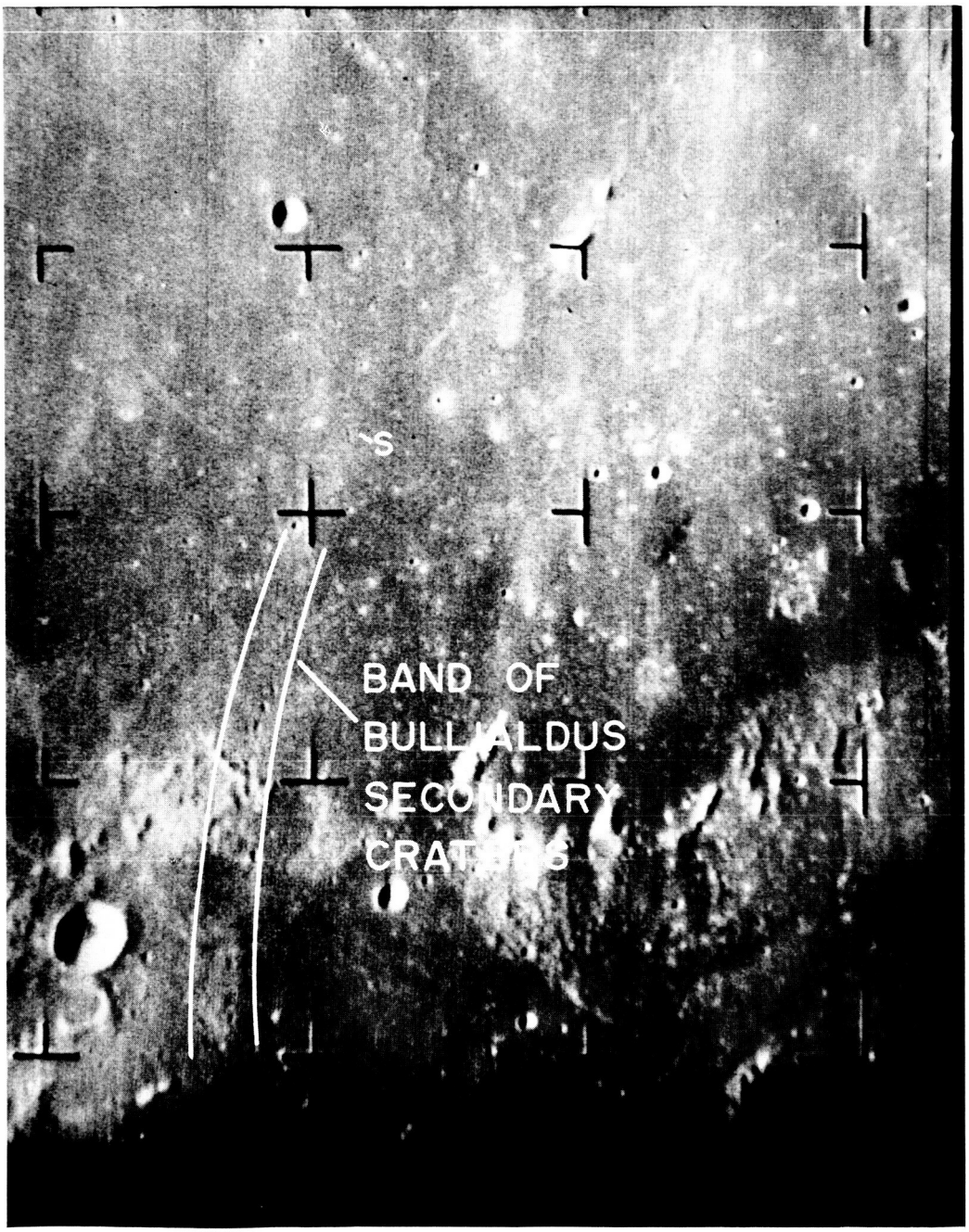

Fig. 16. Part of A-camera photograph 156 showing band of Bullialdus secondary craters. (Large Eratosthenian secondary crater beyond band, designated S, probably also belongs to the Bullialdus secondary crater swarm.)

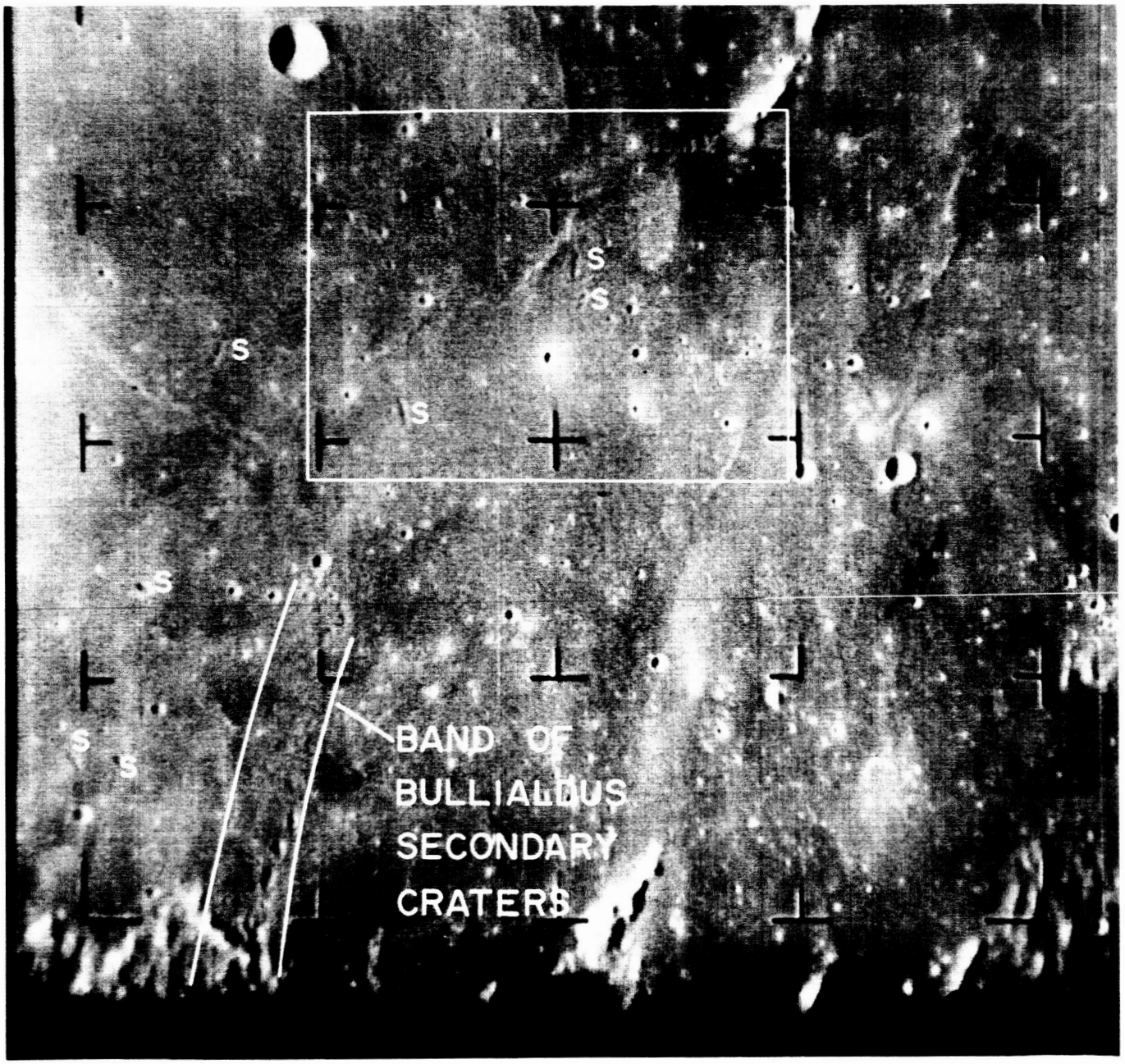



Fig. 17. A-camera photograph 176 showing band of Bullialdus secondary craters and scattered large Eratosthenian secondary craters (designated S) that may belong to Bullialdus secondary crater swarm. (Inset shows position of Fig. 18.)

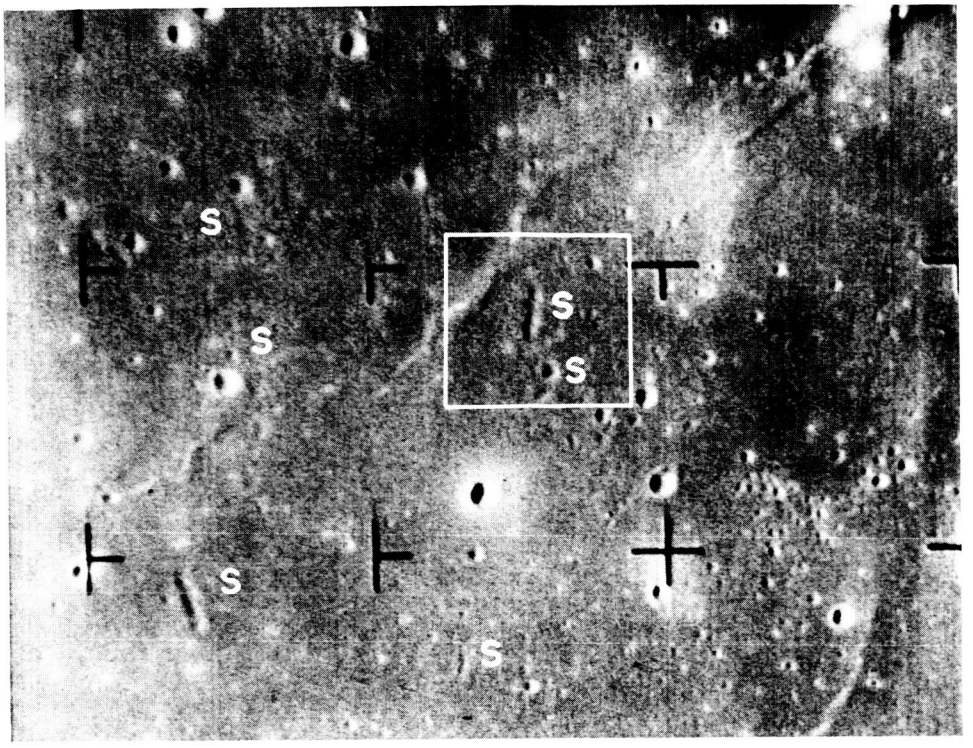

Fig. 18. Part of A-camera photograph 185 showing distribution of large Eratosthenian secondary craters (designated S). (Inset shows position of Figs. 19 and 20.)

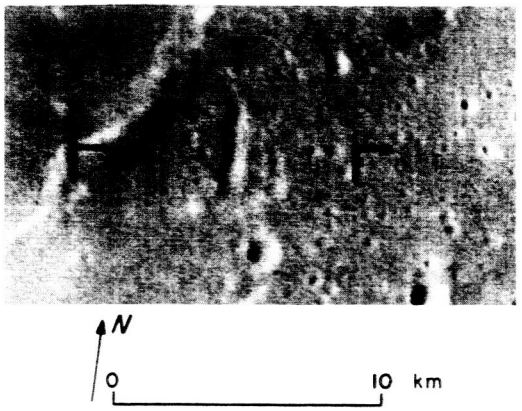

Fig. 19. Part of A-camera photograph 191 showing small cluster of large Eratosthenian secondary craters. (This cluster is probably part of Bullialdus secondary crater swarm.)

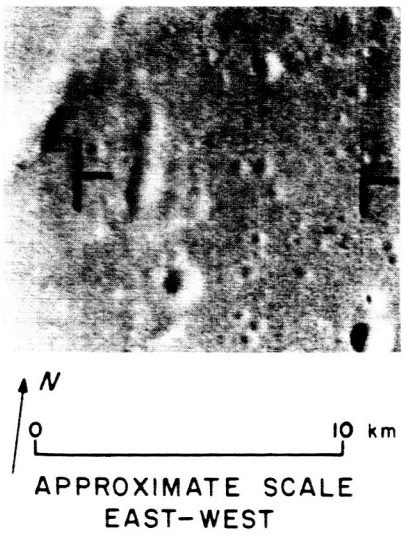

Fig. 20. Part of A-camera photograph 192 showing small cluster of large Eratosthenian secondary craters.

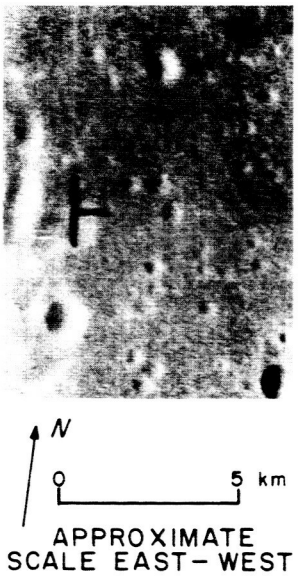

Fig. 21. Part of A-camera photograph 193 showing small cluster of large Eratosthenian secondary craters.

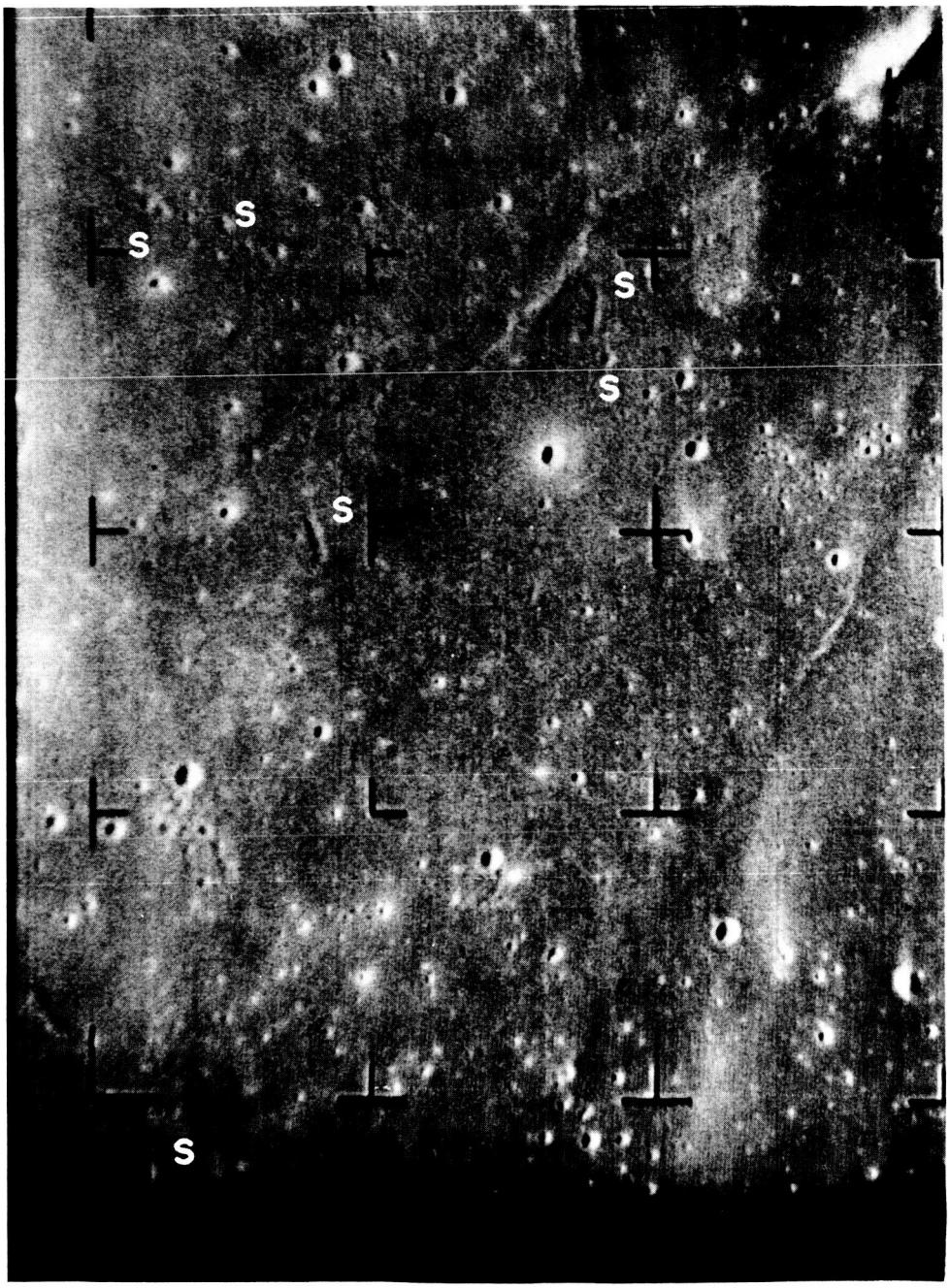

Fig. 22. Part of A-camera photograph 182 showing distribution of large Eratosthenian secondary craters (designated S).

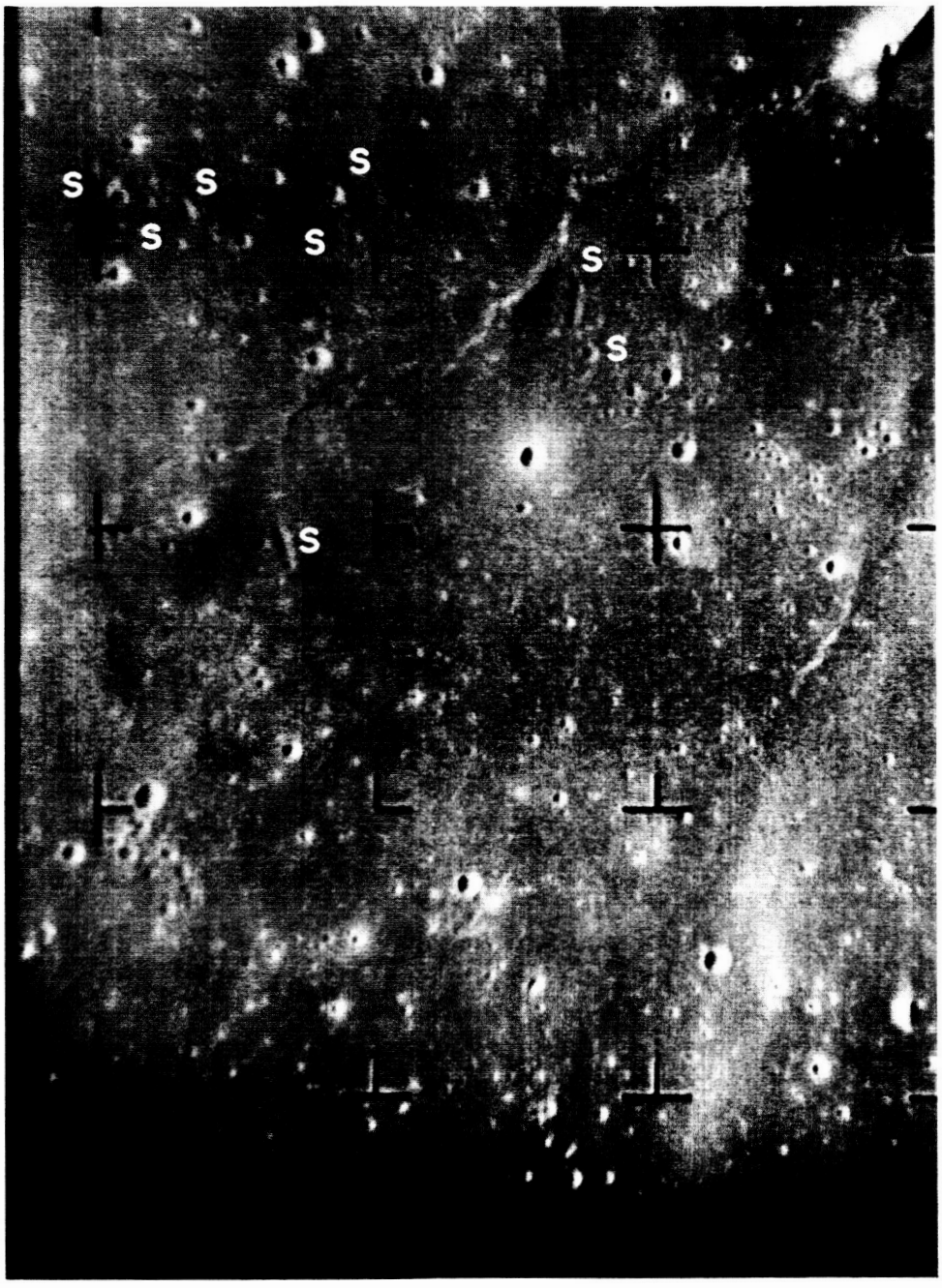

Fig. 23. Part of A-camera photograph 183 showing distribution of large Eratosthenian secondary craters (designated S).

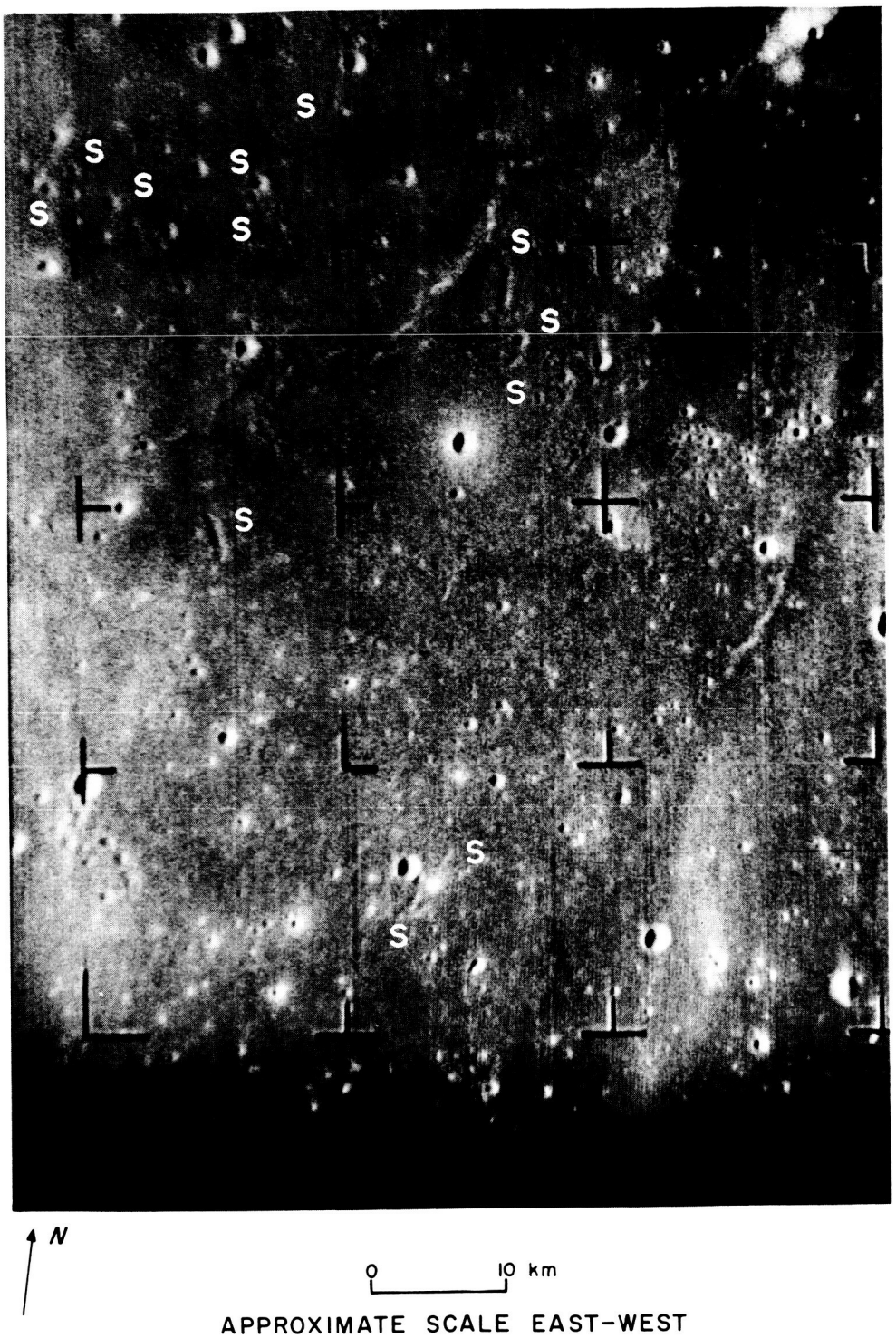

Fig. 24. Part of A-camera photograph 184 showing distribution of large Eratosthenian secondary craters (designated S).

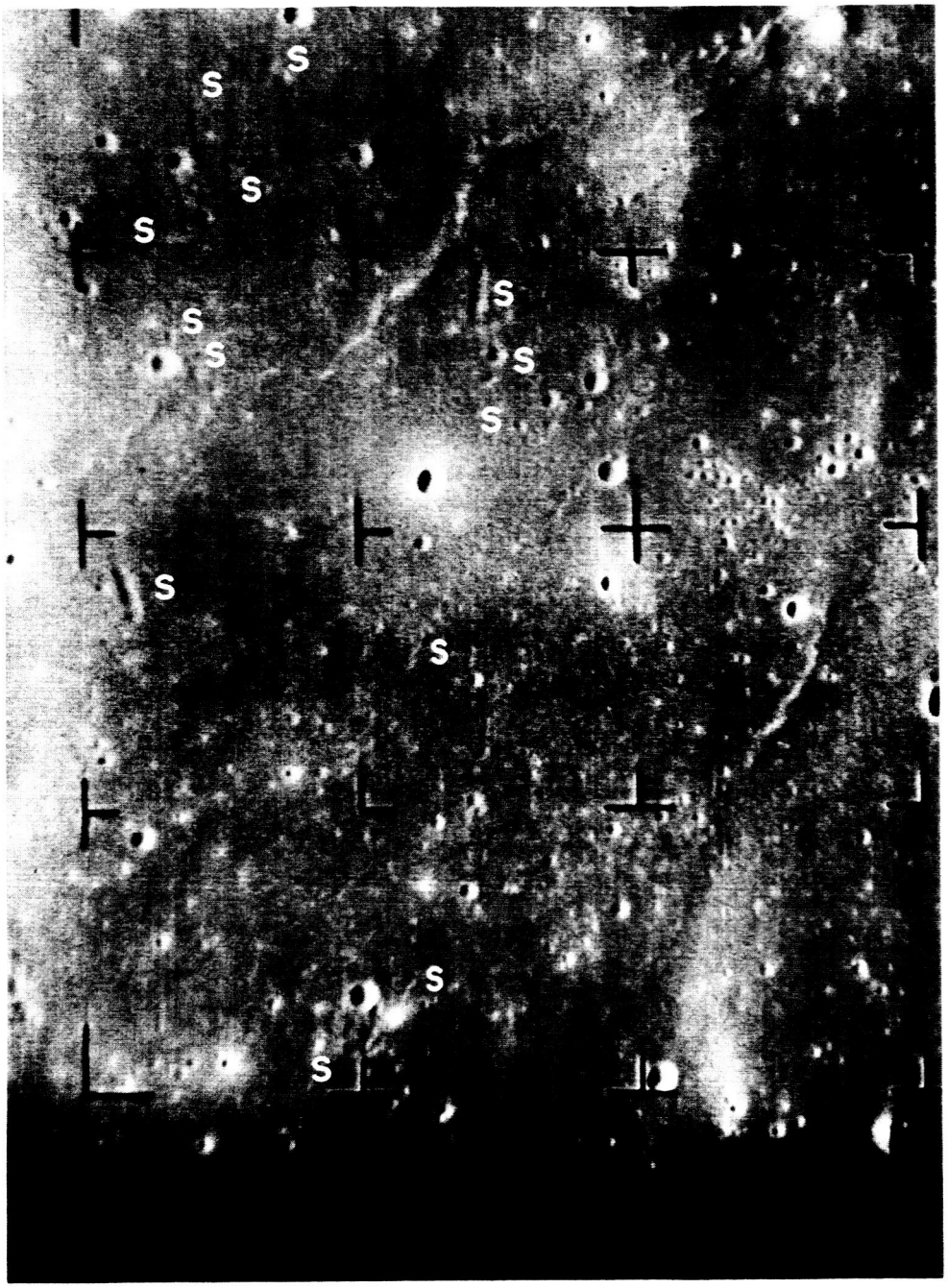

Fig. 25. Part of A-camera photograph 186 showing distribution of large Eratosthenian secondary craters (designated S).

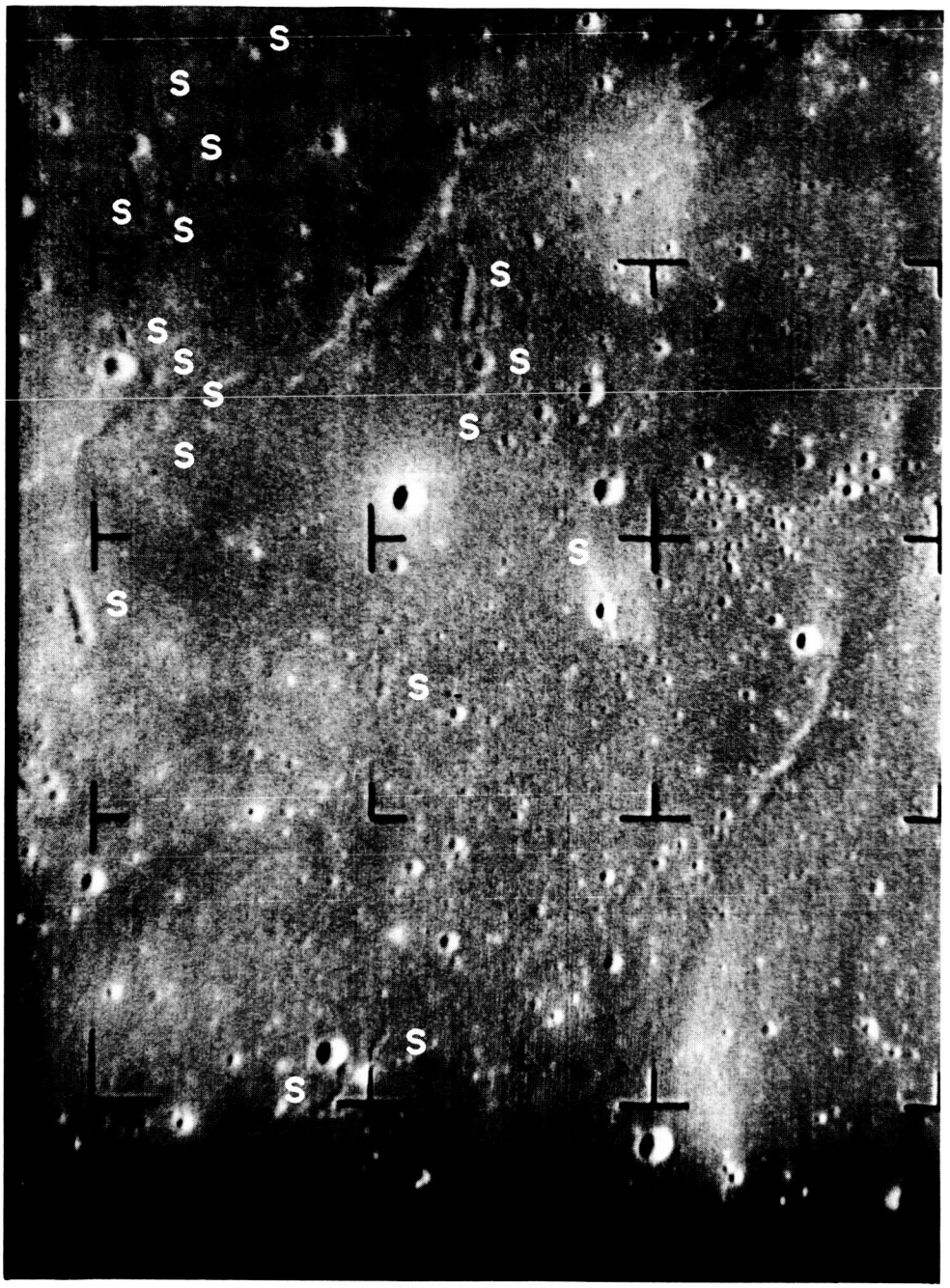

Fig. 26. Part of A-camera photograph 187 showing distribution of large Eratosthenian secondary craters (designated S). (Very shallow craters in upper right-hand corner may belong to a secondary crater swarm older than Bullialdus.)

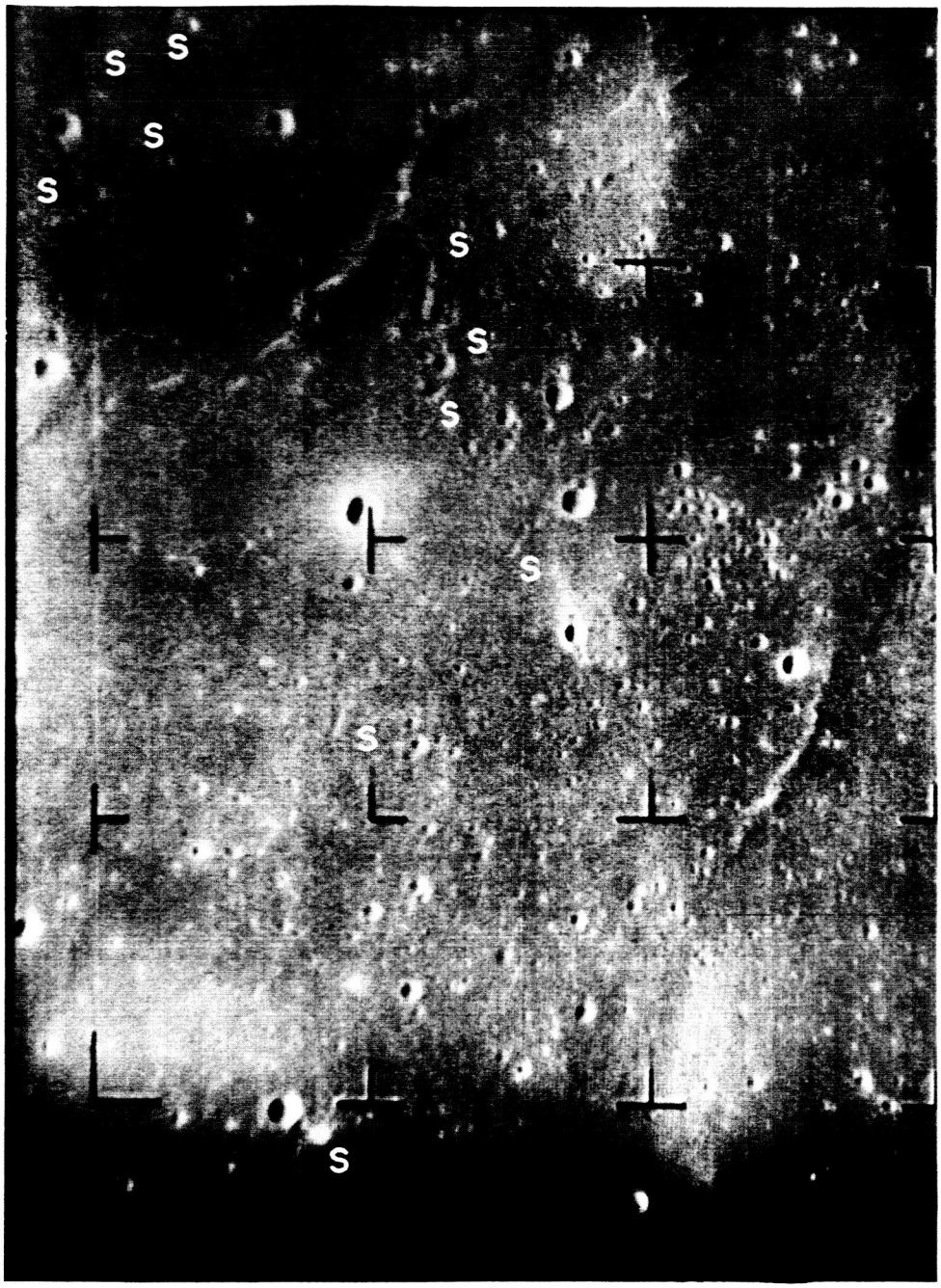

N

0 10 km

APPROXIMATE SCALE EAST-WEST

Fig. 27. Part of A-camera photograph 188 showing distribution of Eratosthenian secondary craters. (Very shallow craters in upper right-hand corner may belong to a secondary crater swarm older than Bullialdus.)

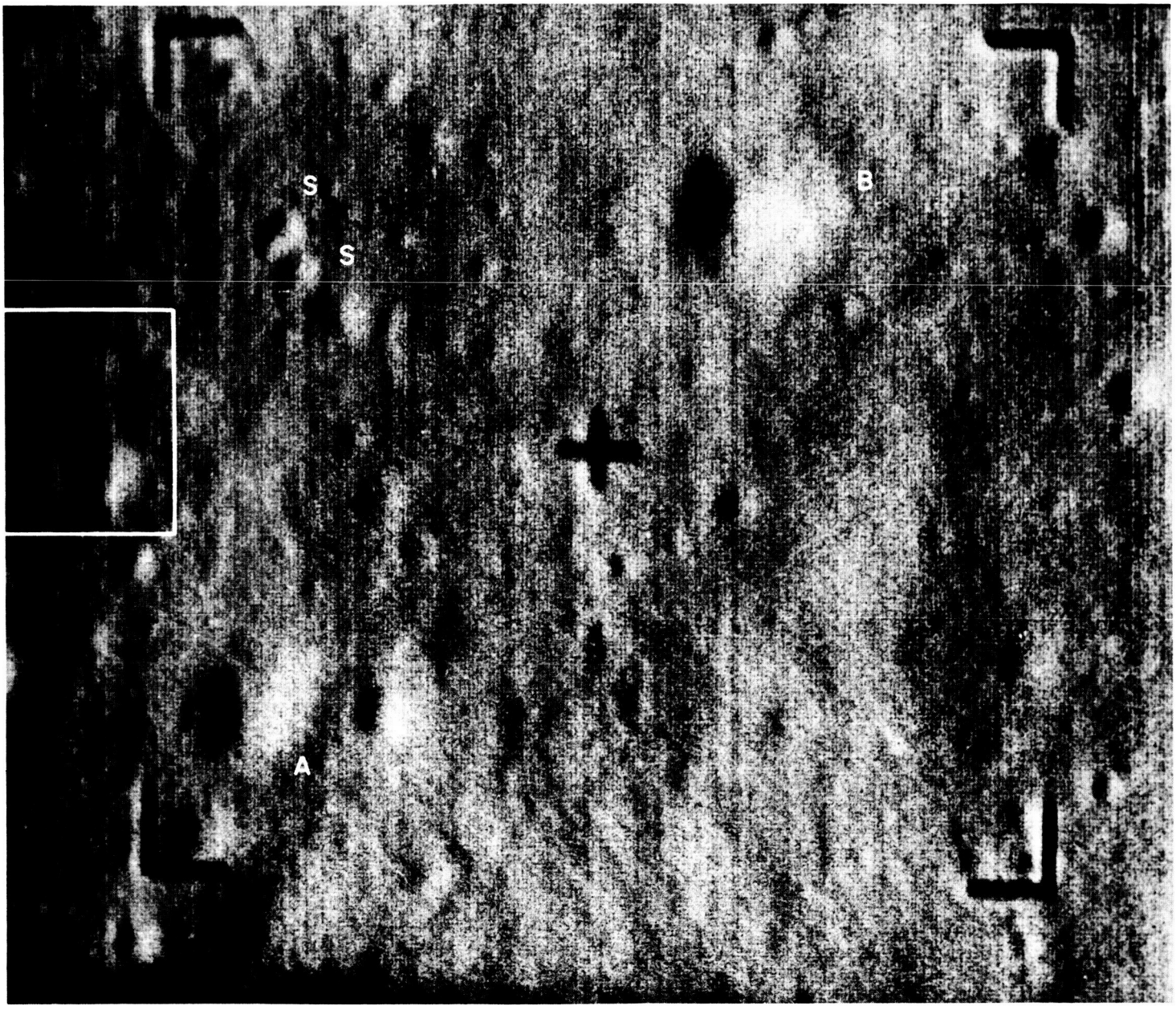

Fig. 28. Last P_4-camera photograph showing small secondary craters (designated S). (Craters A and B are identical with craters marked A and B in Fig. 35. Inset shows position of part of Fig. 36.)



Fig. 29. Last P_3-camera photograph showing small secondary craters (designated S) and mounts with summit craters (designated M). (The length of the secondary craters is exaggerated by image motion, but the secondary craters are also elongated in the general direction of motion of the image as shown by the presence of small circular craters in the same part of the field.)

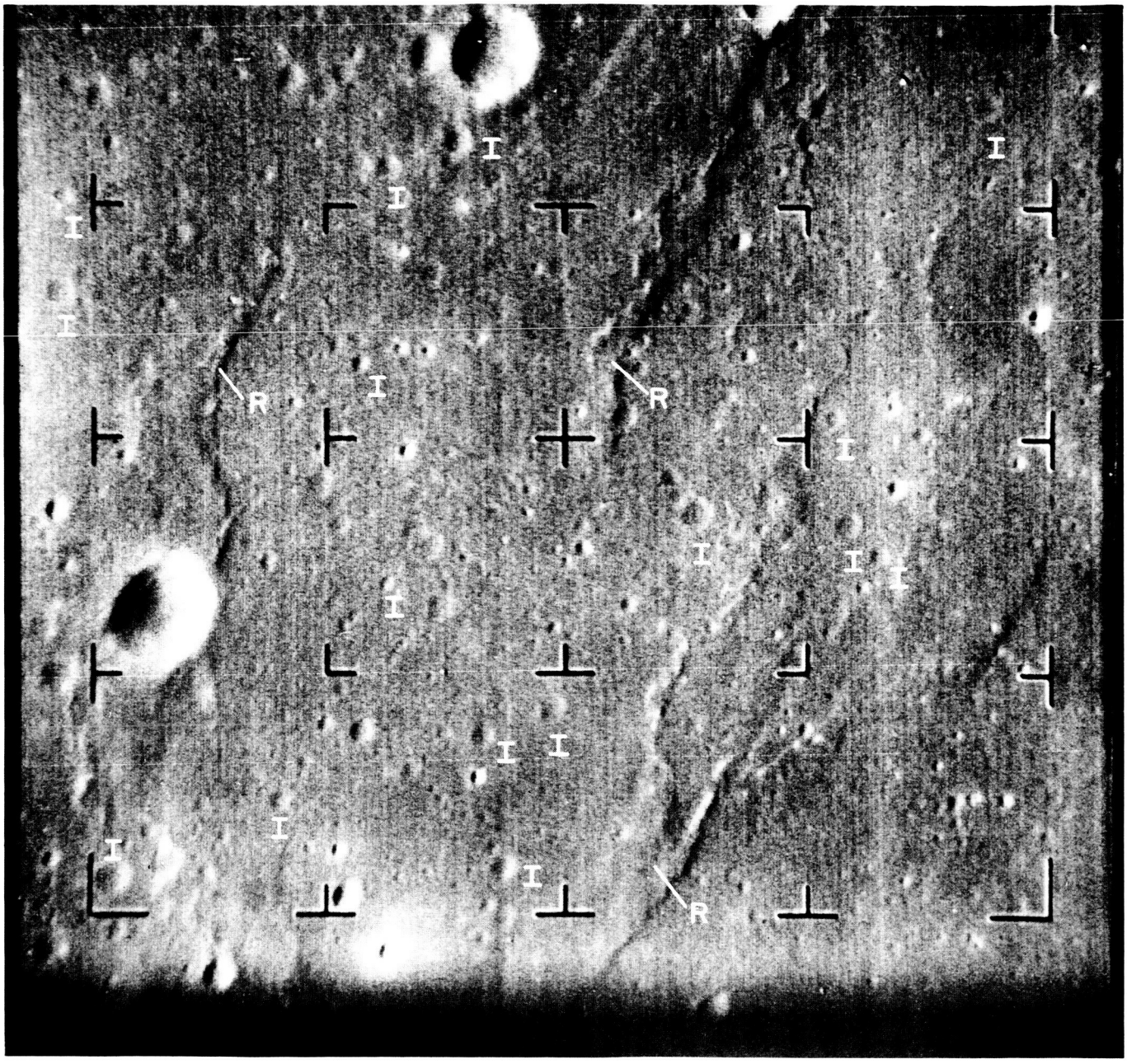

Fig. 30. B-camera photograph 194 showing distribution of shallow circular craters with low rounded rims (designated I) of indefinite classification. (Only the largest of the indefinite craters are marked. Major ridges are designated R. Note craters on ridge in upper right.)

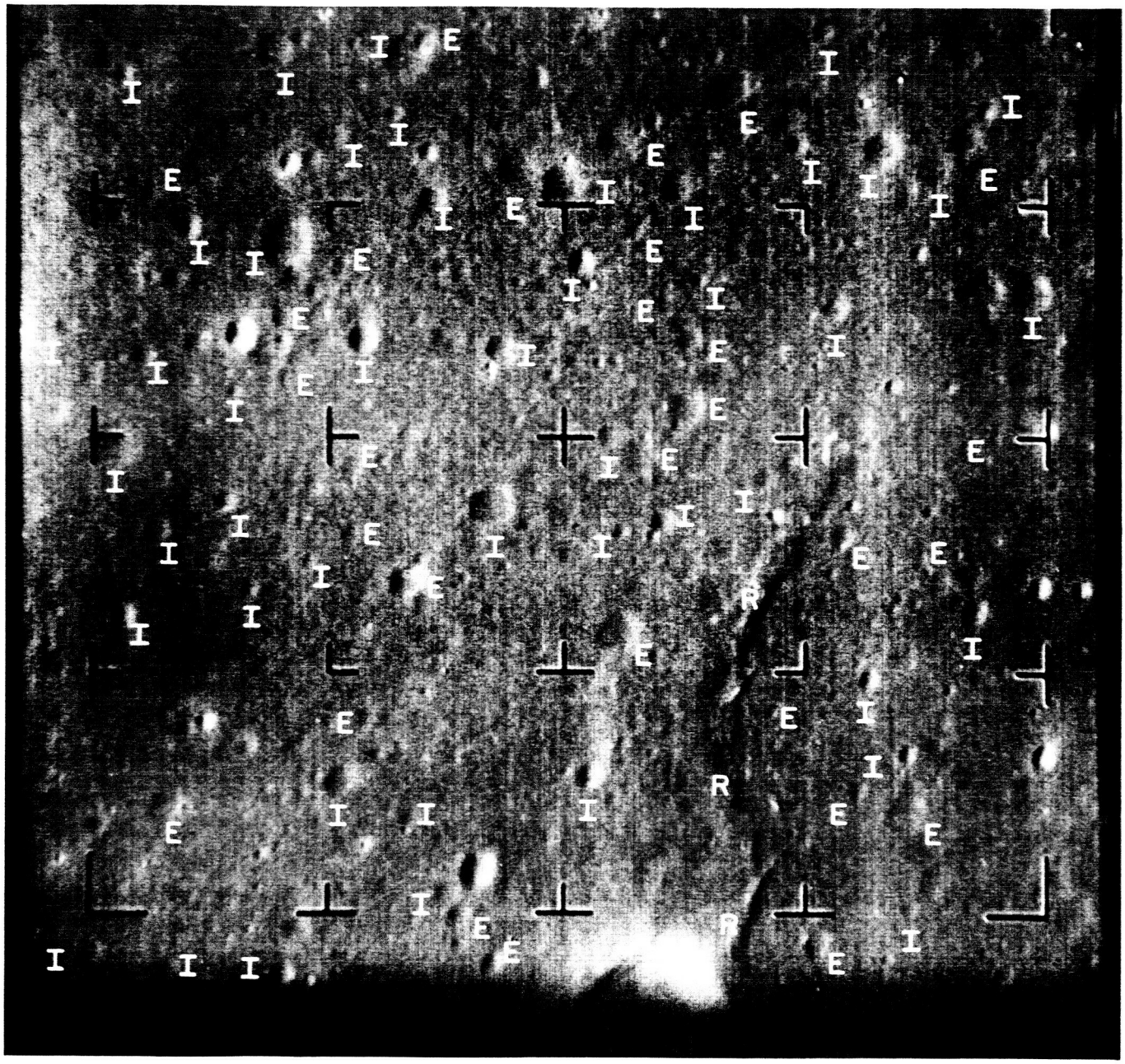

Fig. 31. B-camera photograph 197 showing distribution of shallow circular craters with low rounded rims (designated I) of indefinite classification, and elongate and irregular craters (designated E). Only the largest craters in these two classes are marked. A prominent ridge in the lower right part of the photograph is designated R. Note the presence of sharply defined branches or spurs on the ridge.)

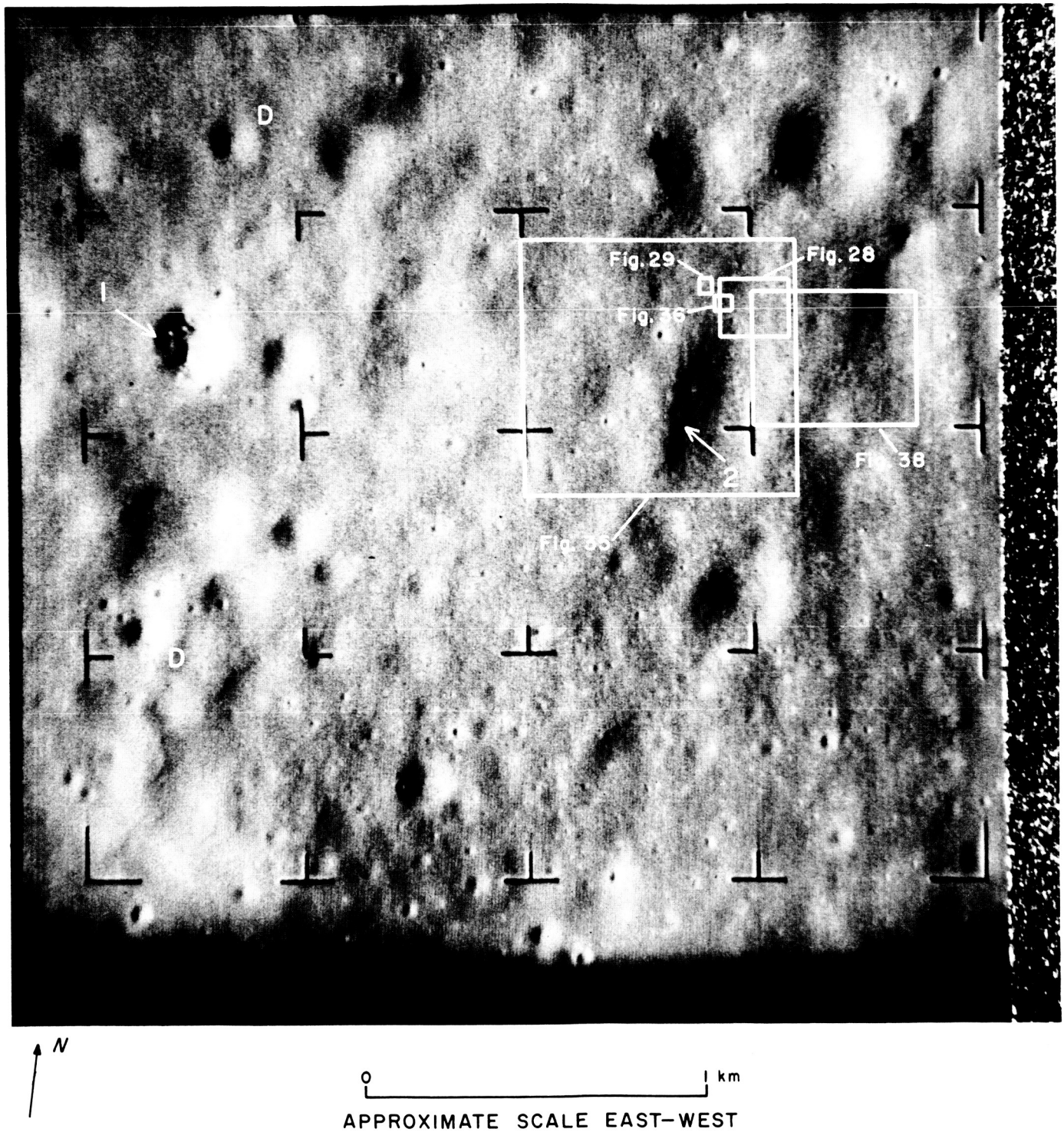

Fig. 32. A-camera photograph 199 showing location of irregular features of craters, dimple-shaped craters (designated D), and other Figures. (Crater with prominent protuberances is designated 1. Scarp in wall of elongate Tycho secondary crater is designated 2. Subdued scarps in nearby secondary crater occur within inset showing position of Fig. 38.)

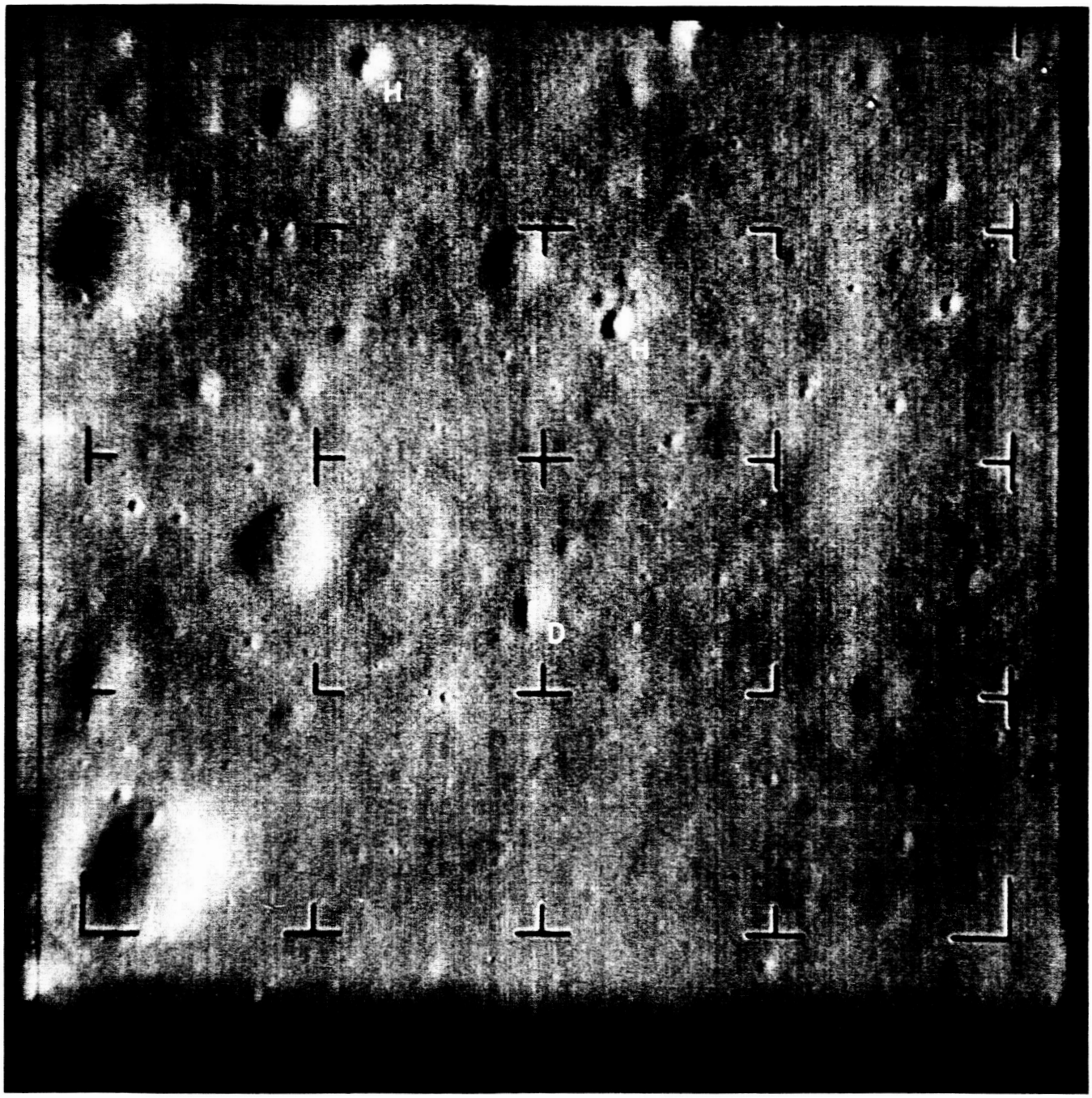

Fig. 33. B-camera photograph 200 showing dimple-shaped crater (designated D) and small craters containing humps or protuberances (designated H).

200-m-diameter crater in A199. In this crater, there appear to be at least three discrete protuberances, one much larger than the other two. Slopes on the sides of these protuberances in places exceed the local Sun elevation angle of 23 deg. In addition to the protuberances, there are two rows of smaller irregular features, consisting of very small bumps and troughs that extend up the walls of the crater. On the west wall, above the largest protuberance, is a distinct scallop or depression that resembles a landslide scar and is about the same width as the protruding mass below. The east wall is distinctly concave except near the floor of the crater, where it is sharply convex adjacent to the protruding body. A radial profile of this wall resembles the longitudinal profile of certain types of small landslides with rounded toes or snouts. The resemblance in form suggests that the east wall of the crater has slumped. Indeed, all of the features seen within the crater may have been formed by slumping, the largest protruding mass having been derived from the upslope scallop or scar.

A plausible alternative explanation of the relatively rare protuberances in small crater floors is that they represent remnants of impacting masses that formed the craters. To account for the survival of the impacting mass and the ratio of the diameter of the largest protuberance to the diameter of the crater, the impacting bodies would most probably be low-velocity lunar fragments ejected from nearby primary craters.

Other features observed in a few craters suggest that slumping has occurred, at least locally. These include scarps, terraces, and a few vague linear features within the craters which may be described as subdued scarps. One of the best examples of an abrupt scarp within a crater occurs in a 500-m-long rounded Tycho secondary crater in A199 (Fig. 32). This is an irregular branching scarp along the western wall of the crater; it is steeper than 23 deg over most of its length. The irregular trace and local branching of the scarp suggest that the material of the lower part of the western wall and crater floor has slipped downward a few meters. Very subdued scarps that are similarly irregular in trace appear in two smaller shallow irregular secondary craters nearby. I believe they are probably similar in origin to the abrupt scarp.

A rounded terrace occurs midway up the western crater wall of a primary crater approximately 1.5 km in diameter in B196 (Fig. 34). This feature has been interpreted by Dr. Urey as the extension of a mare ridge that intersects the rim crest of the crater, and as a laccolith by Dr. Kuiper; it may be related to similar terraces that have probably been formed by slumping in much larger primary craters. A hump in the wall of another crater of about the same size (Fig. 34) resembles a landslide.

A few unusual craters about 100 m across are observed in A199 (Fig. 32) and B200 (Fig. 33) whose form may best be described as dimple-shaped. Each of these craters has a low, broadly rounded rim that is convex upward and a wall which appears to be nearly conical or locally convex upward; at the foot of the wall, in some of these craters, the slope seems to steepen slightly, forming a funnel-shaped pit at the center. It is likely that craters of this form have also been modified by slumping or mass movement, the upper parts of the walls having flowed toward the center, the converging toe of the flowing mass enclosing the pit.

b. Distribution of craters. The *Ranger VII* photographs contain a great deal of critically important new information on the size and spatial distribution of craters less than a kilometer in diameter in Mare Cognitum. The size–frequency distributions in Mare Cognitum of primary and secondary craters greater than a kilometer across are close to the average for other maria. The newly observed distributions of small craters represent extensions of three orders of magnitude of diameters below the previously known size distributions for larger craters on the maria. It is important to distinguish between the distribution of the craters in the major ray systems and the distribution in the areas between the rays.

Ray areas. With increasing resolution, the observed ray areas in Mare Cognitum begin to fill up very rapidly with craters less than a kilometer across, but their distribution within the rays is irregular. Some parts of the crescent-shaped ray shown in the last four A-camera photographs (Figs. 11–14) are more than 50% occupied by secondary craters 300 m across and larger. In the northern part of the same ray, however, only 20% of the ray is occupied by craters of that size. Craters larger than 300 m are similarly sparse in the ray to the northwest of the crescent-shaped ray. For craters much smaller than 300 m in diameter, data are available only for the crescent-shaped ray; all of the highest-resolution photographs depict the northern branch of this ray, where the abundance of larger craters is lower than average for the entire crescent.

The last A-camera frame, 199 (Fig. 14), illustrates what appears to be a fairly representative part of the northern

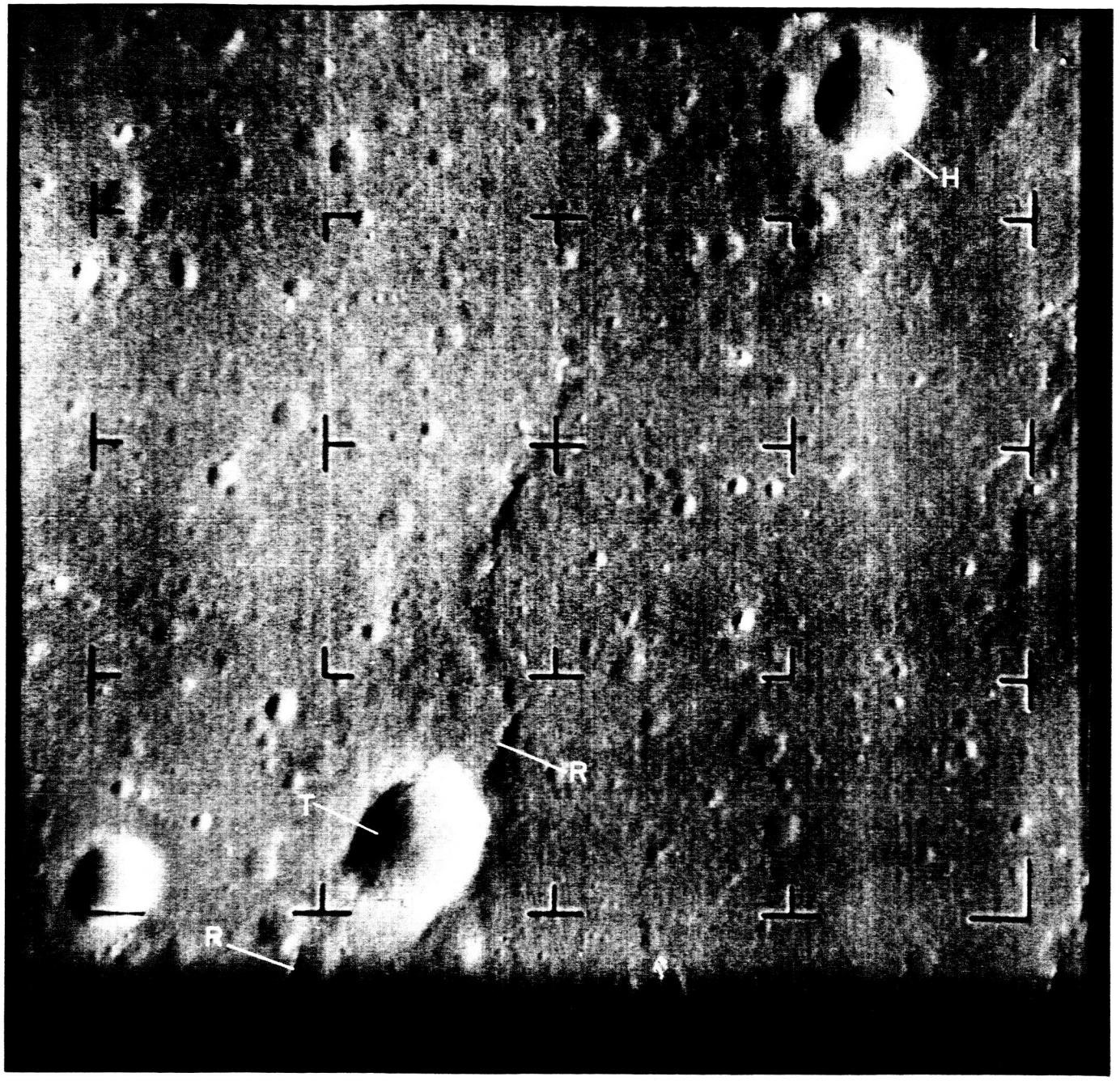

Fig. 34. B-camera photograph 196 showing ridge (designated R) intersected by a crater, position of terrace within crater (designated T), and hump (designated H) in wall of another crater. (Note streaks in wall of crater that intersects the ridge.)

part of the crescent-shaped ray. Craters ranging from 300 to 10 m in diameter can be detected in this photograph. Approximately 50% of the field is covered by craters. The vast majority of these belong to the indefinite class of shallow craters, and many of them are extremely shallow depressions. Craters ranging in size from 10 to 50 m cover 25 to 30% of the field and are scattered more or less uniformly over the larger craters and the areas between them. Many of the smallest craters are difficult to distinguish on the photographs reproduced in the A-Camera Atlas, but their occurrence and distribution can be observed on enhanced photographs from which some of the coherent noise has been removed by Robert Nathan of the Jet Propulsion Laboratory (Fig. 35). The profusion of small craters on the larger craters is well illustrated in a segment of photograph A199 prepared by Nathan. The majority of the smallest craters are very shallow and have rounded rims.

The last photographs obtained from the P_1, P_3, and P_4 cameras (Figs. 36, 29, and 30), which appear to be fairly representative samples of the ray area covered in A199, show that between 25 and 50% of the field is occupied by craters ranging from 1 to 10 m in diameter. Again, smaller craters are scattered over the larger ones.

The cumulative size–frequency distribution of craters in the ray area sampled by the *Ranger* photographs is illustrated in Fig. 37. This Figure shows the distribution for all types of craters, from the largest observed in Mare Cognitum down to craters 1 m in diameter. For craters larger than 1 km across, the curve represents the entire mare, but for smaller craters the data are necessarily restricted to areas covered by the *Ranger* photographs, and only a very minute area is sampled to obtain the estimated frequency of the smallest craters.

Areas between rays. Between the rays, the craters are more evenly distributed than in the rays. The spatial density of craters less than 1 km in diameter increases more slowly with increasing resolution than in the rays. In the sampled areas, covered chiefly by the B-camera photographs, craters greater than 300 m across are fairly widely spaced, occupying about 5% of the total field. With further increase in resolution, the field fills rapidly with craters less than 300 m in diameter. Approximately 20% of the field is covered with craters ranging from 50 to 300 m in diameter in the areas between the rays for which data are available (from highest-resolution B-camera photographs). Again, the large majority of the craters are of the indefinite shallow type, most of them very shallow with gently rounded rims. The distribution of craters much smaller than about 50 m in diameter in the areas between the rays cannot be obtained from the *Ranger VII* photographs because most of the pictures showing smaller craters are within the crescent-shaped ray. Thus, the range within which small craters would be expected to be found abundantly scattered over larger craters lies beyond the limits of best resolution for the *Ranger* coverage of the areas between the rays.

The cumulative size–frequency distribution for all types of craters between the rays is shown as a separate branch of the distribution curve in Fig. 37.

2. Positive-Relief Features

One of the most striking facts revealed by the *Ranger VII* photographs is the rarity of small positive-relief features other than crater rims. New features of this type revealed in the *Ranger VII* pictures include small details on a few mare ridges in areas between major rays and a number of very small low mounds in the crescent-shaped Tycho ray observed in the highest-resolution P-camera photographs.

Mare ridges photographed with resolution much greater than that of previously available photographs are portrayed best in B-camera pictures 194 to 197 (Figs. 30 and 31). The fine details revealed are similar to somewhat larger topographic forms observed on mare ridges through the telescope. Of particular interest are sharply defined branches that extend short distances off the main ridges, generally where the main ridges change strike. Some of these branches and some small cross ridges as short as 300 m in length are 50 m or less in width and have local slopes on their flanks approaching 20 deg. Similar small spines occur locally along the crest of a main ridge. Perhaps one of the most significant observations about these ridges is their local sharpness of form compared to the rounded rims of most of the small craters nearby. Parts of the ridges, however, are pitted with craters (Fig. 30).

At least two kinds of mounds appear to be present in the highest-resolution photographs of the crescent-shaped Tycho ray. These are best portrayed in the last P_1- and P_3-camera photographs (Figs. 36 and 29). Much of the field in the last P_1 photograph is occupied by gentle, irregular, elongate mounds trending north-northeast. Many small craters are superimposed on the mounds, which enhances their irregular appearance. The mounds are 5 to 15 m across and are separated only by narrow, winding, shallow depressions. Similar features are observed with poorer resolution on the next-to-last

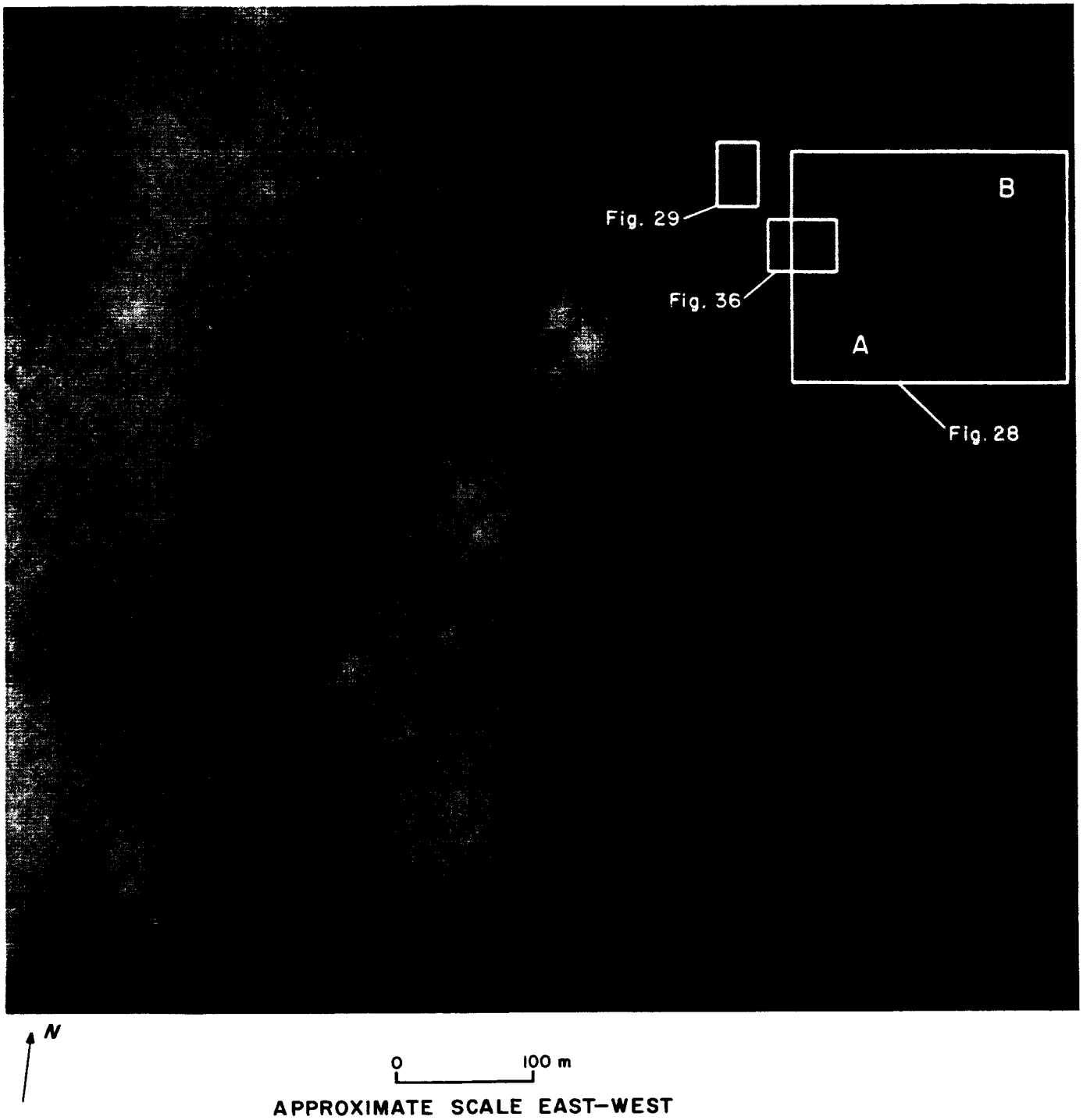

Fig. 35. Part of A-camera photograph 199 reproduced from digitized magnetic tape record after removal of part of coherent noise by digital computer processing. (Contrast has been enhanced to portray small craters more clearly. Computer processing and reproduction of photograph were carried out under the direction of Robert Nathan. Craters A and B are identical with craters marked A and B in Fig. 28.)



Fig. 36. Last P_1-camera photograph. (Note low ridges trending slightly east of north in left half of photograph.)

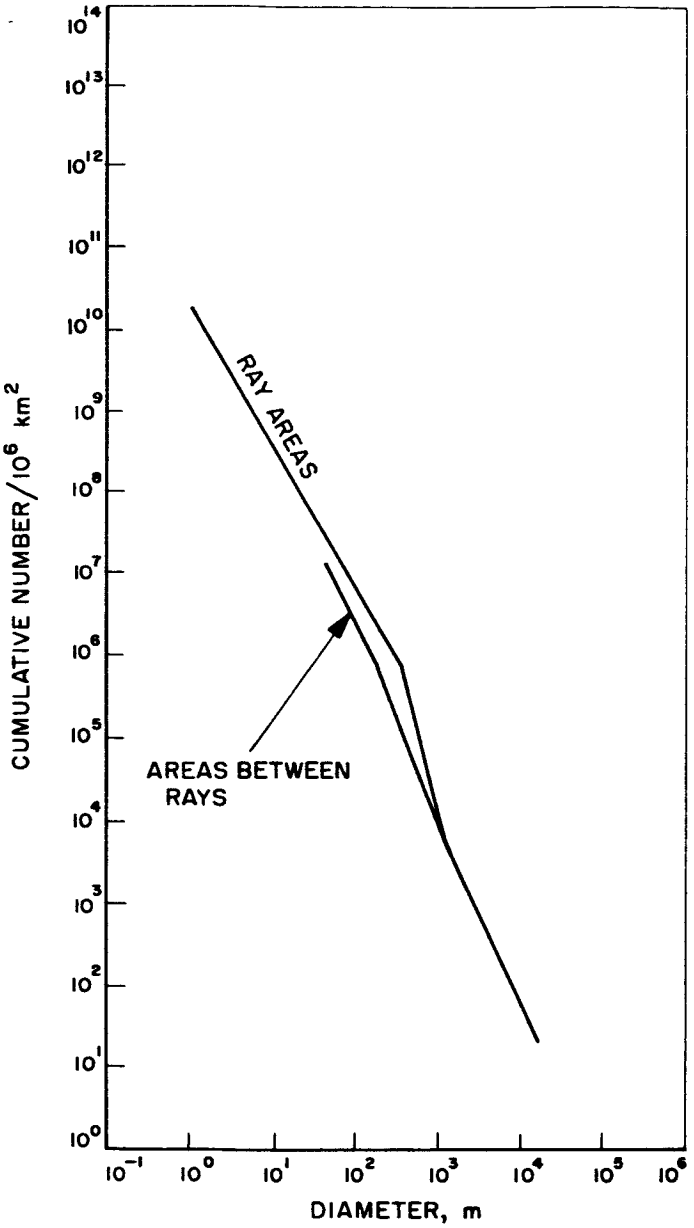

Fig. 37. Cumulative size–frequency distribution of craters in Mare Cognitum (based on distribution of craters observed in *Ranger VII* photographs).

P_3- and P_4-camera photographs (see, for example, Fig. 38). The mounds are locally well defined along a faint curved trough or subdued scarp, to which they give a very ropy appearance. Dr. Kuiper has compared the surface here to the bark of the Ponderosa pine. The bark-like appearance is heightened by the presence of many small craters superposed on and interspersed with the mounds. Relief on most of these mounds probably does not exceed a few meters, and the slopes are predominantly less than 10 deg (estimated). I believe that these gentle mounds are probably an intrinsic feature of the ray and will discuss them in more detail in the interpretive section to follow. A few other gentle mounds, ranging from a meter to a few meters across, have been detected in the last P_3-camera photograph, chiefly by photometric measurements. These features have such gentle slopes that they are not readily detected by visual examination.

One other unusual kind of positive-relief feature occurs in the last P_3-camera photograph (Fig. 29). It consists of a mound with a crater in the summit; it may be regarded as a crater with a greatly exaggerated rim. There are at least two definite examples of this feature in the photograph. The largest is an elongate mound about 5 m in length and 3 m across, with a 1-m-diameter crater in its summit. This mound occurs just inside the rim crest of a 10-m-diameter crater. The height of the mound measured in a direction normal to the large crater wall is about ⅓ m.

3. Albedo Variations

Variations in surface brightness due to variations in albedo of the surface rather than to variations in slope occur at many different scales in Mare Cognitum. Albedo variations over broad areas of the mare surface and local bright halos around primary craters larger than 300 m in diameter are well known from telescopic observations. The major broad variations in albedo are due to ray systems of Tycho and Copernicus. Another well known feature is a local very dark streak in the southeastern part of Mare Cognitum that corresponds with a low irregular ridge about 15 km in length. This ridge has been classified as part of the Procellarum group of Imbrian age by Eggleton (Ref. 3), who considered it to be closely related to domes observed elsewhere on the maria. It is well portrayed in about 100 of the A-camera photographs, but no critical new details of the ridge have been observed from these pictures.

Information of prime interest obtained from the *Ranger VII* photographs about the variations in albedo chiefly concerns the very small features and the sharpness of gradient of albedo variations. The margins of major rays observed through the telescope are diffuse, but the cause of this diffuseness could not be determined from the telescopic observations. One possibility was that the rays were composed of discrete, telescopically unresolved bright patches, and that the bright patches became more widely spaced toward the ray margins. The high-resolution photographs of the Tycho rays obtained by

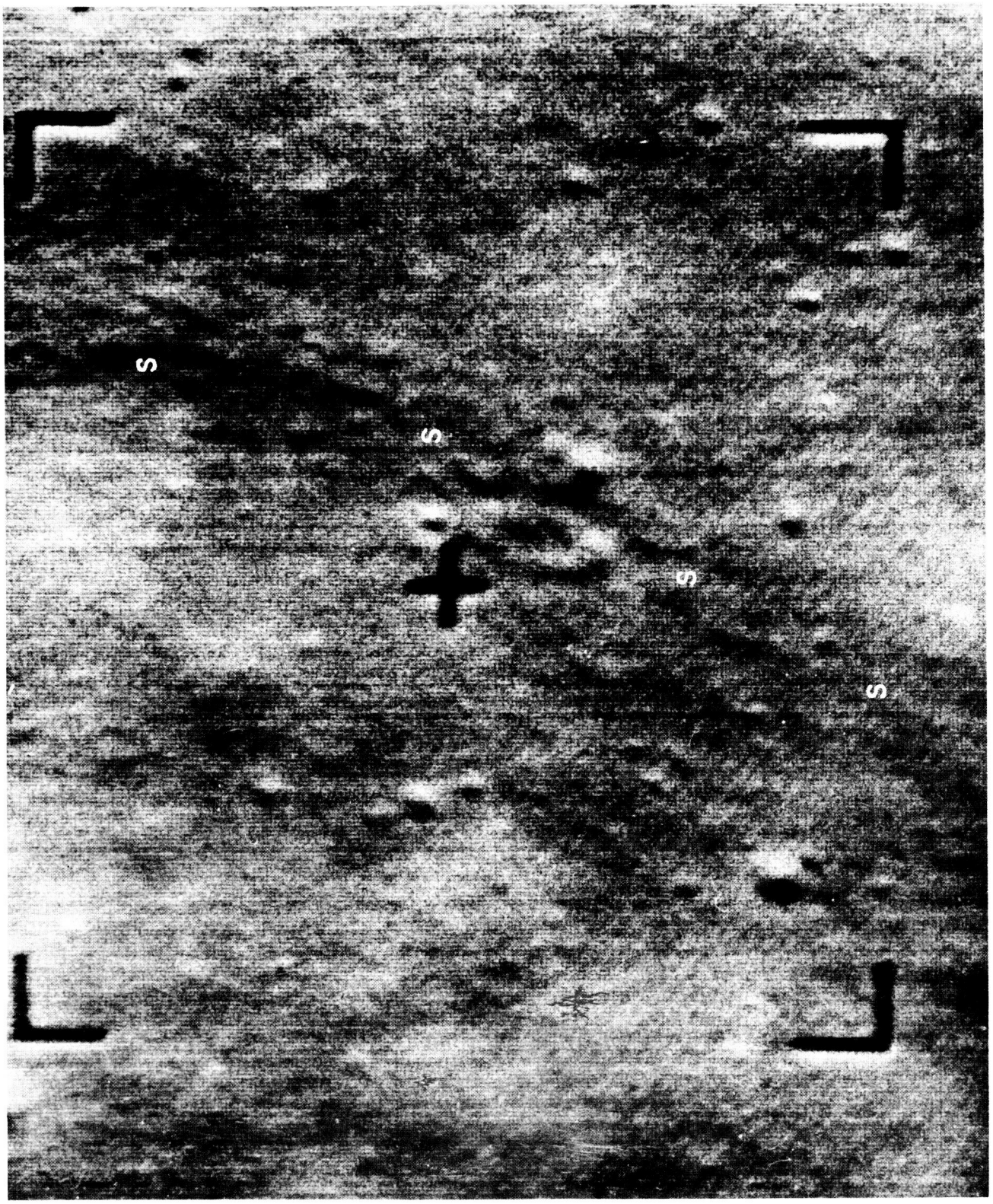

Fig. 38. Second-to-last P_4-camera photograph showing ropy appearance of subdued scarp (designated S).

Ranger have revealed that the bright walls of some of the telescopically unresolvable craters in the rays contribute to the overall ray brightness, but that this effect is superimposed on a background of more uniform albedo between the bright-walled craters. This background albedo of rays diminishes gradually toward the ray margins. The margin of the ray cannot be located more closely than about 1 km because of the gradual change in albedo, even in the high-resolution pictures. Over distances of a few tens of meters, areas in the crescent-shaped Tycho ray appear to be nearly uniform in albedo except near very small superimposed ray craters.

The smallest observed ray craters are about 30 m across and have bright halos or rays of comparable width. The margins of these halos and rays have the steepest gradients of albedo variation observed.

Another albedo variation feature of considerable interest is the pattern of radial and irregular streaks in the walls of certain primary craters. The best example occurs in the crater intersecting the mare ridge shown in B196 (Fig. 33). Alternate bright and dark streaks may be observed running down the illuminated crater wall. Well defined streaks range in width from about 100 m to the limit of resolution, and some taper noticeably downward. These streaks may be produced by sliding of weakly consolidated debris on the crater walls. A more detailed interpretation is given in Section B. Similar but more irregular streaks occur on the wall of a primary crater, 3 km in diameter, shown in Figs. 39–41. These streaks have widths up to several hundred meters.

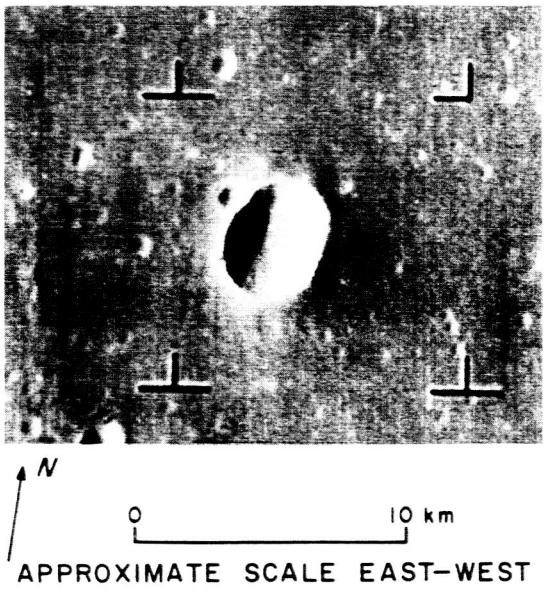

Fig. 39. Part of B-camera photograph 182 showing crater with prominent streaks on crater wall.

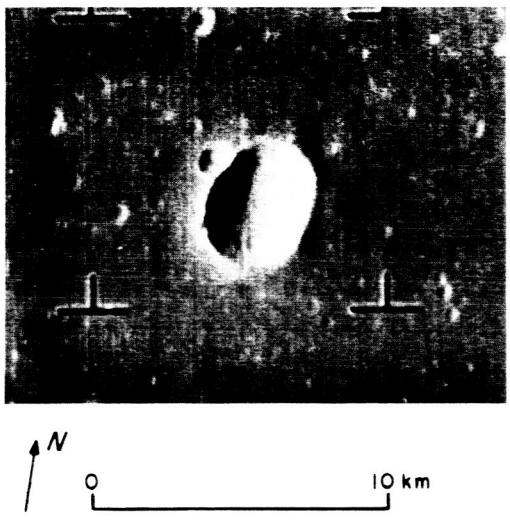

Fig. 40. Part of B-camera photograph 183 showing crater with prominent streaks on crater wall.

B. Cratering as the Dominant Surface Process

So far as may be judged from the *Ranger VII* photographs, cratering is the dominant process responsible for the small relief features of Mare Cognitum. This conclusion was anticipated before the evidence from *Ranger VII* was at hand, because the Moon is essentially devoid of an atmosphere and its surface is directly exposed to the bombardment of small and large meteoroids crossing the Earth's orbit. Because of the lack of an atmosphere, furthermore, most of the familiar processes which sculpt and modify the surface of Earth would not be expected to occur on the Moon. Thus, the bombardment by meteoroids and larger objects from interplanetary space is one of the few processes that, demonstrably, must occur on the Moon, and it is the only process that can also be demonstrated to be capable of producing most of the small surface features observed in Mare Cognitum.

All of the small relief features discovered in the *Ranger VII* photographs can, in my opinion, be explained as being a direct result of the formation of craters by impact. No other process is required, except for local mass movement (slumping), to account for the full range of small features (other than the sinuous mare ridges) and crater shapes observed. In accordance with the principle of simplicity (Occam's razor), impact cratering (with minor mass movement) will be adopted as the single process



Fig. 41. Part of B-camera photograph 184 showing crater with prominent streaks on crater wall.

leading to the development of the present relief in the region of Mare Cognitum around the *Ranger VII* impact point. The adoption of this point of view does not mean that the possible occurrence of other processes is not recognized, but simply that no compelling evidence is known that other processes have had an observable effect on the topography of the features observed.

Darkening of materials near the Moon's surface by high-energy solar radiation will be adopted as an auxiliary process leading, in conjunction with cratering, to the observed albedo variations in Mare Cognitum. It has been well established that high-energy solar radiation must reach the surface of the Moon and that such radiation will produce color centers and darkening of many silicates in the laboratory.

With these initial assumptions, we may proceed to examine how the features observed in Mare Cognitum are to be accounted for, in detail, and then to construct a model of the fine structure of the mare surface that is consistent with the observational facts and assumed processes. It will be shown that such a model can be developed that is also consistent with the presently known facts about the physical characteristics of the Moon's surface obtained from telescopic observations.

1. Cratering Rate as a Function of Crater Size

The primary craters on the maria are here interpreted as having been formed by impact of meteoroids and larger interplanetary objects such as asteroids and comet nuclei. Detailed evidence for this interpretation has been presented elsewhere (Refs. 4 and 5) and will not be reintroduced here. (See also Refs. 6–11.) According to this interpretation, the observed primary craters were formed by solid objects, ranging in diameter from several centimeters to a few kilometers, striking the solid surface of the mare at high velocity and propagating a shock locally in the mare material. (For a discussion of the mechanics of meteorite impact, see Refs. 12 and 13.) This process has probably continued intermittently since the maria were formed, possibly as long as several billion years.

The secondary craters are interpreted as having been formed by impact of comparatively low-velocity fragments of the Moon ejected from primary craters located both on the maria and on other parts of the lunar surface. (For an explicit account of the interior ballistics of a primary crater and the exterior ballistics of secondary crater-forming fragments, see Ref. 2, pp. 329–340.) The rays on Mare Cognitum, under this interpretation, consist primarily of mare material ejected from the secondary craters but contain a small admixture of material derived from the more distant primary craters with which the rays are associated.

a. Primary cratering rate. The rate of primary cratering on the lunar maria may be estimated from three independent sources of information: (1) the present observed fall of meteorites and micrometeorites on the Earth, (2) the distribution and age of ancient impact craters and eroded structures of possible impact origin on Earth, and (3) the distribution of primary craters on the maria and estimates of the absolute ages of the maria. Shoemaker, Hackman, and Eggleton (Ref. 5) showed that their interpretation of the terrestrial geologic record of impact cratering for the past several hundred million years is fairly consistent with a very large extrapolation in time and mass of the observed mass–frequency distribution and rate of fall of meteorites. They further demonstrated that the size–frequency distribution and average number of craters per unit area on the maria that may be predicted from the terrestrial data are consistent with the telescopically observed primary crater distribution on the maria (for all except the largest craters) if (1) the maria are assumed to be several billion years old and (2) the impact rate has remained relatively constant since they were formed. The observational uncertainties of the meteorite infall and of the geologic record of cratering, however, are rather large. Perhaps the greatest source of uncertainty in comparing the terrestrial data with the lunar data is the large extrapolation backward in time of the predicted cratering rate.

The expected or predicted size–frequency distribution of primary craters on the lunar maria, based on extrapolating the estimated size–frequency distribution of meteorites falling on the Earth to very large sizes and on extrapolating the present estimated rate of infall backward in time, is illustrated in Fig. 42. The meteorite infall data used are from Refs. 14 and 15; it is necessary to adopt likely impact velocities for the meteorites striking the Moon and to employ empirical scaling laws in order to derive crater size–frequency distributions. An age of 4.5 billion years, the approximate age of the Earth (Ref. 16), has been arbitrarily assumed for the maria in order to compare predicted primary crater distributions with the observed crater distribution on Mare Cognitum.

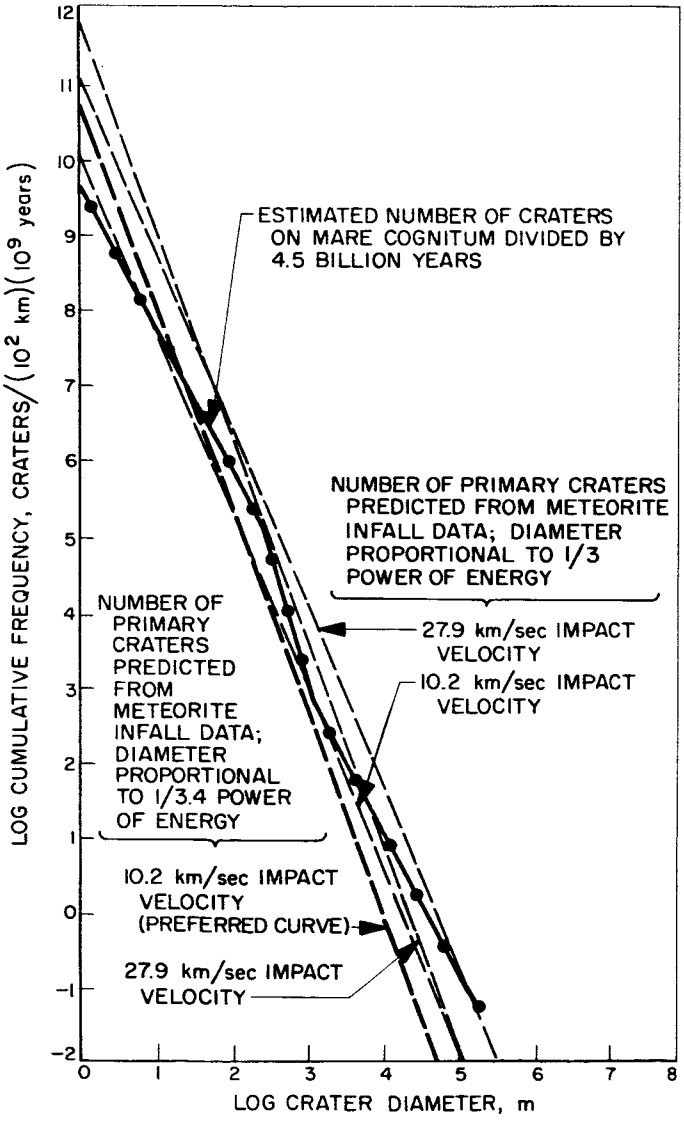

Fig. 42. Cumulative size–frequency distribution of craters in Mare Cognitum compared with cumulative size–frequency distribution predicted for primary craters on the basis of meteorite infall data. (Size–frequency distribution of craters in Mare Cognitum estimated from *Ranger VII* photographs is an average for ray areas and areas between rays.)

Four curves are shown in Fig. 42 which correspond, respectively, to the probable upper and lower limits of average meteorite impact velocity on the Moon and to two empirical scaling laws. A lower limit of average impact velocity of 10.2 km/sec and an upper limit of 27.9 km/sec are adopted. Objects striking the Moon at these velocities would have entered the Earth's atmosphere at 15 and 30 km/sec, respectively, had they encountered the Earth instead. The actual modal velocity of entry of meteorites into the Earth's atmosphere has been estimated as close to 15 km/sec (Ref. 17). The diameters of the craters formed by impact have been assumed to be proportional either to the ⅓ power or to the $\frac{1}{3.4}$ power of the kinetic energy of the meteorites. Diameters of very small hypervelocity impact craters in rock are approximately proportional to the ⅓ power of the projectile kinetic energy (Ref. 18), whereas the diameters of large craters formed by shallow subsurface explosion in rock and alluvium are approximately proportional to the $\frac{1}{3.4}$ power of the energy released (Ref. 19). Crater sizes are scaled from the Jangle U nuclear explosion crater, 82 m in diameter, which is intermediate in size between the largest and smallest craters observed on Mare Cognitum. Small corrections for the differences in size and capture cross-section of the Earth and Moon have been made in estimating the lunar impact rate from the terrestrial meteorite infall. (For a discussion of these corrections and the crater scaling relationships, see Ref. 5.) The four curves define an envelope of the predicted size–frequency distribution of primary craters formed on the lunar maria in 4.5 billion years.

The cumulative size distribution of all craters observed in the *Ranger VII* photographs (data for ray areas and non-ray areas combined) falls within the envelope of predicted distributions of primary craters for all except the smallest and largest craters (Fig. 42). This rough agreement might be taken to indicate that the assumptions adopted in deriving the predicted distributions are approximately correct and that most of the observed craters are of primary impact origin. There is a serious discrepancy, however, between the slopes of the observed crater distribution and the predicted distribution curves. Except for a short segment of the observed crater distribution curve, for craters ranging in size from 250 to

1,000 m, that is steeper than the predicted distribution curves, the observed crater distribution curve is less steep than the predicted distributions. For this reason, there is no way to significantly improve the match between the predicted and observed distributions simply by assuming a different age for the maria.

The predicted crater distribution, based on the best estimate of the modal impact velocity of meteorites on the Moon and the preferred scaling law for craters between 1 and 1,000 m in diameter, is shown in Fig. 42 by a heavy line. The discrepancy between this curve and the observed crater distribution is large. At a diameter of 1 m, the observed cumulative number of craters is an order of magnitude less than predicted. If the age of the maria were reduced an order of magnitude to bring the predicted and observed number of craters into agreement at 1 m diameter, the number of all craters larger than 10 m in diameter would be more than an order of magnitude too great.

The deficiency of observed small craters that can be identified as primary is actually much greater than an order of magnitude. In Fig. 43, the size–frequency distributions of identifiable primary craters and of the total number of craters observed in the *Ranger VII* photographs are plotted as separate curves. The curves join at about 1 km crater diameter, as all craters (in Mare Cognitum) much larger than this that are observed in the *Ranger* photographs are identifiable primaries. At 100 m diameter, the total number of craters is an order of magnitude larger than the number of identifiable primary craters, and at a few meters diameter, the total number of craters is more than an order of magnitude larger than the number of identifiable primaries. The predicted number of primary craters (preferred curve) is more than two orders of magnitude greater than the observed number at a few meters crater diameter. This difference between predicted and observed numbers of primary craters decreases rapidly with increasing crater size, and the two curves intersect at about 400 m diameter.

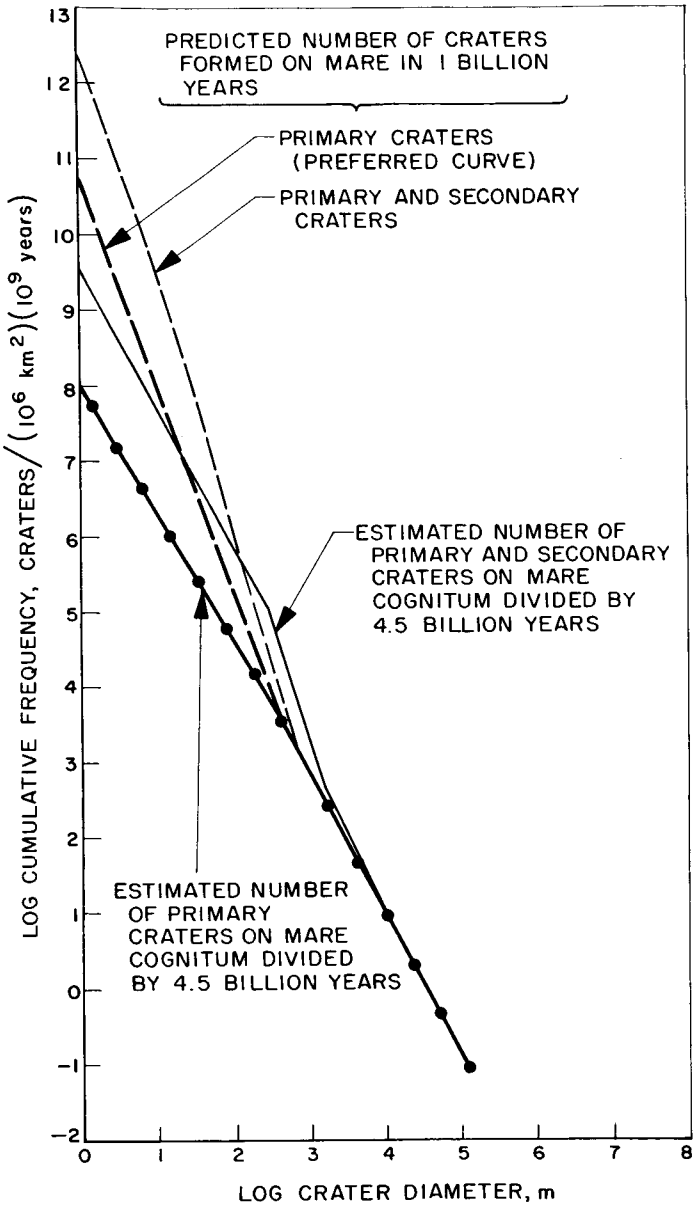

Fig. 43. Cumulative size–frequency distribution of primary craters and of all craters on Mare Cognitum compared with predicted size–frequency distribution of primary craters and of all craters.

b. Secondary cratering rate. The rate of formation of secondary craters on the Moon can be estimated from the primary cratering rate if the size distribution of secondary craters formed by individual primary craters is known. A predicted size distribution of secondary craters on the maria can be derived from the observed distribution of large primary craters, moreover, without any assumptions about the age of the maria or about the cratering rate. To do this, we require empirical data on the size–frequency distribution of secondary craters produced by primaries of different sizes. Around very large craters on the Moon, part of the size distribution of secondary craters can be observed directly. To obtain the expected size distribution of secondaries around small primary craters, such as those near the limit of telescopic resolution, it is necessary to examine experimental craters on the Earth.

Craters formed by large charges of high explosives or by nuclear devices detonated at shallow depth beneath the Earth's surface have the form and structure of primary meteorite impact craters (Ref. 12). Most such explosion craters, if they are larger than about 50 m in diameter, are surrounded by a swarm of secondary impact craters. Secondary craters are also formed around primary impact craters produced by ballistic missiles (Ref. 20), even in cases in which the primary crater is as small as 10 m in diameter. Part of the secondary crater field around the nuclear explosion crater Sedan is illustrated in Fig. 44. This explosion crater is about 400 m in diameter, and is surrounded by more than 5,000 secondaries that may be resolved in the aerial photograph. The secondary craters, which were formed by impact of large masses of rock and alluvium ejected on ballistic trajectories from the main crater, range in diameter or minor axis from 2 to 32 m (Fig. 45). Smaller secondary impact craters were also formed but cannot be distinguished on the aerial photograph. The cumulative number of the larger secondaries is approximately a simple power function of the crater diameters. A power function with an exponent of -4 is plotted in Fig. 45 for purposes of comparison. The cumulative number for the smallest secondary craters observed, however, lies significantly below the comparison curve. This is due in part to the fact that only a few of the craters with diameters near the resolution of the photograph were recognizable and counted.

The size–frequency distribution in each of the large secondary crater swarms on the Moon is similar in form to the distribution observed around Sedan. As an example, the size–frequency distribution of a part of the secondary craters in the swarm around Langrenus is shown in Fig. 46. Only the craters formed on Mare Fecunditatis (Fig. 4) have been measured and counted. Again a power function with an exponent of -4 has been plotted for comparison, and the cumulative number for the smallest observed secondary craters falls significantly below this comparison curve. As in the case of the Sedan secondaries, only a few of the craters with diameters or minor axes near the limit of resolution of the photographic plate were detected and counted. In order to

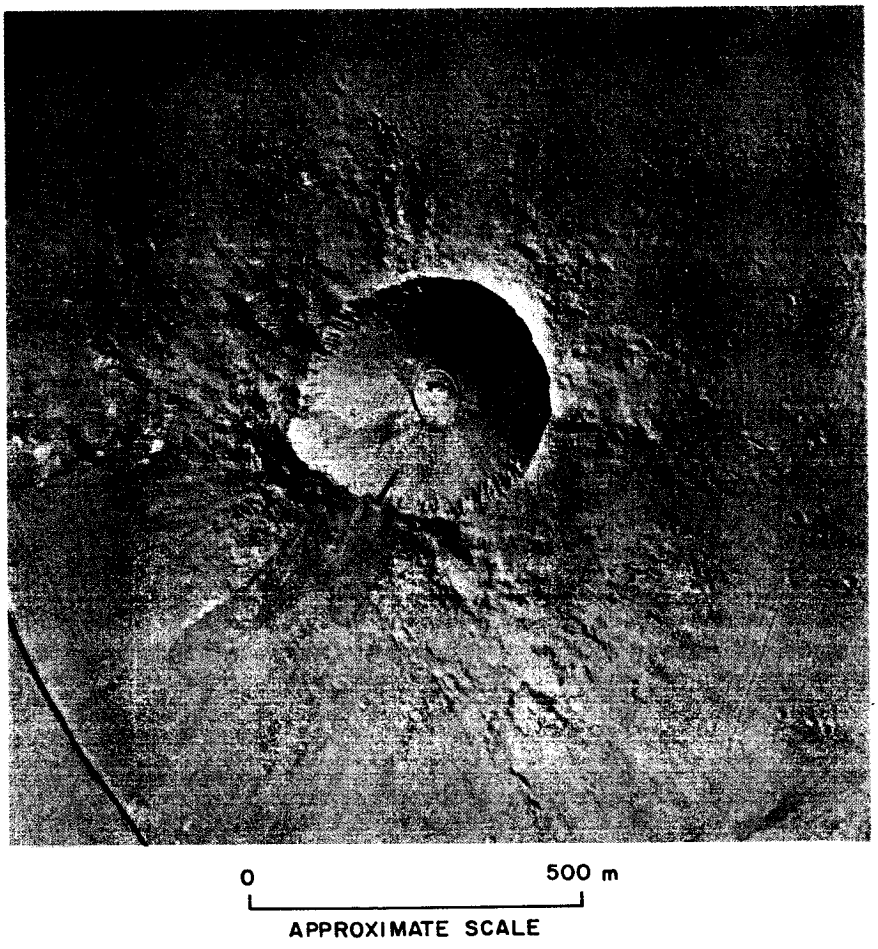

Fig. 44. Aerial photograph of Sedan nuclear-explosion crater (Nevada) showing associated swarm of secondary craters. (Several thousand secondary craters are resolved in the original photograph.)

obtain the true form of the size–frequency distribution of secondaries down to the limit of the smallest formed, it would be necessary to have much higher-resolution photographs, such as those acquired by *Ranger VII*.

If it is assumed that the number and size distribution of secondary craters observed in the crescent-shaped cluster in the highest-resolution *Ranger VII* A-camera photographs is representative of the number and size distribution of small secondary craters in the rest of the Tycho ray system, then we may estimate the cumulative size–frequency distribution of the Tycho secondary craters from the largest secondaries formed around Tycho

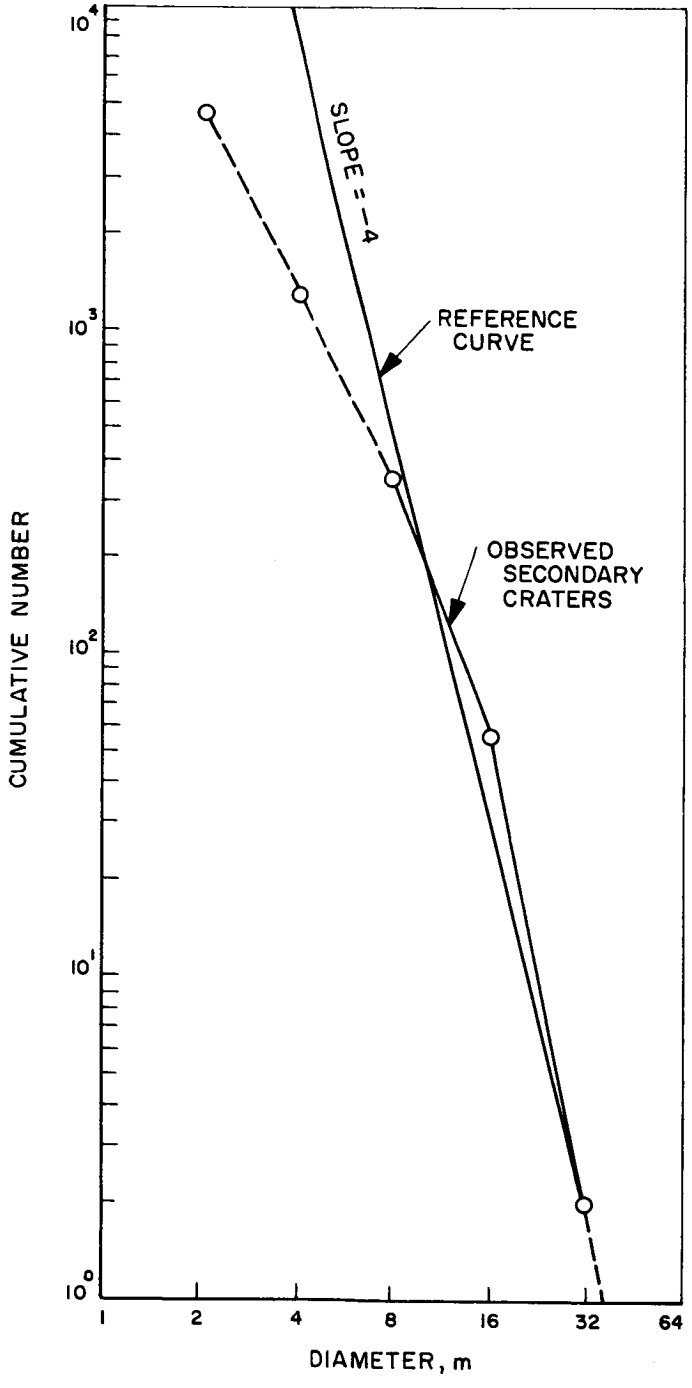

Fig. 45. Cumulative size–frequency distribution of Sedan secondary craters.

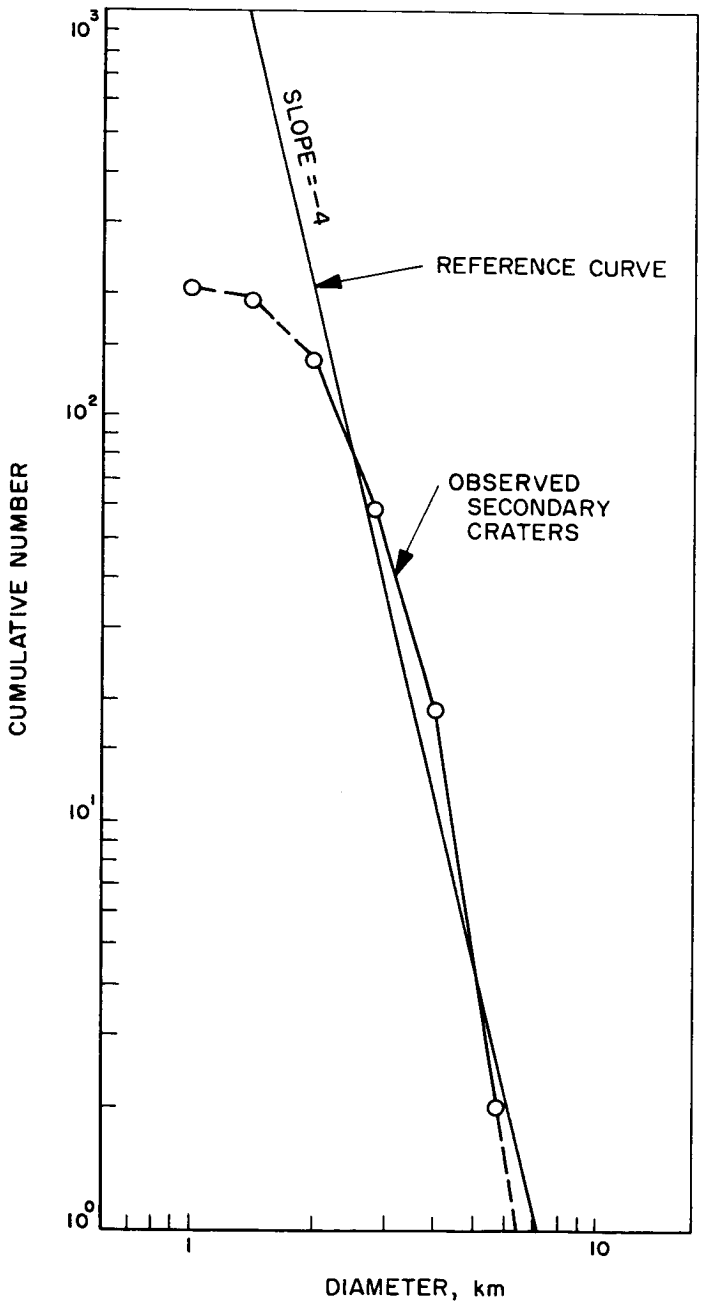

Fig. 46. Cumulative size–frequency distribution of Langrenus secondary craters.

down to 200 m in diameter. It is found, on this basis, that the cumulative number of secondary craters is very closely a simple power function of the diameters up to a cumulative number of 100,000 craters. The exponent of the function that best fits the estimated size distribution is slightly greater than −4. (The absolute value of the exponent is slightly less than 4.) The largest secondary crater formed by Sedan is about 1/12 the diameter of the primary crater, whereas the largest secondary in the swarm around Langrenus is about 1/20 the diameter of the primary. If we assume that this ratio varies smoothly with increasing diameter for primary craters from the size of the Sedan to the largest (Langrenus), it is possible to derive the expected size–frequency distribution of secondaries for any primary crater of intermediate size. Each of these expected distributions will be a simple exponential function with an exponent which may be taken to be the same as that estimated for the Tycho secondary crater swarm. It will be assumed that these distributions extend to a cumulative number of 100,000 craters, as in the case of Tycho.

The observed size–frequency distribution of primary craters on the lunar maria is illustrated by the solid segment of the line labeled "primary craters" in Fig. 47; the dashed segment of this line represents an extrapolation of the telescopically observed distribution of primary craters. The size–frequency distribution of secondary craters, obtained by integrating all of the secondary craters expected for each primary on the lunar maria, is illustrated in Fig. 47 by the line labeled "secondary craters." The solid segment of the line represents that part of the predicted distribution which is observable through the telescope. It may be seen that the total number of predicted secondary craters becomes equal to the number of primary craters (extrapolated) at a diameter a little above 200 m, which is a size just beyond the limit of visual resolution under the best seeing conditions at a large telescope. The actual distribution of secondary craters on the lunar maria observed through the telescope follows the predicted distribution very closely. With decreasing crater size below 200 m, the predicted number of secondary craters rapidly becomes much greater than the number of primaries expected on the basis of extrapolation. At a diameter of 10 m, the predicted number of secondary craters so greatly exceeds the number of primaries that the curve for the distribution of both primary and secondary craters is not distinguishable from the secondary crater curve in the illustration. For diameters smaller than 10 m, several hundred secondary craters are expected for each primary.

A majority of the telescopically resolvable secondary craters are clustered within the major swarms of secondaries around large primary craters. At the outer limits of these swarms and beyond, however, are regions in which a significant number of secondary craters can be found that cannot definitely be assigned to any given primary. These unassigned secondaries constitute a background field of craters with much more uniform distribution than is observed within the swarms. Most of the

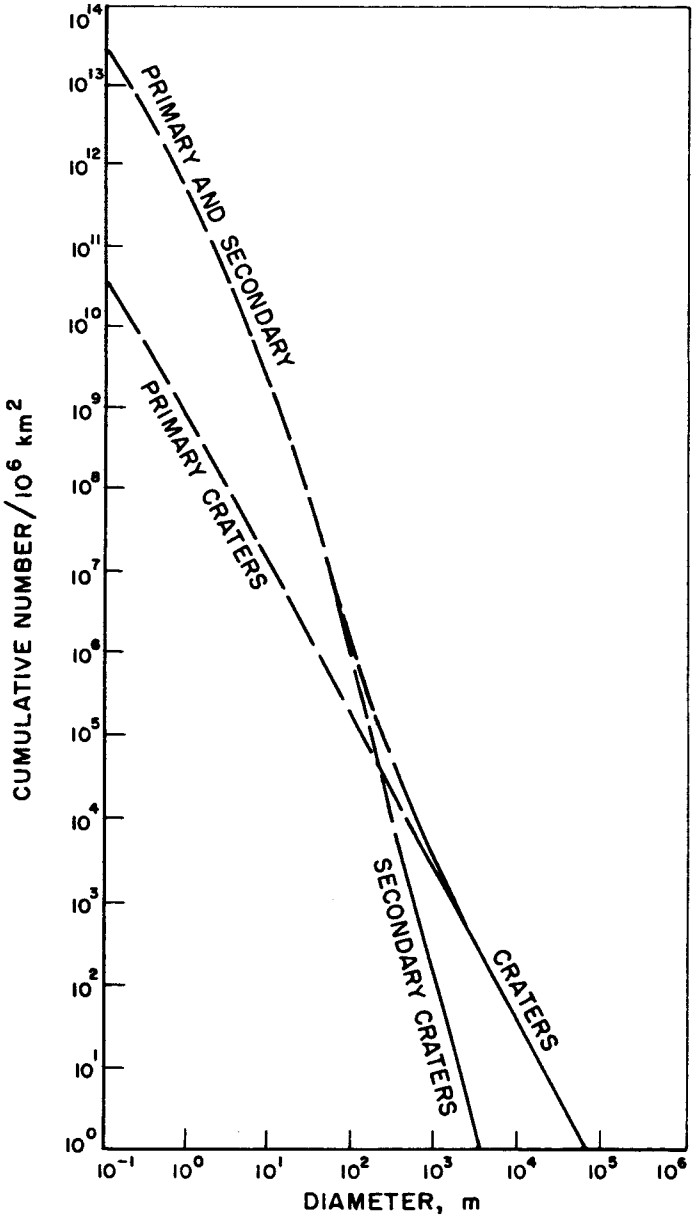

Fig. 47. Cumulative size–frequency distribution of primary craters on lunar maria and calculated distribution of primary and secondary craters. (Solid lines indicate telescopically observed distributions; dashed lines are extrapolated or calculated.)

large number of secondary craters too small to be resolved telescopically will probably not be assignable to individual primary craters because there will be extensive overlap of the swarms associated with small primaries. Thus, the small secondaries will contribute to the background field of craters. The mare surfaces, therefore, not only will contain small secondary crater swarms but also are expected to be more or less uniformly peppered with such craters.

An improved estimate of the number of small secondary craters that have been formed on the maria may be made utilizing the predicted number of small primary craters based on the terrestrial meteorite infall data (Fig. 43). For this estimate, an age of 4.5 billion years is again adopted for the maria. The primary crater distribution curve adopted in making the estimate has two branches: (1) the preferred curve for primary craters based on meteorite infall data, which extends from diameters of 1 m to about 400 m, and (2) the observed crater frequency distribution of the lunar maria for diameters above 400 m. The cumulative number of secondary craters larger than 1 m in diameter, predicted on this basis, is more than 10 times greater than the number based on the observed primary crater distribution extrapolated to small sizes. The predicted cumulative number of all craters larger than 1 m in diameter, however, is only about 50 times greater than the predicted cumulative number of primary craters of that size.

The predicted cumulative number of all craters 1 m in diameter and larger (improved estimate) is more than two orders of magnitude greater than the estimated cumulative number of all craters based on the *Ranger VII* photographs. At diameters of a few meters, the ratio of the cumulative number predicted to the number observed is about the same for all craters (primary and secondary combined) as it is for the primary craters. As in the case of the primaries, this ratio decreases rapidly with increasing crater size, and the predicted and observed curves cross at a diameter between 100 and 200 m. For areas between the rays, the predicted and observed cumulative curves for all craters join at about 300 m.

2. Effects of Interaction of Small Craters

The predicted number of small craters, both primary and secondary, is so great that craters are expected to have been formed everywhere on the lunar maria. On the basis of the improved prediction for the cumulative number of all craters larger than 1 m across, the mare surface would have been cratered repeatedly at any one place. It is impossible, in other words, to observe the predicted number of craters larger than 1 m across because their total area is more than 10 times as great as the area of the mare surface. The effect of repeated cratering is to reduce the total number of craters that are observable. Not only are small craters lost by the superposition of others of the same size or larger, but the repeated formation of small craters will also finally obliterate larger ones.

The effects of repeated formation of small craters on larger ones are complex and can only be worked out in terms of a statistical model of cratering frequency, the mechanics of cratering, and distribution of crater ejecta. For each cratering event, material is removed at the site of the crater and is widely distributed in the surrounding area. On the basis of the velocity distribution of fragments observed in impact experiments with rock targets, about half of the fragments ejected from a small crater on the Moon will land within a kilometer of the crater. The other pieces will be thrown greater distances, and, in the case of primary impact craters, a small percentage of the material thrown out will be widely scattered over the Moon's surface. Some material is even ejected at the velocity of escape from the Moon. For each cratering event that removes material from a small spot and scatters it widely over the surrounding area, there will be many events in the surrounding area that will throw material back.

If no material were lost from the Moon by ejection at escape velocity, the ultimate effect of repeated formation of craters of one size would be the development of a layer of fragments with an average depth approximately equal to the depth of the individual craters. At any one point, this layer of fragments would be removed or reduced in thickness from time to time by the formation of a new crater and would then be gradually covered again by fragments ejected from a large number of craters formed elsewhere. The average time of turnover or renewal of the layer at any one point would be just equal to the time required to form the number of craters whose total area is equal to the surface of the Moon.

If a frequency distribution of crater sizes like the cumulative size distribution predicted for the lunar maria is next considered, the effects of repeated cratering are more complicated. The smaller the crater diameter, the higher the turnover rate of the surface layer. The average depth of the fragmental layer on the maria will be given by the product of the average depth of the craters larger than the size at which the total area of the craters is equal to the area of the maria and the ratio of the specific volume of the crater ejecta to the specific volume

of the original material. The layer will have been stirred to this depth just once on the average. At successively shallower depths, the material is stirred or the layer is rejuvenated more frequently, and, in its uppermost part, the layer is stirred by the repeated formation of very small craters a very large number of times. The turnover rate of the uppermost millimeter of the Moon's surface, on the basis of estimates of the micrometeorite influx (Ref. 21) and the secondary particles generated by this influx (Ref. 22), may be greater than once every 100 years.

On a surface on which a fragmental layer is continuously being formed and reformed, the shapes of craters are modified by two processes. The first process is the actual destruction or removal of a crater by the formation of a new crater the same size or larger. In the second process, a crater is gradually covered over by fragments and peppered with smaller craters in the time intervals between larger cratering events. The latter process, if it continues sufficiently long, will so modify the shape of the crater that it is no longer recognizable. With a given flux of impacting objects, the distribution of observed craters below some limiting size will tend toward a steady size–frequency distribution. Within the size range in which the distribution remains steady, new craters are formed as fast as old ones disappear from the combined effects of the two crater-modification processes. There will be a steady number of craters of any given size, no matter how long the cratering continues, and craters of a given size will exhibit a complete range of shapes from fresh unmodified forms to forms so modified that the crater is barely discernible. Above this limiting size, craters may undergo considerable modification in shape, but those formed do not disappear. With a given flux and size distribution of impacting objects, the limiting size of the steady crater size distribution gradually increases with time.

Craters only slightly larger than the limit of the steady size–frequency distribution will generally be significantly modified by covering with fragmental material and peppering by smaller craters. The precise effects of this process vary with position on the crater. As the majority of smaller craters are expected to be secondary impact craters, formed by fragments traveling generally along relatively low-angle trajectories (Refs. 2 and 23), the rim of the large crater is exposed to a greater flux of impacting objects than the floor. The rim is also exposed to a greater flux than the more level areas surrounding the crater, and the floor is exposed to a lower flux than the surrounding terrain. Thus, more material tends to be ejected from the rim than is thrown back from the surrounding region, and the floor of the crater tends to receive more material from the surrounding region, including the rim, than is thrown out. In the crater floor, the fragmental layer tends gradually to become thicker, whereas the crater rim, or any protruding or positive-relief feature on a mare surface, will tend to be covered by only a thin layer of fragments relative to the surrounding region and to be continuously worn away. As the crater floor slowly fills up and the rim is ground down, the differences in the solid angles of space subtended by points on the surface of the rim and on the floor become less pronounced, the differences in rate of cratering diminish, and the rates of filling of the crater and degradation of the rim decrease. The ultimate effect of repeated formation of smaller craters on a large one, however, would be to reduce the rim and raise the floor to the same level as the surrounding terrain, thus completely eliminating the topography of the crater. A deposit of fragments would be present over the floor of the original crater, with a maximum depth equal to the depth of the original crater below the level of the surrounding terrain.

Let us turn now to the interpretation of the difference between the predicted number of craters and the estimates of the actual size–frequency distributions of craters in Mare Cognitum obtained from the *Ranger VII* photographs, as illustrated in Fig. 43. The predicted curves represent the numbers of craters expected to have been formed in each million square kilometers of the mare surface per billion years, whereas the curves based on the *Ranger VII* data represent the observed distribution of craters per million square kilometers divided by 4.5 to give the equivalent rate of cratering per billion years. If the predicted curves for the number of craters formed are valid, they should join the observed curves, both for primary craters and for primary and secondary craters combined, at the limiting size for steady frequency distribution. This occurs at approximately 400 m for the primaries and at approximately 300 m for all craters in the areas between the rays. Inasmuch as the locations of the points at which the observed and predicted curves join are very sensitive to small variations in the predicted curves, this difference is not judged to be significant. In the ray areas, the observed number of all craters is actually above the predicted curve between 150 m and about 1 km diameter because of the local concentration of Tycho secondary craters in the rays, but is below the predicted curve for diameters less than 150 m. Except for this local concentration of Tycho secondaries, the difference between the observed and the predicted curves

may be interpreted as representing the numbers of craters lost by the effects of crater interaction. At diameters of a few meters, several hundred times as many craters have been formed and subsequently destroyed as are now present on the mare surface. The ratio of craters formed on the maria to those now present is essentially the same for primary and secondary craters.

3. Interpretation of Areas Between Rays

In the areas between the rays, the distribution and shapes of craters observed in the *Ranger VII* photographs are here interpreted as being the result of the cumulative effects of primary and secondary cratering since Mare Cognitum was formed. Many primary craters smaller than 1 km in diameter that are seen in the high-resolution A and B pictures show some rounding of rims and somewhat shallower depths than would be expected for typical primary craters. The rounding of rims is probably due to the eroding effects of the interaction of small unresolved craters, and the anomalously shallow depths are probably the result of partial filling by ejecta from surrounding craters and by landslides and talus derived locally from the crater walls. The almost complete lack of raised rims on the large elongate secondary craters in the Bullialdus secondary swarm and on other secondaries, labeled **S** in Figs. 17 through 27, is also interpreted as due to erosion by repeated formation of small craters. If these craters originally had rims like the larger secondaries of Tycho and Copernicus, 10 to 20 m of rim material has been worn away. The floors of these ancient craters are probably underlain by a fairly thick layer of slowly accumulated fragmental material.

With craters of progressively smaller diameter, it becomes increasingly difficult to distinguish modified primary from secondary craters. Erosion and filling due to small crater interaction apparently have modified the shapes of primaries less than 1 km across so that they approach secondary craters in form. Craters smaller than 300 m in diameter exhibit a complete range of shapes from typical primaries to craters so shallow that they are scarcely detectable in the *Ranger* photographs. In this size range, it is impossible to distinguish eroded primary from circular secondary craters. On the basis of the predicted numbers of primary and secondary craters, the circular craters of the indefinite class larger than about 200 m in diameter (labeled I on Figs. 30 and 31) are predominantly eroded primaries but probably include some secondaries. The elongate to irregular craters (labeled **E** on Fig. 31) are probably chiefly eroded secondaries. The depth of fill of most of the nearly flat circular craters larger than 200 m across may be nearly equal to the depth of uneroded primaries of the same size, between one-fourth and one-third the crater diameter. The average depth of fill in the eroded secondaries is probably significantly less, as the depth of unmodified secondary craters is typically as low as one-tenth of the crater diameter.

Most of the indefinite craters less than 200 m in diameter are believed to be secondary craters, many with forms modified by small crater interaction. All except the youngest probably have been partially filled with fragmental material. The average depth of the fragmental layer in these craters should be less than 10 m.

Between the resolvable craters, the surface of the mare is probably covered nearly everywhere with a fragmental layer of crater ejecta which varies irregularly in thickness from place to place. On the basis of the number of small craters, chiefly secondaries, predicted to have been formed, the average thickness of this fragmental layer in the areas between the rays should be of the order of 1 m. This estimate has a large uncertainty owing primarily to the unknown magnitude of two effects on the small crater ejecta: (1) change in specific volume of the lunar surface material due to fragmentation or to shock compression and (2) loss of material ejected at escape velocity from the Moon. The first effect depends on the initial porosity of the lunar surface material, specifically, the mare material. If it is originally rock with little pore space, a large expansion of specific volume can result from fragmentation and loose stacking of the fragments. This expansion is typically of the order of 30% for fragmentation of dense rocks on the Earth, but it may be much greater for very open stacking of small fragments on the lunar surface. If the mare surface material is initially very porous lava, on the other hand, as Dr. Kuiper has suggested, then shock compression of the ejecta may be greater than the volume expansion normally expected from fragmentation and loose stacking, and the net volume of ejected material may be less than its original volume.

Loss of material ejected at escape velocity from the Moon also depends on the porosity at the lunar surface as well as upon the total flux and velocity distribution of impacting primary particles. Where dense rocks are exposed, as much as an order of magnitude more mass may be ejected from the Moon than strikes the lunar surface, at impact velocities typical for comets and meteor streams (Ref. 22). The amount lost is much less for low-velocity impacts and from porous materials. The total

mass of material lost from the mare surface due to high-velocity impact of small solid particles and to energetic solar protons may be roughly of the same order as the mass of fragments now present on the mare surface.

Original small surface features of Mare Cognitum have probably been strongly modified, and the smallest features completely removed, by repeated cratering. The only small features I have observed in the *Ranger VII* photographs which might be original features of the mare surface are the sinuous ridges and a few low scarps that may be related to the ridges. Some parts of these ridges are pitted with craters, but other parts are surprisingly sharply formed. From telescopic studies, it is known that the ridges cross color and albedo boundaries elsewhere on the maria; they appear to be younger than the mare material. It is possible that some of the ridges have been actively rising late in the history of the Moon, although most of them are probably ancient features of the maria.

Most of the small linear features I have found in Mare Cognitum, and most of the lineaments illustrated by Strom (data presented by Dr. Kuiper) I believe are either secondary craters or rows of secondary craters. The azimuths of the major axes of composite secondary impact craters and of rows of secondary craters are related to the azimuths of major lineaments on the lunar crust through transformations given by the ballistic equations for secondary fragment trajectories and the equations describing particle acceleration during cratering (Ref. 2, pp. 329–334). Relatively few of the lineaments, in my opinion, are related directly to subjacent structures that extend into the mare material beneath the debris layer.

4. Interpretation of Ray Areas and the Highest-Resolution Pictures

The highest-resolution photographs obtained with *Ranger VII* show small parts of the mare surface that lie entirely within a ray of Tycho. The surface features shown in the last few P-camera pictures provide an insight into the fine structure of this ray, possibly a typical ray, but are probably not representative of the areas of the mare surface between the rays.

One of the most significant facts revealed by the last few A-camera pictures is that the ray, which is identifiable on both low- and high-resolution photographs as a bright streak, is coincident with an area of closely spaced secondary craters. Although the spacing and size of craters varies within the ray, the areal density of craters more than 200 m across, particularly the elongated secondary craters, is nearly everywhere greater inside the ray than in the areas adjacent to the ray. The gradational photometric boundary of the ray lies within a kilometer of the limit of the closely spaced secondary crater field.

If the craters are of secondary impact origin, as I believe, the extent of the bright material of the ray is coincident with an area which may be expected to be covered by coalescing and overlapping rim deposits of material ejected from the craters. By far the largest proportion of this material at any one place is probably derived from the nearest large secondary crater, although fragments are probably also present which have come from other secondaries within the ray and from the primary crater.

The ray is thus viewed here simply as an area nearly continuously covered by a layer composed of the collective throwout of the cluster of Tycho secondary impact craters and by the craters themselves. This thrown-out material is brighter than most of the material exposed elsewhere on the mare because of several factors discussed in detail below. The shape and extent of the ray are controlled strictly by the shape and extent of the secondary impact crater cluster.

In the ballistic theory (Ref. 2), the pattern of a secondary crater swarm and the shape of individual crater clusters are controlled by the breakup pattern of the lunar material as it is ejected from the primary crater. The size distribution of secondaries within each ray is related directly to the size distribution of fragments within each ray-forming cluster of fragments ejected from the primary crater. These fragments traveled through space on closely similar but slightly divergent ballistic trajectories as an expanding cluster. Fragments which were on the end of the cluster nearest the center of the primary crater as they left the primary received slightly greater accelerations, were ejected at somewhat higher angles, and traveled farther than the fragments originally farthest from the center of the primary. The radial sequence of points at which the individual fragments struck the lunar surface is, therefore, the reverse of the radial sequence of the positions from which they were ejected from the primary crater. Fragments derived from positions farthest from the center of the primary tend to be larger than fragments from positions nearer the center, and there is thus a general tendency for the largest craters to occur near the end closest to the primary in each secondary crater cluster.

Circular secondary craters are probably formed by impact of individual large secondary fragments, whereas elongate and composite secondaries are formed by impact of two or more fragments that traveled very close together. Both theory and the evidence from "ballistic shadows" in the ray pattern of Copernicus (Ref. 23) indicate that the angles between the horizontal plane at the impact points and the trajectories of the secondary fragments are low. Composite craters, therefore, tend to be elongate roughly in the azimuths of the trajectories, but their major axes will not, in general, be precisely radial from the primary crater. The fact that many of the elongate secondary craters are distinguishably composite and are generally not aligned precisely along radials from the primary shows that they are not just grooves plowed by individual fragments striking the lunar surface at low angles.

The elongate secondary craters in the distal or "downrange" part of the Tycho ray seen in the last *Ranger VII* pictures seem to have more rounded rims than craters of similar size in the proximal or "uprange" end of the ray. This apparent rounding may be due to the smoothing effects of throwout from the craters in the uprange end of the ray. It is possible that many of the shallow craters 10 to 50 m across that are revealed by enhancement of the last A-camera photograph (Fig. 35) are "tertiary" craters—that is, they are secondary craters of the large uprange Tycho secondaries. These small shallow craters are strewn over the larger elongate Tycho secondaries shown on the last A-camera photograph, and their combined effect would be to reduce the relief of the larger craters.

The thickness of thrown-out material on the rims of the secondary craters probably varies with position on the rim. It may be expected to be thickest near the crests of the secondary crater rims and to become progressively thinner at greater distances from the rim crests. A substantial thickness of thrown-out material should be present in the immediate vicinity of the closely spaced Tycho secondary craters shown in the last A-camera photograph. This includes the area shown in the last P-camera pictures. The thickness of thrown-out material on the rim of the 500-m-long secondary crater shown in the last P_1-camera photograph (Fig. 36) should be of the order of 10 m. Material at this locality on the rim probably has been expelled from depths greater than 10 m within the secondary crater. If the craters I have identified as Tycho secondaries in Figs. 13 and 14 are truly of secondary impact origin, I do not believe that the original surface of the mare can possibly be exposed in the area shown in the last half-dozen P-camera photographs. The low mounds of the "tree-bark" structure of the surface revealed in these photographs are probably original features of the throw-out deposits of the large secondary craters. The structure may be the result of flowing motion of the thrown-out material as it skids along the surface after ejection from the secondary crater. I have observed similar topography on material thrown out of explosion craters. Although the tree-bark structure is most easily observed along scarps sloping away from the Sun, it is probably present over most of the area covered by the last P-camera photographs.

The presence of small, possibly original, features of the throw-out deposits suggests that the ray was formed very late in lunar history. Tycho can be shown to be one of the youngest large ray craters on the Moon because its rays are superimposed on most other types of lunar terrain, and no telescopically resolvable younger features have been found to be superimposed on Tycho. Its age may be on the order of one-hundredth the age of the maria—50 million years or less. The smallest craters observed in the highest-resolution P-camera photographs are superimposed on and still younger than the Tycho secondary craters and the ray. Even the smallest craters resolved in the last P-camera pictures may have diameters greater than the upper limit of the steady size–frequency distribution for craters formed since the ray. If this is the case, the ratio between the number of observed and predicted small craters on the ray may give the ratio of the age of the ray to the age of the mare (assuming the cratering rate has remained constant).

The absence of small blocks or pronounced bumps in the ray may indicate an upper limit to the size of fragments in the material thrown out of the secondary craters. If the fragments had dimensions as large as the width of the mounds in the tree-bark structure, one might expect them to stick out here and there. Fragments this size could not have been worn away by repeated cratering, or the mounds would have disappeared, too, although small blocks with dimensions near the limit of highest resolution of the P-camera photographs could have been worn away by still smaller craters. It is tentatively concluded that most of the fragments in the throwout from the 500-m-long secondary shown in the last A-camera photograph are less than 1 m across.

The fine structure of the ray, as interpreted here, is fairly complex. Within the ray, a layer of varying thickness of thrown-out material, derived from varying depths beneath the surface at the sites of the secondary craters,

overlies an older mare surface. Immediately beneath the throw-out layer, there is probably a layer of fragmental debris in most places that is nearly identical with the debris layer exposed in the areas between the rays. The surface of this older debris layer was probably pitted with craters with distributions of size and shape similar to that observed between the rays. Where the layer of ray material is relatively thin, away from the rim crests of the secondary craters, most of the larger craters observed are probably thinly veneered pre-ray craters. A very thin debris layer produced by repeated formation of very small craters is expected to be present on top of the ray material.

5. Interpretation of Photometric Variations

Variations of brightness of the lunar surface recorded in the *Ranger VII* photographs are due to variations in albedo of the lunar surface materials and to variations in slope of the surface. First, the causes of albedo variations on Mare Cognitum will be examined in terms of the cratering processes. A method will then be outlined for estimating the distribution of slopes on the mare surface in areas with uniform albedo.

a. Interpretation of albedo variations. The principal variations of albedo on Mare Cognitum occur across the rays and along steep crater walls. Certain other features in the albedo pattern such as the unusual dark ridge in the mare shown in the A-camera pictures and the relatively high albedo of the highlands surrounding Mare Cognitum and of certain ridges, peaks, and broad high areas within the mare, are observable in the *Ranger VII* photographs and are well known from telescopic observations. Some of the observed differences in albedo are probably related to differences in mineral or chemical composition of the materials exposed, but it is instructive to examine whether most of the albedo variations on the mare can be explained as being a result of physical processes operating on materials of essentially uniform composition.

If it is assumed that the material at the mare surface is susceptible to darkening by high-energy solar radiation, then most of the materials making up the fragmental layer produced by repeated cratering have been affected by the darkening processes, as most fragments in the layer have been at the surface at one time or another. The darkening is assumed to take place as a result of a number of possible solid-state changes produced both by ultraviolet radiation and by solar-proton bombardment.* Laboratory studies of these effects suggest that most of the darkening takes place within a millimeter or a few millimeters of the exposed surfaces of common rock-forming minerals and depends upon the radiation dose, up to the point at which the albedo of the mineral or material in question reaches a limiting minimum value. If this is the case for the materials of the maria, the precise effects of irradiation on a repeatedly stirred layer of fragments on the order of a meter or many meters thick are complex.

The average rate of darkening of the surface of an initially unirradiated fragmental layer would depend on the relative rates of darkening of an undisturbed surface and of turnover and exposure of fresh material. If the time required for the albedo of an undisturbed surface to reach a lower limiting value under solar irradiation is much shorter than the average time of turnover or renewal of the fragmental layer to the depth significantly affected by radiation darkening, then nearly all parts of the surface will be more or less uniformly darkened after a period of time not much greater than the period required to darken an undisturbed surface completely. If, on the other hand, the turnover time of the upper part of the fragmental layer is much shorter than the time required for the albedo of an undisturbed surface to reach a lower limiting value, then the radiation darkening effect will be spread through the material of the fragmental layer during early stages of darkening, and the upper surface of the layer will gradually become darker after a period of time much longer than the period required to darken an undisturbed surface completely. The latter case appears to offer a good model for the lunar maria.

In the case in which the darkening rate is relatively slow, material initially at and near the surface will be partially darkened first, and this partially darkened material will gradually be dispersed downward in the fragmental layer with repeated formation of craters of varying size. As the fragments that are initially at the surface are, on the average, exposed longer than fragments initially near the base of the fragmental layer, fragments nearest the surface will tend to receive a greater radiation dose in a given period of time than

*Since the preparation of the manuscript of this report, Hapke (Ref. 24) has described the primary cause of darkening of fine rock powders by experimental irradiation of 2-kev H and He ions as due to the formation of coatings of nonstoichiometric compounds on the undersurfaces of the particles. The general process of darkening of the lunar surface by this mechanism would not be greatly different than outlined in this Section.

fragments nearest the base of the layer. A vertical gradient of darkening therefore tends to develop in the fragmental layer, the fragments in the lower part of the layer being darkened the least and the fragments in the upper part darkened the most. With increasing time and radiation dosage, this gradient of darkening, scaled to the thickness of the fragmental layer, tends toward a steady vertical distribution of partially darkened and completely darkened material. At any one place, the vertical gradient of darkening will generally be irregular and will depend on the specific history of cratering at that place. The albedo of the material at the surface, if measured on a scale that is coarse with respect to the mean fragment size, tends toward a lower limiting value that is somewhat higher than the lower limiting albedo of an undisturbed surface, because a certain proportion of fresh and partially darkened fragments will always be present.

Fresh craters that penetrate the base of the fragmental layer may be expected to have fresh or relatively unirradiated material in the deposits of throwout on their rims. These deposits form the rays and the bright halos around primary craters on the maria. If the craters are much deeper than the fragmental layer, relatively fresh material may also be expected to be exposed in the crater walls.

Most telescopically resolvable crater walls and other slopes on the Moon that are steeper than 30 deg have relatively high albedos. This is probably attributable to intermittent sliding and rolling of fragments down slopes which are at or near the angle of repose. A steady gradient of darkening will not develop on such slopes because any thoroughly irradiated material exposed at the surface tends to migrate down the slope and accumulate at the foot, and fresh unirradiated or partially irradiated material is continually or intermittently exposed. Crater walls and other steep slopes will tend to become thoroughly darkened only after the slopes are sufficiently reduced by sliding, slumping, and other degradation processes to become stabilized. The slopes with high albedo are thus interpreted as continually or intermittently active talus deposits. The streaks in the steep crater walls revealed in the *Ranger VII* photographs (Figs. 34 and 39–41) probably correspond to individual rock slides. Bright streaks correspond to parts of the talus that have slid or been exposed most recently and the intervening dark streaks to the material that has remained stable the longest.

Interpretation of the albedo of a large ray with many secondary craters is complicated by the presence of high-albedo material on steep secondary crater walls. Variations of albedo across a large ray measured at the telescope are demonstrably due in part to the presence of unresolved bright crater walls. It might be argued that this effect occurs at all scales at which the ray is observed and that the relatively high albedo of a ray is due entirely to the presence of small crater walls and other steep slopes in the ray. Both the observed distribution of slopes in the highest-resolution *Ranger VII* pictures of the Tycho ray and the model of the surface processes presented above, however, suggest that the contribution of high-albedo steep slopes to the integrated albedo of the ray diminishes rapidly with decreasing length of slopes. In areas of the Tycho ray between the recognizable secondary craters, the surface of the ray is probably not significantly rougher, on the average, than areas outside the ray. Yet, at all scales, the albedo of the ray is generally significantly brighter than the areas outside the ray. The high albedo of the ray material should probably be attributed chiefly to the excavation of fresh material from the secondary craters late in lunar history. The period of time elapsed since the ray was formed has been insufficient for the development of a steady gradient of darkening in the debris layer at the top of the layer of ray material.

The rays have gradational boundaries, probably as a result both of the initial distribution of fresh material and of the later processes of darkening of this material. The ray is conceived here as formed by a discrete, nearly continuous layer of ejecta. At the margins of the layer, however, the ejecta are probably discontinuously scattered as individual fragments across the pre-existing terrain. The original boundaries of the ray, therefore, tend to be diffuse. In addition, under the process of darkening suggested for mare material, the thinnest and marginal parts of the ray will become dark more quickly than thicker central parts, because already darkened material surrounding and beneath the ray will be mixed more rapidly with the thin marginal parts of the ray by repeated cratering.

The occurrence and distribution on the mare of very small primary craters with bright halos and rays provide a means of estimating the maximum depth to unirradiated or relatively weakly irradiated material. As the smallest primary ray craters observed in the *Ranger VII* photographs are about 30 m in diameter, the indicated maximum depth to relatively undarkened material at the sides of these craters is about 6 to 8 m, the approximate depth of the craters. The actual depth to undarkened material at these localities in the Tycho ray is probably

much less. Small primary craters are so rare in the highest-resolution photographs that the smallest new ray craters present in the area are not likely to have been photographed.

b. Photometric measurement of slopes. The brightness of any element of the lunar surface recorded by *Ranger VII* depended on the albedo of the surface material, the angle of incidence of the sunlight on the surface, and the angle of emission of the light scattered toward the spacecraft cameras. The relationship between these variables is known as the photometric function of the surface. From photometric measurements of resolvable small areas on the Moon, made through the telescope, it may be shown that the photometric function for small areas of the lunar surface exhibits a characteristic that is highly unusual for scattering surfaces. If the direction of illumination and the angle between the incident ray and the scattered ray (the phase angle) are held constant, then the brightness of a surface element of a given albedo depends only on the component of the slope of the surface in the plane of the phase angle. As the direction of solar illumination is constant and known for any *Ranger VII* photograph and the phase angle may be determined from the orientation of the cameras and position of image elements within the photographs, it is possible to measure the component of slope in the phase-angle plane for each image element from the response of the television camera, if certain assumptions are made about the albedo of the surface. Preflight photometric calibrations of the cameras may be employed to calculate the brightness of the image element either directly from the transmitted video signal, as recorded on magnetic tape, or from measurements of the film records of the pictures obtained with a microdensitometer.

An initial investigation by photometric analysis has been made of the distribution of slopes in the northern half of the area covered by the last *Ranger VII* P_3 photograph.* The small area studied, about 40 m across, lies within the crescent-shaped Tycho ray, a short distance from the rim crest of a relatively large Tycho secondary crater. No demonstrable variations in albedo are present within the area photographed, and it was assumed that the albedo was uniform for purposes of calculating the slopes. A photometric function was adopted for this part of the lunar surface based on numerous telescopic measurements of the lunar maria and adjusted to the estimated albedo of the ray material. The partial photometric function used, for the phase angle of 38 deg, is illustrated in Fig. 48. Here, the brightness of the lunar surface, measured in foot-lamberts, is shown as a function of the component of slope in the phase-angle plane, measured with reference to the local horizontal plane. All phase angles for the part of the photograph analyzed were within about 1½ deg of 38 deg.

The brightness of each image element was calculated from microdensitometer measurements of a duplicate negative prepared from one of the prime negatives of the Goldstone station. Approximately 12,000 measurements were employed. Photometric corrections were made for shading and vignetting in the television cameras. Slope components were calculated from the corrected brightness values using the adopted photometric function. Individual slope components were then connected serially along the approximate traces of the phase-angle planes to construct a sequence of topographic profiles of the surface in the phase-angle planes. A topographic map was prepared from the array of profiles by adopting a series of control points to which the profiles were arbitrarily adjusted and by making simplifying assumptions about the orientation of the phase-angle planes.

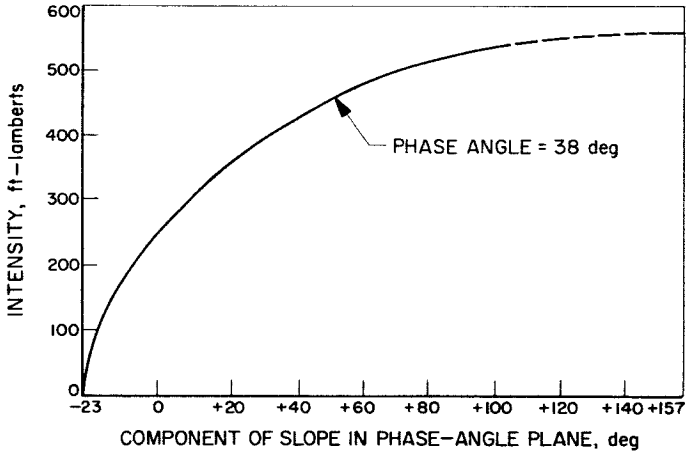

Fig. 48. Partial photometric function adopted for estimation of slopes from highest-resolution *Ranger VII* photographs. (Graph shows relation between brightness of lunar surface and component of slope in the phase-angle plane for a phase angle of 38 deg. Positive angles indicate slopes dipping toward the Sun; negative angles indicate slopes dipping away from the Sun.)

*The work has been carried out for me by a group of my colleagues in the U.S. Geological Survey, among whom Howard A. Pohn and Laurence C. Rowan should receive special mention.

A three-dimensional physical model of the area mapped was next prepared from the map by Howard A. Pohn and Walter C. Black, at an approximate scale of 1/20, and fine topographic details of the surface which had become smoothed out or lost by the measurement and calculation procedures were restored with the aid of light projected on the model from an angle appropriate to simulate the original solar illumination of the lunar surface. A cast of the model was then prepared and photographed, and a new topographic map was prepared by special photogrammetric techniques by Richard H. Lugn.

The cumulative frequency distribution of the components of slope in east-west vertical planes, measured from the improved topographic map, is illustrated in Fig. 49. This distribution is for slope components with a base length of 1 m. The median slope is about 5 deg. About 90% of the slopes are less than 16 deg and 10% less than 1 deg. The form of the frequency distribution is similar to that observed on a number of different terrains on Earth.

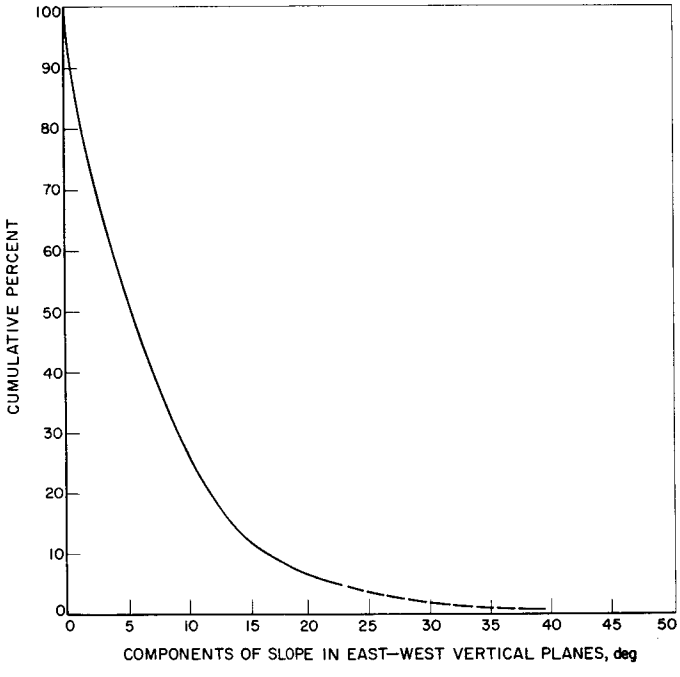

Fig. 49. Estimated cumulative frequency distribution of slopes in half of area shown in last P_3-camera photograph.

C. *Preliminary Model of Fine Structure*

Information on the fine structure of the surface of Mare Cognitum derived from study of the *Ranger VII* photographs is consistent with the evidence about the fine structure that had been obtained previously from physical measurements made at the telescope. The telescopic data that bear on the fine structure may be classified in four categories: (1) photometric properties at the visible wavelengths, (2) polarization of scattered radiation at visible wavelengths, (3) thermal emission at both infrared and microwave wavelengths, and (4) reflection characteristics for microwave radiation. No unique set of physical interpretations can be made from these measurements, but limits can be set on the porosity and probable grain size of the material at and very close to the lunar surface.

The photometric function of small parts of the Moon's surface for visible wavelengths indicates that at some scale appreciably coarser than the wavelengths of light, the texture of the Moon's surface is extremely rough and porous (Ref. 25). The shapes of the pores are such that open holes extend into the surface in all directions. This configuration can be achieved by an open fibrous network, loose stacking of needles or fibres, or extremely open stacking of angular grains. Measurements of the polarization of scattered sunlight with variation in phase show that the scattering surface is covered with very fine, nearly opaque grains (Ref. 26).

Variations of the thermal emission with phase and during eclipses, measured at infrared wavelengths, indicate that the average thermal inertia of the uppermost few millimeters of the lunar surface material is between one and two orders of magnitude less than the thermal inertia of ordinary dense rocks (Ref. 27). The low thermal inertia of the lunar surface material can be readily explained if the density of this material is about an order of magnitude less than ordinary silicates, which suggests that the bulk of the volume of the uppermost few millimeters is open pore space. Thermal emission measured at microwave wavelengths shows that the diurnal thermal wave propagated into the Moon's surface by insolation damps out very rapidly with depth. The lunar surface material is probably highly porous to depths of at least several centimeters.

Interpretation of the physical properties of the surface from measurements of reflected microwave radiation is, unfortunately, ambiguous. The principal reflecting horizon, however, appears to have a dielectric constant close to the value for dry sand (Ref. 28). Probably, the reflection takes place at some shallow depth beneath the surface.

Employing the data available from the *Ranger VII* photographs, together with the information obtained at the telescope, a reasonable model of a typical local area between the rays on Mare Cognitum can be described in the following way:

1. A layer of shattered and pulverized rock covers more than 95% of the mare. It is of variable thickness and rests with irregular contact on the underlying substance of the mare.

2. The fragments in this layer or blanket of shattered rock have been derived by ejection from craters, most of them nearby, but some lying great distances away. Probably, about 50% of the fragments have come from within 1 km of the site at which they are now found, but there is a finite probability, decreasing with the distance to the source, of finding a rock fragment in the debris layer which has been derived from any place on the Moon. Except along the margins of the mare, the pieces of debris will be composed predominantly of mare material.

3. Fragments occurring at the base of the debris layer will, on the average, have been transported on ballistic trajectories a smaller number of times than pieces near the middle or top of the layer. Progressing upward from the base, the layer has been stirred or reconstituted an increasing number of times by smaller and smaller and more and more numerous cratering events. The uppermost millimeter of the debris layer is probably completely reorganized once every 10 to 100 years by the formation and filling of minute craters.

4. The average grain size of the debris layer tends to decrease from base to top because fragments in the upper part have been shocked and broken a greater number of times and have been ejected, on the average, from smaller craters. The exact distribution of mean grain size in the layer is controlled closely by the mass–frequency distribution of impacting interplanetary objects. Unfortunately, this distribution is not well known for objects with masses less than about 10^{-6} g. If the mass distribution of interplanetary particles given by McCracken and Dubin (Ref. 21) is adopted, the size distribution of fragments in the debris layer may be roughly described as follows: Near the base, fragments as large as several centimeters in diameter will be common, whereas most of the material in the uppermost few millimeters will be finely pulverized. Throughout the debris layer, the bulk of the fragments will probably average less than a millimeter in grain size, but heaps of coarse, blocky rocks may be expected to surround the larger craters. At any one locality, the vertical variation of grain size may be expected to be extremely irregular.

5. Beneath the blanket of shattered rock, the mare substance, if originally solid, will in many places show evidence of having been broken to greater depths by shocks of varying strength produced during development of the larger craters. If the original mare substance at a given locality was initially relatively porous, it will have been strongly compressed by shock.

6. The contact between the underlying mare substance and the debris layer has considerable local relief, consisting of the intersecting segments of the original floors of numerous craters that ranged from a meter to a few tens of meters across. Most of these old craters are no longer observable, and their remnants are now buried beneath younger impact debris.

7. The upper surface of the debris layer is pockmarked by craters ranging from less than a millimeter to several tens of meters in diameter (or larger, depending on the local area). Craters larger than 1 m in diameter occupy about 50% of the surface; smaller craters occupy the rest of the surface and are also superimposed on the large craters. Minute craters, with dimensions of the order of a millimeter or less, probably cover nearly all of the surface and are superimposed on nearly all other features.

8. The debris layer typically varies in thickness from a few tens of meters to less than a millimeter. It is thickest where it covers the floors of some of the oldest and largest craters present and is thin, or possibly even absent, along the walls of very young craters that cut through the debris layer into the underlying mare material. Between craters less than 100 m in diameter, the average thickness of the debris layer is probably between ½ and 1 m.

9. The porosity of the debris layer is expected to be of the order of 90% at the surface. It decreases rapidly with depth in most places, probably to less than 50% at depths of a few tens of centimeters. Beneath these depths, the debris will have been compacted by shocks propagated from numerous small impact events.

10. The uppermost few millimeters of the debris layer is conceived as a fragile open network of loosely stacked, very fine grains. It is probably compressible under loads of the order of a few tens of grams per centimeter. The bearing strength and shear strength of the material increase rapidly with depth, and at depths of a few tens of centimeters are probably similar to the bearing and shear strength of moderately consolidated dry alluvium on Earth.

11. The average albedo of the material in the debris layer ranges from that measured at the telescope, about 0.07 at the surface, to intermediate values at the base, probably between 0.10 and 0.15. The immediately underlying mare materials, when pulverized, have an albedo comparable to that of the brightest rays on the mare, about 0.25 to 0.30.

In the ray areas, a layer of coarsely crushed rock overlies the debris layer described here. The fragments in the layer of ray material probably have ordinary rock densities, and the bulk density of the ray material is not much lower than the density of the individual fragments. Depending on the age of the ray, a new porous layer of finely pulverized debris may be expected to form a thin veneer on the ray material. Judging from the shapes of the smallest craters shown in the last *Ranger VII* P-camera photographs, the ray material is essentially unconsolidated. It is probably similar in its gross physical characteristics to a mixture of dry sand and angular gravel.

REFERENCES

1. Kuiper, G. P., "The Exploration of the Moon," *Vistas in Astronautics*, Vol. 2, ed. by Alperin, Morton, and Gregory, New York: Pergamon Press (1959), pp 273–313.

2. Shoemaker, E. M., and Hackman, R. J., "Stratigraphic Basis for a Lunar Time Scale," *The Moon—Symposium No. 14 of the International Astronomical Union*, ed. by Z. Kopal, and Z. K. Michailov, London: Academic Press (1962) pp. 289–300.

3. Eggleton, R. E., "Preliminary Geology of the Riphaeus Quadrangle of the Moon and Definition of the Fra Mauro Formation," *United States Geological Survey, Astrogeologic Studies Annual Progress Report, August 25, 1962, to July 1, 1963*, Pt. A (1964), pp. 46–63.

4. Shoemaker, E. M., "Interpretation of Lunar Craters," *Physics and Astronomy of the Moon*, ed. by Z. Kopal, London: Academic Press (1962), pp. 283–359.

5. Shoemaker, E. M., Hackman, R. J., and Eggleton, R. E., "Interplanetary Correlation of Geologic Time," *Advances in the Astronautical Sciences*, Vol. 8, New York: Plenum Press (1963), pp. 70–89.

6. Gilbert, G. K., "The Moon's Face—A Study of the Origin of Its Features," *Philosophical Society of Washington Bulletin*, Vol. 12 (1893), pp. 241–292.

7. Dietz, R. S., "The Meteoritic Impact Origin of the Moon's Surface Features," *Journal of Geology*, Vol. 54, No. 6 (1946), pp. 359–375.

8. Baldwin, R. B., *The Face of the Moon*, Chicago: University of Chicago Press (1949).

9. Urey, H. C., "The Origin and Development of the Earth and Other Terrestrial Planets," *Geochimica et Cosmochimica Acta*, Vol. 1 (1951), pp. 209–277; correction, Vol. 2, Nos. 5-6 (1952), pp. 263–268.

10. Urey, H. C., "The Origin and Significance of the Moon's Surface," *Vistas in Astronomy*, Vol. 2, New York: Pergamon Press (1956), pp. 1667–1680.

11. Kuiper, G. P., "On the Origin of the Lunar Surface Features," *Proceedings of the National Academy of Sciences*, Vol. 40, No. 12 (1954), pp. 1096–1112; criticism by H. C. Urey, Vol. 41, pp. 423–428; further comments by G. P. Kuiper, pp. 820–823.

12. Shoemaker, E. M., "Impact Mechanics at Meteor Crater, Arizona," *The Solar System, Vol. IV—The Moon, Meteorites, and Comets*, ed. by B. Middlehurst, and G. P. Kuiper, Chicago: University of Chicago Press (1963), pp. 301–336.

13. Bjork, R. L., "Analysis of the Formation of Meteor Crater, Arizona, a Preliminary Report," *Journal of Geophysical Research*, Vol. 66 (1961), pp. 3379–3387.

14. Brown, H., "The Density and Mass Distribution of Meteoritic Bodies in the Neighborhood of the Earth's Orbit," *Journal of Geophysical Research*, Vol. 65, No. 6 (1960), pp. 1679–1683.

15. Brown, H., "The Density and Mass Distribution of Meteoritic Bodies in the Neighborhood of the Earth's Orbit—Addendum," *Journal of Geophysical Research*, Vol. 66 (1961), pp. 1316–1317.

16. Patterson, C. C., Tilton, G. R., and Inghram, M. G., "Age of the Earth," *Science*, Vol. 121, No. 3134 (1955), pp. 69–75.

REFERENCES (Cont'd)

17. Whipple, F. L., and Hughes, R. F., "On the Velocities and Orbits of Meteors, Fireballs and Meteorites," *Journal of Atmospheric and Terrestrial Physics,* Supplement 2 (1955), pp. 149–156.

18. Moore, H. J., Gault, D. E., and Heitowit, E. D., "Change in Effective Target Strength With Increasing Size of Hypervelocity Impact Craters," *United States Geological Survey, Astrogeologic Studies Annual Progress Report, August 25, 1962, to July 1, 1963,* Pt. D (1964), pp. 52–63.

19. Johnson, G. W., *Note on Estimating the Energies of the Arizona and Ungava Meteorite Craters,* UCRL-6227, United States Atomic Energy Commission, 1963.

20. Moore, H. J., Kachadoorian, R., and Wilshire, H. G., "A Preliminary Study of Craters Produced by Missile Impacts," *United States Geological Survey, Astrogeologic Studies Annual Progress Report, July 1, 1963, to July 1, 1964,* Pt. B (1964), pp. 58–92.

21. McCracken, C. W., and Dubin, M., *Dust Bombardment on the Lunar Surface,* United States National Aeronautics and Space Administration Technical Note D-2100, 1963.

22. Gault, D. E., Shoemaker, E. M., and Moore, H. J., *Spray Ejected from the Lunar Surface by Meteoroid Impact,* United States National Aeronautics and Space Administration Technical Note D-1767, 1963.

23. Carr, M. H., "Trajectories of Objects Producing Copernicus Ray Material on the Crater Eratosthenes," *United States Geological Survey, Astrogeologic Studies Annual Progress Report, July 1, 1963, to July 1, 1964,* Pt. A (1964), pp. 33–41.

24. Hapke, B. W., *Laboratory Photometric Studies Relevant to the Lunar Surface,* Paper presented at 118th American Astronomical Society Meeting, Lexington, Kentucky, 1965.

25. Hapke, B. W., "Theoretical Photometric Function for the Lunar Surface," *Journal of Geophysical Research,* Vol. 68, No. 15 (1963), pp. 45–86.

26. Dollfus, A., "The Polarization of Moonlight," *Physics and Astronomy of the Moon,* ed. by Z. Kopal, New York and London: Academic Press (1962), pp. 131–159.

27. Sinton, W. M., "Temperatures on the Lunar Surface," *Physics and Astronomy of the Moon,* ed. by Z. Kopal, New York and London: Academic Press (1962), pp. 407–427.

28. Evans, J. V., and Pettengill, G. H., "The Scattering Properties of the Lunar Surface at Radio Wave Lengths," *The Solar System, Vol. IV—The Moon, Meteorites, and Comets,* ed. by M. Middlehurst and G. P. Kuiper, Chicago: University of Chicago Press (1963), pp. 129–159.

V. OBSERVATIONS ON THE RANGER VII PICTURES

Harold C. Urey
University of California, San Diego
La Jolla, California

The pictures taken by *Ranger VII* are most clear and constitute a remarkable engineering achievement. It has been a pleasant surprise to me that so much information can be secured from these pictures. When further chemical and physical tests of the lunar surface are made by the *Surveyor* program, the interpretation of many features will undoubtedly become more definite.

The following pages record briefly various features of the lunar surface which I have noted by visual observation. No attempt has been made to make a complete statistical survey or to measure quantitatively the dimensions of craters or other features. It is likely that all observers of these pictures will note much the same features but that interpretations may vary considerably.

A. Erosion

The most obvious features of the *Ranger VII* photographs are the general smoothness of the lunar surface and the varying sharpness of the crater outlines. Some craters are very sharp and clear, others less so, and this characteristic varies from those which are partly filled to craters that can barely be seen as slight depressions in the surface. The largest craters which are nearly obliterated are about 300 m in diameter and may be presumed to have been some 40 m deep when they were formed. Thus, material from the lunar surface accumulated in these depressions.

The situation is consistent with the following assumed series of events:

1. The Moon's craters in the land areas and the great maria were formed during the early history of the Moon, some 4.5×10^9 years ago.
2. Bombardment of the lunar surface by meteoritic or cometary objects of various sizes and energies has been occurring since then. The rate of bombardment may or may not have been constant.
3. An erosion process due to bombardment by micrometeorites and protons and to temperature effects has taken place. This process may or may not have been of constant intensity during the history of the Moon.

The bombardment of the surface should have produced small craters and destroyed them many times during lunar history. The surface of the maria must have been "gardened," let us say, to a considerable depth (Ref. 1). The last P picture shows small craters (~5 m in diameter) that should have existed for only brief periods of time, indicating that extensive mixing of the surface region to a depth of some 10 m has occurred. One concludes that the outer surface layers consist of highly fragmented material regardless of what the original material may have been. Moreover, these processes operating in a high vacuum should have produced "fairy castle" structures just as are required by the optical characteristics and thermal conductivity of the lunar surface. Also, all original surface features of the maria to some 10 m in height and depth have been destroyed. Thus, T. Gold's suggestions (Ref. 2) in regard to the lunar surface are borne out, at least in a limited way, although the origin of the erosion is more probably due to micrometeorites, as Hunter and Parkin (Ref. 1) have argued.

Conclusions of the qualitative kind given here could be made more quantitative by extensive measurements and classification of craters along the lines presented by Dr. Shoemaker in Section IV.

B. Secondary Craters

The A pictures particularly show clusters of craters most of which are not very regular in outline. The existence of such clusters indicates that they were produced by objects originating from some large crater on the lunar surface. The crater Tycho has been suggested as a possible source of the objects producing these secondary craters. In this case, they must have been moving with velocities of about 1.1 km/sec or more. The largest of the craters are about 0.9 km in diameter, i.e., comparable to the Canyon Diablo crater (Fig. 1 at **A**). The energy required to produce such a crater is some 10^{23} to 10^{24} ergs (Ref. 3), or a mass of 10^{13} to 10^{14} g or 10^{7} to 10^{8} tons moving at a velocity of 10^{5} cm/sec. It is surprising that such a large object could have been impelled at such a high velocity. Because of the smaller gravitational field of the Moon, the figures for the masses are probably too high. Furthermore, one wonders whether the density of the surface layers of the Moon may not be lower than that of the rocks of the Canyon Diablo crater and whether, as a result, formation of the craters required less energy than estimated here. The question arises as to whether these larger and more nearly circular craters might not be primary craters, since chance clustering of some five objects is not impossible. However, even the somewhat smaller craters of this group would have had to be formed by impacts of objects nearly as large. Whitaker has pointed out that a whitish deposit regularly occurs on the side of the secondary craters away from Tycho. Since this is true for the cluster of five craters near **A** in Fig. 1, this cluster is composed of secondaries.* They are circular in shape without evident slumping on their interiors. The sharp crater to the left of **A** near the first fiducial mark appears to belong to this class also. The other craters with softened outlines to the left of **A** and to the north of the cluster near **A** probably have a different origin. It seems unlikely that craters having such different structures, namely, sharp explosive-type formations on the one hand and smooth irregular gouges on the other, should all be due to massive objects of the same velocity from Tycho. These diffuse depressions will be discussed later.

I would suggest two possible conclusions from this observation.

1. A cometary collision would be more likely than a meteoritic one as the origin of Tycho, since the more volatile constituents of a comet head should give a more propellant character to the gases produced in the collision. The pressures would be lower and last longer and hence impart a more gradual acceleration to objects; thus, larger objects may be accelerated to high velocities without being crushed.

2. It would be expected that many objects smaller than those producing the larger craters would be accelerated to higher velocities and, in fact, to velocities in excess of the escape velocity of the Moon. In this case, many of these objects, probably one-half of them, would eventually reach the Earth and would be regarded as meteorites. The fate of such objects has been studied in detail recently by James Arnold (Ref. 4). Of course, there is no certainty that our present meteorites are such objects, since the lunar events we are discussing may have happened long ago. However, various lines of evidence do suggest that the stone meteorites may be coming from the Moon, e.g., their cosmic ray ages, the possibility of residues of living organisms in meteorites, and mineral composition and structures indicating origins from some fairly large object. It is difficult to estimate the distribution of velocities to be expected, because a comet head collision would be a very complicated process and also because our knowl-

*In Part VI, Whitaker suggests another origin for some of these craters.

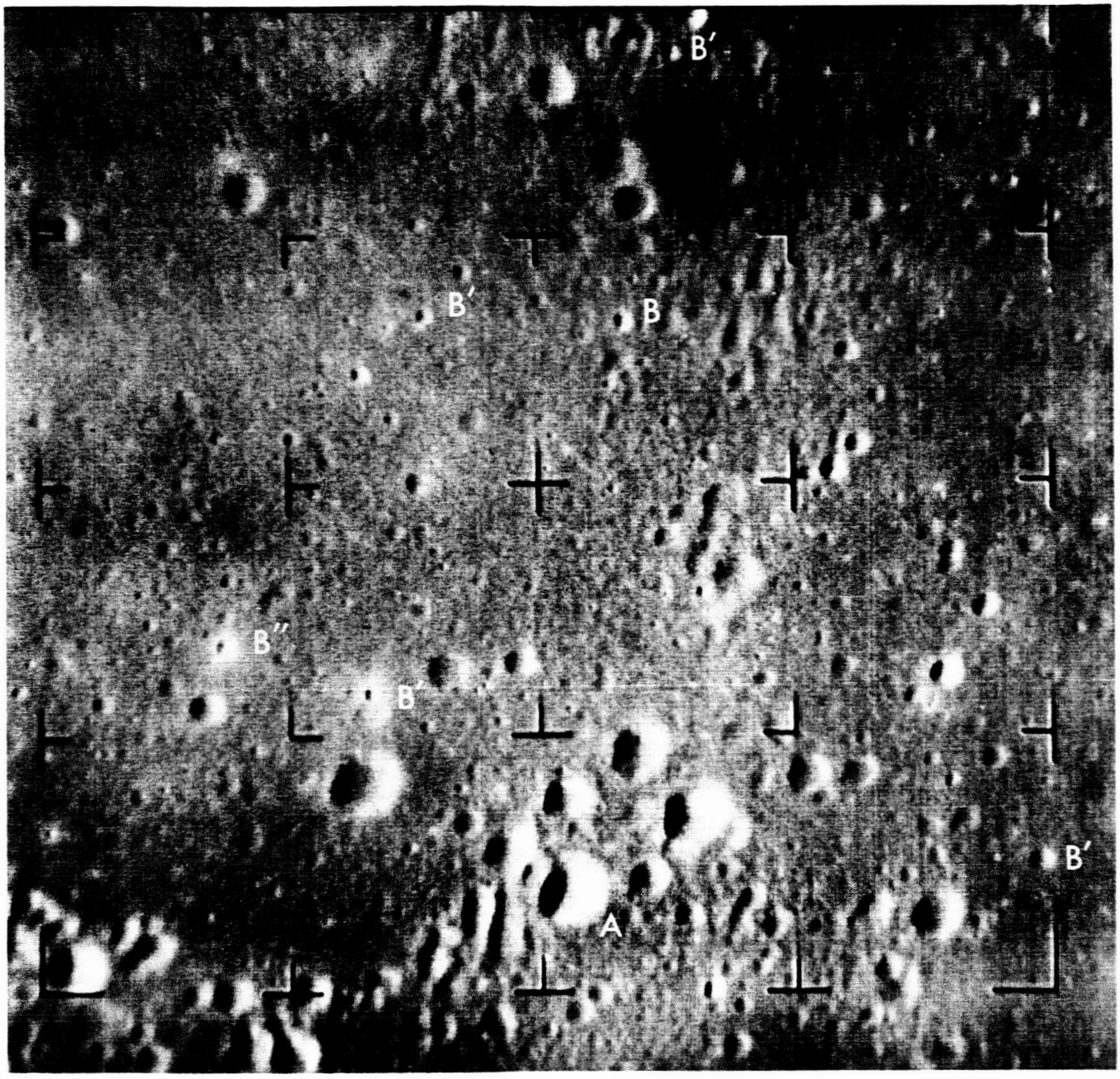

Fig. 1. A-camera photograph 197: A designates a crater 0.9 km in diameter presumed to be a secondary of Tycho; B is the "crater with rocks"; B′ indicates craters of similar size; B″ is a similar crater with two black objects in it.

edge of the characteristics of comet heads is very uncertain. Probably, scaling derived from small experiments such as those of Gault (Ref. 5) would be very uncertain. Evidence that meteorites come from the Moon is suggestive but inconclusive at the present time.

The diffuse elongated craters of this region mentioned above will be discussed later, but, as Gault and Quaide (Ref. 5) have suggested, they may be due to secondaries from Bullialdus 275 km distant. Bullialdus is an older crater than Tycho, and its secondaries should have fallen in this region and their outlines softened by the erosion processes.

C. Rocks in Craters

The most prominent "rock in a crater" is that seen in Fig. 2. The crater is about 250 m in diameter and is of irregular shape. The largest rock mass is 40×60 m; the two smaller ones are round and measure about 15 m in diameter. Assuming the depth of the larger one to be equal to its width, its volume is 10^5 m^3 and, with a density of 3 to 8, its mass is $3\text{–}8 \times 10^5$ tons. If this object arrived at 2.4 km/sec, i.e., the escape velocity of the Moon, its energy would be $7\text{–}20 \times 10^{21}$ ergs, and, according to the curves of Shoemaker *et al.* (Ref. 3), it should have produced a crater of about twice the observed diameter as a minimum. It also seems improbable that such large objects would not be destroyed even if they consisted of iron–nickel.

Nathan (Ref. 6; Fig. 3) has cleaned up the picture of this crater. The results strongly suggest that some opening below the surface may exist and that gases may have escaped at this point.

It may be that this feature is not unique. On photograph A197, one can see a number of craters of approximately the size and appearance of the crater in question. These are indicated by **B′** in Fig. 1. The crater marked **B″** has two black dots in it, which would probably be well developed objects or openings at higher resolution (see Fig. 4). Also, the crater on B200 (Fig. 5) marked **A** has a projection in its bottom, and the two craters marked **B** have darkish patches at the bottom. These craters are rather small, less than 100 m in diameter, and have been eroded markedly. However, it does appear that objects in the bottoms of these smaller craters are of common occurrence, although the smaller and larger objects may not have originated by similar processes.

Some very tentative suggestions for the origin of the larger objects in Fig. 2 have occurred to me: (1) Water with other gases escapes from the lunar interior and deposits dissolved materials as it evaporates. Nathan's pictures particularly support this suggestion. (2) A low-density object, e.g., a small comet head, collides with a lunar surface of fragmented material of low density and compresses a mass into an irregular pellet. I have been unable to construct any reasonable theory for this last process or to get any constructive, or even destructive, criticism from my colleagues in regard to it. At present, I favor the second interpretation, but am not firmly convinced that it is correct. Shoemaker has suggested that the "rock" is a landslide within the crater. It does seem odd that this particular crater is nearly filled with a landslide while so little evidence for landslides exists in other larger craters.

D. Perfect and Imperfect Craters

Kuiper and Whitaker some time ago reported the presence of some perfect lunar craters as observed from the Earth, and their observations are confirmed by the *Ranger VII* pictures. Very smooth and symmetrical craters are found on many of the *Ranger VII* pictures. On the other hand, craters with indications of structure in the walls are seen in some pictures. It seems possible that most primary craters are originally formed as perfect craters and that the first erosion by micrometeorites or small and numerous macrometeorites produces land slips that result in slight imperfections. It is my contention that these perfect craters of various sizes, i.e., from 15 km diameter down, indicate that the material of the Moon must be of very uniform composition over considerable distances and depths. Moreover, since they occur both in the mountainous and maria regions, this conclusion applies to parts of the maria and mountainous regions, at least. Atomic explosion craters that I know of do not have this characteristic. This leads me to question seriously whether the lunar surface does not consist of highly fragmented material produced by the great collisions early in lunar history.

Gault and Quaide (Ref. 5) suggest, on the basis of experimental studies, that these smooth round craters have been produced in material of low physical strength. Of course, materials of low physical strength are, in a way, of nearly uniform physical strength.

On the basis of any theory for lunar origin, the evidence indicates that an intense collisional history occurred at the end of the formation process. The layer

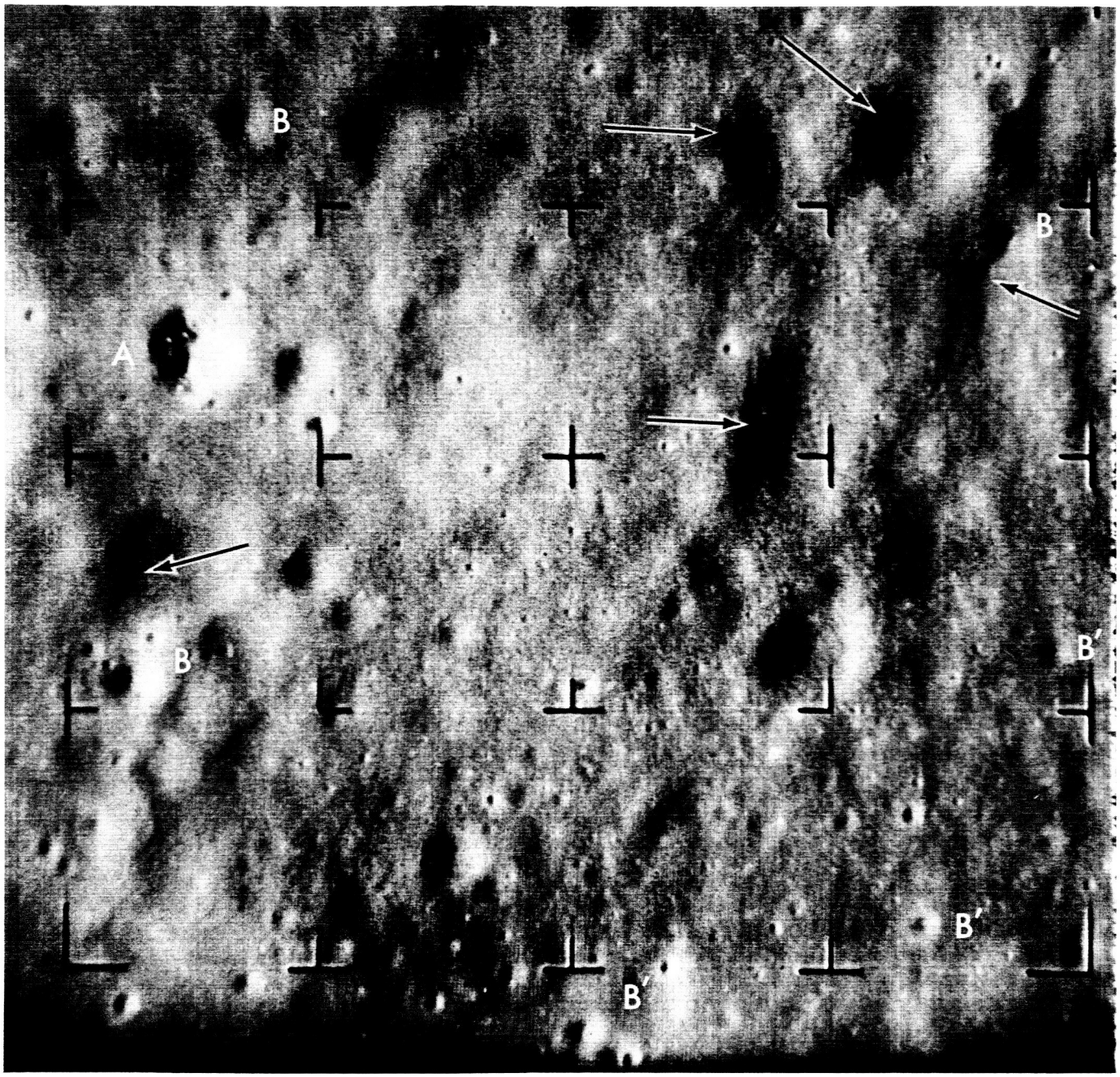

Fig. 2. The last A-camera photograph, No. 199: A designates the "crater with rocks"; B are dimple craters; B′ are imperfect dimple craters.

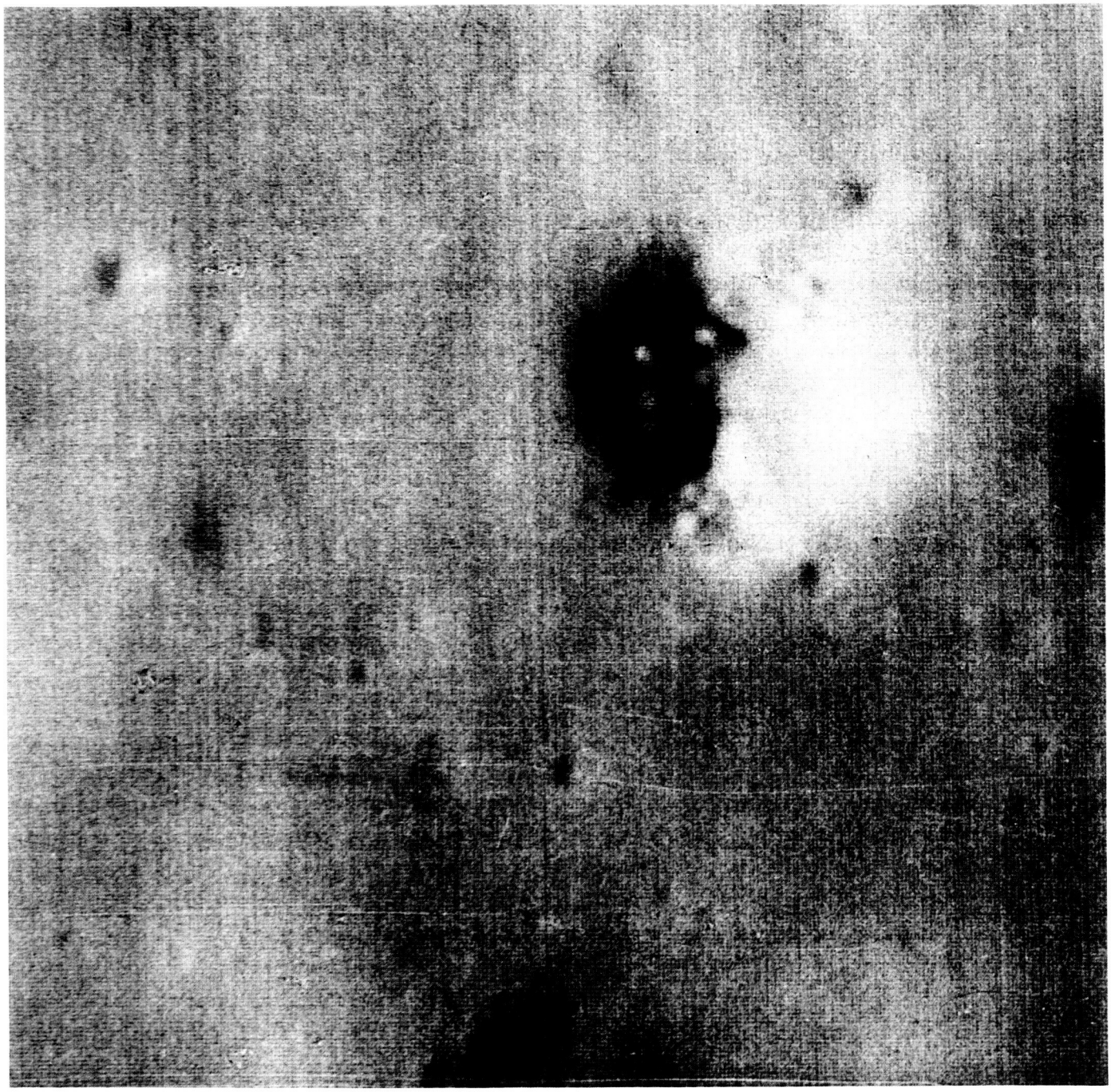

Fig. 3. Nathan's picture of the "crater with rocks."

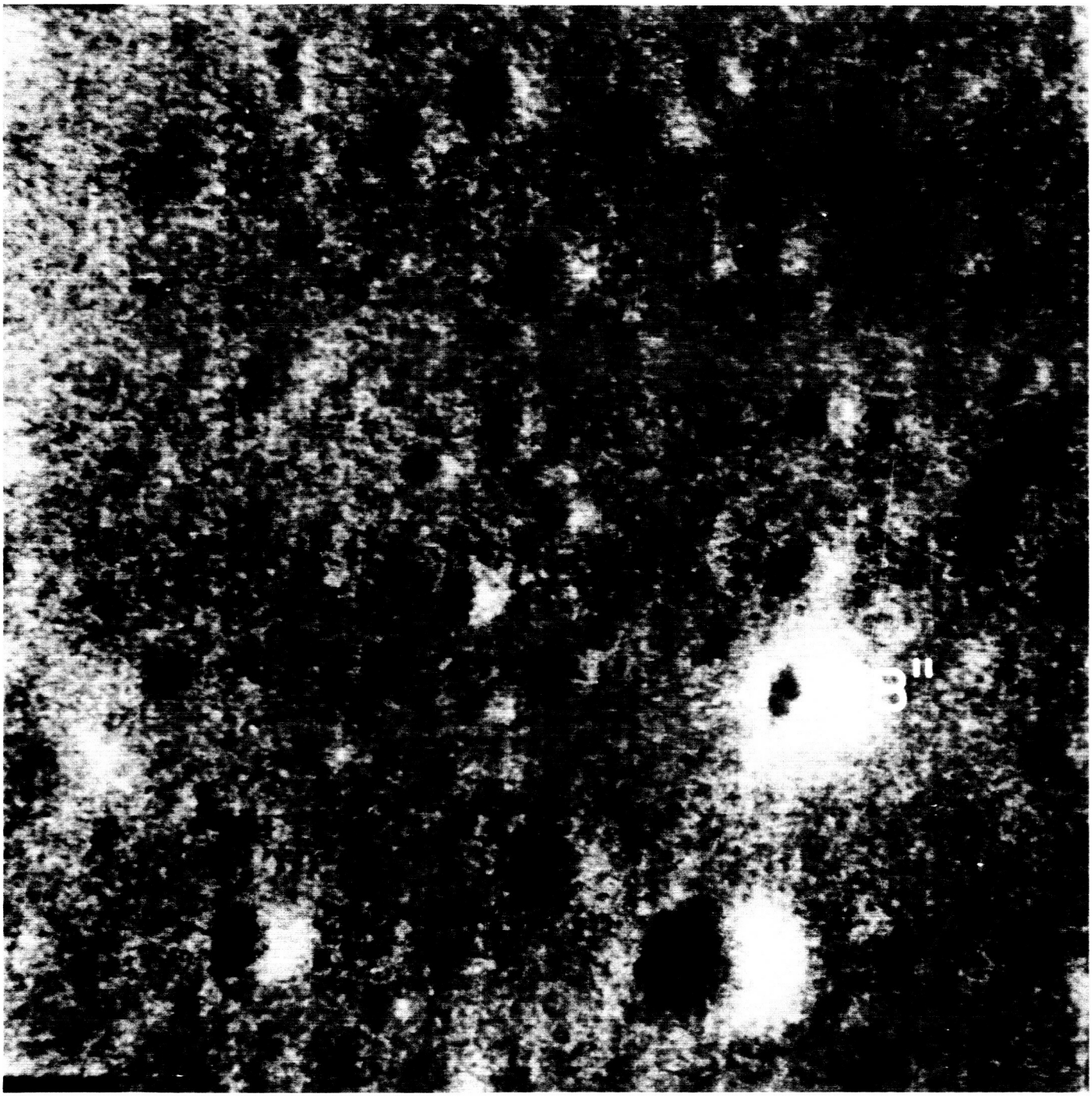

Fig. 4. Enlargement of B″ crater of Fig. 1.

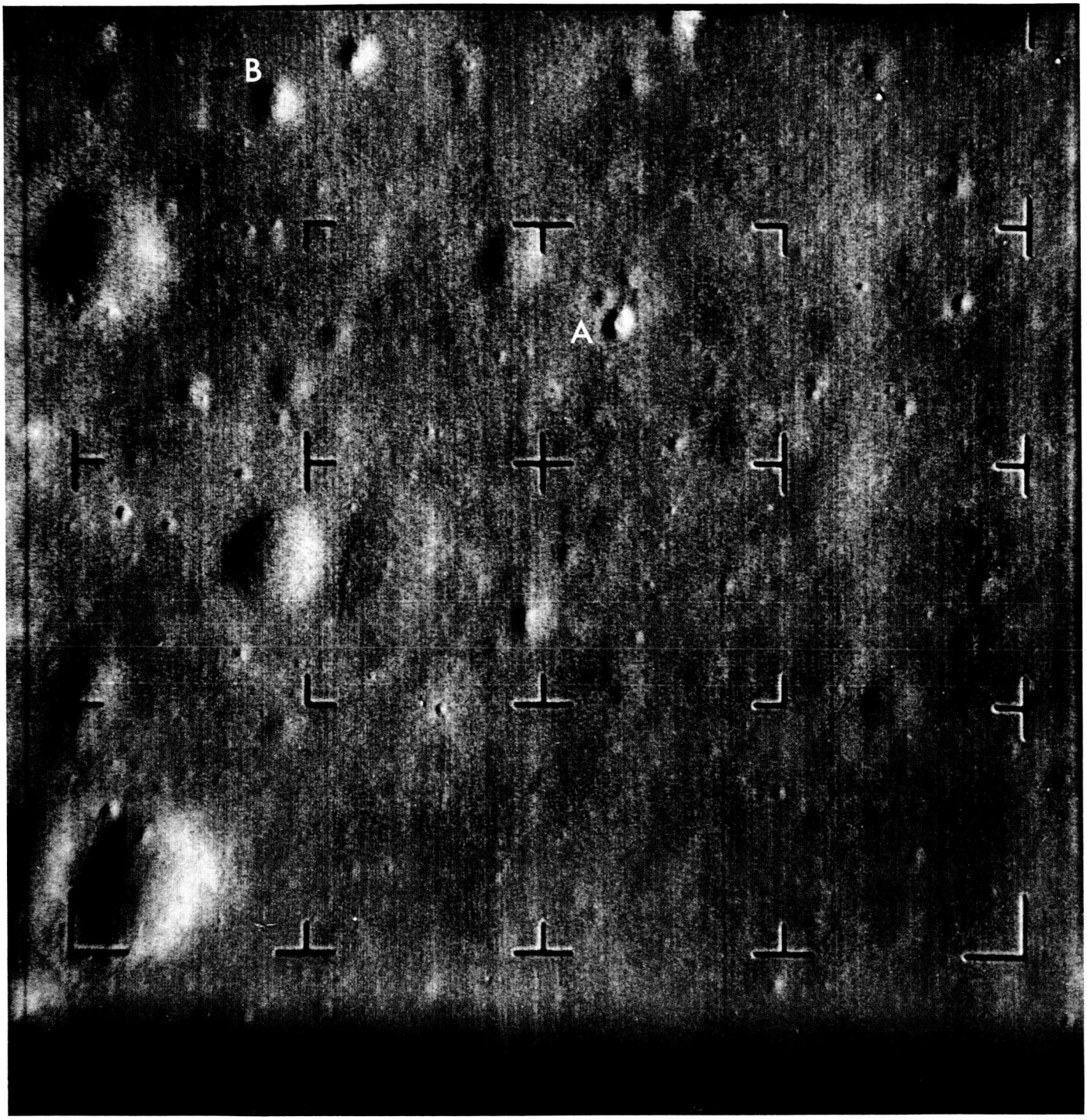

Fig. 5. The last B-camera photograph, No. 200: A and B show two craters with small objects at their bottoms. Note the dimple crater in the center.

of collisions that is visible is probably not the only layer. A layer of material some 10 km thick or more may have been deposited on the Moon in this way. In this case, the outer parts must consist of fragmented material, and hence it is not surprising that the mountainous areas should consist of such material. But it appears from the evidence of both ground-based observations and the *Ranger VII* photographs that the area of Mare Cognitum consists of similar material.

E. Wrinkles on the Lunar Surface

The wrinkles in the maria are very well known, and the *Ranger VII* pictures show that even small wrinkles are present. The A photographs contain wrinkles some 10 km in length, and the B pictures show some of greater length. Their general appearance is similar to the larger ones observed in photographs taken with terrestrial telescopes. It is interesting that these small structures have survived the erosional processes, and this suggests that they are of fairly recent origin.

A study of photographs B193, B194, B195 (Fig. 6) and B196 shows that one wrinkle traverses one of the craters. The wrinkle enters the crater at the upper right-hand edge, passes along the inner edge through the shadows, turns left inside the rim as a whitish line, and joins the wrinkle at the lower left-hand rim. Another case is seen imperfectly at the bottom edges of B193 and B194. The wrinkle enters the crater, only half of which was caught in the photographs. The arrows on Fig. 6 point out these features.

The photographs indicate that these wrinkles are comparatively late structures. It has been suggested that they are pressure ridges due to thermal contraction of the Moon, as indicated by MacDonald's calculations (Ref. 7), although the evidence presented below for an extensive crevasse structure underneath the surface argues against this. However, the pictures only indicate that these structures formed after the craters and that they are not a surface phenomenon of lava flows, for example, or that they are older structures but have depth such as would be expected for intrusions of modified materials along crevasses.

F. Dimples, Valleys, and Cracks

In Fig. 2, three well defined dimples (marked **B**) are evident, and several less well defined craters of this type (marked **B′**) appear. One of these craters is seen near the upper right of the photograph. The dark bands in a valley lead into it, as pointed out to me by Whitaker. It has no rim and has a small, round, button-like bottom. With a little imagination it can be traced to another dimple marked **B′**. Another is at the upper left of Fig. 2 in a smooth area. There are slight indications of a rim, but these could be variations in elevation of the general plane. A third is at the left near the second fiducial mark from the bottom of the picture. The button-like bottom is not evident. These three objects are about the same size, but it is difficult to measure diameters because of the indefinite rim or absence of a rim. Also, the depth is difficult to measure. If the fiducial marks are 647 m apart, these dimples are about 100 m in diameter and possibly 20 m deep. Another well defined dimple occurs in the middle region of the last B frame. It is of about the same size as those on the last A frame. On the A198 frame, other craters that may have this dimple-like structure can be seen. One near the fiducial mark at $x = 1$, $y = 1$ looks well defined, with the bright "button" at the bottom. In fact, these curious craters seem to be remarkably common in this area.

It has occurred to me that these dimples look as though slumping into a crevasse below has occurred. If it were freely flowing sand, one would expect the walls to be funnel-shaped. However, particles of sticky, fragmented solids or more rigid material such as expected in the lunar high vacuum would not flow and hence must have been moved by sputtering or by micrometeorite or small macrometeorite bombardment. Hence, if a hole is present at the bottom, the material which was not sprayed back from this area would give rise to the dimple-like shape, i.e., steeper walls near the center of the crater.*

On the other hand, dimples may be explained as being due to some chunks of material, possibly metal or solid rock, at their centers. Under bombardment by micrometeorites, etc., material would be scattered to great distances, while the neighboring regions, consisting of soft and easily penetrated matter, would absorb much of the energy of the bombarding particles and hence scatter material to smaller distances. In this way, material is lost

*Note added in proof: Dr. Leonard D. Jaffe of the Jet Propulsion Laboratory has sprinkled finely divided solids over small models of lunar craters and has produced a very good imitation of lunar dimple craters. This work possibly supersedes the suggestion made here in regard to the origin of these objects. The dimple craters were quite certainly produced by the fall of finely divided material produced in great collisions at some indefinite time in lunar history.

by being spread over a large area, and the hard objects move downward. In fact, as mentioned previously, several of the photographs show that some of the dimples have small objects at the bottom. This interpretation would indicate that there are numerous rocky or metallic objects lying near the surface in a layer of soft porous material and that the depth of such material is at least equal to the depth of the dimples, i.e., up to some 20 m.

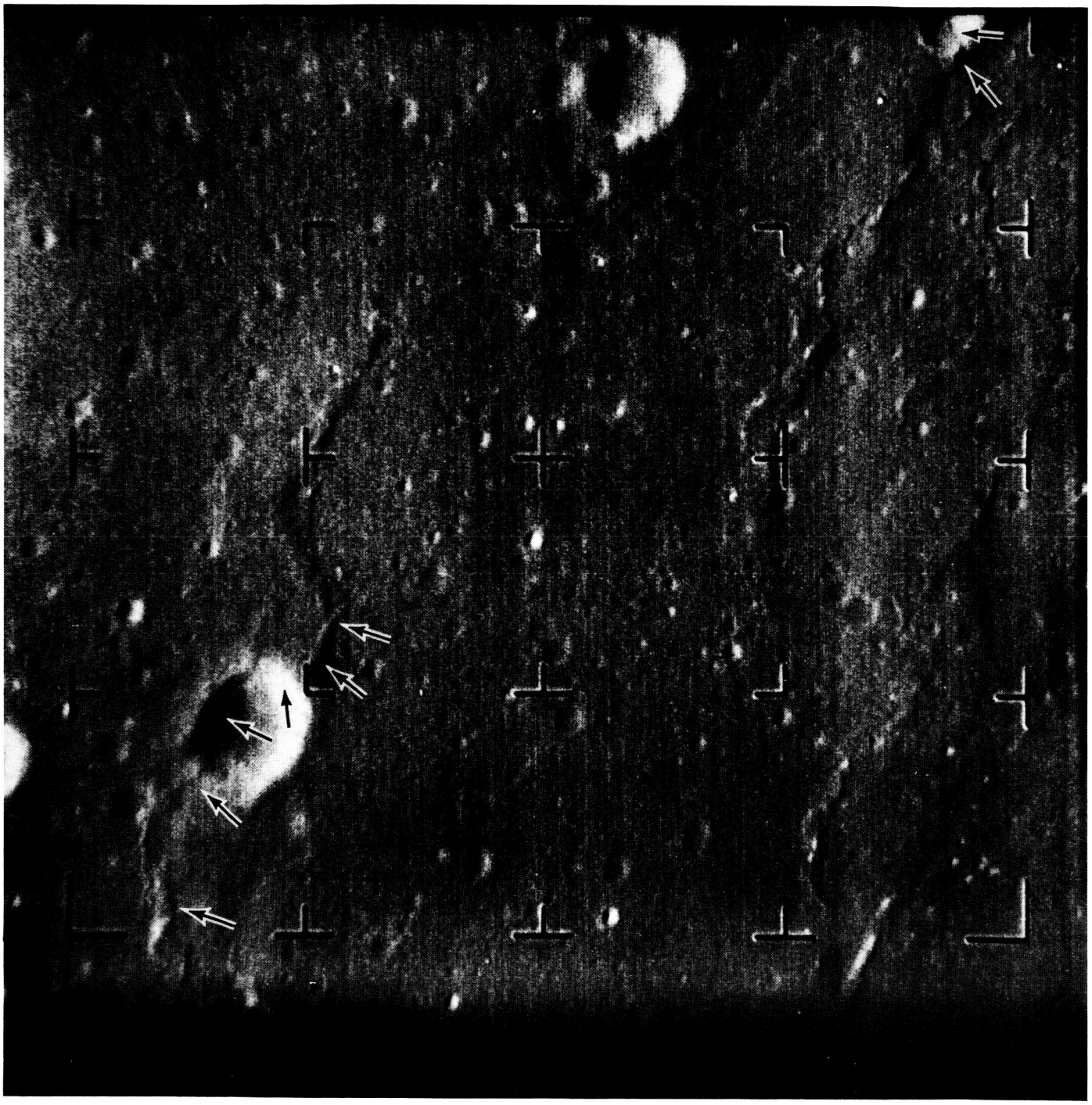

Fig. 6. B-camera photograph 195: Arrows indicate one wrinkle passing through one crater and another entering a crater.

In Fig. 2, there are cracks of considerable length (~500 m), generally running north and south, giving the impression that there may be crevasses below the surface which are bridged over by a layer of the smooth gray material. If they are cracks, they must be very shallow, since they are seen only in the slopes forming a small angle with the Sun's rays. These cracks are particularly prominent in the upper right-hand quarter of the Figure. Also, one is evident in the left middle just below the crater with the rocks.

A very dark irregular area appears on the right edge of Fig. 7 and the preceding and following pictures. It shows no evidence of elevation or depression, and hence, the color is probably due to some darker coloration of the surface. One immediately thinks of chemical coloration due to the escape of gases from the interior along fissures. Thus, there are several bits of evidence for activity of this kind from the lunar interior.

In the A pictures I find some elongated craters without well defined rims which I prefer to call valleys. Examples are seen in the A180–195 (e.g., Fig. 7) pictures as elongated smooth gouges in the smooth surface. These elongated valleys are similar to gouges observed near the great craters, but they seem to have no orientation that systematically relates them to any large crater in this region. They are of various sizes and orientations, the largest being some 3–4 km long and about 1 km wide. If they were produced by objects thrown from craters, these objects must have been of large size and of great energy. On the other hand, they may be features produced by slumps into sublunar cavities or settling of loosely aggregated materials. The elongated valleys near the landing area appear on A194 and on the subsequent A pictures. Some of these valleys are indicated in Fig. 2.

On A177 (Fig. 7) and pictures preceding and following it, I recognize a fairly well defined long valley which may connect with a wrinkle leading to the well defined peak just north of the landing area. The wrinkles, the crevasses, and these valleys, as well as the two large peaks north and south of the landing area, have a direction nearly north and south; however, some valleys run at quite different directions. Some craters appear to be lined up in rows as well. I believe that these features indicate that the valleys, some rows of craters, and the wrinkles are probably related to each other. Some of these features are shown in Fig. 7 between the curved lines. (It is possible to think that one sees other features of this kind in the A pictures, but it is difficult to be certain, and I have marked only those that I regard as certain.)

It seems to me that these features may indicate that great crevasses, covered by smooth grey material, occur below the surface. The open crevasses and the valleys, and possibly the dimples, represent regions in which slumping has occurred. Photographs taken by terrestrial telescopes show great crevasses and wrinkle ridges on the lunar surface. One such ridge to the right of Copernicus, with north at the top of the picture, continues toward the shore of Mare Imbrium and may be continued into the mare as a large wrinkle ridge. Similarly, the lines suggested covered crevasses in Fig. 7 and others near them can be connected (using a little imagination) to ridges and to mountainous ridges at the north. In fact, all of these ridges and crevasses of all sizes may well be related to each other. The wrinkles may be crevasses through which water has come to the surface, hydrated the silicates, and caused a swelling of the rocks along the region of the crevasses, as suggested by the Salisbury–Urey hypothesis (Ref. 8).

The interpretation of these features as being due to crevasses leads one to speculate on their origin. Mac Donald (Ref. 7) has estimated that the Moon has expanded by 3–5 km or by 1 in 350 to 1 in 600 in linear dimensions. Such expansion does not appear to furnish an adequate order of magnitude for these crevasses. Gold (Ref. 9) postulates large masses of ice below the surface, but this does not seem consistent with the appearance of very symmetrical craters of varying sizes distributed over the mare surface as seen in the *Ranger* pictures. Possibly, I have overlooked some distinguishing features to be expected in these photographs. Solidifying lava flows might produce fissures. Also, it seems likely that great collisions would have produced large cracks below the surface regardless of the origin of the smooth grey material.

G. Summary

The history of the Moon may be the following. The body of the Moon was formed by some here unspecified process. The outer part consists of the debris of a terminal accumulation process. It hardly seems likely that the surface collisions which we recognize produce the only layer resulting from such processes, but the thickness of the materials so collected is unknown. The maria were formed by the largest collisions, and the surfaces of the maria consist of some smooth material, possibly lava



Fig. 7. A-camera photograph 177, showing valleys and linear features as indicated.

flows and/or fragmented material produced by these great collisions. This initial collision process decreased in intensity gradually, but quickly as measured in terms of planetary times. A possibly, and indeed probably, steady bombardment process by meteorites, micrometeorites, and ionized particles, mostly of hydrogen and helium but other atoms also, began and continued throughout the last 4.5×10^9 years. These collisions produced craters of large and small size and caused a wearing down of the larger features, which are clearly recognized on the *Ranger VII* photographs for the first time. The transport of material by the collision and erosion processes was sufficient to fill craters 300 m or less in diameter and completely covered smaller craters, so that these were formed and covered a number of times.

The larger collisions in the post-formation period expelled massive objects to great distances at high velocities, i.e., objects up to 10^6 or 10^7 tons at velocities of 1 km/sec. These objects can be recognized on the *Ranger VII* pictures. It is fairly certain that many smaller objects, perhaps 1 ton in size and smaller, escaped from the Moon. Such objects should have arrived at the Earth and would be classified as meteorites. Our present meteorites may be, but are not necessarily, this class of object.

One of the wrinkles passes through one of the craters (Fig. 6). Such wrinkles are possibly compression ridges, though other explanations are possible; in fact, they may be due to the hydration of silicates along fissures. One wrinkle probably originated after one of the craters and is not the residue of a surface feature of a lava flow. Shoemaker points out that side branches on one of the wrinkles give an indication that these features have emerged so recently that erosion processes have not had time to smooth them out.

The large rocks seen in some small craters probably originated during the collisions that produced the craters, but may have been formed by deposits from water escaping from the Moon.

The remarkably perfect symmetrical craters, ranging in size up to diameters of 15 km, indicate that the lunar surface has very uniform physical properties, both in the maria and terrae, for a considerable depth (i.e., a kilometer or more) and over great distances (as far as 15 km). It is unlikely that any terrestrial materials would have characteristics sufficiently similar to make such craters possible. This indicates a different origin for the surface materials of the Moon from those characteristic of the Earth. It is my opinion that the lunar craters are more in accord with the hypothesis of a surface of fragmented material than any other.

The evidence for crevasses beneath the lunar surface is suggestive but not conclusive. It seems likely that the many collisions of very great magnitude required to produce the observed surface of the Moon have covered the craters and maria formed by previous collisions and a substantial layer of material accumulated in this way. It is not surprising that such collisions should have produced a fragmented material for some depth both in the maria and terrae, and crevasses can reasonably be expected to exist below the surface. Thus, a large collision may have opened great cracks and crevasses, which then partially but not completely settled down again. This process may have been repeated many times and produced large openings below the surface.

The dimples may be due to the loss of material into holes below the surface or to rocky or metallic objects lying on the surface and scattering material to great distances.

It appears probable that both the wrinkle ridges and the surface crevasses range in size from those seen in photographs taken from the Earth to the smallest ones shown on the last *Ranger* pictures, and that these two types of features may be intimately related to each other.

The suggestion that the maria consist of ice overlaid with dust made by Kopal and Gold (Ref. 9) has been referred to several times. They have supported this suggestion by comparisons to the degassing of the Earth. However, the Earth has certainly had a vigorous volcanic history, while, according to my interpretation, the Moon has not. Thus, although I am willing to assume and have assumed that some water has come to the lunar surface from the interior, it is my belief that the amount has been small and has not been sufficient to fill the maria basins.

However, as I have pointed out (Ref. 10), it is possible, and indeed probable, that the Moon received water and other materials from the Earth during its separation from or its capture by the Earth. I have assumed that the amount of water received by the Moon was small, but it may have been sufficient to fill the maria basins. I

see no unique evidence in the *Ranger VII* pictures supporting or disproving such a hypothesis.

The evidence from the *Ranger VII* pictures is most interesting, but the photographs raise more questions than they answer unequivocally. Some think that they show that the maria are surely lava flows, and others, including myself, believe that this is not the case. It seems probable that Mare Cognitum consists of fragmented material as Gold (Ref. 2) has argued, although the origin of this material is more reasonably postulated as coming from the Imbrian and other collisions as suggested by Urey (Ref. 11). I see no reason to modify in any important details previous ideas which I have advanced relative to the origin and structure of the Moon (Ref. 12). Hopefully, future exploratory space probes will answer more conclusively questions that are raised by these pictures.

REFERENCES

1. Hunter, W., and Parkin, D. W., "Cosmic Dust in Tertiary Rock and the Lunar Surface," *Geochimica et Cosmochimica Acta*, Vol. 24 (1961), pp. 32–39.
2. Gold, T., "The Lunar Surface," *Monthly Notices of the Royal Astronomical Society*, Vol. 115 (1955), pp. 585–604.
3. Shoemaker, E. M., Hackman, R. J., and Eggleston, R. E., "Interplanetary Correlation of Geologic Time," *Advances in the Astronautical Sciences*, Vol. 8, New York: Plenum Press (1963), pp. 70–89.
4. Arnold, J. R., *Astrophysical Journal* (In press).
5. Gault, D., and Quaide, W., Private communication (1964).
6. Nathan, R., Private communication (1964).
7. McDonald, G. J. F., "Stress History of the Moon," *Planetary and Space Science*, Vol. 2 (1960), pp. 249–255.
8. Urey, H. C., "The Origin and Nature of the Moon," *Smithsonian Report for 1960* (1961), pp. 251–265.
9. Gold, T., "Processes on the Lunar Surface," *The Moon*, ed. by Z. Kopal and Z. K. Mikhailov, London: Academic Press (1962), pp. 433–439.
10. Urey, H. C., "Origin of Life-like Forms in Carbonaceous Chondrites," *Nature*, Vol. 193 (1962), pp. 1119–1123; "Meteorites and the Moon," *Science*, Vol. 147 (1965), pp. 1262–1265.
11. Urey, H. C., "The Origin of the Moon's Surface Features—I and II," *Sky and Telescope*, Vol. 15 (1956), pp. 108–111 and 161–163.
12. Urey, H. C., "The Chemical Evidence Relative to the Origin of the Solar System," *Monthly Notices of the Royal Astronomical Society* (In press).

VI. FURTHER OBSERVATIONS ON THE RANGER VII RECORDS

Ewen A. Whitaker
Lunar and Planetary Laboratory, University of Arizona
Tucson, Arizona

As mentioned in Part III, there is now considerable evidence to support the theory that the lunar maria were originally formed by processes involving the flow of material rather than by gradual dust transport or sudden deposition of shattered surface materials resulting from very large impacts. It is less easy to decide whether the maria are lava flows, ash flows, or combinations of the two, since one cannot readily predict the results of even terrestrial types of volcanic activity under the high vacuum and reduced gravity conditions existing at the lunar surface. However, one would expect a very porous, fragile structure for the surface layer in either case.

These original mare surfaces have presumably been subjected to at least the following modifying agents:

1. Mechanical stresses (tensions, compressions, shear stresses) due to tectonic motions in the mare beds, tidal effects, etc.
2. Bombardment by meteoritic bodies of all sizes
3. All solar radiations

The difficulty in trying to specify the present nature of the mare surfaces from a study of the *Ranger VII* records, made in conjunction with reliable Earth-based data, lies in predicting the effects of at least these three agents on the original surface layers, whose properties can only be surmised anyway.

It is generally agreed that large, ray-bearing craters such as Copernicus, Tycho, etc., were formed by the explosive energy release of massive bodies impacting the lunar surface at interplanetary velocities. It has not been established, however, whether the rays represent finely powdered lunar materials ejected from the explosion site, finely powdered debris of the impacting body, material displaced by the impact of chunks of lunar material hurled from the explosion site, the debris of these chunks, a combination of one or more of these effects, or some entirely different phenomenon (e.g., surface stains). Telescopic observation, study of good-quality Earth-based photographs, and now the *Ranger VII* records, show that those ends of ray elements lying closest to the parent crater apparently always contain a round or elongated crater, or cluster of craters. It is difficult to accept the first explanation as it stands, at least in the case of the more distant elements, because one cannot readily visualize tight clusters of ray material

remaining intact over distances in excess of 1000 km, with each cluster containing crater-forming chunks which invariably reach the lunar surface before the ray material. An extreme case is the crater Messier A in Mare Fecunditatis (Fig. 1), which displays the well known "comet-tail" double ray, precisely radial to the more northerly of the two intense ray systems situated on the Moon's far side at 120°E longitude, 10°N latitude (derived from the *Lunik III* photographs). Another possible example is the crater Rosse in Mare Nectaris (Fig. 2), which is situated just beyond the apex of a major ray element of Tycho. The apex of this ray also appears to contain a small cluster of craters.

It seems, therefore, that at least in the case of the more distant ray elements, the ray material is associated in some way with those craters situated at the apices of the elements rather than with the parent crater, although the direction of the ray is clearly governed by the location of the parent crater. However, the difficulty now arises that the craters Messier A, Rosse, and a considerable percentage of the smaller craters located in the apices of the ray elements shown in the *Ranger VII* records are indistinguishable from what are usually considered to be meteorite impact craters. The only obvious difference is that some of the supposed meteorite craters display roughly circular nimbi or ray systems of their own. Since crater circularity suggests an explosive origin, why has the bright material all fallen to one side in the case of the ray craterlets? A possible explanation might be that any large disturbance of the lunar crust causes the release of trapped gases, vapors, etc. (e.g., from the permafrost layer postulated by T. Gold), and the expansion of these gases and vapors might cause a thin, temporary wind across the lunar surface. This wind might be expected to travel with velocities of an order of magnitude similar to those of the ejected chunks of material (from large ray craters such as Tycho). Fine material ejected by the collision of these chunks with the lunar surface would be transported downwind from the parent crater. The fact that many of the ray-element craterlets resemble explosion craters rather than collision scars might possibly be due to the sudden release of previously trapped gases or vapors on collision.

However, a major stumbling block to all of these explanations is the existence of such ray systems as those surrounding the small craters Stevinus A and Furnerius A (Fig. 2). The former crater, for example, has a diameter of about 7 km, and yet displays a straight ray over 1000 km in length. While the volume of the crater is sufficient to cover the entire ray area to a depth of almost 1 m, it is difficult to reconcile the perfect symmetry of the crater, suggesting a violent explosion, with the very marked asymmetry of the ray system. Furthermore, some of the secondary craters situated in the apices of the ray elements have diameters a considerable fraction of that of the parent crater. It seems very unlikely that the primary explosion could have produced blocks of a size sufficient to form the observed secondary craters, and that these blocks would largely be ejected in one preferred direction. In addition, this impact should have produced sufficient gas or vapor to fan ejecta from the secondary impacts for distances up to 1000 km is inconceivable.

Urey suggests in Section V that large ray craters such as Tycho may have been caused by cometary collisions, the energy of the expanding dome of vaporized ices being largely responsible for the impetus given to the large masses which, he assumes, produced the secondary craters visible in several ray elements shown in the *Ranger* A frames. This explanation does not seem plausible in the case of the Stevinus A system, however.

An examination of high-quality full-Moon photographs shows that the majority of the small, regular, conical craters, which are usually acknowledged as being due to high-velocity impacts, have no ray systems whatever. Yet, adjacent craters of indistinguishable shape, presumably formed in material of identical properties, may possess extensive ray systems. Similarly, the *Ranger VII* records show that the crater clusters seen in the apices of ray elements are frequently indistinguishable from other clusters which display no rays. This fact strongly suggests that the rays are not composed of lunar material. The existence of such asymmetric objects as the Stevinus A system shows that the rays are not composed of the fragmented impacting body either.

In order to try to account for these facts, the following suggestion is put forward. The small, conical type of craters which possess no trace of a nimbus or ray system have been formed by impacting meteorites, presumably similar to the stones and irons which still abound in the solar system. Craters possessing ray systems, however, were formed by the impact of comet nuclei.

Without elaborating details, it is suggested that the ray crater was formed by the impact of the main cometary nucleus, which consists of meteoritic types of bodies cemented together by frozen gases and vapors ("ices"). Detached fragments of the nucleus, and meteoritic material released by evaporation prior to impact, account

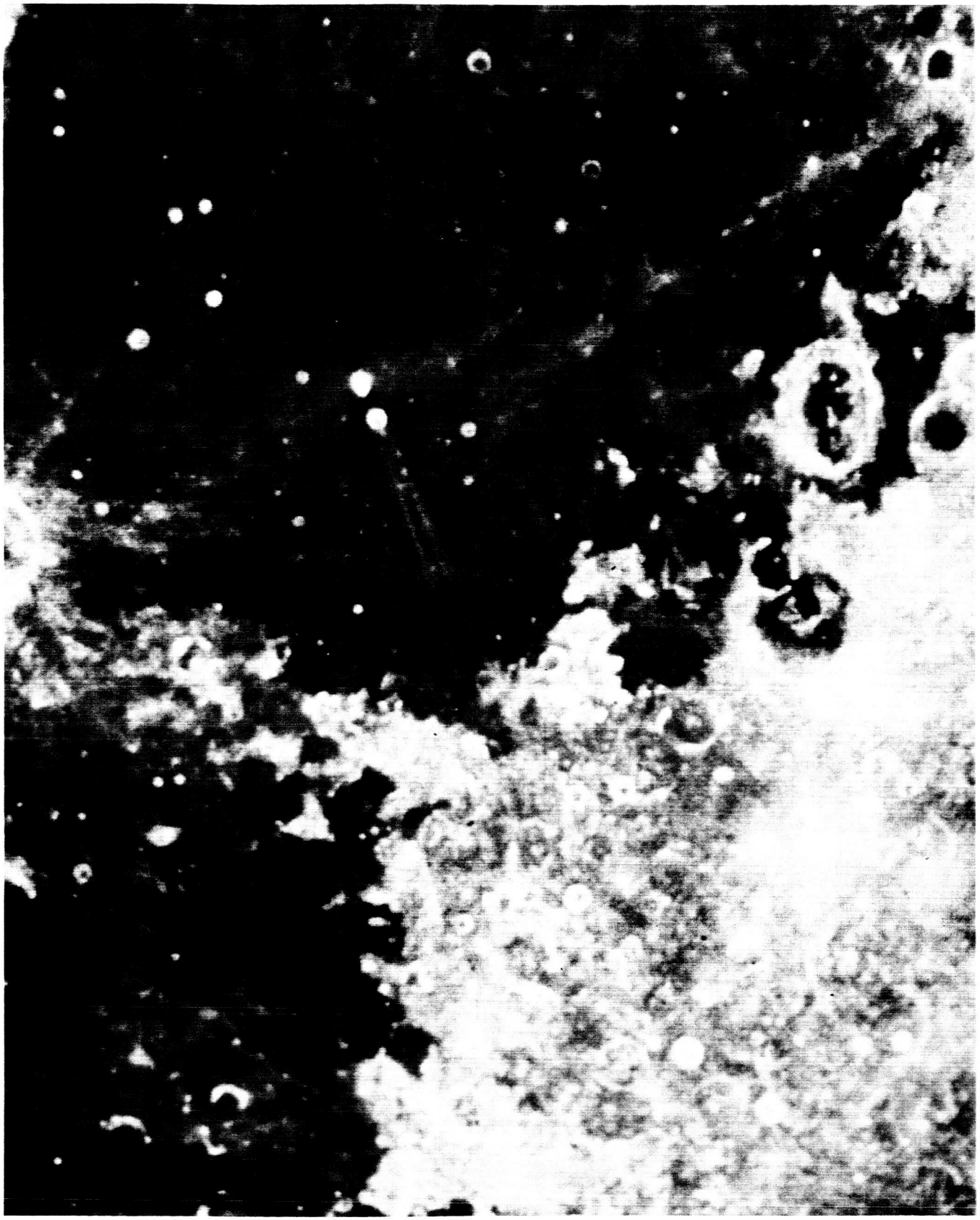

Fig. 1. Rectified view of Mare Fecunditatis at full Moon, showing the double ray associated with the craters Messier (right) and Messier A (left).

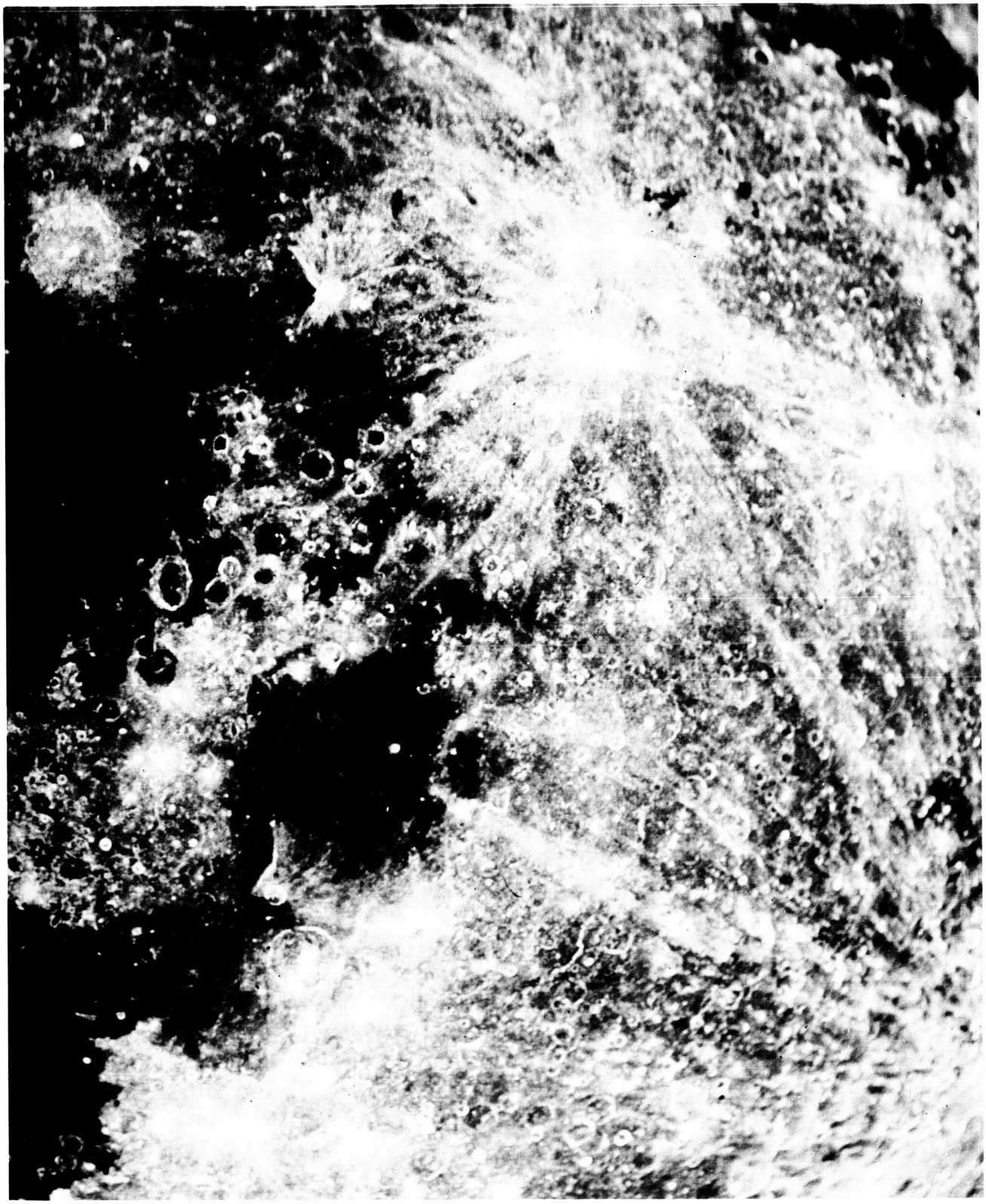

Fig. 2. Rectified view of the southern Mare Fecunditatis area showing the extensive ray systems associated with the small craters Furnerius A (right member of pair) and Stevinus A (left member of pair). The crater Rosse and its associated Tycho ray can be seen in Mare Nectaris (above and left of center).

for the rays and the "secondary" impact craters. The radial aspect of the rays is produced by the effect of the rapidly expanding dome of gases and vapors resulting from the almost instantaneous evaporation of the ices upon the still falling clots of meteoritic material. Under these conditions, the finer particles are deposited downwind from the heavier pieces, exactly as observed. If this assumption is correct, then asymmetric ray systems, like that of Proclus, are merely a reflection of the asymmetric distribution of detached meteoritic dust and other larger bodies around the original cometary nucleus. The long thin rays emanating from such craters as Stevinus A and Olbers A can be accounted for by the existence of strings of clots of meteoritic material in the vicinity of the cometary nuclei. This hypothesis differs from Urey's in that the former postulates that all lunar rays consist of cometary dust and debris, and that the "secondary" craters formed in clusters in and near ray elements are actually impacts.

Ranger VII impacted in the barely discernible boundary of a very minor ray which appears to be associated with Tycho. This ray is shown in all A-camera frames, while the higher-resolution P-camera frames feature areas in which the ray merges into imperceptibility. Other rays are recorded in many of the A frames. Wherever depressions do not interfere, the rays present an entirely unmottled appearance, no matter what the resolution. It is found that the ray areas tend to contain more shallow depressions than the non-rayed areas, although some of the latter display conspicuous clusters of such depressions. The depressions situated in the ray in which *Ranger VII* impacted exhibit a very marked NNE–SSW alignment; other depressions situated in non-rayed regions show precisely the same alignment, so that the apparent connection between rays and elongated depressions is presumably fortuitous.

The appearance of the elongated depression lying due south of the *Ranger VII* impact point is very suggestive of a collapse structure. The shaded area under the crest of the west wall is seen to consist of four or five straight segments, each of which lies parallel to one of the lineament systems of the entire mare and surroundings. Comparison between this depression and adjacent circular depressions fails to reveal any obvious structural differences. All of these observations suggest that the shallow, soft-edged depressions are not connected with lunar rays, that they are not impact structures, and that the rounding is not primarily due to erosion. It appears that the different apparent brightnesses of adjacent areas are due almost entirely to different angles and directions of slope, and that the tree-bark structure is rendered visible in the darker regions because of lower angles of illumination. This view has been further strengthened, since the completion of Part III, by the production of a somewhat improved mosaic of the last few P frames, in which the tree-bark structure can be traced in many of the lighter areas as well as the darker ones (Fig. 3). This structure tends to follow contour lines, although the NNE–SSW direction appears to predominate in the more level areas.

Thus, the main segment of shade in the elongated depression lying south of the impact point, continued northward, passes through two P frames of high resolution, in which the tree-bark appearance is clearly visible. One may tentatively conclude, therefore, that the tree-bark appearance is the outward manifestation of a system of fractures, those in the more level regions having their origin in the same stresses which produced the overall lineament systems and those on the inner slopes of the soft-edged depressions being caused by tensions induced by the collapse or slumping of the floors.

The above observations lead to the following conclusions:

1. Smooth conical lunar craters are presumably formed by impacting solid meteoritic bodies.

2. The larger ray systems appear to be more readily explainable on the basis of impacts with cometary nuclei. The ray crater is assumed to be formed by the impact of the main nucleus. The rays are assumed to be thin deposits of cometary dust, fanned radially by the expanding gas and vapor dome produced by the vaporized ices. The craters situated in or near the apices of the ray elements are assumed to have been formed by the impacts of meteoritic bodies or clots of meteoritic material loosely or partially cemented together by ices, which had become detached from the main nucleus prior to impact through evaporation of ices by solar radiation.

3. The ray material is evenly distributed, and has not been deposited in discrete clumps. The general dimness of the Mare Cognitum rays, as compared with bright rays, suggests that nowhere do these rays completely blanket the mare surface material.

4. The shallow, round or elongated, soft-edged depressions seen in some of the ray elements are believed to have no connection with the rays. They are tentatively assumed to be collapse features.

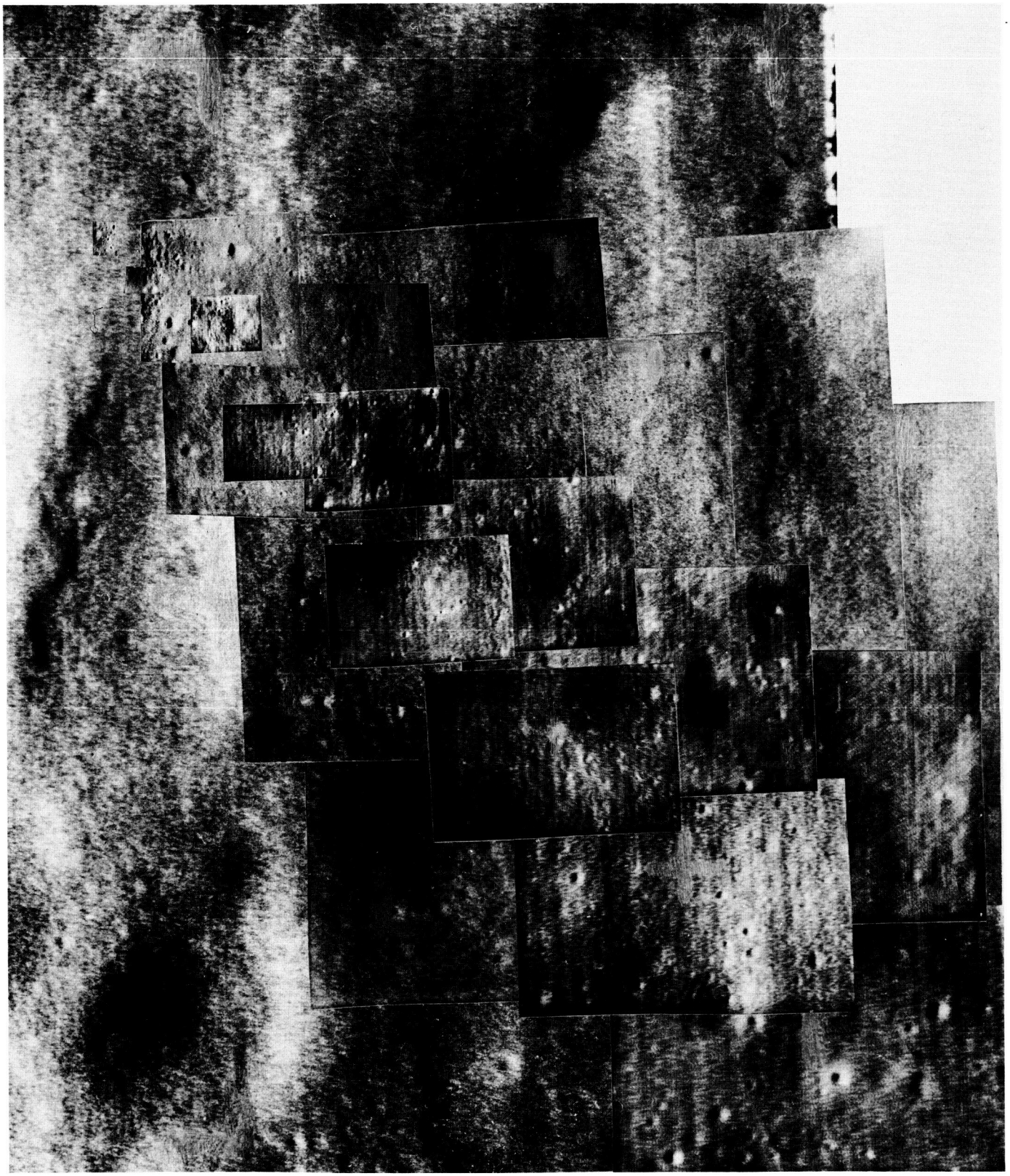

Fig. 3. Mosaic of the last few P frames on a portion of the last A frame. (Although densities are not well matched, the "tree-bark" structure is readily visible.)